



**HAL**  
open science

# Probabilistic seismic hazard assessment in Ecuador : inputs, practical applications and communication

Hugo Alfonso Yepes Arostegui

► **To cite this version:**

Hugo Alfonso Yepes Arostegui. Probabilistic seismic hazard assessment in Ecuador : inputs, practical applications and communication. Earth Sciences. Université Grenoble Alpes, 2015. English. NNT : 2015GREAU020 . tel-01330748

**HAL Id: tel-01330748**

**<https://theses.hal.science/tel-01330748v1>**

Submitted on 13 Jun 2016

**HAL** is a multi-disciplinary open access archive for the deposit and dissemination of scientific research documents, whether they are published or not. The documents may come from teaching and research institutions in France or abroad, or from public or private research centers.

L'archive ouverte pluridisciplinaire **HAL**, est destinée au dépôt et à la diffusion de documents scientifiques de niveau recherche, publiés ou non, émanant des établissements d'enseignement et de recherche français ou étrangers, des laboratoires publics ou privés.

## THÈSE

Pour obtenir le grade de

### DOCTEUR DE L'UNIVERSITÉ GRENOBLE ALPES

Spécialité : **Sciences de la terre et univers, environnement**

Arrêté ministériel : 7 août 2006

Présentée par

« **Hugo Alfonso YEPES AROSTEGUI** »

Thèse dirigée par « **Fabrice Cotton** » et  
codirigée par « **Céline Beauval** »

préparée au sein du **L'Institut des Sciences de la Terre**  
dans l'**École Doctorale Terre. Univers, Environnement**

# Probabilistic Seismic Hazard Assessment in Ecuador: inputs, practical application and communication

Thèse soutenue publiquement le « **6 juillet 2015** »,  
devant le jury composé de :

**M. Philippe GUÉGUEN**

Directeur de recherche, IFSTTAR, Président du jury

**M. Eric CALAIS**

Professeur, Ecole Normale Supérieure, Rapporteur

**M. Ross STEIN**

Scientist Emeritus, USGS, Rapporteur

**M. Philippe CHARVIS**

Directeur de recherche, Université de Nice-Sophia Antipolis, Examineur

**M. David BAUMONT**

Ingénieur Sismologue Senior, Geoter International–FUGRO, Examineur

**M. Fabrice COTTON**

Professeur, University of Potsdam and GFZ, Directeur de thèse

**Mme. Céline BEAUVAL**

Chargé de recherche, IRD-ISTerre, co-Directrice de thèse

**Mme. Laurence AUDIN**

Chargé de recherche, IRD-ISTerre, collaboratrice et jury invité





**Probabilistic Seismic Hazard  
Assessment in Ecuador: inputs,  
practical application and  
communication**

## *Preface*

Two of the largest Latin American disasters in Mexico City and Nevado del Ruiz-Armero, Colombia, in 1985 and the ensuing 1987 Mw 7.1 earthquake in eastern Ecuador taught me that the seismic and volcanic risk in our countries is enormous but very few people were recognizing it and even less were doing something about it. At the time, earth scientists were trying to understand the hazard at the regional (South America) scale and social scientists were talking about disaster preparedness and response. National Civil Defense systems claimed that they were ready to rescue survivors and to efficiently bury the victims as part of the relief effort. The more proactive times when the discussion was about reducing human and economic losses, vulnerability and resilience were still to come.

The Ecuadorian engineering community was practically absent from the discussion about the physical vulnerability and safety of constructions. Engineers and practitioners claimed victory when horizontal accelerations of  $\sim 0.06$  g did not produce major structural damage in Quito (80 km W from the epicenter) but did cause extensive, visible non-structural effects on modern buildings. Current analysis techniques are showing us now that structural damage did occur.

At the time my convictions were, and still are, that we as scientists are responsible for generating the best possible science not only to answer our research curiosity but also, or maybe first of all, to answer the practical questions that society poses to us. But in a context where society thought that catastrophes were natural and that God's design had a lot to do with them, I have found myself in the position of having a dual responsibility: to formulate or illuminate—in the name of that society I belong to—those practical questions for coping with the risk and to help answering them through my scientific activity.

The big efforts I devoted to create and sustain an institution such as the Instituto Geofísico (along with my professor and mentor Minard 'Pete' Hall) had a toll on my scientific production. I was involved among other duties in getting permanent funds for continuous long-term operation of the IG, implementing nation-wide geophysical observation networks for monitoring seismic and volcanic sources, promoting the scientific interest among young students for them to go abroad to study at renowned institutions and to come back with a higher level education, issuing early warnings or responding to authorities' demands during ongoing seismic or volcanic crises with limited monetary, instrumental and human resources, communicating our science to society translating the scientific knowledge into practical information, and much more.

At the maturity of my academic career, I have had the privilege over the last couple of years to stop running back and forth, to stop swimming against bureaucratic currents, to spend my time reading, observing, and thinking about several scientific ideas I had related to the geodynamics and seismotectonics of NW South America. I have benefited from new data, from better techniques used in the treatment of those data and from a new wealth of knowledge about the earthquake science in active subduction zones. With these advantages I was able to propose my own interpretations.

It has also been a privilege to work in France with my French and Ecuadorian colleagues to construct the road for assessing the seismic hazard of Ecuador at international standards and to contribute to the advancement of science, but also to the well-being of my society through the vulgarization of the scientific knowledge.

<b>Table of Contents</b>		p.
	<i>Preface</i>	i
	<i>Contents</i>	ii
	<i>PLATE A</i>	viii
<b>1</b>	<b>Introduction</b>	<b>1</b>
1.1	A brief earthquake history and the human impact	2
1.2	A perspective about potential outcomes during future earthquakes and the importance of assessing the seismic hazard	5
1.3	Previous efforts in assessing PSH in Ecuador	7
1.4	Methodological approach	13
1.5	References	15
<b>2</b>	<b>Overview of the papers</b>	<b>18</b>
2.1	Construction of the Ecuadorian earthquake catalog for PSHA	18
2.1.1	<i>Locations and magnitudes of historical earthquakes in the Sierra of Ecuador (1587–1996) (Appendix 1, Chapter 3)</i>	18
2.1.2	<i>An Earthquake Catalog for Seismic Hazard Assessment in Ecuador (Chapter 3)</i>	19
2.2	Definition of the seismic source zones SSZ for PSHA	20
2.2.1	<i>A new view of Ecuador’s geodynamic context and its implications for seismogenic sources definition and seismic hazard assessment (Chapter 4)</i>	21
2.3	Application study using the new information	23
2.3.1	<i>Probabilistic Seismic Hazard Assessment in Quito, Estimates and Uncertainties (Chapter 5)</i>	23

2.4	References	25
<b>3</b>	<b>An Earthquake Catalog for Seismic Hazard Assessment in Ecuador</b>	<b>27</b>
	Introduction	27
	A Homogeneous Earthquake Catalog	27
	<i>Instrumental Earthquake Catalogs</i>	27
	<i>Merging Different Instrumental Earthquake Catalogs</i>	29
	<i>Homogenization of Magnitudes to Moment Magnitude</i>	30
	<i>The Historical Catalog</i>	32
	<i>Final Unified Earthquake Catalog</i>	33
	Recurrence Times of Earthquakes in the Cordillera	34
	<i>Declustering of the Catalog</i>	34
	<i>Recurrence Times of Potentially Destructive Earthquakes in the Cordillera</i>	36
	Conclusions	38
	Data and Resources	38
	Acknowledgments	39
	References	39
<b>4</b>	<b>A new view for the geodynamic context of Ecuador and its implications for seismogenic sources definition and seismic hazard assessment</b>	<b>41</b>
	<b>Introduction</b>	<b>41</b>
	<b>1. REVISITING GEODYNAMICS AND SEISMOTECTONICS IN ECUADOR</b>	<b>43</b>

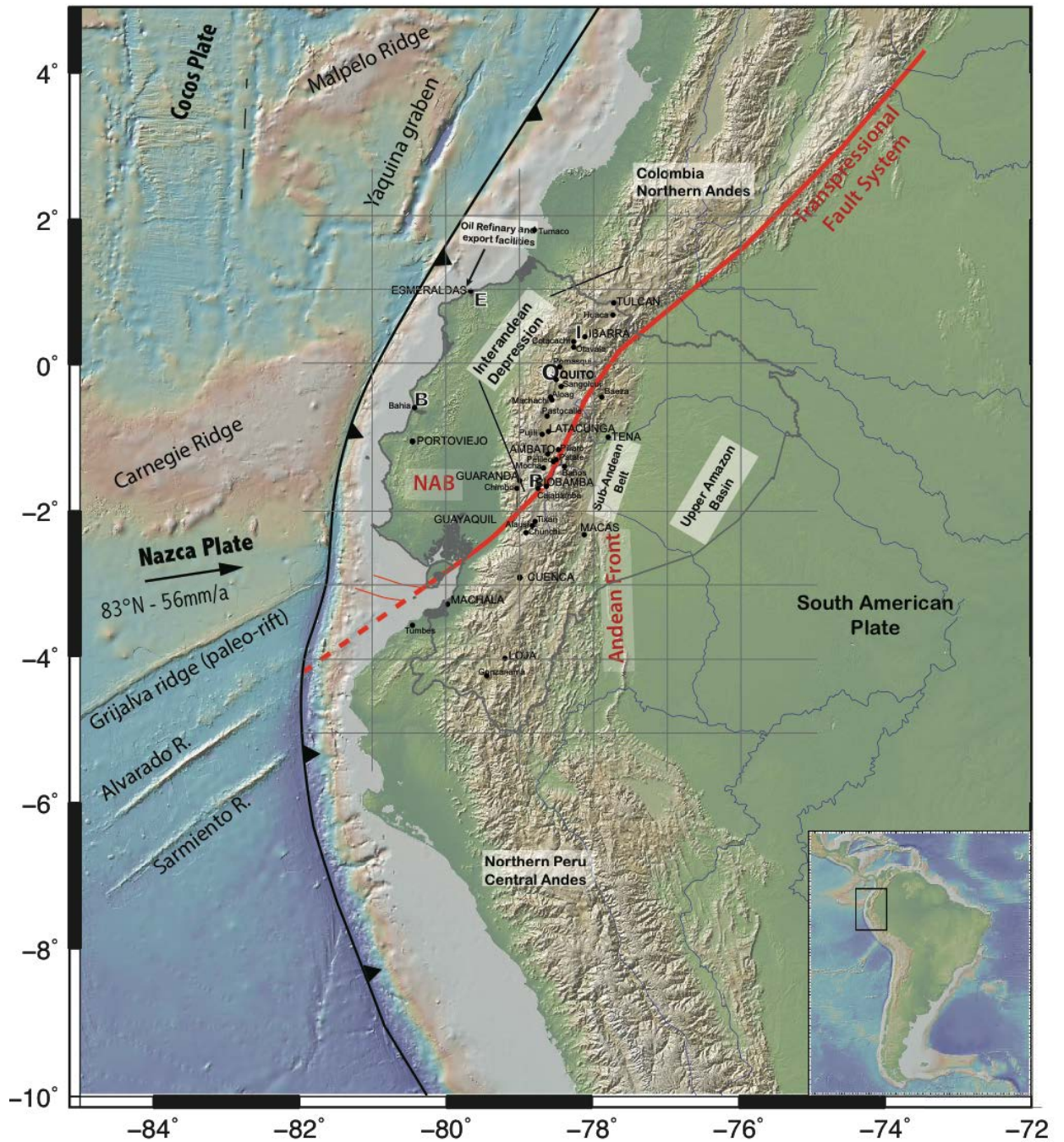
<b>1.1 Overview of geomorphic features and shallow seismicity of the intervening plates</b>	<b>43</b>
<i>Nazca Plate: two plates with different densities in contact</i>	43
<i>Interface seismicity: one of the most seismically active convergent margins</i>	45
<i>Crustal morphology: evidence of continuous oblique convergence</i>	48
<i>Crustal seismicity: localized activity with strong shallow earthquakes</i>	49
<b>1.2 Consequences of the oblique convergence along the convex continental margin of northwestern South America</b>	<b>50</b>
<i>Subduction along a convex margin</i>	51
<i>Slab geometry from south to north as given in the literature</i>	51
<i>Relocated Intermediate depth seismicity as a key to interpret moment release, shapes, and dipping angles</i>	54
<i>Oblique convergence tectonics</i>	58
<b>2. CONSTRUCTION OF A NEW SEISMIC SOURCE ZONES MODEL FOR ECUADOR</b>	<b>62</b>
<b>2.1 Interface megathrust sources</b>	<b>64</b>
<i>Esmeraldas SMT-1</i>	64
<i>Bahía SMT-2 and Talara SMT-3</i>	68
<b>2.2 Inslab sources</b>	<b>69</b>
<i>Farallon ISF sources</i>	69
<i>Nazca ISN sources</i>	71
<b>2.3 Crustal sources</b>	<b>72</b>
<i>CCPP fault system</i>	74
<i>Eastern sub-Andean uplifts, thrust faults and fold</i>	76
<i>Western Cordillera faults</i>	76
<b>3. DISCUSSION</b>	<b>78</b>
<i>Subducting slabs</i>	78

	<i>Carnegie Ridge and the interface</i>	81
	<i>Grijalva to Mendaña interface</i>	82
	<i>Crustal structures</i>	84
	<i>Outer-trench seismicity</i>	86
	<b>Conclusion</b>	86
	<b>References</b>	88
	Table 1 (as electronic supplement in the submitted paper)	97
<b>5</b>	<b>Probabilistic Seismic Hazard Assessment in Quito, Estimates and Uncertainties</b>	110
	Introduction	110
	Probabilistic seismic hazard in Quito: the host zone is controlling the hazard	111
	Variability of the uniform hazard spectrum at 475 years	113
	<i>Host Zone: Frequency–Magnitude Distributions</i>	113
	<i>Variability of the Uniform Hazard Spectrum (UHS)</i>	115
	<i>Frequency–Magnitude distributions based on the slip rate and corresponding hazard</i>	116
	Restricting large earthquakes to the Quito fault and hanging-wall effect	118
	<i>PGA at 475 Years: Profile Perpendicular to the Fault</i>	118
	<i>Scenarios and Hazard Values at 475 Years</i>	118
	Conclusions	119
	Acknowledgments	120
	References	120

<b>6</b>	<b>Communicating the hazard</b>	<b>122</b>
6.1	Introduction	122
6.2	Lessons learned in communicating hazard and risk during the Tungurahua volcano eruption	124
6.2.1	<i>The scientific–community interface over the fifteen-year eruptive episode of Tungurahua Volcano, Ecuador (Appendix 2)</i>	126
6.2.1.1	<i>Initial eruptions and difficulties in the relationship between scientists and the community</i>	128
6.2.2	<i>The vigías network, a fruitful initiative to establish effective communication between scientists and the community</i>	130
6.2.3	<i>Discussion</i>	133
6.3	A strategy for earthquake risk community-based risk management in Quito	136
6.3.1	<i>Theoretical grounds</i>	136
6.3.2	<i>Outline for a CBDRM strategy in Quito</i>	137
6.3.3	<i>Conclusion</i>	143
6.4	References	144
<b>7</b>	<b>Summary and perspectives</b>	<b>147</b>
7.1	Summary	147
7.2	Perspectives	150
7.3	References	156
 <b>APPENDICES</b>		
	<i>Appendix 1 – Chapter 3: Locations and magnitudes of historical earthquakes in the Sierra of Ecuador (1587-1996)</i>	1-A
	<i>Appendix 2 – Chapter 6: The scientific–community interface over the fifteen-year eruptive episode of Tungurahua Volcano, Ecuador</i>	22-A

*We need to encourage students to take a step back and see the big picture rather than becoming overly specialized at a young age or locked into conventional ways of thinking.*  
*H. Kanamori (2012)*

# Plate A: General setting and geographic references



# 1 Introduction

Roger Bilham [2009] in his paper “The seismic future of cities” predicts that the urban population living along the earthquake geography will continue to be killed by earthquakes in the foreseeable future, and in greater numbers than in the documented past. This may well be true for Ecuadorian cities for several reasons related to the country’s active tectonics, historical seismicity, and socio-economic situation. For Ecuador, the following statements are true:

- A long history of strong earthquakes and a large number of casualties that rise above 60.000 during the last four and a half centuries (Ecuador’s written history epoch).
- A rapid urbanization process by which ~64% of the dwellings are now built in crowded cities.
- Poor building practices that includes the lack of professional advise, the use of substandard materials and assembly methods, and inappropriate siting of buildings.
- A loosely regulated, controlled and supervised construction industry.
- Non-existent and/or inadequate formal education and professional training given by Ecuadorian universities in matters related to seismic hazard and seismic design, construction safety and urban planning for earthquake environments like Ecuador’s.
- A generalized absence of public seismic awareness that precludes the adoption of policies and strategies to cope with the risk.

One of the tools to revert this reality is to improve the knowledge about seismic hazard as one of the two main components of the seismic risk. More and better knowledge in the citizens’ hands for them to take informed decisions means less risk. Therefore, it is very important for the future security and development of the country to quantify Ecuador’s seismic hazard and risk. This work deals with the first, the probabilistic seismic hazard assessment –PSHA– for Ecuador.

## 1.1 A brief earthquake history and the human impact

In order to have a quick grasp of the overall seismic history of the country Figures 1 and 2 have been prepared to show a synthesis of the most important earthquakes identified from instrumental and historical seismicity respectively. Ecuador's general setting is presented in Plate A and will be referenced throughout this manuscript for geographic sites and tectonic features location.

Ecuador is one of the four countries located on the active, convergent plate boundary along the western South American coast (Plate A). The fast Nazca plate subduction ( $\sim 6$  cm/year) underneath the continental plate provokes repetitive large ( $6 < M_w \leq 7$ ) to great ( $7 < M_w \leq 8$ ) interface earthquakes. Rare mega-earthquakes  $M_w > 8$ , such as the  $M_w$  8.8 1906 event -one of the 10 largest earthquakes recorded by seismometers in the world-, have also broken the northern Ecuadorian subduction zone at least once during historical times. During the 20<sup>th</sup> century a total of five  $M_w \geq 7.5$  earthquakes ruptured different segments along the Ecuadorian interface (Fig. 1). For individual segments responsible for the great earthquakes the recurrence time is 100-150 years, and several centuries-long for the rare mega-events evidencing a dual cyclic pattern [Chlieh *et al.*, 2014]. The recurrence time for smaller, independent  $7.5 > M_w \geq 6.5$  events is around 10 years for the entire coastal length ( $\sim 600$  km) (see Fig. 1).

A second active plate boundary crosses the country from SW to NE (Plate A). Along this boundary crustal faulting generates frequent, moderate ( $M_w \leq 6$ ) to large shallow earthquakes and occasional great ones that have devastated several Andean cities in the populated Interandean Depression during the last 450 years. These earthquakes are related either to continental-size, transpressional fault systems developed along the contact between the North Andean Block –NAB– and the South American plate, or to internal deformation within the NAB or the Andean front (Plate A). The former is the case of the catastrophic 1797  $M_{ic}$  7.6 Riobamba event, one of the largest historical crustal earthquakes in South America (Fig. 2) [Baize *et al.*, 2014].  $M_{ic}$  is the “intensity magnitude” calculated at the intensity center equivalent to  $M_w$  for the Ecuadorian seismic catalog [Beauval *et al.*, 2010].

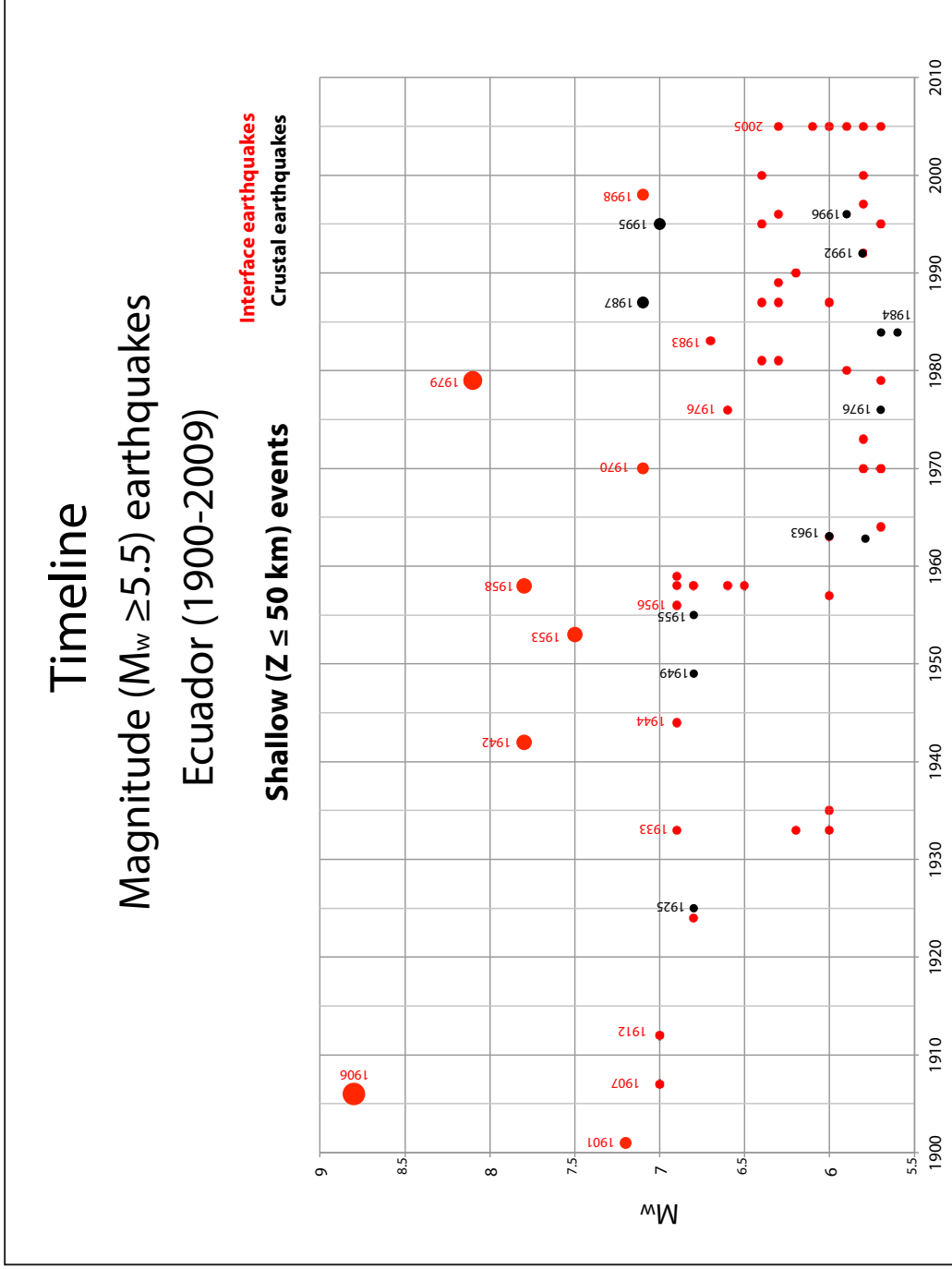


Fig. 1: Timeline for  $M_w \geq 5.5$  earthquakes listed in the PSHA-ready Ecuadorian earthquake catalog (Beauval et al. 2013). Interface and crustal earthquakes are red and black, respectively. Most of the interface events without a year are aftershocks.

The 1868  $M_{ic}$  7.25 Ibarra earthquake [Beauval et al., 2010], the second deadliest event in Ecuador's history, is an example for the latter (Fig. 2).

F2

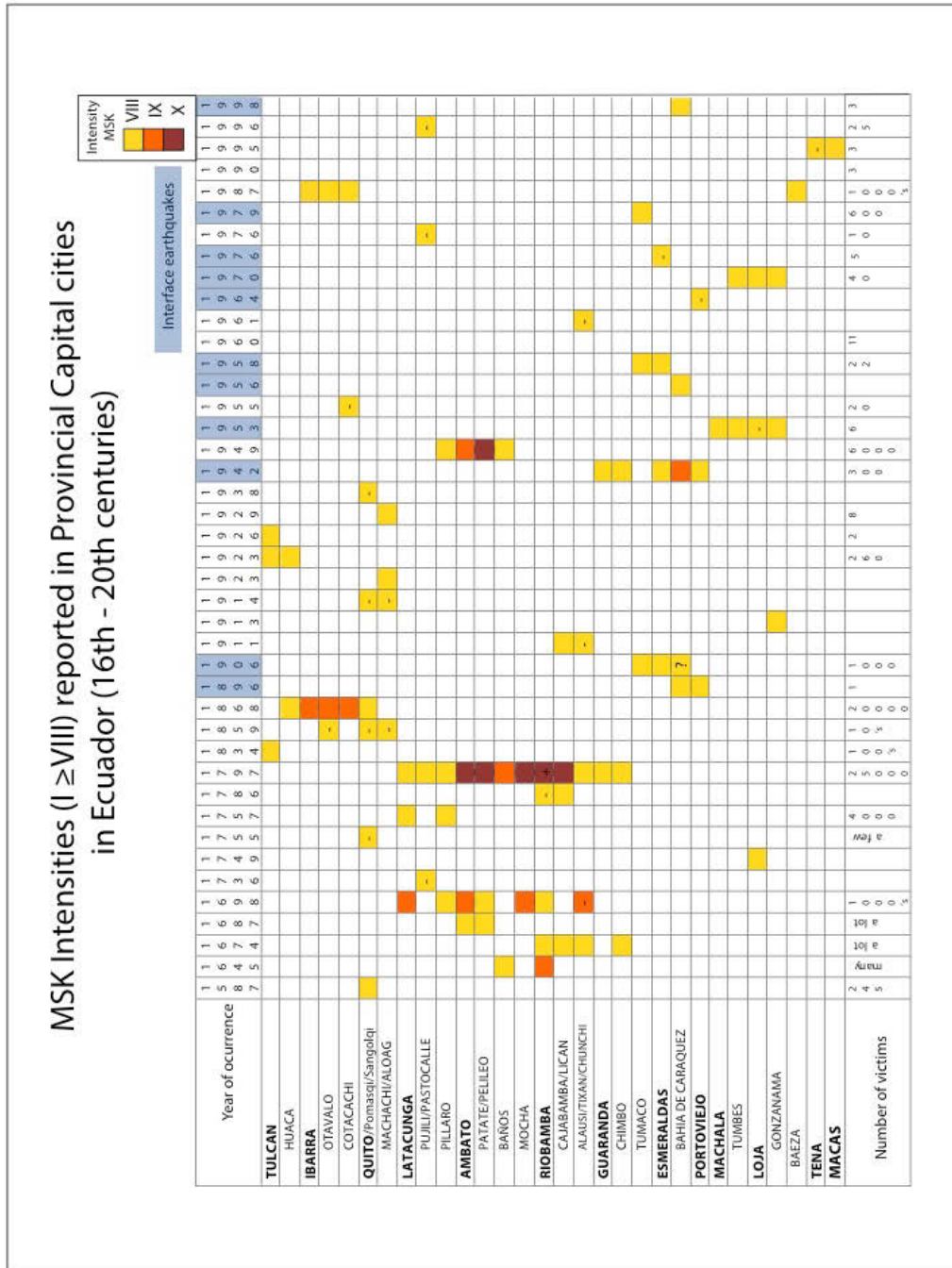


Fig. 2: Intensity chart for the historical earthquakes in Ecuador with reported intensities (MSK scale) equal or greater than VIII. Interface earthquakes are marked in light blue. Provincial capital cities are written in bold. Other towns with repetitive high intensities in the province are also listed. Towns list is arranged so that intensities from the same event group together and show the geographical extension of the damage. Minus or plus signs denote intermediate intensity values. Localities are shown in Plate A. The number of victims was modified from the IGEPN internal archives after the work of J. Eged and collaborators.

Surprisingly, although the seismic moment released by interface earthquakes largely surpasses that of crustal faulting (see Figs. 7 and 10 in

Chapter 4), the casualties toll related to shallow crustal earthquakes (~60.000 during the 480 years of written history) is one order of magnitude higher than that from subduction earthquakes (Fig. 2). This is directly related to two factors:

- the proximity of shallow crustal earthquakes to Andean towns (a few kilometers) in contrast to hypocentral distances of tens of kilometers for interface earthquakes
- different type of construction along the Interandean Depression in contrast with that in the Coastal region.

Historically, before concrete, the Andean highlands dwellings have been constructed with clay (adobe bricks, mud-walls, heavy tile roofs) which is the weakest structure to sustain lateral seismic forces. Meanwhile, in the hotter, humid Coast the predominant construction type was a mixture of wood frames and armored clay walls, more flexible and resistant to earthquakes.

But these circumstances have dramatically changed. With the aggressive urbanization process that started during the second half of the 20<sup>th</sup> century, city construction is now almost ubiquitously of the type known as concrete frames, i.e. reinforced concrete columns and beams filled with heavy cooked-clay or concrete bricks. Moreover, low rise dwellings have given way to tall buildings which are susceptible to experience much stronger shaking under the effect of long period waves generated by great to mega interface earthquakes. While the known seismic sources will probably be generating earthquakes in more or less the same sites and at the same pace –of course surprises are not discarded– the seismic risk has shifted from rural areas to cities and vulnerability from adobe to concrete.

## 1.2 A perspective about potential outcomes during future earthquakes and the importance of assessing the seismic hazard

Although recently built-concrete structures in theory perform better than old, clay dwellings, reinforced concrete buildings are not necessarily much safer

in developing countries, as it was painfully experienced during the 2010 Port-au-Prince earthquake [O'Brien *et al.*, 2011]. Damage to concrete frame structures may be caused by [Bilham, 2009]:

- incorrect design –short columns, soft stories, flat slabs with embedded beams, torsion-prone layouts,
- incorrect assembly—weak concrete, brittle steel, an absence of stirrups, a lack of through-going steel-work at columns.

Unfortunately in the local Ecuadorian construction practices, both situations are present as has been repeatedly demonstrated by the effects caused by the interface 1998 Mw 7.1 Bahía de Caraquez earthquake [CERESIS *et al.*, 1998], the 1987 Mw 7.1 Napo crustal event [Schuster *et al.*, 1991] or the 1976 Mw 6.6 Esmeraldas subduction earthquake, just to name some of the most notorious ones. It is even more worrisome that small events like the 2014  $M_w$  5.1 Pomasqui (Quito suburb) earthquake also produced light structural damage in newly constructed concrete reinforced structures (F. Yopez, personal communication).

Guidelines exist for Ecuador's seismic-resistant construction, but it is not unusual for these guidelines to be ignored by builders either to reduce costs or simply because they do not understand how seismic waves and structures interact. Under the category of 'builders' we can find architects, in lesser extent civil engineers, but mostly home owners trying to save money at the construction stage. It is estimated that over 70% of the dwellings have not been designed and/or constructed by qualified construction industry professionals (Flores, H., 2014), therefore the physical vulnerability in the country is really high. From this perspective, it is a valid and important contribution for reducing the seismic risk to elaborate methodologically sound hazard assessment maps with purposes of reducing the seismic risk via establishing national and local seismic building codes and building retrofitting programs.

It is also worth mentioning that other types of vulnerability have already been highlighted by recent earthquakes. During the 1987  $M_w$  7.1 transpressive

fault system earthquake (see Chapter 4 for details), ~40 km of the Trans-Ecuadorian oil pipeline were wiped out by massive ground-shaking-triggered landslides impacting the epicentral zone located in the Sub-Andean Belt, 80 km east of Quito. At the time, the country's economy was deeply dependent –and still is– from its oil exports. Due to five months of inability to pump oil through its only pipeline, Ecuador's economic growth during 1987 was negative; its Gross Domestic Product (GDP) annual average variation dropped 10 points to -6% in comparison to a sustained annual growth of the economy of ~3.5% during the previous three years [*Cornejo et al.*, 1999]. This huge impact on the economy signified a halt on public investment, less jobs and more poverty, among other consequences.

In spite of these lessons, at the beginning of this century the country built its second oil pipeline parallel (10 m apart) to the one destroyed in 1987, exposing not one but the two ducts to similar effects along the 450 km long path from the upper Amazon basin, across the Andes, to the northern Ecuadorian Pacific coast (Plate A). Even worst, a new oil refinery, the largest investment in the decade, is planned to be built at the southern termination of the 1906 mega-earthquake rupture zone (see Chapter 4 for details).

With all of the above in mind, it is not only likely that Bilham's statements (2009) may become truth, but also that the country's sustainable development is in peril if the seismic hazard and the consequent risk are not taken seriously by the national and local authorities and the general population.

### 1.3 Previous efforts in assessing PSH in Ecuador

Although both seismic hazard and risk are evidently high, in the international literature very little scientific production is found regarding SHA in Ecuador. During the previous century probabilistic seismic hazard maps were mostly calculated by means of international projects, either at the South American or global scales and were not country-specific. All these analyses

followed the Cornell-McGuire probabilistic methodology [*Cornell*, 1968; *McGuire*, 1976].

Ecuador is part of a venerable organization called CERESIS (South American Regional Center For Seismology) since its foundation by all South American countries in the early 70s. CERESIS was fundamental in generating the first regional seismic catalog and an historical database for PSHA calculations at the subcontinent scale through the USGS funded SISRA project (Earthquake Mitigation Program in the Andean Region, [*Giesecke et al.*, 2004]). The first internationally published seismic hazard map for Ecuador is included in the CERESIS' 1:5'000.000 South-American map (CERESIS, 1996; taken from [*PREDECAN*, 2009]), obtained on the basis of the regional seismicity. As part of this regional effort, national scientific/technical institutions such as the Geophysical Institute and the Astronomic Observatory (in charge of seismology in Ecuador until 1983), both in Quito, generated the local historical and instrumental catalogs under common regional criteria. Since PSH analysis was done outside the local institutions, there was not an effective knowledge transference to build up local capacities in PSHA calculations.

In the framework of the GSHAP (Global Seismic Hazard Assessment Program, [*Giardini*, 1999]), one of the United Nations demonstration projects launched during the International Decade for Natural Disaster Reduction (UN/IRNDR), a second seismic hazard evaluation at the regional scale was obtained for Ecuador. A consortium of five Andean and three European institutions performed the regional South American PILOTO project [*Dimaté et al.*, 1999] with the aim of producing a unified SHA for five countries: Bolivia, Perú, Ecuador, Colombia and Venezuela. The main activities and setbacks were the following:

- National earthquake catalogs were integrated in a regional single catalog with homogeneous magnitude via linear regressions derived independently for each country catalog and a prioritizing scheme.
- Magnitudes reported in the national seismic catalogs were homogenized in terms of  $M_s$ . Notwithstanding the advantage of

having a common magnitude throughout the region, very little efforts were made to verify the quality and the meaning of magnitudes calculated for local seismicity in each country and to compare them for unifying the catalog beyond magnitudes extracted from international standardized bulletins.

- Maximum intensities reported for historical events were used to calculate  $M_s$  utilizing the Gutenberg and Richter (1956) equation. The problems for calculating magnitudes using one single maximum intensity value are well known, leading to an overestimation of magnitudes for shallow crustal events and an underestimation for interface and in-slab earthquakes. Besides, intensities are not equally determined throughout the region precluding an homogeneous characterization of magnitudes.
- Seismic source zones were jointly defined using the regional catalog, along with emerging knowledge of active faults and contemporary geodynamic models. Since this was a regional, small scale project aiming to produce results at the sub-continental scale, and Ecuador is a small country, only two source zones were defined exclusively for Ecuador. Five other multinational source zones, hundred if not more than one thousand kilometers long and comprising seismicity in two or three neighboring countries, were used to perform PSHA. Important local active faults and subduction zone details were concealed by this broad modeling.
- Two regional ground motion prediction equations –GMPEs– were used for the calculations, one for subduction sources developed for Chile [Saragoni *et al.*, 1981] and one for crustal sources developed for Venezuela [Quijada *et al.*, 1993]. These GMPEs have not been peer-reviewed by the international community and the lack of enough native recordings suggests that the epistemic uncertainty for these models is large.

Several authors [Shedlock and Tanner, 1999; Tanner and Shedlock, 2004] profited from the work done within the region and recalculated the PSH using

up-to-date GMPEs. The resulting maps represent the concatenation of various national and regional maps and approaches. The maps were done with the intent of providing a global seismic hazard framework to national and international agencies to be used as a starting point for further detailed studies [Shedlock and Tanner, 1999]. The GSHAP Global Map presents a slightly different version than the original PILOTO Project [Giardini, 1999]. In Fig. 3 the different seismic hazard maps described above are presented for comparison. All of them show peak ground acceleration (PGA) values in rock and were produced for a 475 years return period.

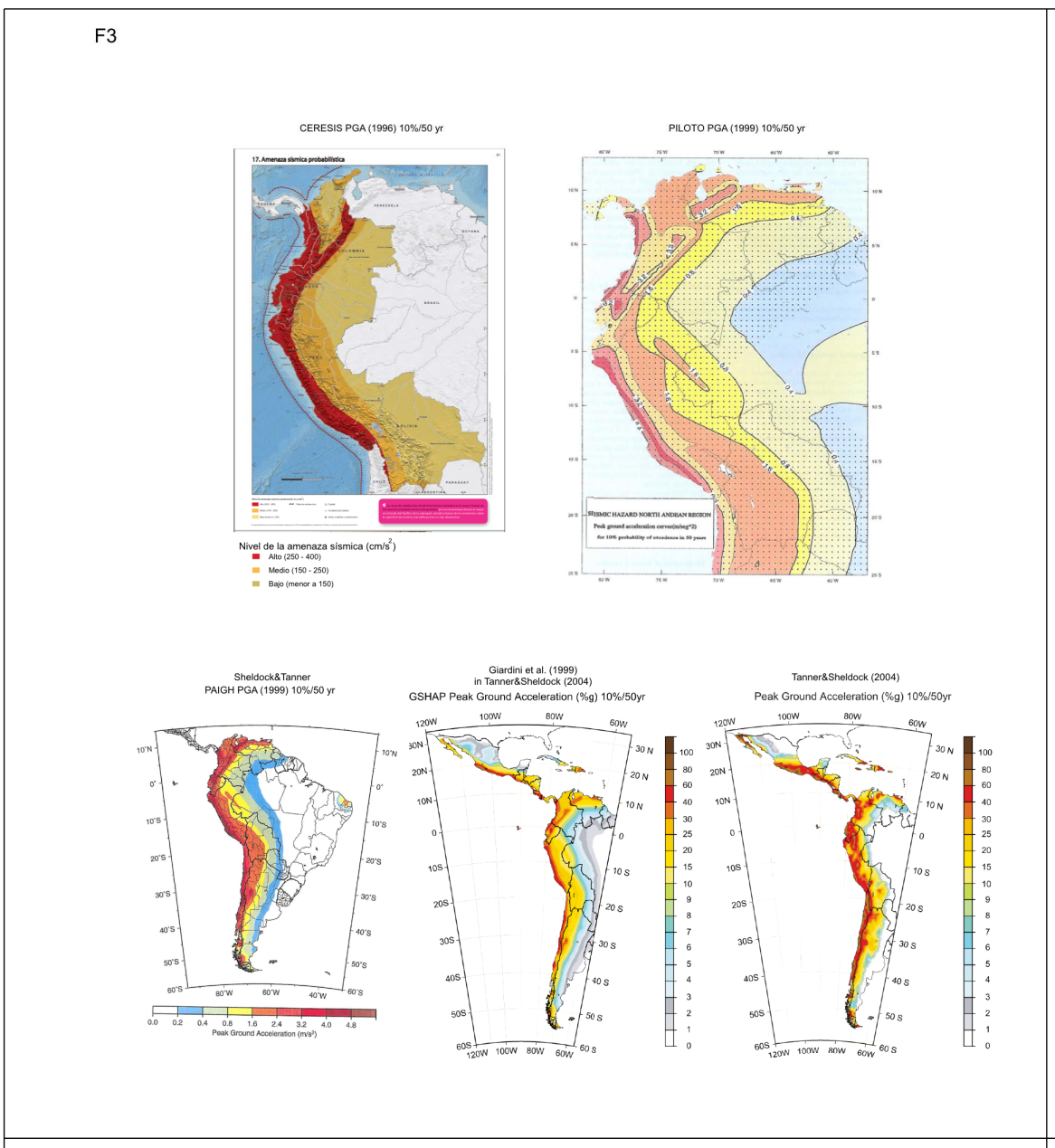


Fig. 3. Regional PSHA maps produced for the South-American region.

Finally, the last published international effort to assess the PSH in South America was in charge of the USGS group for modeling the seismic hazard, in cooperation with CERESIS and the Global Earthquake Model –GEM– [*Petersen et al.*, 2013]. GEM is a new private/public organization that aims to be the uniform, independent standard to calculate and communicate earthquake risk worldwide. Each of these groups has interest in standardizing the hazard methodologies and data that pertain to hazard analysis, and although the region has made important advances in that direction there is still a need for standardization as a means to improve the local PSHA practices. This assessment follows the methodology developed by Petersen et al. [2008] for the United States and profits from fault databases published after the previous calculations [*Egüez et al.*, 2003]. Since the published report includes only the map for 2475 years return period, the results are not directly comparable with those in Fig. 3. Once again, source zones defined for calculating seismicity statistics span over areas larger than Ecuador.

Local efforts to assess PSH for the country have been made in the framework of the requirements for the Ecuadorian Building Code –EBC. The first EBC was launched in 1951 after the 1949 earthquake (6000 victims, Fig. 2). There was, as it always occurs, a major revision after the 1976  $M_w$  6.6 interface earthquake that killed five people but badly damaged modern structures in the city of Esmeraldas (Fig. 1, 2). None of these versions presented a seismic zonation of the territory as part of the EBC provisions.

The following ECB was launched in 2001 [*CEC*, 2001], influenced by the 1998 Bahía de Caráquez  $M_w$  7.1 interface earthquake, the latest event to produce considerable damage in Ecuador. The 2001 ECB includes a map of four equal-value PGA seismic zones, known as the seismic zonation map –SZM– or seismic design value maps for buildings. The PSHA which is the basis for the 2001 SZM was obtained as follows [*CEC*, 2001]:

- The Ecuadorian section of the PILOTO project [*Dimaté et al.*, 1999] catalog was reviewed. Overall, 22000 local events were analyzed. A national homogeneous magnitude was obtained by means of an  $m_b$ –

$M_s$  regression. The minimum homogeneity magnitude was established as  $M$  3.9 and  $M_{max}$  was 8.6.

- Historical earthquakes were qualitatively analyzed in terms of their maximum intensities. Since historical earthquakes produced large quantities of victims the intensities assigned to those events were very high. These intensities were related not only to the strong ground shaking but also to the very poor quality construction of the adobe-brick or mud-wall dwellings. Therefore intensity values were clipped or not overestimating the magnitudes.
- Every meaningful local neotectonic study –developed mainly during the 90’s– was incorporated and a seismotectonic scheme for the country was adopted.
- 53 seismogenic sources were modeled in ten seismotectonic provinces and their seismic parameters for PSHA were obtained. The seismotectonic provinces were useful to define regional seismic parameters.
- Two GMPEs were used for the two distinct tectonic environments: Katayama-1982 (in [Douglas, 2011]) for crustal events and Youngs-1997 [Youngs et al., 1997]. The Katayama-1982 equation was adopted in a deterministic fashion because of its better fit –in comparison with more modern GMEPs– with the only accelerographic recording available for the country: the EPN (Quito) accelerogram of the 1987  $M_w$  7.1 NAB boundary earthquake located 80 km to the east of the instrument’s site. The dispersion was set at one standard deviation.

Unfortunately there is no technical publication documenting the followed procedure to calculate the PSHA. In Fig. 4 the EBC 2001 SZM is presented.

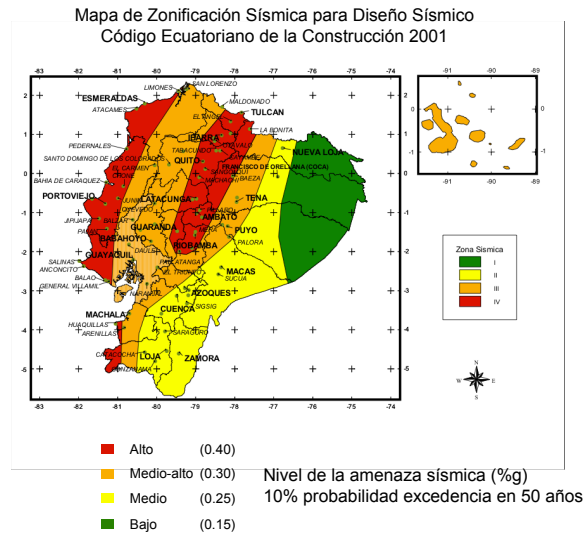


Fig.4: Seismic Zonation Map for the Ecuadorian Building Code 2001

Although agreed-upon drafts of the new EBC were ready much earlier, the latest official ECB's release dates from January this year, after a shoddy process lead by the Ecuadorian Housing Ministry (MIDUVI) of validating it among the engineering community. The 2015 version of the EBC [NEC, 2015] includes a SZM outlined from earlier versions of the seismic hazard map that was calculated based on a single best-estimate model (no logic tree and no exploration of uncertainties). All the analysis was made by means of the products presented in this doctoral work in the following chapters.

Last but not least, there were several earlier academic efforts to calculate the PSH in Ecuador. Among them one could mention the work done by Bonilla and Ruiz (1992) and Bernal (1998). It is important to mention them since they were independently performed from the regional approaches and started the local learning process to calculate PSHA in the country. Finally, Chunga [2010] proposed a different approach (pattern recognition) for obtaining a crustal seismic zonation for Ecuador.

#### 1.4 Methodological approach

“The goal of earthquake engineering analyses is to ensure that a structure can withstand a given level of ground shaking while maintaining a desired level of performance. But what level of ground shaking should be used to perform

this analysis? There is a great deal of uncertainty about the location, size, and resulting shaking intensity of future earthquakes. Probabilistic Seismic Hazard Analysis (PSHA) aims to quantify these uncertainties, and combine them to produce an explicit description of the distribution of future shaking that may occur at a site” [Baker, 2008].

Probabilistic seismic hazard analysis is then meant to quantify, at a given site, the level of ground shaking with a given probability of exceedance over a specified time window. For that, all possible contributing earthquakes and their resulting ground motion (by means of the application of the pertinent GMPEs) should be considered, along with their associated probabilities of occurrence. In this sense, PSHA is fundamentally composed of five steps:

- Identify all earthquake sources capable of producing damaging ground motions.
- Characterize the distribution of earthquake magnitudes (the rates at which earthquakes of various magnitudes are expected to occur).
- Predict the resulting distribution of ground motion intensity as a function of earthquake magnitude and distance.
- Combine uncertainties in earthquake size, location and ground motion intensity, using a calculation known as the total probability theorem.
- Estimate the epistemic uncertainties through methodologies such as logic trees.

During more than seven years of collaboration the Institut de Recherche pour le Développement (IRD), the Institut des Sciences de la Terre (ISTerre) in Grenoble and the Instituto Geofísico de la Escuela Politécnica Nacional (IG-EPN) in Quito have undertaken a systematic approach for calculating the PSH for Ecuador assuming the steps described above in a broader or lesser extend according to the local conditions. The traditional approach where area source zones are modeled around seismicity and/or seismic capable tectonic structures for the calculation of seismic hazard [see Cornell, 1968] has been adopted. My dissertation is part of this fruitful cooperation.

The manuscript follows a multi-paper model. Two original studies that address mainly the first and second steps, i.e. the generation of the seismicity information and the modeling of the earthquake sources for PSHA, are presented, A third paper shows a first application of the new knowledge for estimating the PSH in Quito and its uncertainties. Each paper corresponds to a chapter of the present dissertation. Two more papers are included as appendixes in the respective chapters showing previous work in historical seismicity necessary for PSHA and my experience in communicating natural hazards to communities, as a way of reducing the risk via inducing better knowledge in the community and therefore having more capacity to make informed decisions.

## 1.5 References

- Baize, S., L. Audin, T. Winter, A. Alvarado, L. Pilatasig Moreno, M. Taipei, P. Reyes, P. Kauffman, and H. Yepes (2014), Paleoseismology and tectonic geomorphology of the Pallatanga fault (Central Ecuador), a major structure of the South-American crust, *Geomorphology*, 1–15, doi:10.1016/j.geomorph.2014.02.030.
- Baker, J. W. (2008), An introduction to probabilistic seismic hazard analysis (PSHA), *White paper, version, 1*, 72.
- Bernal, Z.R., 1998. Estimación bayesiana del peligro sísmico en el Ecuador Tesis de Matemática. EPN-Quito, 123 p.
- Beauval, C., H. Yepes, W. H. Bakun, J. Egred, A. Alvarado, and J.-C. Singaicho (2010), Locations and magnitudes of historical earthquakes in the Sierra of Ecuador (1587-1996), *Geophysical Journal International*, doi:10.1111/j.1365-246X.2010.04569.x.
- Bilham, R. (2009), The seismic future of cities, *Bull Earthquake Eng*, 7(4), 839–887, doi:10.1007/s10518-009-9147-0.
- Bonilla, L.F. y Ruiz, M.C., 1992, El Peligro Sísmico en el Ecuador, Tesis Ing. Geotécnico, EPN-Quito, 212 p.
- CEC (2001), Requisitos generales de diseño: Peligro sísmico, espectros de diseño y requisitos mínimos de cálculo para diseño sismo-resistente, edited by INEN, *Instituto Ecuatoriano de Normalización*, 1–32.
- CERESIS (Centro Regional de Sismología para América del Sur) (1996) Mapa Probabilístico de Peligro Sísmico de Sudamérica. Compilado por J. C. Castaño y M. H. Millán. Escala 1:5'000.000.

- CERESIS, UNESCO, EPN (1998), El terremoto de Bahía de Caraquez - Ecuador, edited by J. Fernandez and H. Yepes, *Misiones de Reconocimiento - CERESIS*, 1–1.
- Chlieh, M. et al. (2014), Distribution of discrete seismic asperities and aseismic slip along the Ecuadorian megathrust, *Earth and Planetary Science Letters*, 400(C), 292–301, doi:10.1016/j.epsl.2014.05.027.
- Chunga, K. (2010), Terremoti crostali e zonazione sismica dell'Ecuador attraverso l'integrazione dei dati geologici, sismologici e morfostrutturali, *Università degli Studi dell'Insubria Sede di Como Dipartimento di Scienze Chimiche ed Ambientali*, 1–165.
- Cornejo, B., M. Naranjo, and F. Pareja (1999), *Gasto público en servicios sociales básicos en América Latina y el Caribe: análisis desde la perspectiva de la iniciativa 20/20 - Ecuador*, edited by E. Ganuza, A. Leon, and P. S. Fiatt, CEPAL.
- Cornell, C. A. (1968), Engineering seismic risk analysis, *Bulletin of the Seismological Society of America*, 58(5), 1583–1606.
- Dimaté, C., L. Drake, H. Yezpe, L. Ocola, H. Rendon, G. Grünthal, and D. Giardini (1999), Seismic hazard assessment in the Northern Andes (PILOTO Project), *Annali di Geofisica*, 42(6), 1039–1055.
- Douglas, J. (2011), Ground-motion prediction equations 1964–2010, *BRGM Final Report*, 1–446.
- Egüez, A., A. Alvarado, H. Yepes, M. Machette, C. Costa, and R. Dart (2003), Database and Map of Quaternary faults and folds of Ecuador and its offshore regions, *USGS Open file Report 03-289*, 1–77.
- Flores, H. (2014, September 7). 5 puntos hacen vulnerables a las edificaciones. *El Comercio Quito*, p.10.
- Giardini, D. (1999), The global seismic hazard assessment program (GSHAP)-1992/1999, *Annali di Geofisica*, 42(6), 957–974.
- Giesecke, A., A. G. Capera, I. Leschiutta, E. Migliorini, and L. R. Valverde (2004), The CERESIS earthquake catalogue and database of the Andean Region: background, characteristics and examples of use, *Annals of Geophysics*, 47(2-3).
- McGuire, R. K. (1976), FORTRAN computer program for seismic risk analysis, *Open-File Report*.
- NEC (2015), CARGAS SÍSMICAS - DISEÑO SISMO RESISTENTE, *Ministerio de Desarrollo Urbano y Vivienda*, 1–139.
- O'Brien, P., Marc Eberhard, O. Haraldsson, Ayhan Irfanoglu, D. Lattanzi, S. Lauer, Santiago Pujol (2011), Measures of the Seismic Vulnerability of Reinforced Concrete Buildings in Haiti, *Earthquake Spectra*, 27(S1), S373–S386, doi:10.1193/1.3637034.

- Petersen, M. et al. (2008), Documentation for the 2008 update of the United States National Seismic Hazard Maps, *U.S. Geological Survey, Open-file report 2008-1128*, 60 p.
- Petersen, M., K. Haller, C. Mueller, N. Luco, G. P. Hayes, and J. Dewey (2013), *Preliminary Seismic Hazard Model for South America*, edited by CERESIS, CERESIS.
- PREDECAN (2009), *ATLAS de las dinámicas del territorio andino: Población y bienes expuestos a las amenazas naturales*, CAPRADE.
- Quijada, P., E. Gajardo, M. Franke, M. J. Kozuch, J. Grases Galofre, and V. U. de los Andes Departamento de Estructuras (1993), Análisis de amenaza sísmica de Venezuela para el nuevo mapa de zonificación con fines de ingeniería, edited by U. de los Andes, *Memorias : 8 seminario latinoamericano de ingeniería sismo resistente y primeras jornadas andinas de ingeniería estructural*, 92–101.
- Saragoni, R., J. Crempien, and R. Araya (1981), *Características de los movimientos sísmicos fuertes de Chile*, edited by U. de Chile Dpto Ing Civil.
- Schuster, R. L. et al. (1991), The March 5, 1987, Ecuador Earthquakes: Mass Wasting and Socioeconomic Effects, *NATURAL DISASTER STUDIES*, 5, 1–179.
- Shedlock, K. M., and J. G. Tanner (1999), Seismic hazard map of the western hemisphere, *Annali di Geofisica*, 42(6).
- Tanner, J. G., and K. M. Shedlock (2004), Seismic hazard maps of Mexico, the Caribbean, and Central and South America, *Tectonophysics*, 390(1-4), 159–175, doi:10.1016/j.tecto.2004.03.033.
- Youngs, R. R., S. J. Chiou, W. J. Silva, and J. R. Humphrey (1997), Strong Ground Motion Attenuation Relationships for Subduction Zone Earthquakes, *Seismological Research Letters*, 68(1), 58–73, doi:10.1785/gssrl.68.1.58.

## 2 Overview of the papers

### 2.1 The construction of the Ecuadorian earthquake catalog for Probabilistic Seismic Hazard Assessment PSHA

The estimation of probabilistic seismic hazard requires models of occurrence of earthquakes in time, space, and magnitude. These models rely notably on earthquake catalogs covering the longest time period possible [Beauval *et al.*, 2013].

In a high seismicity region, a sound seismic catalog is the most effective way to model all earthquake sources capable of producing damaging ground motions. The catalog should include all the events that have an assigned location and magnitude. From this catalog seismic recurrence models used in PSHA are established. The longer the time span covered by the catalog the more representative of the seismic potential of the region it will be. In the catalog two types of information are combined: the more recent and precise instrumental parametric data and equivalent data derived from historical intensities.

The two publications that deal with the construction of the Ecuadorian earthquake catalog are described in the following paragraphs.

#### *2.1.1 Locations and magnitudes of historical earthquakes in the Sierra of Ecuador (1587–1996) (Appendix 1, Chapter 3)*

By definition, earthquake catalogs are never complete, but in order to expand the time span covered by the catalog beyond the instrumentally recorded seismicity, it is necessary to locate epicenters and assign magnitudes to the pre-instrumental seismicity.

In Ecuador there are around five centuries of registered macroseismic intensities (CERESIS, 1985). Using this information and the IG-EPN archives with historical information generated by J. Egred and collaborators (unpublished IG-EPN internal reports), Beauval, Yepes *et al.* [Beauval *et al.*, 2010] applied the Bakun & Wentworth method [1997] to 25 events from 1587 to 1996. We

obtained 19 new epicentral locations, yielding equivalent moment magnitudes  $M_w$  between 5.0 and 7.6, and their respective uncertainties. All these are crustal events and correspond to the Andean Cordillera. No pre-20th century interface events were re-localized due to a lack of intensity data.

An intensity-magnitude attenuation model was derived and intensity data were inverted in order to obtain the events' most likely epicentral locations. An association between large earthquakes ( $M_w > 6$ ) and strike slip faults of the North Andean Block boundary with stable South America was found, while moderate earthquakes ( $M_w \leq 6$ ) seem to be associated to thrust faults located on the western internal slopes of the Interandean Depression.

By means of the analysis of the macroseismic intensities, the period of completeness of the Ecuadorian earthquake catalog was extended to 1587 for earthquakes larger than  $M_w 7.0$  and to 1860 for earthquakes larger than  $M_w 6.0$ , making it more representative of the seismicity in the Cordilleran region.

### *2.1.2 An Earthquake Catalog for Seismic Hazard Assessment in Ecuador (Chapter 3)*

The seismic catalog for PSHA has to be as complete as possible, unified (i.e. just one entry for each event) and homogeneous (i.e. same type of magnitude for the entire set of events). There is a variety of international catalogs reporting the seismicity in Ecuador since ~1900 from a global seismic networks perspective. From the local perspective, the IG-EPN started to report local earthquakes at the beginning of the 1990's.

In order to produce one single catalog with the aforementioned characteristics, the strengths, weaknesses and uncertainties of these catalogs were analyzed in terms of the geographical coverage, completeness, quality of the reported parameters and reported types of magnitudes. To extract an event and incorporate it in the Ecuadorian catalog as a unique entrance, a prioritizing scheme was developed. The priorities were related to the year of occurrence and geographical location of the event on the one hand, and the type and quality of the reported magnitude on the other. For the homogeneous moment

magnitudes two options were decided: either magnitudes were selected so that a proxy for a moment-magnitude catalog was obtained or they were transformed applying custom regressions developed by comparison of local and international data.

A second effort was also made to complete the historical catalog with those events whose intensity data set did not allow the application of the B&W method used in the 2010 paper [*Beauval et al.*, 2010], but have enough historical information for their parameters to be obtained bearing higher uncertainties. Twelve more historical earthquakes were added to the catalog.

The unified Ecuadorian earthquake catalog 1587–2009 integrates instrumental and historical earthquakes, from magnitude 3 and above. It comprises 10,823 instrumental events plus 32 historical earthquakes. The catalog is much more complete for the Andean region than for the Coast. For the Andes, between latitudes 2.5°S and 1°N, the 500 years of data enable us to derive a recurrence curve for crustal earthquakes with magnitudes 4.0 and above, predicting on average an earthquake with magnitude  $M_w$  6.0 every 10–20 years.

The earthquake catalog is ready for use in seismic hazard studies in Ecuador. Of course, it is intended to evolve as new information emerges, especially when the country has established a nation-wide, modern, dense broadband seismic network after 2009, the final year covered by the catalog.

## 2.2 Definition of the seismic source zones SSZ for PSHA

Seismic sources could be defined either as distributed seismicity or as fault sources. Distributed seismicity sources are geometric volumes where seismicity may be considered uniformly distributed in space and stationary in time, rendering their seismic potential as homogeneous. They encompass seismogenic structures with similar tectonic behavior [*Meletti et al.*, 2008; *Baize et al.*, 2013]. On the other hand, the fault source model requires the geometry and slip rates of mapped fault sources in order to develop a single characteristic

earthquake (magnitude and frequency) for each source [Stirling *et al.*, 2012]. The size, geometry, and slip rates of individual faults or fault systems are poorly known in Ecuador. Just a few segments have been characterized with enough detail for them to be modeled as such. The Quito fault system is one example of that and we will show the shortcomings and uncertainties found during the exercise of estimating the PSH in Quito using the modeled fault as a fault source in Chapter 5.

Consequently, a distributed seismicity seismic source zones model has been constructed for Ecuador. The proposed model is based on a new view of the geodynamics and seismotectonics of the country that reflects some of my own old-dated ideas and the current knowledge in these matters, highlighted by the greatly improved seismic catalog described in Chapter 3.

### *2.2.1 A new view of Ecuador's geodynamic context and its implications for seismogenic sources definition and seismic hazard assessment (Chapter 4)*

This is a review paper that has been divided in two parts. The first one reviews the geodynamics and seismotectonics of Ecuador and identifies some key elements to explain the earthquake generation patterns, while the second deals with the construction of the new seismic source model using the new interpretation. The following points highlight the main findings:

- The subduction of the oceanic Nazca plate underneath the continent is the major geodynamic engine that controls the generation of earthquakes in Ecuador. The Nazca plate shows a complex structure at equatorial latitudes since it is a patchwork of oceanic crusts with different histories consolidated in a single plate nowadays. Each assimilated portion influences the geodynamic behavior differently.
- The Grijalva paleo-rift –GPR– (Plate A) is an important feature on the oceanic plate marking a sharp age and rheology contrast in the plate. GPR is actually separating to plates of different origin: To the south the older Farallon plate and to the north the younger Nazca plate. On

top of the younger portion, the prominent Carnegie ridge has developed.

- The subduction interface zone shows a different seismic behavior to both sides of GPR. Along the northern segments the most powerful earthquakes ( $M_w \geq 8$ ) in Ecuadorian history have occurred and the seismic coupling is high [*Chlieh et al.*, 2014]. The great earthquakes have not ruptured through the Carnegie ridge. On the contrary, the interface the south of GPR is known as a seismic gap [*Nishenko*, 1991], but in fact it has generated  $M_w \sim 7.6$  tsunamigenic earthquakes. The seismic coupling south of GPR is very weak or non-existent [*Nocquet et al.*, 2014]. Although there also are  $M_w \sim 7.5$  earthquakes in the transition zone from the northern to the southern segments around GPR, it is not clear whether or not they belong to the interface.
- The vast majority of intraplate earthquakes are generated inside the Farallon domain of the subducted plate. There is a conspicuous seismic cluster at the northeastern edge of the dipping Farallon plate related to a sharp contortion of this edge. On the contrary, the younger Nazca portion of the subducted plate seems to be too hot to generate sizeable intraplate events at least up to  $2^\circ\text{N}$ .
- The convex curvature of the continental margin in Ecuador and the oblique convergence between Nazca plate and the continent are responsible for partitioning the shear stresses at the interface. This partitioning and the high coupling along the northern Ecuadorian interface are responsible for the block tectonics found in northwestern South America.
- Due to this block tectonics, the North Andean Block is moving to the northeast with respect to stable South America. The major crustal earthquakes in Ecuador's history are located along the block's boundary faults. There is also deformation inside the NAB which may also suggest a slivers tectonics [*Nocquet et al.*, 2014]. In any case important historical earthquakes are also related to active faulting to

the west of the NAB's boundary along the western margin of the Interandean Depression (Plate A).

- With all these elements in mind a total of 19 distributed seismicity source zones have been modeled for PSHA purposes in Ecuador: one outer-trench, three interface, six intraplate and nine crustal. Each is a finite, regular volume and each has a homogeneous seismogenic potential, containing  $M_w \geq 5$  cataloged events.

The next step is to model the seismic recurrence in each source zone and calculate a new generation of probabilistic seismic hazard maps for Ecuador, updating the latest 2011 exercise.

## 2.3 Application study using the new information

As an application of both, the Ecuadorian earthquake catalog and earlier versions of the SSZ model [Alvarado, 2012] from where the seismic parameters for PSHA were obtained, a study to estimate PSH in Quito was conducted. The objective was to identify the uncertainties in the characterization of the seismic sources, uncertainties in the recurrence of earthquakes expected in the sources and uncertainties on the ground motions that these earthquakes may produce. The OpenQuake engine (Global Earthquake Model, [www.globalquakemodel.org/](http://www.globalquakemodel.org/)) was used for all PSH calculations. The focus was on hazard estimate at 475 years return period, corresponding to a 10% probability of exceedance over 50 years. The approach was first to identify the controlling conditions, and then to evaluate the uncertainties on the parameters of each condition and the corresponding impact on the hazard levels.

### 2.3.1 Probabilistic Seismic Hazard Assessment in Quito, Estimates and Uncertainties (Chapter 5)

The city and its suburbs are built along a piggy-back basin on the hanging wall of a reverse fault system that has been recognized as seismically active in previous studies. The Quito fault is approximately 60 km long and as such is capable of producing large earthquakes. There is a recent GPS survey

[Alvarado *et al.*, 2014] that shows a horizontal movement of the hanging wall of  $\sim 4$  mm/a. No large earthquake has released the stored seismic deformation for close to 500 years that the city's history covers, although one major event was identified between the 10<sup>th</sup> and the 16<sup>th</sup> centuries that could have ruptured the entire Quito fault reaching a magnitude 6.5–7.0.

On the basis of seismological, geodetic and tectonic data several combinations of models have been tested.

In regard to the source zone definition and using the catalog, our study shows that, on the one hand, for 475 years return period the seismic hazard is controlled by the crustal SSZ in which Quito is located. The hazard is governed by the short distance from the fault source to the city and the contribution of the interface sources is negligible. On the other hand, the choice of the GMPE selected for this zone also has a clear influence in the results. Both factors, source definition and their modeled seismic parameters and GMPEs, equally control the hazard variability (20%-35% and 30%-45% respectively) for all spectral periods up to 0.5s.

Considering slip rates inferred from geodetic measurements across the Quito fault system to calculate the earthquake recurrence, two assumptions were made: (1) most of the deformation released in earthquakes and, (2) only 50% of the deformation occurs seismically (partially locked fault). The partially locked fault calculations are close to the mean acceleration level predicted by the catalog's earthquake recurrence. If the fault is highly locked, the mean predicted value in Quito increases by 40%.

If the Quito tectonic structure is modeled as a fault source where the occurrence of magnitudes 6–7 are restricted to the fault, and the hanging wall effect is included in the choice of the GMPEs, the hazard increases by 20%–40% at sites located above the fault plane.

With this in mind, the paper proposes uniform hazard spectra for a generic rock site in Quito, which has a mean value around 0.4g for the PGA at 475 years. Variability related to uncertainties and the influence of site effects need to

be further taken into account. These results are in accordance with the acceleration level recently adopted by the new Ecuadorian Building Code [NEC, 2015].

## 2.4 References

- Alvarado, A. (2012), *Néotectonique et cinématique de la déformation continentale en Équateur*, Thèse, Université de Grenoble, Grenoble.
- Alvarado, A., L. Audin, J.-M. Nocquet, S. Lagreulet, M. Segovia, Y. Font, G. Lamarque, H. Yepes, P. Mothes, and F. Rolandone (2014), Active tectonics in Quito, Ecuador, assessed by geomorphological studies, GPS data, and crustal seismicity, *tectonics*, 33(2), 67–83, doi:10.1002/(ISSN)1944-9194.
- Baize, S., E. M. Cushing, F. Lemeille, and H. Jomard (2013), Updated seismotectonic zoning scheme of Metropolitan France, with reference to geologic and seismotectonic data, *Bulletin de la Societe Geologique de France*, 184(3), 225–259.
- Bakun, W. H., and C. M. Wentworth (1997), Estimating earthquake location and magnitude from seismic intensity data, *Bulletin of the Seismological Society of America*, 87(6), 1502–1521.
- Beauval, C., H. Yepes, P. Palacios, M. Segovia, A. Alvarado, Y. Font, J. Aguilar, L. Troncoso, and S. Vaca (2013), An Earthquake Catalog for Seismic Hazard Assessment in Ecuador, *Bulletin of the Seismological Society of America*, 103(2A), 773–786, doi:10.1785/0120120270.
- Beauval, C., H. Yepes, W. H. Bakun, J. Egred, A. Alvarado, and J.-C. Singaicho (2010), Locations and magnitudes of historical earthquakes in the Sierra of Ecuador (1587-1996), *Geophysical Journal International*, doi:10.1111/j.1365-246X.2010.04569.x.
- CERESIS (Centro Regional de Sismología para América del Sur) (1985) Catálogo de terremotos para América del Sur: Datos de hipocentros e intensidades. Programa para la Mitigación de los Efectos de los Terremotos en la Región Andina, SISRA, Volumen 6: Ecuador. Lima, Perú.
- Chlieh, M. et al. (2014), Distribution of discrete seismic asperities and aseismic slip along the Ecuadorian megathrust, *Earth and Planetary Science Letters*, 400(C), 292–301, doi:10.1016/j.epsl.2014.05.027.
- Meletti, C., F. Galadini, G. Valensise, M. Stucchi, R. Basili, S. Barba, G. Vannucci, and E. Boschi (2008), A seismic source zone model for the seismic hazard assessment of the Italian territory, *Tectonophysics*, 450(1-4), 85–108, doi:10.1016/j.tecto.2008.01.003.
- NEC (2015), CARGAS SÍSMICAS - DISEÑO SISMO RESISTENTE, *Ministerio de*

*Desarrollo Urbano y Vivienda*, 1–139.

Nishenko, S. P. (1991), Circum-Pacific seismic potential: 1989–1999, *Pure Appl. Geophys.*, 135(2), 169–259.

Nocquet, J. M. et al. (2014), Motion of continental slivers and creeping subduction in the northern Andes, *Nature Geosci.*, (7), 287–291, doi:DOI: 10.1038/NGEO2099.

Stirling, M. et al. (2012), National Seismic Hazard Model for New Zealand: 2010 Update, *Bulletin of the Seismological Society of America*, 102(4), 1514–1542, doi:10.1785/0120110170.

# 3 An Earthquake Catalog for Seismic Hazard Assessment in Ecuador

Bulletin of the Seismological Society of America, Vol. 103, No. 2A, pp. 773–786, April 2013, doi: 10.1785/0120120270

## An Earthquake Catalog for Seismic Hazard Assessment in Ecuador

by Céline Beauval, Hugo Yepes, Pablo Palacios, Monica Segovia, Alexandra Alvarado, Yvonne Font, Jorge Aguilar, Liliana Troncoso, and Sandro Vaca

**Abstract** Building a unified and homogeneous earthquake catalog is a preliminary step for estimating probabilistic seismic hazard in a country. Ecuador, a territory of  $\sim 600 \text{ km} \times 500 \text{ km}$ , is characterized by an active seismicity, both in the shallow crust and in the subduction zone. Several international and local earthquake catalogs are available, covering different time and spatial windows, characterized by different magnitude types and uncertainties. After a careful analysis of each catalog, in particular for completeness and uncertainty levels, we propose a priority scheme for merging the instrumental catalogs. Moreover, several historical earthquakes are analyzed to estimate epicentral location and magnitude, completing the solutions obtained in a previous publication. Once the historical earthquakes are appended to the instrumental catalog, the resulting catalog covers five centuries in the Cordillera region. Next, homogenization of magnitudes and removal of aftershocks is performed; different options are studied and the impact on the recurrence curve is evaluated. For the Cordillera region within  $-2.5^\circ$  and  $1^\circ$  latitude, the average occurrence of an earthquake with  $M_w \geq 6.0$  is 10–20 years based on the historical catalog.

### Introduction

Ecuador is a seismically active country, with destructive earthquakes occurring both along the subduction zone and in the central part of the territory, in the shallow crust (see Fig. 1). The Geophysical Institute in Quito, at the Escuela Politécnica Nacional (IGEPN), is in charge of estimating the seismic hazard over the national territory. The present study is part of a broader program aimed at evaluating the probabilistic seismic hazard and producing the next seismic building code for the country. The estimation of probabilistic seismic hazard requires models of occurrence of earthquakes in time, space, and magnitude (see, e.g., Beauval and Scotti, 2003, 2004). These models rely notably on earthquake catalogs covering the longest time period possible (e.g., Braunmiller *et al.*, 2005; Grunewald and Stein, 2006; or Yadav *et al.*, 2010). In Ecuador, seismic history extends over five centuries in the Cordillera, and roughly over one century on the Coastal region (Fig. 2). The first entry in the historical database corresponds to the year 1541, shortly after the arrival of the Spaniards. Until the end of the nineteenth century, the historical information mostly describes effects of earthquakes in the Cordillera. The first coastal event for which several intensities are reported is in 1896 (Fig. 2).

Since the beginning of the 1990s, there have been a few studies aimed at developing earthquake catalogs at the scale of the Northern Andes (e.g., Dimate *et al.*, 1999; Giesecke *et al.*, 2004). The objective of this new study is to focus on Ecuador and the surrounding area, to take into account the revised IGEPN local catalog, the recently improved characterization

of historical earthquakes (Beauval *et al.*, 2010), and the overall improved localization of earthquakes at the international scale (e.g., Engdhal and Villaseñor, 2002; and the updated “EHB” catalog, ISC, 2010). The spatial window considered here covers a region that extends in latitude from  $-7^\circ$  to  $+4^\circ$  and in longitude from  $-84^\circ$  to  $-74^\circ$  (roughly  $1100 \times 1000 \text{ km}$ ; Fig. 1). This spatial window encloses all seismic sources able to generate significant ground motions in the Ecuadorian territory. In the first part of this paper we detail the process of building the earthquake catalog: analysis of the available information sources, schemes to merge the different instrumental catalogs, tests to homogenize the magnitude, and extension of the historical catalog with new analysis of several past earthquakes. In the second part, we focus on the Cordillera region. The analysis of the unified catalog, completeness issues, and removal of short-term clustered events enable us to derive frequency–magnitude distributions. Recurrence times for significant earthquakes are determined for the Cordillera region.

### A Homogeneous Earthquake Catalog

#### Instrumental Earthquake Catalogs

Ecuador’s seismicity can be studied through international and local catalogs (Tables 1 and 2; Fig. 2). The Ecuadorian seismic network (RENSIG) is run by the Geophysical Institute in Quito. The local catalog (IGEPN) provides earthquake solutions for the time period 1990–present. The reported

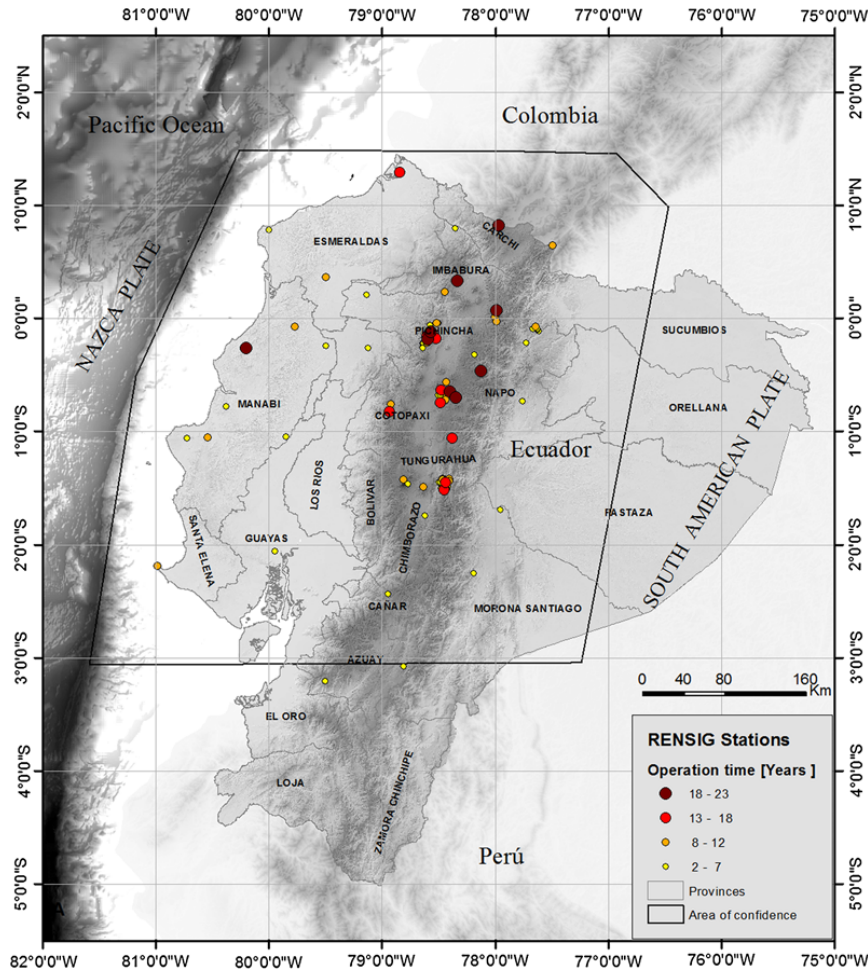


**Figure 1.** IGEPN seismological network, circles. Radius of circle: operation times of stations. Area of confidence for the IGEPN network, polygon (see text). Province names are indicated. The color version of this figure is available only in the electronic edition.

magnitude is duration magnitude ( $M_D$ ) calculated on the Coda waves (Palacios and Yepes, 2011). The RENSIG stations guarantee reliable solutions inside a spatial window that encompasses the area identified by the polygon in Figure 1. Within this zone, the network exhaustively records events with magnitudes down to  $\sim M_D = 3.5$ . As Font *et al.* (2013) have been working on improving the locations of the IGEPN events, their locations are preferred to IGEPN locations when they exist. For the rest of the country, southern Ecuador and the Amazonia to the East, the IGEPN solutions are not reliable and are not included in the catalog. In these zones, the international catalogs National Earthquake Information Center Preliminary Determination of Epicenters (NEIC-PDE from the U.S. Geological Survey) and International Seismological Centre (ISC) provide more accurate solutions than the RENSIG, though with a higher completeness

magnitude (body-wave magnitude,  $m_b = 4.5$ ). Note that RENSIG has evolved considerably since 2010, as more stations have been installed and the network now homogeneously covers the territory. The local catalog's completeness in space and in magnitude will be greatly improved over the next years.

The ISC catalog reports solutions beginning in 1900 (International Seismological Summary [ISS]) and its own solutions since 1964; the NEIC-PDE catalog is providing solutions for earthquakes beginning in 1963 (see, e.g., Johnston and Halchuk, 1993, who provide some useful information on the history of these catalogs). Moreover, three other catalogs are worth integrating into our study, as they contain events with magnitudes usually larger than  $\sim 5.5$ . The first one is the Centennial catalog compiled by Engdahl and Villaseñor (2002) covering the twentieth century, for which earthquakes are relocated using the Engdahl *et al.* (1998) method. They

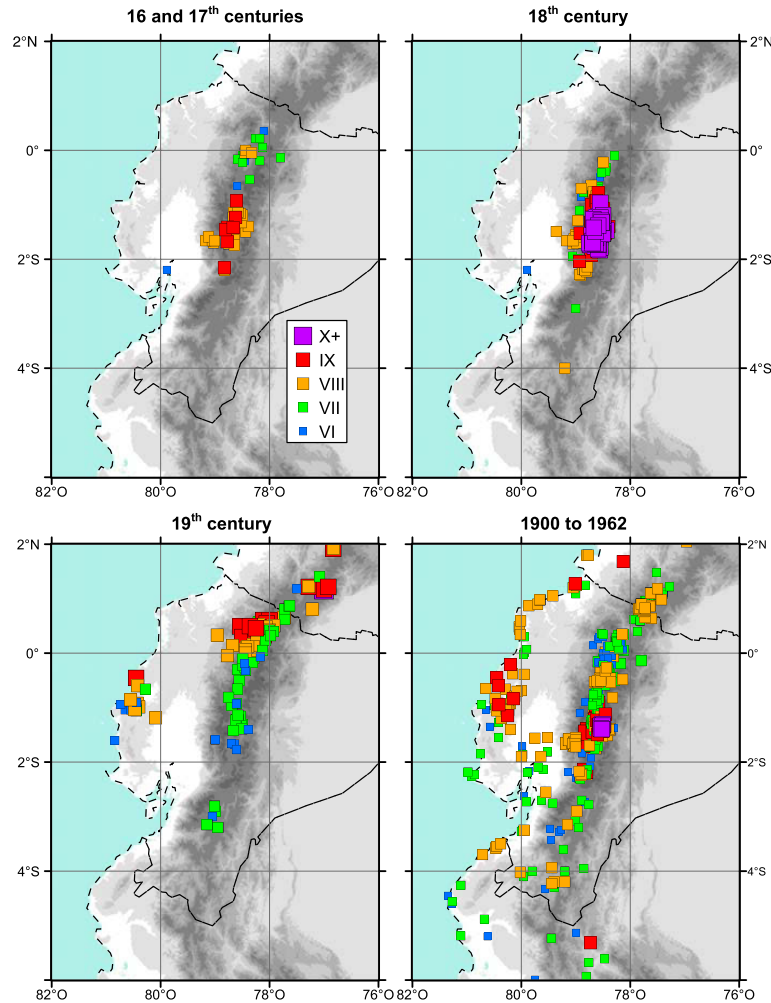


**Figure 2.** Intensity database for Ecuador (Egred, 2009), containing events with at least one intensity VI reported. All individual intensity assignments are plotted on the maps, considering all earthquakes reported in the database. First information for coastal events at the end of the nineteenth century. The color version of this figure is available only in the electronic edition.

report existing magnitude estimates (with a priority order, see p. 667 of their paper). The second catalog is the EHB-ISC catalog (2009), a refined version of the ISC catalog. From 1960 until 2009, Engdahl *et al.*'s (1998) algorithm has been used to significantly improve routine hypocenter determinations made by the ISS, ISC, and PDE. Last, another international catalog worth considering is the Global Centroid Moment Tensor catalog (GCMT; Ekström *et al.*, 2012), which since 1976 has been reporting moment magnitude ( $M_w$ ) for some moderate-to-large events all over the world. The time periods covered by each catalog and the magnitude types reported are described in Tables 1 and 2 and Figure 3. Note that for four major subduction earthquakes, the 1906 ( $M_w$  8.8), 1942 ( $M_w$  7.8), 1958 ( $M_w$  7.8), and 1979 ( $M_w$  8.1) events,

with fault planes extending over hundreds of kilometers, the epicenter coordinates are extracted from specific studies (for the 1906 event: Swenson and Beck, 1996; for the other three events: Mendoza and Dewey, 1984).

#### Merging Different Instrumental Earthquake Catalogs

The first step toward building a unique and homogeneous catalog for the country consists of identifying the same events in the different catalogs. This task can be difficult as there might be uncertainties or lack of entries in the time, magnitude, coordinates, and depth of the solutions. Several tests were performed, which are not detailed here, to understand the uncertainties associated to each catalog and to produce a master catalog with all available solutions

**Table 1**  
Earthquake Catalogs Used for Magnitude Selection in Descending Priority Order

Catalog	Covered Time Period	Magnitude Type
GCMT/HRV	1976–2009	$M_w$
Centennial	1900–2001	Unknown, $m_B$ , $m_b$ , $M_S$ , $M_w$
ISC, determined by BRK, PAS	1900–1963	$M_S$ and unknown
ISC, determined by ISC	1964–2009	$m_b$ from 1964 $M_S$ from 1978
NEIC, determined by USGS-NEIC	1963–2010	$m_b$ from 1963 $M_S$ from 1968 $M_w$ from 1982
IGEPN	1997–2009	$M_D$

**Table 2**  
Earthquake Catalogs Used for Location Selection (see Fig. 3)

Catalog	Time Period	Spatial Area of Confidence
IGEPN-FONT	1994–2007	See Figure 1
IGEPN	1993–2009	See Figure 1
EHB (in the ISC)	1960–2007	The whole window
Centennial	1900–2001	The whole window
ISC, determined by ISS/GUTE	1900–1962	The whole window
ISC, determined by ISC	1964–2009	The whole window
NEIC, determined by USGS-NEIC	1963–2009	The whole window

The spatial window considered is in latitude  $-7^\circ$  to  $4.0^\circ$ , in longitude  $-84^\circ$  to  $-74^\circ$ .

listed per event. All events reported by different catalogs, separated by  $<2$  minutes in time and 100 km in distance, have been manually checked. International catalogs are used only for magnitudes 4.0 and above, which limits the number of events to be checked manually and the problems of mistakenly associating earthquakes. Then, a hierarchy is required for the selection of the location and for the selection of the magnitude for each event in the master catalog (Fig. 3).

This study develops a proxy for a moment-magnitude catalog of earthquakes in which the selection of the magnitude is as follows, by decreasing priority order:  $M_w > M_S > m_b > M_D$  (Table 1, Fig. 3). Inside the spatial window considered, only 242 events of the master catalog have moment magnitude directly calculated by the GCMT/HRV. From 1964 on, most events with a magnitude  $\geq 4.5$  have  $m_b$  (body-wave magnitude) determined by the ISC. A surface-wave magnitude  $M_S$  is selected prior to  $m_b$  whenever  $M_S$  exists and is  $> 5.5$ , as  $m_b$  saturates around 5.8–6.0 (e.g., Utsu, 2002). The magnitude  $M_D$  calculated by the IGEPN is based on an equation calibrated on  $m_b$ . Note that  $M_D$  is not reliable before 1997 (Palacios and Yepes, 2011); therefore, events occurring before that year described by a unique magnitude  $M_D$  are not taken into account.

The selection of the preferred location depends on the location of the event. If the earthquake is located inside the area

of confidence of the RENSIG network (Fig. 1), the IGEPN/FONT solution is considered the best solution, the second-best solution being the original IGEPN one. Even though RENSIG has been running since 1990, it was not until 1993 that hypocentral solutions were calculated using verifiable standards. If the earthquake falls outside this area of confidence, or if the earthquake occurred before 1993, the location solution is selected from solutions provided by international networks. In this case, the priority order that has been used is EHB  $>$  Centennial  $>$  ISC  $>$  NEIC (Table 2, Fig. 3). The EHB solutions (ISC, 2010) are the most recent solutions obtained applying the Engdhal *et al.* (1998) relocation technique. Moreover, as the ISC usually uses the greatest number of stations, its location is preferred over the NEIC solution.

Earthquakes in the catalog have minimum magnitudes greater or equal to 3.0 ( $M_D$ ), as the completeness of smaller magnitudes is highly space dependent, and thus they cannot be used in the development of recurrence models. Events with magnitudes lower than  $m_b = 4$  outside the RENSIG window of confidence are likewise excluded. Neither the RENSIG network nor the international networks are able to determine reliable solutions for such events. The final catalog, containing for each event the best solutions in magnitude and in location, has 10,823 events. As indicated in Table 3, the majority of these events are described by an  $M_D$  (7541). This proportion drops if considering higher minimum magnitude threshold (165 events out of 3139 for  $M4+$ , and 10 out of 1639 for  $M4.5+$ ). Approximately 70% of the earthquakes with  $M \geq 4$  are described by an  $m_b$  as calculated by the ISC.

#### Homogenization of Magnitudes to Moment Magnitude

The entire set of earthquakes in the catalog must be characterized by  $M_w$  or an equivalent  $M_w$ , as the recent ground-motion prediction equations are in terms of  $M_w$ . To homogenize magnitude in a catalog, different techniques may be considered. The obtained catalog contains 68 events for the period prior to 1963, described with varied magnitude types (unknown,  $m_B$ ,  $M_S$ ,  $M_w$ ) and authors (see Engdhal and Villaseñor, 2002). Using the Centennial catalog, Engdhal and Villaseñor (2002) conclude that magnitude estimates listed by Abe (1981, 1984; ABE  $M_S$ ) and by Pacheco and Sykes (1992; P&S  $M_w$ ) are consistent with GCMT/Harvard  $M_w$  estimates. Furthermore, they demonstrate that magnitudes reported by Gutenberg and Richter (1954, G&R), Rothé (1969, ROTHE), and Pasadena (PAS) before 1960, are systematically larger than Abe (1981)  $M_S$  by 0.2 magnitude units on average. Thus, a 0.2 magnitude unit reduction is applied on the magnitudes with sources G&R, ROTHE, and PAS of our catalog.

The magnitudes of earthquakes belonging to the more recent part of the catalog, from 1963 on are (1) body-wave magnitude  $m_b$  calculated by either the ISC or the NEIC-PDE, (2) duration magnitude  $M_D$  estimated by the IGEPN, (3) surface-wave magnitudes  $M_S$ , calculated by either the ISC or

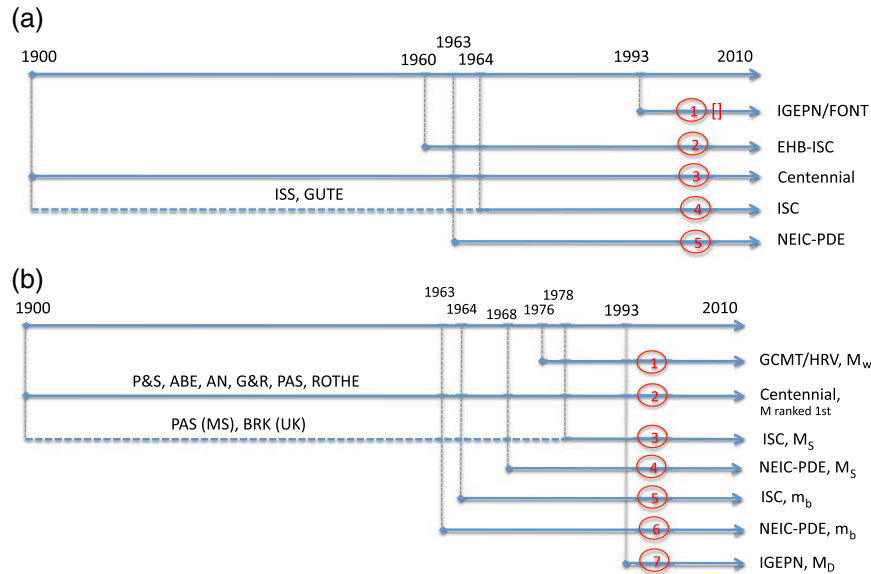


**Figure 3.** (a) Prioritized list for assigning the preferred location for an event of the master catalog. Time periods covered by each catalog are indicated. The IGEPN/FONT is the only catalog used on a restricted spatial window (see Fig. 1). (b) Prioritized list for assigning the preferred magnitude. Magnitude types are specified. See the text for abbreviations. Note: if the magnitude reported in the Centennial catalog has been calculated by the ISC, it is taken directly from the ISC catalog. The color version of this figure is available only in the electronic edition.

the NEIC-PDE, and (4) moment magnitude  $M_w$  determined by GCMT/Harvard. The data used to establish an equation of magnitude conversion usually show that dispersion can be large (e.g., Scordilis, 2006) and that applying an equation may have a great impact on a catalog. Our practice in the current work is to use a conversion equation only when it is considered mandatory. Among others, Utsu (2002) has shown that magnitudes  $m_b$  and  $M_S$  can be considered approximately equivalent to  $M_w$  for magnitudes  $m_b$  up to 6.0 and magnitudes  $M_S$  up to 8.0, respectively (fig. 1 in Utsu, 2002). At first, we decide to use magnitudes  $m_b$  and  $M_S$  as surrogates for  $M_w$  in the appropriate magnitude ranges.

For earthquakes with low magnitudes, usually only a local  $M_D$  is available. The  $M_D$  is calculated using an equation calibrated on magnitudes  $m_b$  (Palacios and Yepes, 2011). In Figure 4, the  $m_{bISC}$  magnitude is plotted against the corresponding  $M_D$ , for all events described by both magnitude types.  $M_D$  shows to be on average equivalent to  $m_{bISC}$ , with some dispersion. Plotting the difference between both

magnitude estimates versus time (Fig. 5), the difference proves to be centered on zero and rather stable with time. Therefore, we also consider  $M_D$  to be a reasonable surrogate for  $M_w$ . This option is called the surrogate option.

A second option consists of applying empirical conversion relationships. For this purpose, the relations between different magnitude types in the region of interest need to be studied. The relations between magnitudes  $m_{bISC}$  and  $m_{bNEIC}$ , and between  $m_{bISC}$  and  $M_{wGCMT}$ , must be analyzed (Fig. 6). We show that  $m_{bISC}$  is approximately equivalent to  $m_{bNEIC}$  (using 2218 events in the spatial window considered). Scordilis (2006), based on worldwide data, came to the same conclusion. Furthermore, we propose the following relation between magnitudes  $m_{bISC}$  and  $M_{wGCMT}$  (valid for the interval 4.5–6 in the considered spatial window; Fig. 6):

$$M_{wGCMT} = 0.93m_{bISC} + 0.6. \tag{1}$$

This equation is close to the equation derived by Scordilis (2006), using data on a global scale ( $M_{wGCMT} = 0.85$

**Table 3**  
Number of Earthquakes in the Final Unified Instrumental Catalog (Surrogate Option)

Number of Events 1901–2009	Number of Earthquakes in the Final Unified Instrumental Catalog (Surrogate Option)					
	In Total	With $M_D$	With $m_b$ (ISC)	With $m_b$ (NEIC)	With $M_S$ (ISC or NEIC)	With $M_w$ (GCMT)
$M3+$	10,823	7541	2580	365	16	242
$M4+$	3139	165	2296	343	14	242
$M4.5+$	1639	10	1160	135	13	242

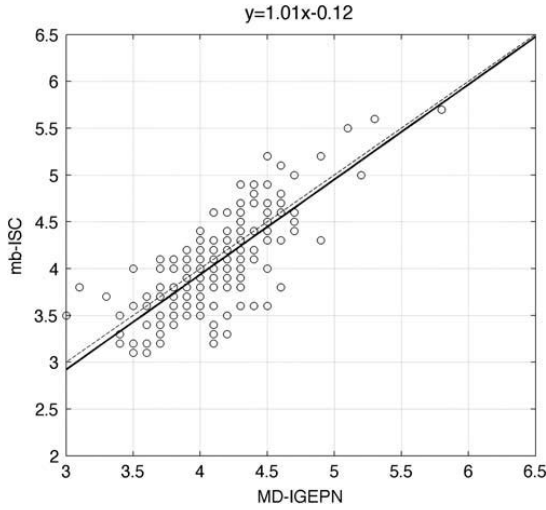


**Figure 4.** Correlation between  $m_b$  (ISC) and  $M_D$  (IGEPN): from 201 earthquakes described by both magnitudes types ( $M_D$  [IGEPN]  $\geq 3$  and  $m_b$  [ISC]  $\leq 5.8$ ), in the spatial window with latitudes from  $-3^\circ$  to  $1^\circ$  and with longitudes from  $-80^\circ$  to  $-77.5^\circ$ .

$m_{b_{ISC/NEIC}} + 1.03$ ; see p. 231, Scordilis, 2006). For the homogenized catalog option, all  $m_b$  as well as local  $M_D$  are converted into an equivalent  $M_w$  using equation (1). The equation is valid only on the magnitude interval of the generating data set, that is to say, for magnitudes  $m_b$  above 4.5 (Fig. 6). Applying the equation to the whole catalog, the equation is extrapolated toward lower magnitudes (down to  $M_D$  3.0). Magnitudes concerned are  $M_D$  between 3.0 and 4.5, resulting in  $M_w$  between 3.4 and 4.8. Moreover, to check the dependence of equation (1) with the depth of earthquakes, two equations were derived separately considering events with depths below and above 40 km (respectively, 107 and 103 events). The equations obtained were close to

equation (1), and we decided not to include a depth dependence in this conversion equation.

Uncertainties and hypothesis underlie both options of building the final catalog. In the section on the [Recurrence Times of Earthquakes in the Cordillera](#), we illustrate the impact on the seismicity rates of choosing one option or the other.

#### The Historical Catalog

In a previous work, Beauval *et al.* (2010) analyzed the intensity database of Egred (2009) and derived locations and magnitudes for nineteen historical earthquakes (1587–1976,  $5.0 \leq M_w \leq 7.6$ ; tables 4 and 5 in Beauval *et al.*, 2010). The Bakun and Wentworth (1997; B&W) methodology was applied to provide locations and magnitudes with associated uncertainties. Many events in the intensity database were left aside, as their intensity data sets did not allow the application of the B&W method. These data sets are either too small or are made of only one or two intensity degrees. In the present study, the earthquake catalog is built for seismic hazard purposes, and it must be as complete as possible. These earthquakes must be analyzed, and ways to evaluate potential locations and magnitudes are needed. These solutions will bear large uncertainties that must be evaluated. Note that aftershocks are not taken into account (e.g., the 27 December 1926 event, which is an aftershock of the 18 December 1926 event on the El Angel–Guachucal fault system at the Colombian border).

For each of the earthquakes listed in Table 4, the distribution of the intensities in space has been checked and the potential responsible fault has been identified based on tectonic arguments (Alvarado, 2012). The preferred epicentral location is selected on the fault. The magnitudes corresponding to different locations on the fault are obtained by simply calculating the mean value of all magnitude values inferred from the individual intensity assignments (as done in the B&W method; see equation 3 in Beauval *et al.*, 2010).

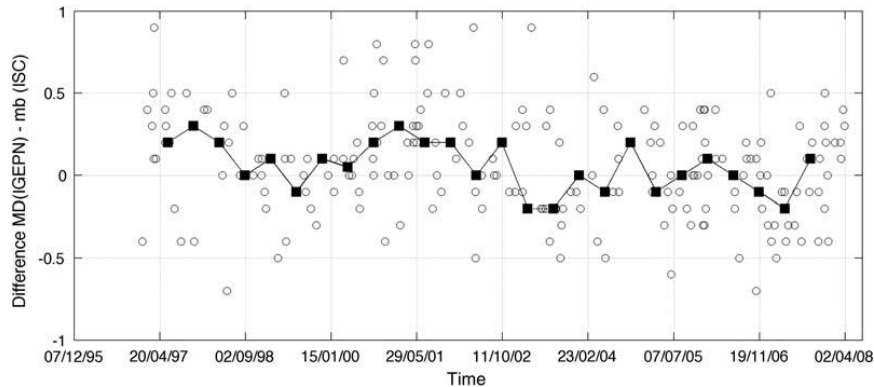


**Figure 5.** Differences between  $M_D$  calculated by the IGEPN, and  $m_b$  calculated by the ISC, for all earthquakes with  $M_D$  (IGEPN)  $\geq 3$  and  $m_b$  (ISC)  $\leq 5.8$  described by both magnitudes types, in the spatial window with latitudes from  $-3^\circ$  to  $1^\circ$  and with longitudes from  $-80^\circ$  to  $-77.5^\circ$ . Differences are plotted against time to check the stability of the duration magnitude determination with time. Mean differences calculated in sliding time windows, squares.

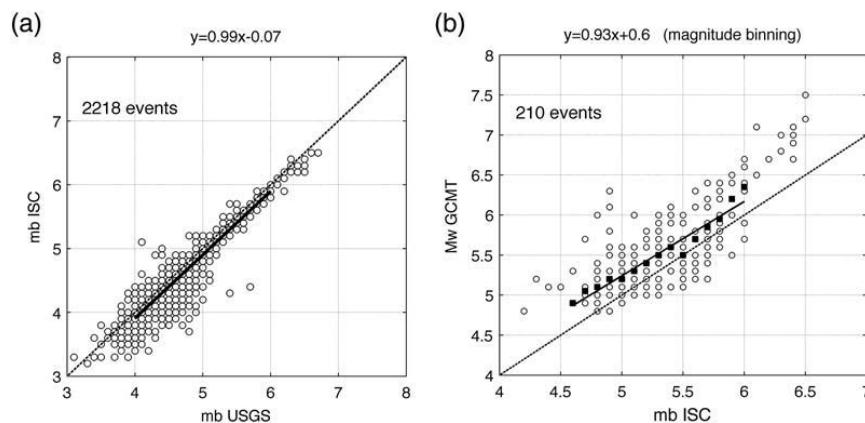


**Figure 6.** (a) Correlation between  $m_b$  (ISC) and  $m_b$  (NEIC/USGS), considering all earthquakes described by both magnitude types in the spatial window within latitudes from  $-6^\circ$  to  $+3.0^\circ$  and longitudes from  $-83^\circ$  to  $-75^\circ$ . The thick segment is the conversion equation obtained from  $4 < m_b(\text{NEIC}) < 6$ . (b) Correlation between  $M_w$  (GCMT) and  $m_b$  (ISC), considering all earthquakes in the magnitude range  $[4.6; 6.0]$ , in the spatial window with latitude  $-6^\circ$  to  $+3^\circ$ , longitude  $-83^\circ$  to  $-75^\circ$ . The regression is performed after applying a magnitude binning (0.1-unit  $m_b$ -bins).

Magnitudes from individual intensities are estimated using the attenuation equation established for the Cordillera region in Beauval *et al.* (2010; equation 2). In the B&W technique, the uncertainty in the magnitude and location estimates is inferred from bootstrapping on the intensity data set. The data sets considered here are very small, and the bootstrapping technique would not give meaningful results.

We adopt another strategy for taking into account the uncertainty on the intensity data set. For previous centuries, when all structures were made of adobe, there has always been doubt of assigned intensities higher than VIII, as intensity descriptions may “saturate” at VIII. In the Andes, all colonial structures such as churches and towers were built either with adobe bricks, mud walls, or stones, with heavy tile roofs. These are vulnerability type A structures in the EMS-98 intensity scale (Grünthal, 1998). Grade 4 (very severe) or grade 5 (total destruction) damages in type A structures should be described with intensity VIII. Before detailed intensity descriptions in scales like EMS-98, widespread destruction during colonial earthquakes has been related to higher intensities. In Beauval *et al.* (2010), tests have been led for various events to check that the highest intensity degrees were not biasing the results. Considering the present earthquakes with much smaller data sets, where only upper intensity degrees are available, such tests cannot be done. The strategy we adopt for taking into account the uncertainty on the available intensity sample is as follows: two calculations are performed, one based on the original intensity set, and the other one on a data set made of these intensities decreased by one degree. The ranges obtained for the magnitude are large (Table 4), but we believe that they are representative of the true uncertainty. Solutions are obtained for thirteen earthquakes located in the Cordillera, from 1645 until 1953, with magnitude estimates ranging from 5.7 to 7.6.

To further improve the magnitude and location estimates for these earthquakes, a thorough historical work will be required, which includes reviewing the archives for more information. Around 20 earthquakes with maximum intensity VII or VIII in the intensity database are still not included (e.g., in 1541, 1557, 1575...). They are described by less than five intensities, and there is currently not enough information to propose a responsible fault and derive earthquake parameters. Finally, some work is required in the future to also provide solutions for the two historical earthquakes that affected the coast (3 May 1896 and 17 April 1898, Manabí province).

#### Final Unified Earthquake Catalog

The unified earthquake catalog 1587–2009 integrates instrumental and historical earthquakes, from magnitude 3 and above. It comprises 10,823 instrumental events plus 32 historical earthquakes. As expected, the seismicity distribution reflects the two major tectonic features in the country: the subduction of the Nazca plate and the active crustal deformation occurring in the Andean Cordillera (Fig. 7).

Regarding the subduction zone, the largest earthquakes are concentrated north of  $\sim 1^\circ\text{S}$ . The two  $M_w > 8$  earthquakes present in the catalog are related to this segment of the subduction zone. In this zone, the seismogenic part of the interface extends over 120 km from the trench, penetrating  $\sim 50$  km inland. Almost no earthquakes deeper than 120 km are found farther east. South of  $2^\circ\text{S}$ , the distribution of the subduction seismicity is not clear, and earthquakes in the depth range 40–120 km are distributed almost uniformly regardless of the physiographic region or the distance from the trench. Significant earthquakes  $M_w$  7–8 are concentrated in the southwestern portion of the Guayaquil Gulf area around  $4^\circ\text{S}$ . These two dissimilar patterns in the seismicity

Table 4  
Historical Earthquakes Analyzed in This Study

yyyy/mm/dd	Epicentral Region (Fig. 1)	IV	V	VI	VII	VIII	IX	X	XI	Fault or Fault System*	Preferred Location of Epicenter <sup>†</sup>	$M_w$ <sup>‡</sup>
1645/03/15	Chimborazo	1	—	—	3	2	1	—	—	Pallatanga	-1.73; -78.8	6.7–7.3
1674/08/29	Bolivar	—	—	—	—	7	—	—	—	San Jose de Chimbo	-1.67; -79.05	6.1–6.8
1687/11/22	Tungurahua	—	—	1	4	5	—	—	—	Pucara	-1.25; -78.42	5.9–6.6
1736/12/06	Cotopaxi	—	—	1	5	1	—	—	—	Saquisilí-Poalo-Yambo (SPY)	-0.75; -78.75	5.7–6.2
1757/02/22	Latacunga	—	1	1	4	3	—	—	—	SPY	-0.92; -78.56	5.9–6.4
1786/05/10	Chimborazo	—	—	—	9	4	—	—	—	Pallatanga	-1.68; -78.78	5.4–6.2
1834/01/20	Carchi/Nariño	2	1	—	2	3	5	1	1	Sibundoy	1.12; -77.00	7.2–7.6
1868/05/17	Tungurahua	—	—	1	8	—	—	—	—	Pucara	-1.25; -78.42	5.7–6.7
1923/02/05	Pichincha	—	—	—	2	6	—	—	—	Machachi	-0.55; -78.63	5.8–6.5
1923/12/14	Carchi/Nariño	1	1	3	8	12	—	—	—	El Angel-Guachucal	0.88; -77.8	5.8–6.5
1926/12/18	Carchi/Nariño	2	—	1	4	3	—	—	—	El Angel-Guachucal	0.87; -77.78	5.7–6.4
1953/12/23	Carchi/Nariño	—	4	5	6	—	—	—	—	Guaitara	1.05; -77.36	5.7–6.3

Intensity data, potential responsible fault, location, and equivalent moment magnitude deduced from the magnitude isocontours.

\*Potential responsible fault (see Beauval *et al.*, 2010, in particular Table 6).

<sup>†</sup>Preferred epicenter location selected on the responsible fault.

<sup>‡</sup>Interval of uncertainty for the magnitude.

distribution are related to the differences in dip of the Nazca plate; the downgoing slab has a shallower dip in the south. There is a concentration of deeper earthquakes (depth > 120 km) around latitude 1.5° S and longitude 78° W known as the Puyo seismic cluster. These are intraslab events with moderate magnitudes clustered in space (but not in time). Within this cluster, the largest known recorded magnitude occurred outside the time window analyzed in the present work ( $M_w$  7.2 in 2010). Their focal mechanisms reflect tearing of the subducting slab with strike ~N45°W (Segovia and Alvarado, 2009).

The crustal seismicity along the Cordillera also shows two different patterns north and south of 2° S (Fig. 7). Along the southern latitudes, to the east, a northwest–southeast trend of moderate  $M_w$  6–7 events with large  $M_w$  7–7.5 earthquakes is clear along the Andean foothills in the Amazon basin in northwestern Peru. This trend is parallel to the direction of the Andean Cordillera and could be related to its active growth to the east. North of 2° S, the seismicity is concentrated in the Cordillera and shows shallow depths in relationship with the deformation of the North-Andean block (Alvarado, 2012). Most of the historical events are located in this region, and five of them show large magnitudes  $M_w$  7–7.6. Instrumental events are also shallow and have similar epicentral distribution along the Andean Cordillera in agreement with locations of historical events, therefore adequately reflecting the seismic potential in Ecuador.

## Recurrence Times of Earthquakes in the Cordillera

### Declustering of the Catalog

From Christophersen *et al.* (2011, p. 2): “Declustering, i.e., the removal of earthquakes that occur in clusters such as aftershock sequences and swarms, is not an exact science, as no physical difference are known to exist between fore-

shocks, mainshocks, and aftershocks. Therefore, earthquake clusters are usually defined by their proximity in time and space.” Keeping this in mind, clustered events need nonetheless to be retrieved from the earthquake catalog, so that the recurrence curves reflect the occurrences of earthquakes related to the regional tectonics and are not biased by overestimated low-magnitude rates. As in many seismic hazard studies, the catalog is declustered using Reasenberg’s (1985) algorithm. Reasenberg’s (1985) code is known as a “linking” algorithm, where clusters are linked by smaller earthquakes and are allowed to grow in time and space (for more details, see Lolli and Gasperini, 2003; Christophersen and Smith, 2008). In brief, the time interaction window is based on the Omori decay for aftershock activity, whereas the spatial interaction zone depends on the magnitude of prior events. Its extension is inferred from the stress redistribution around the most recent and the largest earthquakes in the sequence.

The impact on the declustering of the calibrating parameters is analyzed through a simple sensitivity study based on the surrogate earthquake catalog. Three parameters constraining spatial and time interaction zones are considered: the minimum and maximum look-ahead time  $\tau_{\min}$  and  $\tau_{\max}$ , and the factor for the spatial interaction distance  $r_{\text{fact}}$ . The minimum look-ahead time is used in the case of earthquakes not already associated to a cluster. Note that the location errors of earthquakes are taken into account by fixing the horizontal and vertical errors to 10 km until 1992, and 5 km from 1993 on. Table 5 displays the percentage of aftershocks identified in the catalog, modifying one by one the three parameters. The first set of parameters ( $\tau_{\min} = 2$ ,  $\tau_{\max} = 10$ ,  $r_{\text{fact}} = 10$ ) corresponds to the default parameters in Reasenberg’s (1985) code. The minimum and maximum look-ahead times are extended up to 10 and 20 days, respectively, whereas the distance factor is increased to 15. The

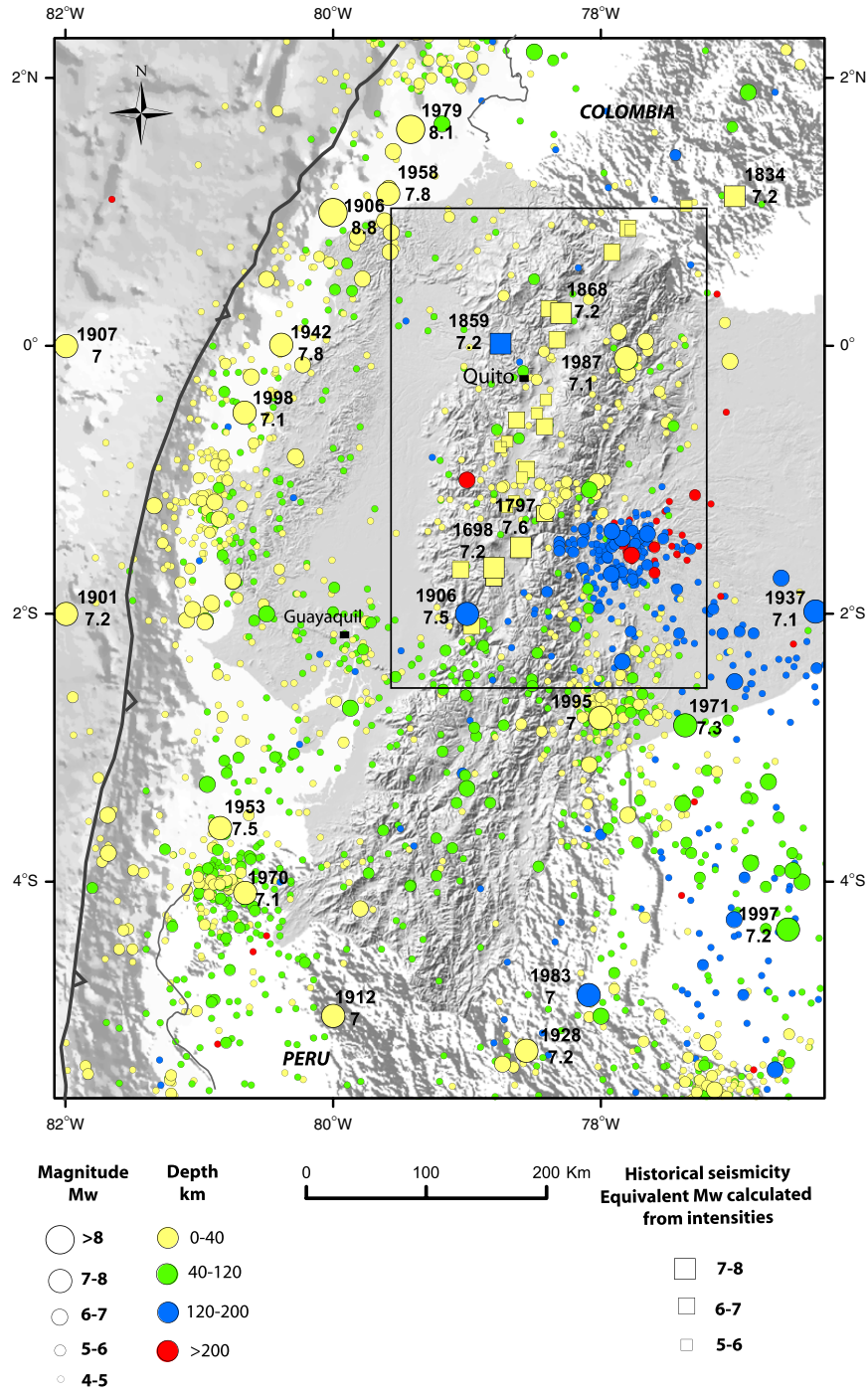


**Figure 7.** Epicenters from the unified earthquake catalog 1587–2009, integrating instrumental and historical earthquakes, displaying magnitude 4 and above (surrogate option, see the text). The recurrence is estimated for crustal earthquakes within a zone focused on the Cordillera (rectangle). Year of occurrence and magnitude are indicated for earthquake with  $M_w \geq 7.0$ . The color version of this figure is available only in the electronic edition.

**Table 5**  
Five Parameters Combinations, Used for Applying the Reasenberg (1985) Declustering Algorithm on the Earthquake Catalogue (Surrogate Option)

$\tau_{\min}$ (days)	$\tau_{\max}$ (days)	$r_{\text{fact}}$	% Aftershocks
2	10	10	21
2	20	10	24
4	20	10	26
4	20	15	27
10	20	15	32

$r_{\text{fact}}$  is a multiple of the circular crack radius.

percentage of aftershocks identified in the Ecuadorian catalog varies between 21% and 32%. We have checked on well-identified sequences (such as the 1996 Pujilí event or the 1987 Salado–Reventador events) that the declustering procedure correctly identifies clustered events. In the following, a recurrence curve is obtained for the Cordillera based on the five declustered catalogs, showing very little impact of using one or the other declustered earthquake catalog. The declustered catalog selected as reference is the one obtained after removing 32% of clustered events. Applying the same set of parameters on the catalog homogenized in magnitude leads to a reduction of 33% of the total number of earthquakes.

#### Recurrence Times of Potentially Destructive Earthquakes in the Cordillera

Based on the declustered earthquake catalog, mean recurrence times can be estimated for earthquakes with given magnitudes. Because of the history of settlements and a climate favorable to document conservation, the information on past earthquakes extends over a longer time window in the Cordillera than in other parts of the country (five centuries; Fig. 2). Moreover, until very recently most stations of the local network were installed mainly on the active volcanoes within the Cordillera (Fig. 1). Therefore, the completeness in the recording of earthquakes is best within the Cordillera. Average recurrence times for significant earthquakes within the volcanic chain, between latitudes  $-2.5^\circ$  and  $+1^\circ$  are determined (see Fig. 7 for the area considered). Several cities with large populations, among them the capital Quito, are located in this area.

To establish a recurrence curve, seismic rates need to be calculated over the complete periods of the catalog. Time periods of completeness are determined from the classical plots displaying cumulated number of events versus time, for different magnitude intervals (four intervals are displayed in Fig. 8). The most recent linear segment, indicating a stable seismic rate with time, provides the lower bound of a completeness period. The plots are displayed for the two optional earthquake catalogs, one based on the surrogate assumption and the other resulting from applying magnitude conversion equations (see [Homogenization of Magnitudes to Moment Magnitude](#)). Based on Figure 8, the same set of completeness time windows is selected for both catalogs (Table 6 and

Fig. 9). As in most hazard studies in any part of the world, identifying complete time periods is not an easy task; none of the plots in Figure 8 shows a perfect linear segment. The dates selected based on the cumulated number of events, however, also correspond to meaningful key dates in the development of seismological networks: 1997 is the beginning date for the IGEPN catalog we are using, whereas 1963 marks the beginning of international seismological networks.

Finally, from the observed rates, the Gutenberg–Richter parameters are calculated (Weichert, 1980) and the recurrence curve is modeled (Figs. 10 and 11). Initially, the recurrence is modeled for the five optional declustered catalogs (see Table 5 and [Declustering of the Catalog](#)). The Gutenberg–Richter parameters do not vary much depending on the declustered catalog considered (Fig. 10). Note that if considering smaller source zones, as will be done in the probabilistic seismic hazard calculations, the impact on the recurrence curve might be more significant. From now on, the catalog that is used is the catalog resulting from the removal of 32% of the clustered events (33% in the case of the homogenized catalog). The observed annual rates considering magnitudes 4.0–6.0 in the surrogate catalog suggest a  $b$ -value of 0.9. For higher magnitudes the observed rates are more scattered (Fig. 11), but they still fall within the modeled recurrence rates taking into account the uncertainty on the  $b$ -value (Weichert, 1980). High magnitude rates are expected not to line up, as the recurrence times of such events are long with respect to the observation time window. As for the earthquake catalog homogenized in magnitude, the observed rates fall on a linear segment on the magnitude interval 4.25–6.0 (again with a slope close to 0.9–1). Applying the magnitude conversion on  $m_b$  and  $M_D$  magnitudes produces an increase of rates for all magnitudes up to 5.5. For both catalogs, there are many more events with magnitudes 3.5–4.0 than expected if one extrapolates the recurrence curves modeled on  $M4+$  down to these magnitude intervals. This is a feature that we have observed in all catalogs, varying the degree of the declustering and/or removing zones characterized by dense swarms (such as the Pisayambo zone; Troncoso, 2009). For now, we have no clear explanation for this observation.

Comparing the recurrence curves obtained from both catalogs, the impact of the decision on the homogenization of magnitudes proves to be noticeable up to magnitudes 5.5–6. From magnitudes  $\geq 6$ , the rates are quite similar. The average rate, for an earthquake with a magnitude  $\geq 6.0$  inside the spatial zone considered, varies between 0.05 and 0.1, resulting in an average recurrence time within 10 and 20 years (Fig. 12). As the clustered events have been excluded from the catalog, the recurrence curve describes the frequencies of Poissonian independent events. A recurrence time of 20 years leads to an  $\sim 37\%$  probability of not observing such an earthquake in the next 20 years in the area, or an  $\sim 18\%$  probability of observing two such events in the same future time window (Fig. 12; see also Beauval *et al.*, 2008).

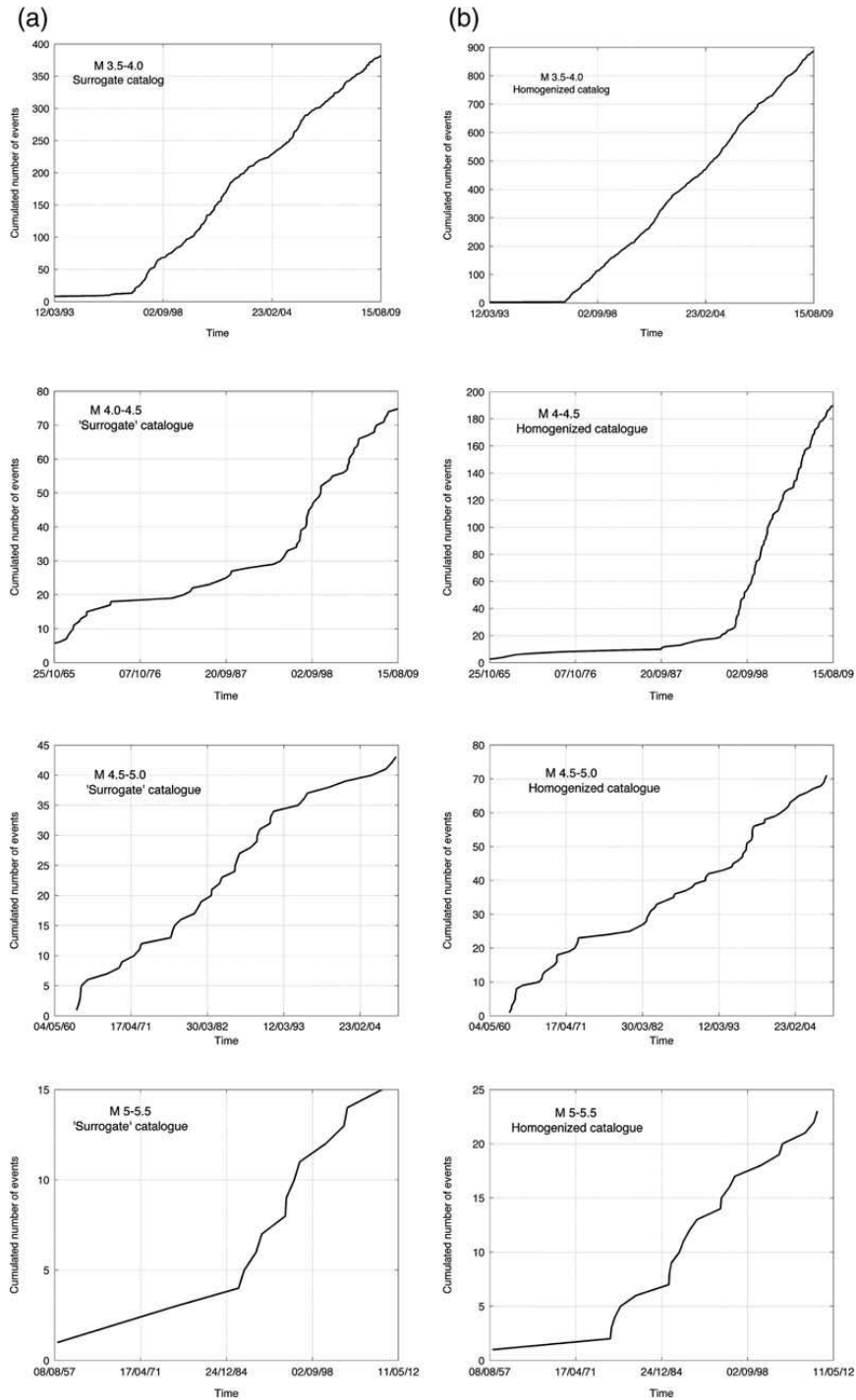


**Figure 8.** Cumulated number of events versus time, for different magnitude intervals, based on the declustered catalog enclosed in the spatial window focused on the Cordillera (Fig. 7): longitude  $-79.5^{\circ}$  to  $-77.25^{\circ}$ , latitude  $-2.5^{\circ}$  to  $+1^{\circ}$ , down to 40 km. (a) Plots based on the “surrogate” catalog (no conversion of magnitudes). (b) Plots based on the catalog homogenized in magnitude.

Table 6  
Completeness Time Windows Valid for the Cordillera Region  
(Longitudes  $-79.5^\circ$  to  $-77.25^\circ$  and Latitudes  $-2.5^\circ$  to  $1^\circ$ )

Magnitude Interval	[3.5–4.0[	[4.0–4.5[	[4.5–5.0[	[5.0–5.5[	[5.5–6.0[	[6.0–6.5[	[6.5–7.0[	[7.0–7.5[
Time period of completeness	1997	1997	1963	1957	1920	1860	1860	1587

### Conclusions

The earthquake catalog is ready for use in seismic hazard studies in Ecuador. Standard techniques and well-established criteria are applied to merge different instrumental sources and select the best earthquake solutions among existing ones. This catalog is intended to evolve as new information emerges, and some solutions will need updating. The historical part is appended to the instrumental unified catalog. Thirteen historical events are analyzed so that magnitudes (equivalent to  $M_w$ ) and locations can be assigned for these events. They complete the initial historical data set published in Beauval *et al.* (2010), made of well-described historical earthquakes. Until more data is available with an intrinsic  $M_w$ , we believe that the uncertainty on the magnitude must be taken into account. Therefore, the earthquake catalog includes both the original magnitudes (calculated on waveforms) and  $M_w$  obtained through conversion equations, and we recommend that users do calculations with both options.

The catalog is much more complete in the Cordillera region than on the coast. At least one historical earthquake of the nineteenth century (3 May 1896), that might be a subduction event, still needs to be analyzed. In the absence of more written documents, however, the length of the earthquake history along the coast will remain short (from the end of the nineteenth century on). For estimating the recurrence of large subduction events, other types of information are needed, such as geodetic measurements (ongoing work in

Ecuador) and paleoseismic techniques (trenching for tsunamigenic deposit analyses or coral dating). For the Cordillera region, between latitudes  $-2.5^\circ$  and  $+1^\circ$ , the 500 years of data enable us to derive a recurrence curve for crustal earthquakes with magnitudes 4.0 and above, predicting on average an earthquake with magnitude  $M_w \geq 6.0$  every 10–20 years. This result includes the uncertainty on the homogenization of magnitudes, as well as an uncertainty on the declustering step.

This work is part of a broader program aimed at estimating probabilistic seismic hazard at the level of the country. Others are currently working on the seismotectonic zoning, using knowledge of active tectonics, and taking advantage of this new unified earthquake catalog (Alvarado, 2012). The next step is the building of frequency–magnitude distributions for each source zone of this zoning. These distributions will be key inputs for the calculation of probabilistic seismic hazard maps. Where possible, the distributions will be combined with geodetic analysis and paleoseismology results (currently only the Pallatanga fault system has been analyzed using paleoseismology; S. Baize *et al.*, unpublished manuscript, 2012).

### Data and Resources

International Seismological Centre online bulletin, <http://www.isc.ac.uk/iscbulletin/search/bulletin/> (last accessed November 2012). GCMT earthquake catalog, <http://www>

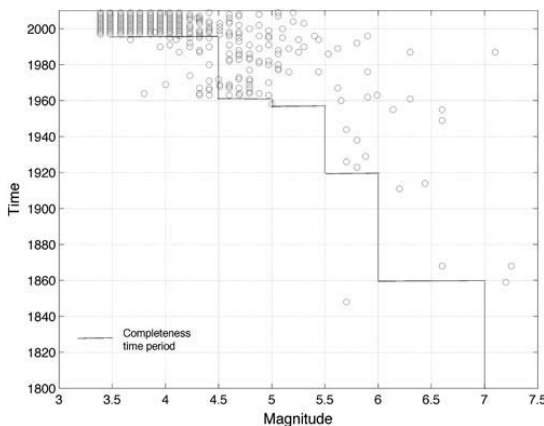


Figure 9. Declustered and homogenized catalog in the Cordillera: distribution of crustal earthquakes in time and magnitude, spatial window: longitude  $-79.5^\circ$  to  $-77.25^\circ$ , latitude  $-2.5^\circ$  to  $+1^\circ$ . Completeness time windows are indicated, see Table 6.

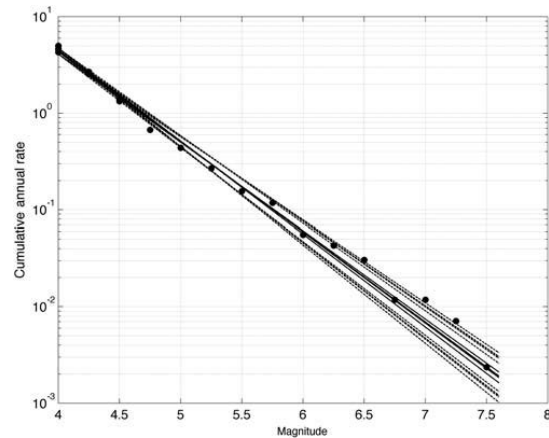
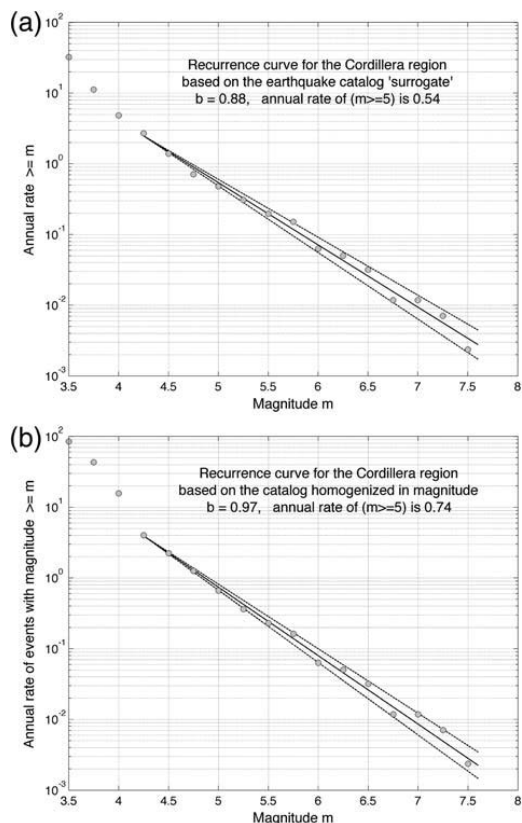


Figure 10. Implications of the declustering on the modeling of the Gutenberg–Richter curve, based on the surrogate earthquake catalog. Five sets of parameters in Reasenberg's (1985) algorithm are tested (Table 5). Observed rates plus parameters  $a$  and  $b$  are calculated five times and superimposed.



**Figure 11.** Recurrence curve for the Cordillera region (spatial window: longitude  $-79.5^\circ$  to  $-77.25^\circ$ , latitude  $-2.5^\circ$  to  $+1^\circ$ ), calculated using the completeness time windows per magnitude interval. Observed seismicity rates (cumulated), gray circles. Recurrence curve taking into account the uncertainty on the  $b$ -value, dashed lines. The earthquakes are taken into account down to 40-km depth. The maximum magnitude for this zone is 7.6 (1797). (a) Surrogate catalog. (b) Homogenized catalog.

[globalcmt.org/CMTsearch.html](http://globalcmt.org/CMTsearch.html) (last accessed November 2012). PDE-NEIC earthquake catalog, <http://earthquake.usgs.gov/earthquakes/eqarchives/epic/> (last accessed November 2012). Centennial catalog, <http://earthquake.usgs.gov/research/data/centennial.php> (last accessed November 2012). Code cluster 2000 (Reasenberg, 1985), <http://earthquake.usgs.gov/research/software/index.php> (last accessed November 2012).

**Acknowledgments**

This work was partially supported by the laboratory ISTerre, by the Agence Nationale de la Recherche through the project Andes du Nord (Contract Number ANR-07-BLAN-143) and by IRD (Institut de la Recherche pour le Développement). On the Ecuadorian side, partial support was available from the Secretaría Nacional de Educación Superior, Ciencia y Tecnología SENESCYT (Proyecto PIN\_08-EPNGEO-00001). This work was

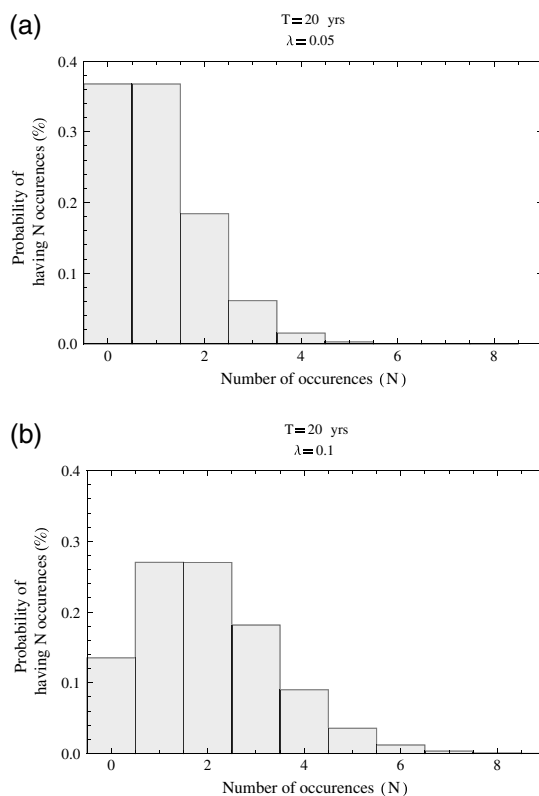


**Figure 12.** Expected number of earthquakes with magnitude  $\geq 6.0$ , in a 20-yr time window, within the Cordillera zone considered (spatial window: longitude  $-79.5^\circ$  to  $-77.25^\circ$ , latitude  $-2.5^\circ$  to  $+1^\circ$ ). (a) Poisson process with annual rate 0.05 (recurrence time 20 yr). (b) Poisson process with annual rate 0.1 (recurrence time 10 yr).

finalized within the recently created IRD joint international laboratory between France and Ecuador, LMI “Séismes et Volcans”. We are grateful to F. Hollender for his kind help in drawing the second figure of the manuscript.

**References**

Abe, K. (1981). Magnitudes of large shallow earthquakes from 1904 to 1980, *Phys. Earth Planet. In.* **27**, 72–92.  
 Abe, K. (1984). Complements to “Magnitudes of large shallow earthquakes from 1904 to 1980”, *Phys. Earth Planet. In.* **34**, 17–23.  
 Alvarado, A. (2012). Néotectonique et cinématique de la déformation continentale en Equateur, *Thèse de doctorat (PhD)*, Université de Grenoble, France, 259 pp.  
 Bakun, W. H., and C. M. Wentworth (1997). Estimating earthquake location and magnitude from seismic intensity data, *Bull. Seismol. Soc. Am.* **87**, 1502–1521.  
 Beauval, C., and O. Scotti (2003). Mapping  $b$ -values in France using two different magnitude ranges: Possible non power-law behavior, *Geophys. Res. Lett.* **30**, no. 17, 1892, doi: [10.1029/2003GL017576](https://doi.org/10.1029/2003GL017576).  
 Beauval, C., and O. Scotti (2004). Quantifying sensitivities of Probabilistic Seismic Hazard Assessment for France to earthquake catalog uncertainties, truncation of ground-motion variability and magnitude limits, *Bull. Seismol. Soc. Am.* **94**, 1579–1594.

- Beauval, C., P.-Y. Bard, S. Hainzl, and P. Guéguen (2008). Can strong motion observations be used to constrain probabilistic seismic hazard estimates? *Bull. Seismol. Soc. Am.* **98**, 509–520.
- Beauval, C., H. Yepes, W. H. Bakun, J. Egred, A. Alvarado, and J.-C. Singaicho (2010). Locations and magnitudes of historical earthquakes in the Sierra de Ecuador (1587–1996), *Geophys. J. Int.* **181**, 1613–1633, doi: 10.1111/j.1365-246X.2010.04569.x.
- Braunmiller, J., N. Deichmann, D. Giardini, S. Wiemer, and the SED Magnitude Working Group (2005). Homogeneous moment-magnitude calibration in Switzerland, *Bull. Seismol. Soc. Am.* **95**, no. 1, 58–74.
- Christophersen, A., and E. G. C. Smith (2008). Foreshock rates from aftershock abundance, *Bull. Seismol. Soc. Am.* **98**, no. 5, 2133–2148.
- Christophersen, A., M. C. Gerstenberger, D. A. Rhoades, and M. W. Stirling (2011). Quantifying the effect of declustering on probabilistic seismic hazard, in *Proc. of the Ninth Pacific Conf. on Earthquake Engineering: Building an Earthquake-Resilient Society*, Auckland, New Zealand, 14–16 April, 8 pp.
- Dimate, C., L. Drake, H. Yepes, L. Ocola, H. Rendon, G. Grünthal, and D. Giardini (1999). Seismic hazard assessment in the Northern Andes (PILOTO project), *Ann. Geofisc.* **42**, no. 6, 1039–1055.
- Egred, J. (2009). Catalogo de Terremotos del Ecuador 1541–2009, Escuela Politécnica Nacional, Instituto Geofísico, internal report.
- Ekström, G., M. Nettles, and A. M. Dziewonski (2012). The global CMT project 2004–2010: Centroid-moment tensors for 13,017 earthquakes, *Phys. Earth Planet. In.* **200–201**, 1–9.
- Engdahl, E. R., and A. Villaseñor (2002). Global Seismicity: 1900–1999, in *International Handbook of Earthquake and Engineering Seismology*, Part A, Chapter 41, W. H. K. Lee, H. Kanamori, P. C. Jennings, and C. Kisslinger (Editors), Academic Press, 665–690.
- Engdahl, E. R., R. Van Der Hilst, and R. Buland (1998). Global teleseismic earthquake relocation with improved travel times and procedures for depth determination, *Bull. Seismol. Soc. Am.* **88**, 722–743.
- Font, Y., S. Segovia, S. Vaca, and T. Theunissen (2013). Seismicity pattern along the Ecuadorian subduction zone: New constrains from earthquake location in a 3D a priori velocity model, *Geophys. J. Int.* (in press).
- Giesecke, A., A. A. Gómez Capera, I. Leschiutta, E. Migliorini, and L. R. Valverde (2004). The CERESIS earthquake catalog and database of the Andean Region background, characteristics and example of use, *Ann. Geophys.* **47**, 421–435.
- Grunewald, E. D., and R. S. Stein (2006). A new 1649–1884 catalog of destructive earthquakes near Tokyo and implications for the long-term seismic process, *J. Geophys. Res.* **111**, B12306.
- Grünthal, G. (Editor) (1998). European Macroseismic Scale 1998 (EMS-98), *Cahiers du Centre Européen de Géodynamique et de Séismologie 15*, Centre Européen de Géodynamique et de Séismologie, Luxembourg, 99 pp.
- Gutenberg, B., and C. F. Richter (1954). *Seismicity of the Earth and Associated Phenomena*, Princeton University Press, Princeton, New Jersey.
- International Seismological Centre (2010). *EHB Bulletin*, Internat. Seis. Cent., Thatcham, United Kingdom, <http://www.isc.ac.uk> (last accessed November 2012).
- Johnston, A. C., and S. Halchuk (1993). The seismicity database for the Global Seismic Hazard Assessment Program, *Ann. Geofisc.* **3–4**, 133–151.
- Lolli, B., and P. Gasperini (2003). Aftershocks hazard in Italy. Part I: Estimation of time-magnitude distribution model parameters and computation of probabilities of occurrence, *J. Seismol.* **7**, 235–257.
- Mendoza, C., and J. W. Dewey (1984). Seismicity associated with the Great Colombia-Ecuador earthquake of 1942, 1958, and 1979: Implications for barrier models of earthquake rupture, *Bull. Seismol. Soc. Am.* **74**, 577–593.
- Pacheco, J. F., and L. R. Sykes (1992). Seismic moment catalog of large shallow earthquakes, 1900 to 1989, *Bull. Seismol. Soc. Am.* **82**, 1306–1349.
- Palacios, P., and H. Yepes (2011). Analysis de la magnitud de duracion, Instituto Geofísico, Escuela Politécnica Nacional, Quito, internal report, 18 pp (in Spanish, available on request).
- Reasenber, P. A. (1985). Second-order moment of central California seismicity, *J. Geophys. Res.* **90**, 5479–5495.
- Rothé, J. P. (1969). *The Seismicity of the Earth, 1953–1965*, UNESCO, Paris.
- Scordilis, E. M. (2006). Empirical global relations converting  $M_S$  and  $m_b$  to moment magnitude, *J. Seismol.* **10**, 225–236.
- Segovia, M., and A. Alvarado (2009). Breve análisis de la sismicidad y del campo de esfuerzos en el Ecuador, in *Geología y geofísica marina y terrestre del Ecuador: desde la costa continental hasta las Islas Galápagos*, J.-Y. Collot, V. Sallares, and N. Pazmiño (Editors), Guayaquil-Ecuador, 131–150.
- Swenson, J. L., and S. L. Beck (1996). Historical 1942 Ecuador and 1942 Peru subduction earthquakes, and earthquake cycles along Colombia-Ecuador and Peru subduction segments, *Pure Appl. Geophys.* **146**, 67–101.
- Troncoso, L. (2009). *Estudio sismológico del Nido de Pisayambo, Memoria Master 2*, Université Nice Sophia-Antipolis, France, 26 pp.
- Utsu, T. (2002). Relationships between magnitude scales, in *International Handbook of Earthquake and Engineering Seismology*, Part A, Chapter 44, W. H. K. Lee, H. Kanamori, P. C. Jennings, and C. Kisslinger (Editors), Academic Press, 733–746.
- Weichert, D. H. (1980). Estimation of the earthquake recurrence parameters for unequal observation periods for different magnitudes, *Bull. Seismol. Soc. Am.* **70**, no. 4, 1337–1346.
- Yadav, R. B. S., P. Bormann, B. K. Rastogi, M. C. Das, and S. Chopra (2010). A homogeneous and complete earthquake catalog for Northeast India and the Adjoining region, *Seismol. Res. Lett.* **80**, no. 4, 609–627.

ISTerre  
IRD-CNRS-UJF  
BP 53, 38041 Grenoble Cedex 9  
France  
celine.beauval@ujf-grenoble.fr  
(C.B.)

Instituto Geofísico,  
Escuela Politécnica Nacional  
Ladrón de Guevara E11-253, Apto 2759  
Quito, Ecuador  
(H.Y., P.P., M.S., A.A., L.T., S.V., J.A.)

Géoazur  
IRD-CNRS-UNS-OCA  
250 rue Albert Einstein  
Sophia-Antipolis 06560 Valbonne  
France  
(Y.F.)

Pontificia Universidad Católica del Ecuador  
Av. 12 de Octubre y Patria  
Quito, Ecuador  
(J.A.)

## 4 **A new view for the geodynamic context of Ecuador and its implications for seismogenic sources definition and seismic hazard assessment**

### **A new view of Ecuador's geodynamic context and its implications for seismogenic sources definition and seismic hazard assessment**

Hugo Yepes <sup>1,2</sup>, Laurence Audin <sup>2</sup>, Alexandra Alvarado <sup>1</sup>, Céline Beauval <sup>2</sup>, Jorge Aguilar <sup>1</sup>, Yvonne Font<sup>3</sup>, Fabrice Cotton <sup>2</sup>

<sup>1</sup> Instituto Geofísico, Escuela Politécnica Nacional, Quito

<sup>2</sup> ISTERre, Grenoble, France

<sup>3</sup> GeoAzur, Nice, France

### **Introduction**

Adequate understanding of long-term crustal deformation processes is essential for accurate determination of seismic hazard. Present day seismogenic structures are palpable evidences of tectonic forces that have slowly evolved during geologic times but remain invariant in terms of the short timeframe observed for seismic hazard assessment. Once those tectonic processes are unveiled and the resulting main fault systems are linked to historical and instrumental seismicity on the one hand, and ground motion prediction equations are adopted on the other, seismic hazard experts have the main inputs to calculate the probabilities of experiencing different levels of ground shaking within a specific exposure time. The output of this intricate modeling process, known as probabilistic seismic hazard assessment –PSHA–, is especially valuable for engineering design and planning purposes in earthquake prone countries.

In PSHA it is current practice to use geodynamic and tectonic information as well as geodetic data for modeling seismic sources (Caputo et al., 2013; Meletti et al., 2008; Muir-Wood, 1993; Stirling et al., 2012). Seismic sources could be defined either as distributed seismicity or as fault sources. Distributed seismicity sources are geometric volumes where seismicity may be considered uniformly distributed in space and stationary in time, rendering their seismic potential as homogeneous. They encompass seismogenic structures with similar tectonic behavior (Baize et al., 2013; Meletti et al., 2008). On the other hand, the fault source model requires the geometry and slip rates of mapped fault sources in order to develop a single characteristic earthquake (magnitude and frequency) for each source (Stirling et al., 2012). Knowledge about the size, geometry, and slip rates of individual faults or fault systems is poor in Ecuador, consequently only distributed seismicity sources or seismic source zones – SSZ– are discussed in this paper.

Previous attempts of defining SSZs in Ecuador date back to the early 90's (Bonilla et al., 1992). More comprehensive studies were aimed at doing PSHA for seismic design of infrastructure (e.g. Gajardo et al., 2001; Yepes et al., 2006) and at producing seismic zonation maps for the Ecuadorian Building Code 2001 and the 2011 versions (CEC, 2001; NEC, 2014), but they were not published in the scientific literature. Alvarado revisited the 2011 zones in her Ph.D. work (2012) and Beauval et al. (2014) used them for PSHA in Quito, the capital city, for estimating uncertainties related to both the definition of distinct source zones and the differences in the chosen ground motion prediction equations.

Our approach to develop the new SSZ scheme for Ecuador is to revisit the previously published geodynamic and seismotectonic models with the goal of matching the seismic sources zonation to the novel geodynamic interpretation presented here. Our fresh view on Ecuador's geodynamics is based on the recently published countrywide *Earthquake Catalog For Seismic Hazard Assessment* (Beauval et al., 2013) which combines the most reliable magnitude and hypocentral solutions extracted from different instrumental catalogs,

including reprocessed results from the local seismic network (Font et al., 2013a). For this analysis we divide the catalog in shallow (0-50 km) and intermediate depth (50-300 km) seismicity. For this subdivision we have observed the failure domains of interface megathrust faults (Lay et al., 2012); that is, brittle rupture of crustal faults for the former and internal tearing of the subducting slab for the latter. The 300 km depth limit reflects the fact that there are few deep earthquakes in the catalog (just three events are deeper than 300 km, the strongest dated in 1925).

The sharper picture of the country's seismicity provided by the new catalog depicts the down-going slab geometry and confirms the relationship of the involved plates at depth where inherited oceanic plate structures have an influential role. For the continental domain, convergence obliquity, and tectonic stress partitioning, focal mechanisms and seismic energy release patterns are analyzed along with new knowledge obtained from recent geologic investigations on active continental faults (Alvarado et al., 2015; Baize et al., 2014). We merge all that information with the seismic catalog and active deformation data to better define geometries and boundaries of continental source zones corresponding to the seismotectonic model.

## **1. REVISITING GEODYNAMICS AND SEISMOTECTONICS IN ECUADOR**

### **1.1 Overview of geomorphic features and shallow seismicity of the intervening plates**

#### ***Nazca Plate: two plates with different densities in contact***

The subduction of the Nazca plate since early Miocene (convergence direction N83; 56 mm/a at equatorial latitudes (Kendrick et al., 2003)) is the most obvious and major geodynamic process taking place in northwestern South America. Before stabilizing during the late Miocene when the Panama Basin spreading centers became extinct, active spreading axes, rifts, transform

faults, and grabens along ridge crests populated the basin as can still be noticed in Fig. 1.

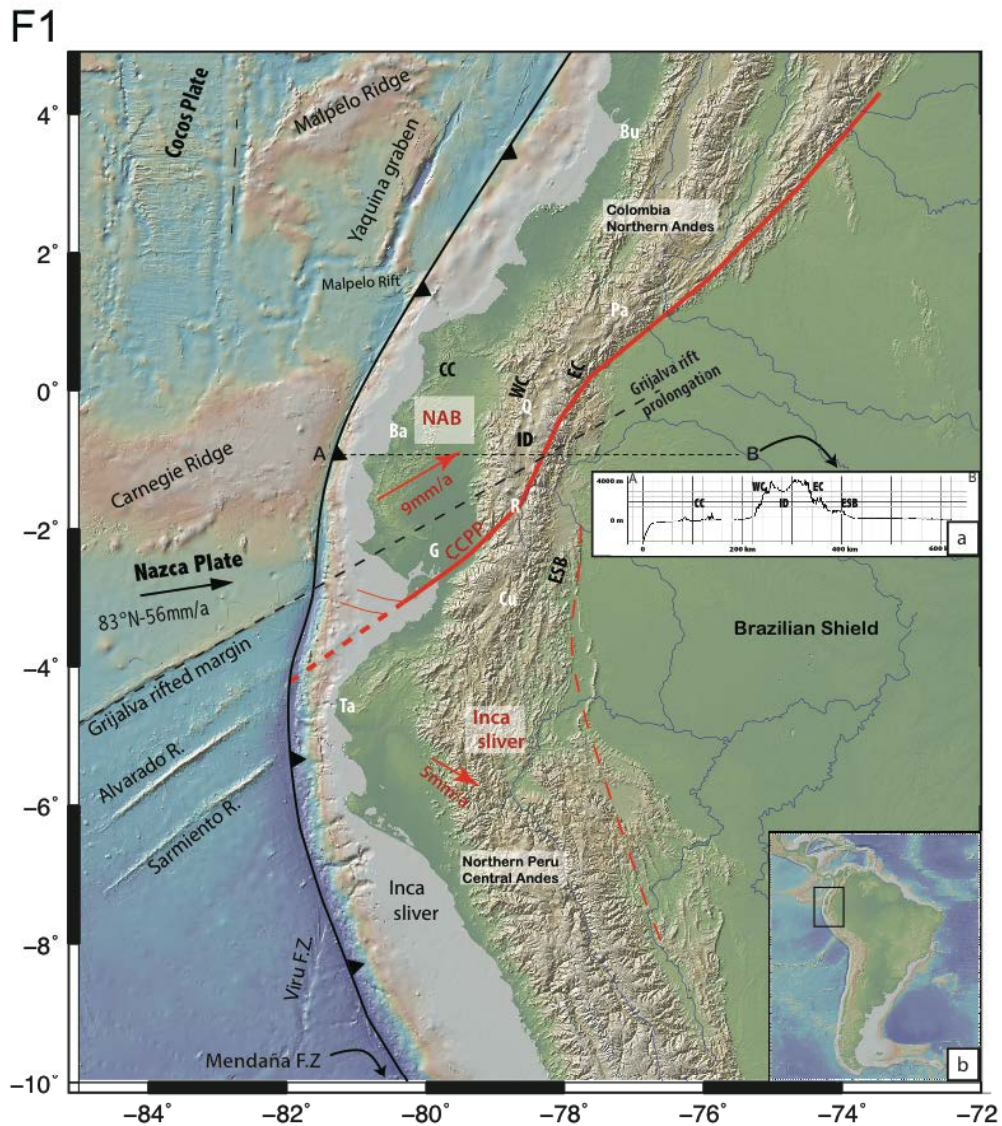


**Fig. 1. Geodynamic setting of Ecuador and neighboring countries.** The Nazca plate is converging at equatorial latitudes relatively to the Brazilian shield at 56 mm/a. Due to the acute convexity of the margin (trench is the thick black line with indents), oblique convergence is driving two different continental slivers away from each other. The North Andean Block – NAB – is moving towards the NNE at 9 mm/a along localized right-lateral strike-slip or reverse faults –CCPP– (red thick line). The Inca sliver is moving towards the SSE at ~5 mm/a along the proposed limit in the eastern Peruvian Sub-Andean Belt (dashed red line). The Grijalva rifted margin is separating two oceanic plates of different ages. The black segmented line is marking the inland prolongation of the rifted margin. The approximate location of main cities has been highlighted with white letters: Bu=Buenaventura; Pa=Pasto; Q=Quito; R=Riobamba; B=Bahía; G=Guayaquil; Cu=Cuenca; Ta=Talara. Base map modified from GeoMapApp (<http://www.geomapapp.org>). **a.** Topographic A-B profile showing the relief across the central Ecuadorian Andes. CC=Coastal Cordillera; WC=Western Cordillera; ID=Interandean Depression; EC=Eastern Cordillera; ESB=Eastern Sub-Andean Belt; AB=Amazon Basin. **b.** Region covered in our study.

Nowadays, the subduction of two major topographic elements complicates the penetration of the Nazca beneath the continent: (a) the Carnegie ridge, a ~200 km-wide, 2000 m-high aseismic ridge, and (b) the ~500 m bathymetric difference north and south of the Grijalva ridge related to the density contrast between the younger Nazca crust to the north and the older Farallon crust to the south. The density contrast is related to an up-to-nine million years difference in oceanic crustal age resulting from the latest fission of the Farallon plate that progressively resulted in the Nazca and Cocos plates at the beginning of the Miocene (Hey, 1977; Lonsdale, 2005; Lonsdale and Klitgord, 1978). Grijalva is the remaining evidence of the rifting of the Farallon lithosphere and will be named as the Grijalva rifted margin hereinafter. To the south, Alvarado and Sarmiento (Fig. 1) are 2 km-high topographic fossil ridges generated by fissural eruptions (Lonsdale, 2005). They do not constitute rifting features and thus don't show any density contrast. Both the Carnegie ridge and Grijalva rifted margin have been entering the subduction zone from at least 3-6 Ma ago and are thought to have penetrated up to 300-500 km under the continent (Gutscher et al., 1999; Lonsdale, 2005; Michaud et al., 2009). This implies that two plates of different densities are in contact underneath the Ecuadorian Andes; the northern-most includes the Carnegie ridge's lower density, buoyant, thickened oceanic crust. North of the Carnegie ridge a clear bathymetric feature belongs to the Yaquina graben: an abandoned transform fault (Lonsdale, 2005) or fracture zone (MacMillan et al., 2004) (Fig. 1).

***Interface seismicity: one of the most seismically active convergent margins***

The scientific literature (Beck and Ruff, 1984; Chlieh et al., 2014; Collot et al., 2004; Font et al., 2013a; Kanamori, 1977; Kanamori and McNally, 1982; Kelleher, 1972; Mendoza and Dewey, 1984; Swenson and Beck, 1996) has extensively shown that the subduction zone along northwestern edge of South America is one of the convergent margins most seismically active in the world. Along this approximately 1300 km long subduction zone, eight  $M_w > 7.0$  events ruptured the seismogenic interface during the 20<sup>th</sup> century (Fig. 2a which includes five in the Nazca plate domain north of the Grijalva rifted margin and

three south of it. No historical subduction earthquakes have been described prior to 1896 either due to a lack of seismicity or to absence of historical records. The only possible exception would be the 1619 Trujillo, Peru earthquake, not verified as an interplate event (Dorbath et al., 1990).

In the northern group, the  $M_w$  8.8 1906 Ecuador-Colombia megathrust earthquake ranks among the ten most powerful earthquakes ever recorded by

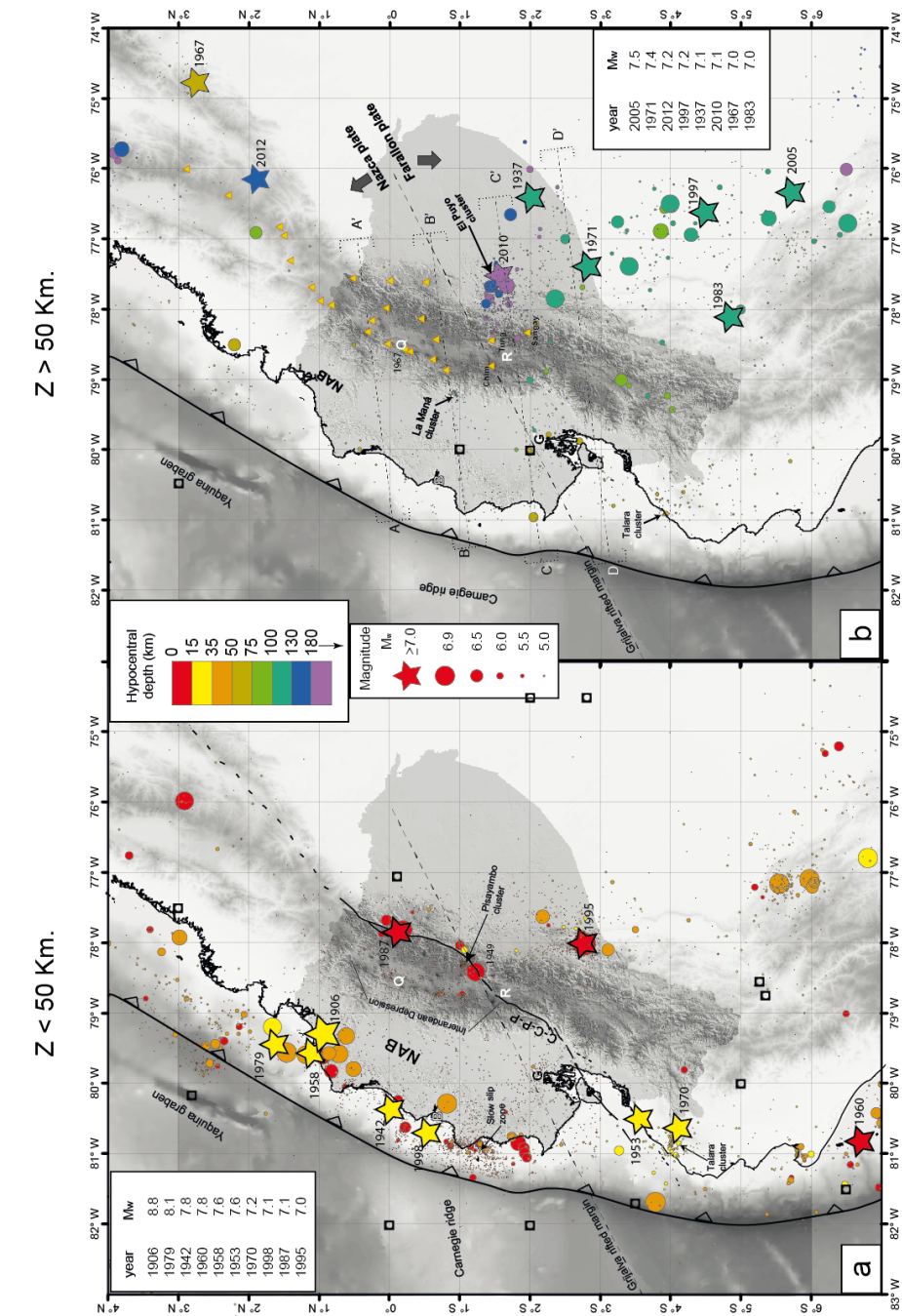


**Fig. 2. 110 years of instrumental seismicity in Ecuador 1900-2009.**  $M_w \geq 7$  earthquakes are plotted as stars. Years and magnitudes are listed in the respective insets.  $M_w < 7$  events are plotted as circles. Sizes are proportional to the seismic moment release  $M_o$  of individual events. Circle's radii are obtained assuming circular faults releasing seismic moment at a constant stress drop of 3MPa. Black hollow squares are pre-1930  $M_w \geq 7$  earthquakes whose location and depth are considered not reliable. Hypocentral depths ( $Z$ ) are classified by colors. **a.** Shallow seismicity (hypocentral depth  $\leq 50$  km). C-C-P-P fault system marks the North Andean Block boundary. **b.** Intermediate depth seismicity (hypocentral depth  $> 50$  km). The dotted line represents the inland prolongation of Grijalva rifted margin. Notice that the line separates slabs with different origin and ages. Cross sections A-A' to D-D' presented in Fig. 4 are marked here. Letters are main cities: Q=Quito; B=Bahía; R=Riobamba; G=Guayaquil. Seismicity from Beauval et al. (2013).

seismometers in the world (Kanamori, 1977) and released seismic energy from a ~500 km long interface segment immediately north of Carnegie ridge. Within the 1906 rupture area, three other large earthquakes occurred during the 20<sup>th</sup> century, depicting a dual rupture cycle where megathrust earthquakes may represent supercycles recurring every 200 to 600 years (Beck and Ruff, 1984; Chlieh et al., 2014; Kanamori and McNally, 1982; Mendoza and Dewey, 1984), while smaller  $M_w$  7–8 events occurred at a pace of three per century during the 20<sup>th</sup> century (Fig. 2a).

Southwards, no  $M_w \geq 8$  event has been recorded along the subduction segment between the Grijalva rifted margin and the Mendaña fracture zone (~10°S, outside the analyzed region). This segment of the South American subduction zone is considered to have greater than average repeat times for great earthquakes (Nishenko, 1991) or to be freely slipping as a second alternative (Nocquet et al., 2014). The strongest recorded magnitude corresponds to the rare tsunamigenic 1960 earthquake ( $M_w$  7.8) (Fig. 2a) characterized by slow rupture that only involved the shallow portion of the subduction zone (Bilek, 2010). From Fig. 2a it is also apparent that south of 2°S the interface seismicity is sparse and less conspicuous, with the exception of an epicenter cluster at Latitude 4°S where two  $M_w \geq 7$  events are located. This concentration of earthquakes is named here as the Talara seismic cluster. Notice that the Grijalva rifted margin encounters the trench at Lat. 2.9°S, suggesting a differential influence of each plate on the generation of interface earthquakes.

The small 100-120 km long subduction segment located between Lat. 1.8°S and the reported southern rupture limit of the great 1906 thrust earthquake at Lat. ~0.7°S (Collot et al., 2004; Kelleher, 1972) is characterized by dense background seismicity with a maximum magnitude of  $M_w$  6.1. Here, most of the seismic energy of the interface is released during intense seismic swarms related to the activity of persistent shallow slow-slip events (Vallée et al., 2013). There is also a concentration of five  $M_w$  6-7 earthquakes immediately

to the south of the slow-slip zone, but it lacks the presence of smaller events (Fig. 2a).

***Crustal morphology: evidence of continuous oblique convergence***

In continental Ecuador, four physiographic zones can be defined from west to east as a result of long term crustal deformation (Fig. 1): (1) the low, wide coastal region with smoother topography and a coastal range located at the western margin (~300 m above sea level –a.s.l.); (2) the Andean ranges, 150 km wide on average in Ecuador, that display a general N-S direction and rise above 3000 m a.s.l.; (3) the sub-Andean belt (ESB) with lower average altitudes (~2000 m a.s.l.) than the main Andean Cordillera; and, (4) the Amazon Basin gently dipping to the east (~300 m a.s.l.). The Ecuadorian Andes show distinct morphology, north and south of Lat. 1.7°S. To the north, two parallel ranges are distinguishable (the Western and Eastern Cordilleras at ~4000-4400 m a.s.l.) separated by the Interandean Depression (~2200-3000 m a.s.l.), that is not wider than 30 km (Fig. 1a). An active volcanic arc with up to four rows of volcanoes is associated with the top of the western and eastern ranges, with intra-Depression edifices and with the ESB. Active volcanism is not present south of Lat. 2°S. No distinctive ranges are found south of 1.7°S and the Interandean Depression gives way to individual intra-mountainous sedimentary basins that lack the widespread Quaternary volcanic deposits observable to the north. Farther south in Peruvian territory, the northern Peruvian Andes consist of a more massive range ~300 km-wide.

This morphology is the consequence of a shared geodynamic history of the Northern Andes (Ecuador-Colombia-Venezuela: Pindell and Kennan, 2009), which is very different from that of the Central Andes (Peru-Chile-Bolivia: Barnes and Ehlers, 2009). Indeed, present day Ecuador's tectonic setting results from a transpressive evolution that has occurred throughout the Paleocene as a consequence of oblique subduction and progressive, accretionary continental growth (Cediel et al., 2004; Daly, 1989; Toro, 2007). Subsequently, the onset and development of the current subduction scheme began during the Oligocene (Jaillard et al., 2009) characterized by continuous

oblique subduction (Daly, 1989). As a result of oblique convergence and the accretion of oceanic terranes, a tectonic block began to be pushed towards the northeast, in response to partitioning of shear stresses and high coupling along the northern Ecuadorian interface (Egbue and Kellogg, 2010; Nocquet et al., 2014), as will be described in more detail later. This continental block is known as the North Andean Block –NAB– and is bordered to the east by a long-lived, transpressive right-lateral fault system, the Chingual-Cosanga-Pallatanga-Puna (CCPP) system, that forms the western limit of the stable South America plate (Alvarado et al., 2015; Ego et al., 1996b) (Fig. 1).

***Crustal seismicity: localized activity with strong shallow earthquakes***

In continental Ecuador, high-energy seismic moment release is mostly concentrated in the northern Andes, especially in the Interandean Depression and along the sub-Andean belt (Fig. 2a). Two shallow continental crust earthquakes of  $M_w \geq 7$  have been instrumentally recorded during the past 110 years. The 1987  $M_w$  7.1 shock is related to the NAB - South American transpressive boundary while the second event is located in the Ecuadorian ESB but probably still in the Central Andes compressive domain (Yepes et al., 1996) (Fig. 2a). Several events with  $M_w$  6.0-7.0 also cluster in the northeastern Peruvian Central Andes domain (Lat.  $\sim 6^\circ\text{S}$ ) and are aligned in a direction perpendicular to Nazca plate convergence.

The largest intra-Andean instrumental event corresponds to the 1949 Ambato earthquake, ( $M_w$  6.5) (Fig. 2a). This devastating earthquake is also related to the NAB – South American boundary zone (Beauval et al., 2010). Several moderate earthquakes ( $5 < M_w \leq 6$ ) have also been recorded along a 130 km long, N15°E lineament that coincides with the western slopes of the Interandean Depression (Fig. 2a).

Pre-instrumental earthquakes are also fairly common in the Interandean Depression (Beauval et al., 2010; Giesecke, 1988; Giesecke et al., 2004). Seven out of 30 Andean historical earthquakes relocated by Beauval et al. (2010) and Beauval et al. (2013) have an intensity-derived magnitude  $M_{IC} \geq 6.5$

( $M_{IC}$  = intensity magnitude calculated at the intensity center using Bakun and Wentworth (1997) methodology equivalent to  $M_w$ ) in a time span of 368 years and 21 have  $M_{IC} \geq 6.0$ . The recurrence interval for  $M_w \geq 6$  historical and instrumental crustal earthquakes along the 300 km long segment of the Ecuadorian north-central Andes is estimated to be 10-20 years (Beauval et al., 2013), for events that originated along both NAB boundary faults and at the smaller thrust faults marking the borders of the heavily populated Interandean Depression. Although the total moment release along these structures is not comparable with that at the interface, hypocenters are very shallow and have a high damaging potential as reflected by the high number of fatalities and widespread destruction during historical earthquakes. It is noteworthy that NAB's CCPP Pallatanga fault segment, to the SW of the Interandean Depression, and which was broken by the 1797 event –one of the largest historical crustal earthquakes in South America (Baize et al., 2014) with a death toll between 15000 and 30000 (Egred, 2000)–, exhibits very little seismic energy release during the catalog's instrumental time span (Fig. 2a). Historical earthquakes will be addressed in more detail when discussing individual source zones.

## **1.2 Consequences of the oblique convergence along the convex continental margin of northwestern South America**

Subduction of oceanic plates is a complex geodynamic process responsible not only for the release of more than 90% of the total seismic moment globally, but also for most of the first-order tectonic features that characterize continental plates at convergent margins. It has been recognized that along-strike variations in the margin geometry, such as convexity and concavity, have effects on the shape and stress field in the descending slab (Bevis, 1986) and on the stress regime and the strain pattern in the upper plate (e.g. Bonnardot et al., 2008). Additionally, the resulting obliquity of the convergence leads to partitioning of the convergence vector in its thrust and shear components that are perpendicular and parallel to the trench, respectively

(McCaffrey, 1993). The parallel-to-the-trench component may give rise to the development of large continental faults in response to continental block movements.

### ***Subduction along a convex margin***

As observable in Fig. 1, the trench displays a great curvature at the equatorial latitudes, giving rise to complexities in the geometry of the slab (Barazangi and Isacks, 1976; Bevis and Isacks, 1984a; Bonnardot et al., 2008; Cahill and Isacks, 1992; Heuret et al., 2007; Isacks and Barazangi, 1977). Therefore, different subduction angles and geometries should be expected along the strike of this convex margin. The new global subduction plate geometry model –SLAB 1.0–(Hayes et al., 2012) describes the 3-D shape of the down-going slab underneath South America. SLAB 1.0 reproduces very well the wider flat slab geometry described by several authors in central and northern Peru up to Lat.  $\sim 4^{\circ}\text{S}$ . (Cahill and Isacks, 1992; Tavera and Buforn, 2001) Farther north it models a gentle change of the Benioff zone to steeper dipping angles in central Ecuador. However, insufficient data make it difficult for the model to fit the true subduction interface in a narrow region of complex geometry based upon worldwide seismic catalogs (see Fig. 6a in Hayes et al., 2012), which is the case for central and northern Ecuador. Therefore, in order to model intermediate-depth seismic source zones, we have reviewed the literature and carried out an independent analysis of a more comprehensive set of seismicity data supplied by local networks (Beauval et al., 2013), in order to recognize and identify potential shapes and boundaries of plate segments along the subduction.

### ***Slab geometry from south to north as given in the literature***

In Central Peru (Lat.  $\sim 10^{\circ}\text{S}$ ), the Nazca plate is subducting with a gently dipping angle that increases to  $30^{\circ}$  until it reaches  $\sim 100$  km depth; then the plate becomes almost horizontal for distances of  $\leq 500$  km from the trench (Barazangi and Isacks, 1976; Cahill and Isacks, 1992; Jordan et al., 1983; Stauder, 1975; Suarez et al., 1983). This pattern is also found in northern Peru

between  $\sim 4^{\circ}\text{S}$  and  $\sim 8^{\circ}\text{S}$ , where the Nazca plate initially dips beneath the continent at a  $10^{\circ}$  angle, then dives with a steeper angle until the slab reaches depths of  $\sim 130$  km, and then it flattens out (Tavera and Buforn, 2001). Local seismicity studies (Tavera et al., 2006) helped to determine these subduction angles to  $10^{\circ}$  and  $28^{\circ}$ , respectively, measured along cross sections oriented  $\text{N}70^{\circ}\text{E}$ , but did not recognize the flat slab portion.

In south-central Ecuador, between  $4^{\circ}\text{S}$  and  $1^{\circ}\text{S}$ , the Nazca plate undergoes a sharp contortion similar to that observed in southern Peru where there is a southward transition from a flat to a normal ( $30^{\circ}$ ) plunging slab at Lat.  $\sim 15^{\circ}\text{S}$  (Cahill and Isacks, 1992; Hasegawa and Sacks, 1981). First Pennington (1981) and later Bevis and Isacks (1984a) and Hall and Wood (1985) proposed a sharp flexure of the subducted Nazca plate beneath Ecuador associated with the Carnegie ridge. Chen et al. (2008) statistically analyzed along-strike dip variations of the subducted Nazca plate from Lat.  $1^{\circ}\text{N}$  to  $3^{\circ}\text{S}$  using focal mechanisms of intermediate-depth earthquakes given in Harvard's CMT catalog (Dziewonski et al., 1981). They determined that the slab is dipping at  $20^{\circ}$  and has a general strike of  $\text{N}300^{\circ}$ . This averaged strike represents a counterclockwise  $\sim 45^{\circ}$  rotation as compared to the  $\text{N}345^{\circ}$  strike found for the subducted slab southwards of Lat.  $5^{\circ}\text{S}$ , using focal mechanism solutions. This is interpreted as a sharp flexure of the descending slab (Tavera et al., 2006).

Instead of favoring the contortion or flexure of a coherent slab Gutscher et al. (1999) postulated that the oceanic lithosphere is torn along the Grijalva *scarp or fracture zone [sic]* due to the buoyancy of the adjoining slab segment to the north, which carries the Carnegie ridge. For them, this segment corresponds to a flat slab that is also bounded to the north by a series of tears arranged in steps from Lat.  $1.5^{\circ}\text{N}$  to  $3^{\circ}\text{N}$ . For this same segment, several authors propose that the slab is subducting eastward at  $25^{\circ}$  to  $35^{\circ}$  dip angles (Guillier et al., 2001; Hall and Wood, 1985; Manchuel et al., 2011; Pennington, 1981; Pontoise and Monfret, 2004; Taboada et al., 2000), whereas others conceive dipping planes up to  $50^{\circ}$  (Pedraza et al., 2007).

These differences concerning the general shape, orientation, dip, and proposed tears of the Nazca plate and of its predecessor, the former Farallon plate, are fueled by the given interpretation about the role that the Carnegie ridge plays in the subduction process and even in many superficial characteristics of Ecuadorian geology since the mid-Miocene (Michaud et al., 2009). From 2°S to 0.5°N the presence of such a bathymetric relief is appealing (Fig. 1) and the age of collision, inland penetration, buoyancy and coupling have different levels of influence on the down going and upper plates (Cloos, 1993). Nevertheless a closer look at the available information downplays the role of Carnegie. Local microseismicity studies (Guillier et al., 2001; Manchuel et al., 2011; Pontoise and Monfret, 2004) have contradicted the flat subduction hypothesis (Gutscher et al., 1999). Michaud et al. (2009) conclude that there is no need for tears in the plunging slab to explain the anomalous geochemical (adakitic) signature of volcanoes in the broad Ecuadorian volcanic arc. Furthermore, they consider that there is no clear deformation in the continental realm linked solely to the arrival and later subduction of the Carnegie ridge, either on the coastal plains or in the Cordillera.

Finally, at the northern end of our studied area, several authors (Taboada et al., 2000; Vargas and Mann, 2013) have recognized the so-called Caldas tear at Lat. 5.6°N (not in our figures). At this latitude there is a 240 km offset of the intermediate depth seismicity to the east related to the presence of two very distinct slabs, the shallow-dipping Panama indenter to the north and the normal-dipping Nazca plate to the south (Taboada et al., 2000). South of the Caldas tear, from 5.6°N to 2°N, the Nazca plate is subducting at 30°-40° to the east (Vargas and Mann, 2013). The intermediate depth seismicity disappears southwards of Lat. ~2°N. We observe that the disappearance of this seismicity to the south coincides with the inland projection of the fossil Malpelo rift spreading center (Fig. 1) (Lonsdale, 2005).

***Relocated Intermediate depth seismicity as a key to interpret moment release, shapes, and dipping angles***

Let's now look at the intermediate depth seismicity distribution in order to elucidate the moment release, shape, and dipping angles of the Nazca and Farallon slabs from the perspective of the newly published catalog (Beauval et al., 2013; Font et al., 2013a). Intermediate depth earthquakes (hypocentral depths between 50 km and 300 km) have very distinct distributions in northern and southern Ecuador (Fig. 2b). Seismicity is bounded by the inland projection of the Grijalva rifted margin, an aspect that was not recognized by previous authors.  $M_w \geq 6$  earthquakes have not been recorded between this projection line and Lat. 2°N during the 110 years of catalog coverage. Intermediate depth seismicity is almost exclusively located south of the Grijalva projection, implying a strong control of the intermediate depth seismicity by differing mantle rheology of the older Farallon plate to the south and the younger Nazca plate to the north.

A clear alignment of sizable earthquakes is also apparent along a narrow 600 km long NNW-SSE band in the Farallon plate, stretching from Lat. 1.5°S to 6.5°S (Fig. 2b). Six of them show  $M_w \geq 7$  with depths ranging from 120 to 200 km. The moment release everywhere else in the subducting slab is secondary to this seismic strip, which may be related to the transition from a flat to a much steeper angle of the slab, as modeled in SLAB 1.0 (see Fig. 7a in Hayes et al., 2012). The northern termination of the strip is marked by a conspicuous concentration of earthquakes around Lat. 1.5°S, Long. 77.8°W, which have hypocentral depths ranging from 130-210 km and have had a maximum  $M_w$  7.1 (2010). We name this concentration hereafter as the El Puyo seismic cluster (Fig. 2b).

In Fig. 3 we present all the focal mechanism solutions (depth 50-300 km) obtained from the Harvard Global Centroid Moment Tensor catalog (Dziewonski et al., 1981). Normal-faulting focal mechanisms are ubiquitous in the Farallon down-going slab. Nodal plane's strikes show a remarkable parallelism with the direction of the magnetic anomalies offshore (Fig. 3), suggesting that gravity

driven stretching of the subducted oceanic lithosphere is tearing the plate along the inherited fabric. If this is the case, the  $\sim 20^\circ$  counterclockwise rotation in the nodal planes' strikes observed in El Puyo seismic cluster (Fig. 3) and the hypocentral deepening as shown in Fig. 2b should be related to the bending of the subducted lithosphere. The east-dipping slab of northern Peru begins flexing at about  $3^\circ\text{S}$  and after  $\sim 100$  km of horizontal distance it begins to dip to the northeast towards the El Puyo cluster. The slab bending may be responsible for concentrating stresses that trigger the intermediate depth seismicity in the cluster. The details of the shape and complexities of the bending slab are

F3

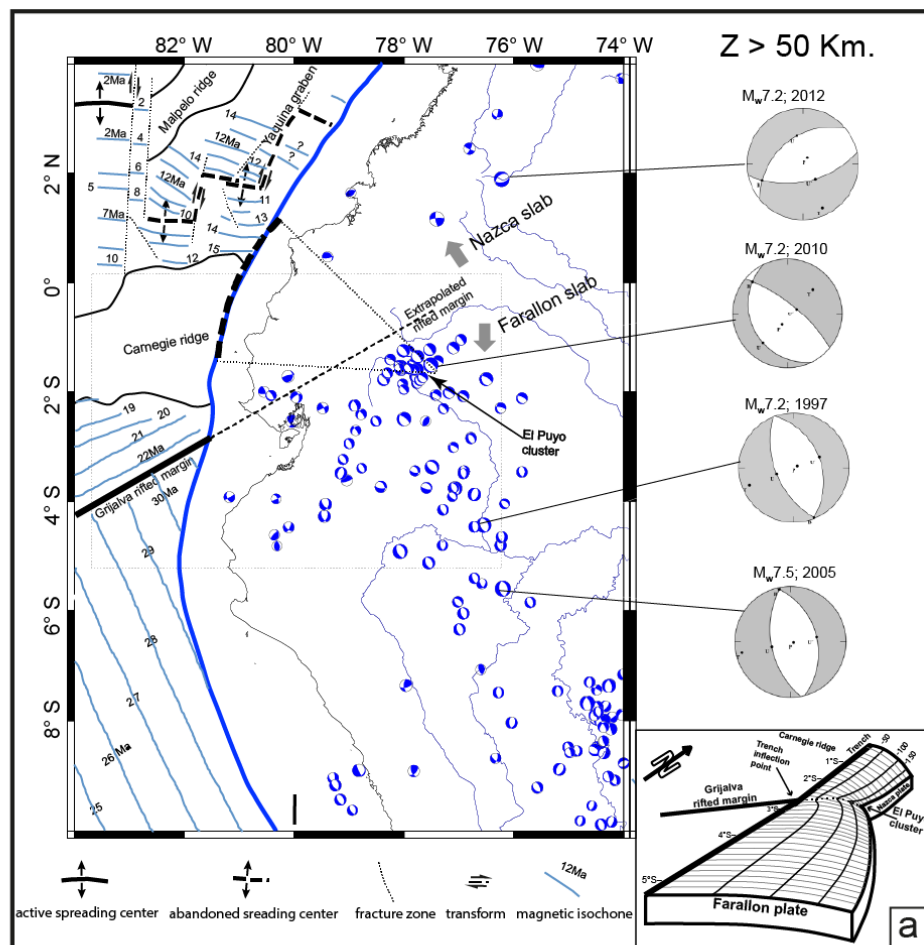


**Fig. 3. Focal mechanisms for intermediate depth earthquakes ( $55\text{km} < Z \leq 300$  km)** obtained from the Harvard Global Centroid Moment Tensor catalog Dziewonski et al. (1981) from 1976 to 2013. The Grijalva rifted margin northeastern prolongation (thin hachured line) constitutes a sharp boundary for intermediate depth seismicity which is sporadic north of it. Focal mechanisms for the four largest events have been highlighted. Notice the along-strike counter-clock rotation of fault plane azimuths from south to north in the Farallon plate. The thick hachured line at the trench show a circle's arch centered at El Puyo cluster (see the text for explanation). Offshore lines represent magnetic isochrones modified from Lonsdale (2005). Associated numbers are crustal ages in million years. **a.** Sketch showing internal flexure of the subducting plates. The margin convexity (concavity from the perspective of the continental plate) forces the slab to flex and shorten at depth. The trench axis inflection point coincides with the present day position of the Grijalva rifted margin at the trench. The light dotted rectangle in the main figure depicts the sketched portion of the subduction.

beyond the scope of the present work, but a schematic drawing has been attempted to help visualize the structure and the possible depth iso-contours of the subducted plates (Fig. 3a).

In order to explore the slab's dipping angles across the Nazca-Farallon boundary, four 50 km wide cross-sections with azimuths parallel to the Nazca plate's convergence direction are shown in Fig. 4. Sections A-A' and B-B' include hypocenters exclusively located in the Nazca plate while section D-D' corresponds to events in the Farallon plate; the remaining section C-C' has events in both (Fig. 2b).

Two aspects clearly stand out in cross section A-A and B-B' (Fig. 4) and in Fig. 2b. Inslab Nazca plate seismicity is not observable below the Ecuadorian volcanic arc, stopping abruptly about 240 km east of the trench, and is not deeper than 140 km. There is only a conspicuous small volume-small energy seismic cluster at 0.9°S, 79.1°W in section B-B' –named here La Maná cluster– with magnitudes  $M_w < 4$ . The almost complete absence of seismicity below the Ecuadorian volcanic arc precludes us from proposing a dip for the younger Nazca plate from cross section A-A' below central and northern Ecuador by looking exclusively at the recorded earthquakes. The fact that active volcanism is present above the aseismic segments indicates that the plate continues to dip eastwardly. As Syracuse and Abers (2006) point out, it has been extensively discussed in the literature that the top of the slab below the front arc volcanoes is at a depth of roughly 100–120 km and that this depth is the same for all subduction zones, regardless of slab dip and plate age (Davies and Stevenson, 1992). If these values hold for the Ecuadorian front arc volcanoes, the young Nazca plate should be dipping at about 20°, if the upper earthquakes of La Maná cluster were used along with the mentioned depth to define the slab top as seen in section B-B' (Fig. 4). By analogy, Nazca is probably dipping with the same angle below the active volcanic arc in northern Ecuador and southernmost Colombia (section A-A', Fig. 4). The lack of seismicity is probably related to the age of this subducted portion of the Nazca plate, since in young plates intermediate depth seismicity is largely absent (Syracuse and Abers,

F4

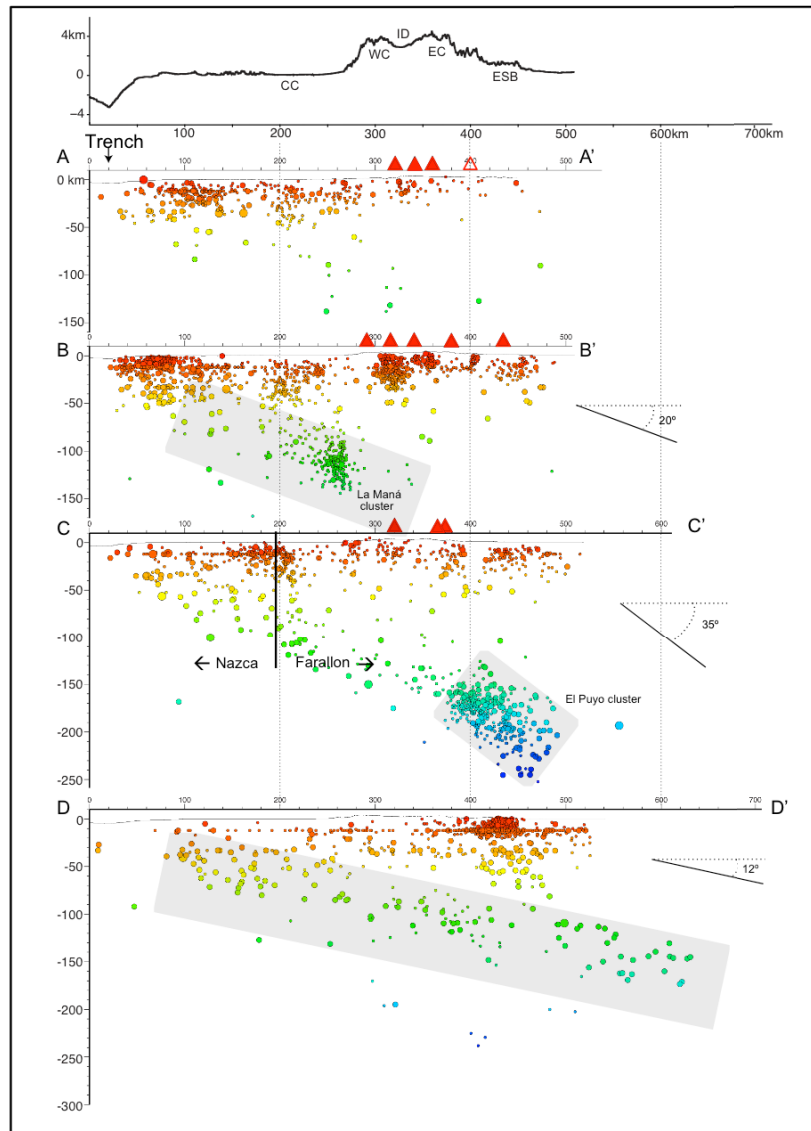


**Fig. 4. Vertical cross sections (50 km-wide) showing instrumental seismicity.** Seismicity is from Beauval et al. (2013). Cross sections location is marked in Fig. 2b. Colors reflect hypocentral depth. Solid triangles are active late Holocene volcanoes; open triangles are Holocene dormant volcanoes. The vertical line in cross section C-C' shows the approximate contact between Nazca and Farallon plates. The shaded areas capture the general dip of the plate or of portions of it distinguishable through seismicity: for B-B' the dipping angle is obtained using magma generating conditions (see text); for C-C' the angle reflects El Puyo cluster apparent dip as result of plate contortion; for D-D' the general dipping trend of tearing seismicity inside the plate has been measured. The upper topographic profile shows a generalized topography for Ecuador north of Lat. 2°S. CP=Coastal Cordillera; WC=Western Cordillera; ID=Interandean Depression; EC=Eastern Cordillera; ESB=Eastern Sub-Andean Belt.

2006). Earthquakes with  $M_w > 6$  only reappear north of 2°N although they are far less abundant than in the older Farallon plate (Fig. 2b).

Immediately south of the Grijalva rifted margin, i.e. in the Farallon plate domain, inslab seismicity in section D-D' indicates a gently dipping slab (~12°)

that can be traced for more than 600 km inland (Fig. 4). This dip differs from the  $28^\circ$  angle reported by Tavera et al. (2006) 200 km to the south. Seismicity in section C-C' cannot be interpreted as a single slab profile, since it comprises events from both Nazca and Farallon plates. Besides, the El Puyo seismic cluster is part of a contorted portion of the older slab and is anomalously deeper than the rest of the Farallon slab directly to the south (Figs. 2b, 4). The Nazca dipping angles mentioned above in the literature review are thus systematically overestimated, once the El Puyo cluster is included as part of the Nazca plate seismicity.

Here we analyze the location of the El Puyo seismic cluster in relationship with the convex Ecuadorian margin. It is surprising that the horizontal distance from El Puyo cluster to any point along the trench for approximately 350 km, from  $\sim 1.3^\circ\text{S}$  to  $\sim 1.3^\circ\text{N}$ , varies only five per cent. Thus, the curving trench describes an almost perfect circle's arch centered upon the El Puyo cluster as drawn in Fig. 3. Any slab's dipping angle determined from cross-sections perpendicular to the trench along these latitudes will be invariant. Those cross-sections intersect the inland prolongation of Grijalva ridge, thereby creating a false spatial association between shallower Nazca plate earthquakes at the trench with intermediate depth Farallon plate earthquakes at the El Puyo seismic cluster to the east (cross section C-C', Fig. 4). This in turn defines an apparently continuous slab with dipping angles around  $25^\circ$ . Consequently, we consider that hypocenters in the El Puyo seismic cluster should not be associated with eastward-dipping Nazca plate interface events for slab description purposes, but should be treated separately.

### ***Oblique convergence tectonics***

In the context of convexity of the northwestern South American margin and the subsequent oblique convergence, in Figure 5 we have compared obliquity with the trench azimuth and with fault plane strikes of interface earthquakes. We observe that the total change in obliquity is about  $60^\circ$  in the 1200 kilometers from  $2^\circ\text{N}$  to  $10^\circ\text{S}$ . Perpendicular convergence is taking place at around Lat.  $5^\circ\text{S}$  where null partitioning is expected. North of  $5^\circ\text{S}$ , i.e. in Ecuadorian territory,

there is a gradual, northward increase in obliquity that reaches its maximum value north of the Carnegie ridge. In Peru, south of Lat. 5°S, the trench rapidly assumes a southeasterly direction and obliquity is negative, remaining invariant south of the Mendaña fracture zone (Fig. 5).

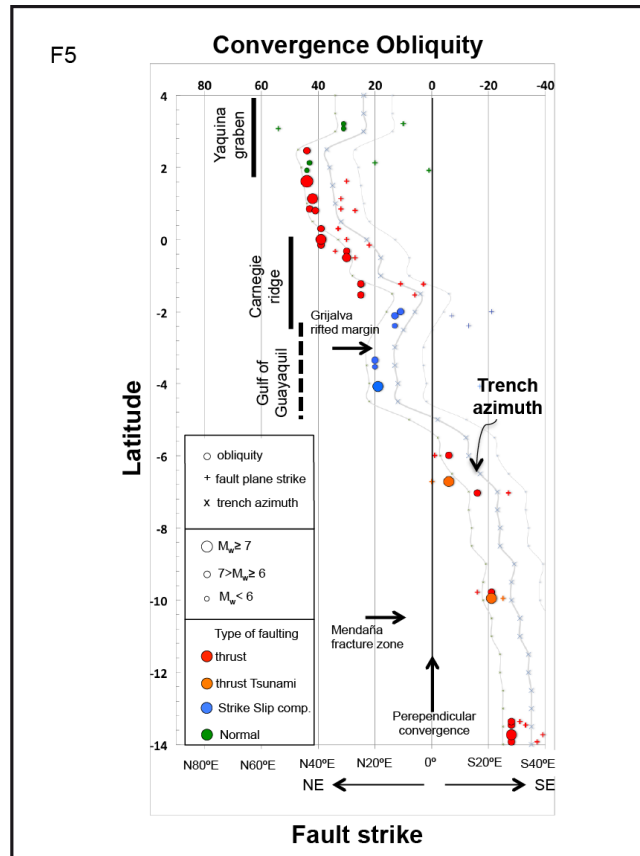


**Fig. 5. Convergence obliquity.** Circles represent obliquity values calculated at each epicentral latitude for  $M_w \geq 6$  earthquakes. Plus signs represent ruptured fault plane strikes obtained from focal mechanisms assuming the most probable fault plane candidate. We have used the Harvard focal mechanisms catalog (<http://www.globalcmt.org>) from 1976 to 2013. Colors indicate focal mechanism. Tsunami events are highlighted, but they also correspond to thrust events. Light gray lines are the trench azimuth (crosses)  $\pm 10\%$  error. Notice the good agreement between faults strike and trench azimuth for thrust interface events. Some  $M_w < 6$  earthquakes have been included to show lack of agreement for non-interface events such as the Yaquina graben normal and the Grijalva rifted margin strike slip events.

Both partitioning and coupling transfer the trench-parallel shear stresses to the continental crust, thereby inducing northeastward motion of the fore-arc north of the Gulf of Guayaquil and southeastward movement south of it. Partitioning reaches similar levels at around 20-25% in both domains (Nocquet et al., 2014). As a result of this, the NAB is moving as a rigid block towards the northeast while a newly defined continental sliver –the Inca sliver proposed by

Nocquet et al. (2014)– is moving to the southeast (Fig. 1) and prompting the opening of the Gulf. Based upon observed GPS data and the geodetic velocity field in Ecuador (Freymueller et al., 1993; Nocquet, 2009; Trenkamp et al., 2002; White et al., 2003), general consensus is achieved on  $\sim 7 \pm 2$  mm/a northeastward motion of the NAB relative to South America (Egbue and Kellogg, 2010; Nocquet et al., 2014; Nocquet, 2009).

In Ecuador, the NAB translation takes place along a narrow corridor of crustal deformation –the Chingual-Cosanga-Pallatanga-Puna (CCPP) transpressive right-lateral system– that sharply determines the limit of the block with the rest of stable South America (Alvarado et al., 2015; Ego et al., 1996b) (Fig. 6) and is the loci of large earthquakes (Baize et al., 2014; Beauval et al., 2010). Soulas et al. (1991), based on morphodynamic analysis, were the first to depict these four major active fault sub-systems and their deformation rates in continental Ecuador. Several authors (Alvarado et al., 2015; Baize et al., 2014; Dumont et al., 2005; Ego et al., 1996a; Fiorini and Tibaldi, 2012; Lavenu et al., 1995; Tibaldi et al., 2007; White et al., 2003; Winter et al., 1993) have described in further detail various aspects of the fault systems and given different tectonic interpretations, but the first proposed picture remains unchanged.

By contrast, in southern and central Colombia convergence obliquity decreases rapidly (Fig. 5) and internal deformation in the block appears, all related to the complex interaction of three plates: the Paleo-Caribbean, Nazca, and South American plates (Ego et al., 1996b; Taboada et al., 2000). Major strike-slip faults resulting from this deformation, such as the Cauca-Patía and Romeral fault systems, run parallel to the NNE-SSW striking Andes. This faults trend turns to a N-S orientation from Lat.  $\sim 0^\circ$  to the south and adopts a reverse dip slip movement (Ego et al., 1995) (Fig. 6), joining the NAB boundary in central Ecuador. In northern Ecuador the NNE-SSW strike-slip faults of El Angel belong to this first order tectonic structure (Ego et al., 1995; Taboada et al., 2000).

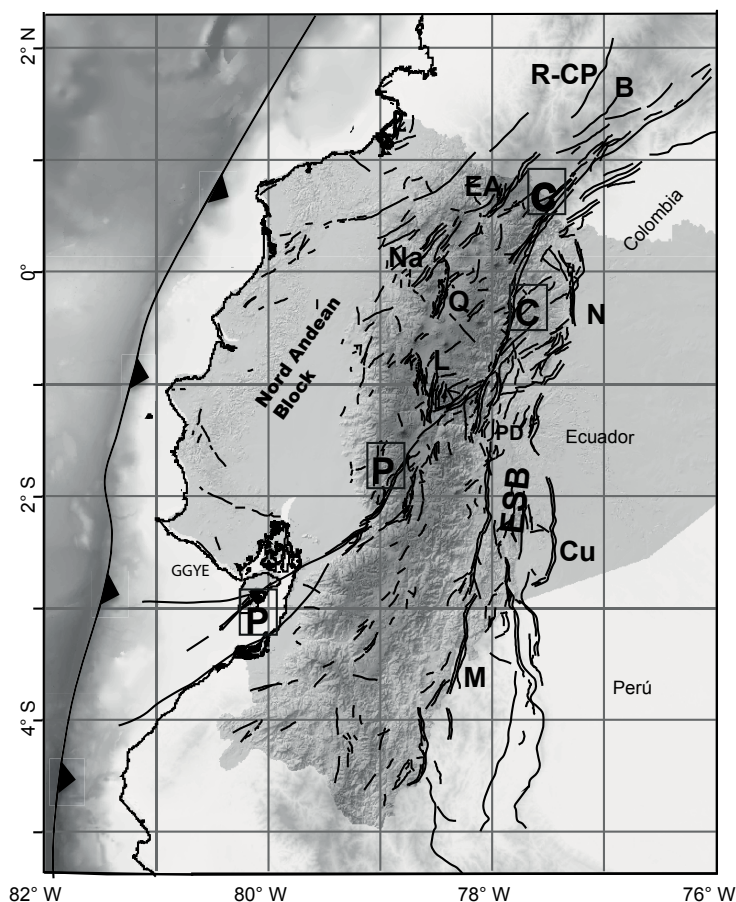


**Fig. 6. Main crustal fault systems in Ecuador** (modified from Alvarado et al. 2014). Thick continuous lines: North Andean Block east boundary –CCPP– composed by four major transpressive segments from NE to SW: C= Chingual, C=Cosanga, P=Pallatanga, P=Puna. The type of faulting is determined by faults' orientation and is mainly right-lateral strike-slip and reverse. The thick-dotted line represents the northeastward continuation of the system not modeled for this study. Double-dotted-dashed lines: Eastern Sub-Andean thrust-and-folds Belt –ESB– divided in two main uplifts: N=Napo and Cu=Cutucu separated by the PD=Pastaza Depression. The M=Macas fault system is considered to be part of ancient tectonic systems that may have been reactivated by present day tectonics. All three families show compressional deformation. Dashed lines: The Quito-Latacunga fault system –Q-L– is related to blind thrusts separated in two main segments: Q=Quito and L=Latacunga. Reverse faulting is dominant throughout the system. Single-dotted-dashed lines: The El Angel fault system –EA– comprises a series of right-lateral strike-slip faults and could be part of the Romeral-Cauca Patía major fault system in Colombia – R-CP (thin-dotted line). Parallel segments go from B=Buesaco to Na=Nanegalito. Three-dotted lines: Low angle detachment normal faults in the Gulf of Guayaquil (GGYE) continental margin. Thin lines are the complete inventory of cataloged faults, folds and lineaments Egüez et al. (2003).

To the east and southeast of the NAB–South America boundary, shortening across the active Andean back-arc is taking place along the easternmost thrust-and-fold belts (ESB) (Bès de Berc et al., 2005; Ego et al., 1996b) i.e. the Napo and Cutucu uplifts, and along thrust faults on the eastern

slopes of the Eastern Cordillera, such as the Macas fault system (Alvarado et al., 2015) (Fig. 6). The belt's N10 general direction is approximately parallel to the trench between Lat. 1°S - 5°S, where obliquity is smaller (Fig. 5). This favors thrust faulting due to a larger trench-perpendicular partitioning of the plate movement than that to the north. The Southern Ecuador - northern Peru Andes seem to be entirely included in the Inca sliver, if its boundary lies along the thrust-and-fold belts as proposed by Nocquet et al. (2014). The sliver shows a fairly constant 4.5-6.0 mm/a southeastward motion between latitudes 3°S and 10°S (Fig. 1), but a major, single, continental size structure that takes up most of the deformation has not been identified yet, as is the case with the NAB.

To the west of the NAB boundary, moderate historical earthquakes ( $M_w \leq 6$ ) are associated with thrust faults concentrated along the western internal slopes of the Interandean Depression from Lat. 0.5°N to 1.7°S, collectively known as the Quito-Latacunga fault system (Fig. 6) (Alvarado et al., 2014; Beauval et al., 2010; Ego et al., 1995). At these latitudes convergence obliquity rapidly decreases from north to south (Fig. 5) promoting a compressional environment. The Depression is a compressional basin ('push-down' type) bounded by N-S trending reverse faults which have been active since the Miocene at a shortening rate of  $1.4 \pm 0.3$  mm/a. Lavenu et al. (1995) and Alvarado et al (2015) postulate that these faults are related to internal deformation of the NAB at a rate of 1 to 4 mm/a. North of Lat. 0° newly described strike-slip faults by Alvarado et al. (2014) could be transferring the regional strain from the compressive Q-L faults to CCPP's Chingual strike-slip faults or to the Romeral – Cauca-Patia fault systems in Colombia as part of a major transpressive dextral zone proposed by some authors (e.g. Ego and Sébrier, 1996; Ego et al., 1995; Taboada et al., 2000), Fig. 6).

## **2. CONSTRUCTION OF A NEW SEISMIC SOURCE ZONES MODEL FOR ECUADOR**

Our new interpretation of the geodynamic and seismotectonic scheme for Ecuador is fundamental for defining the new seismic source model presented here. The model comprises the area from 4°N to 6°S and from 75°W to 82°W

and covers Ecuador and the southern part of Colombia and the northern part of Perú.

In this section we describe 19 seismicity source zones (SSZ) –three interface, six inslab, nine crustal and one outer-trench zones. Each SSZ has a homogeneous seismogenic potential, containing all  $M_w \geq 5$  cataloged events. Interface and subducting inslab sources are bounded by limits that reflect, as much as possible, physical features in the subducting plates that could condition earthquake generation and/or rupture propagation in agreement with the geodynamic model. On the other hand, crustal sources are described by the main tectonic structures and by the shallow seismicity related to brittle fracture in the crust. We have also defined small complementary SSZ –all of them below the main interface zones– as a means of grouping left-outside seismicity spatially related to the interface SSZs. This seismicity may reflect inaccuracies in hypocentral locations or tectonic complexities not included in the main zones. We let practitioners the option to include it in the sources or to treat it as background seismicity.

In the following pages we briefly describe the criteria used to define and limit the seismic sources. Schematic descriptions, parameters, and boundaries for each source zone are provided as Table 1 in the Electronic Supplement. For each tectonic domain we provide further details on some of the most significant sources in each tectonic domain, chosen as typical examples of the applied approach. The criteria include morphotectonic aspects and/or neotectonic and structural features as well as seismic, geodetic, paleoseismic, and other geophysical factors. Every historical earthquake reported in Beauval et al. (2010) is correlated with a specific source zone. To each source zone, a predominant focal mechanism is defined. Focal mechanism solutions of instrumental earthquakes are analyzed, obtained either from the Harvard Centroid Moment Tensor (CMT) catalogue (Dziewonski et al., 1981) or from specific individual studies. If different types of focal mechanisms are present in the same source zone, all of them are shown in Table 1, but only one kinematic style is identified as predominant. The main faulting style reflects

structural/tectonic evidences collected in the literature or from our own field observations. Simple statistics related to hypocentral data are used to obtain the mean depth for each source, and is presented in Table 1. The moment release density (Mo per unit volume normalized for 100 years) was calculated for each source as a way to have a first-hand approximation of their seismic activity and their sources were colored accordingly.

In Figures 7 and 10 we present schematic views of subduction and crustal SSZ respectively, with the names, codes, relative position of the sources and of the dominant structures. These schemes serve as a guide for identifying the sources in the following discussion.

### **2.1 Interface megathrust sources**

Along the Ecuadorian margin, interface sources encompass seismicity recorded from the trench to the downdip edge of the seismogenic zone. For great megathrust earthquakes such as the Esmeraldas 1906 event, this depth could reach to 45-55 km as observed in the Sumatra, Chile, and Japan mega-earthquakes during the 21<sup>st</sup> century (Lay et al., 2012). For the smaller  $M_w < 8$  events the interface rupture could reach depths around 35 km, according to the present interseismic coupling (Chlieh et al., 2014) (Fig. 7).

#### ***Esmeraldas SMT-1***

During the 20<sup>th</sup> century, four  $M_w$  7.6 to 8.8 thrust earthquakes repeatedly ruptured segments of a ~500 km long stretch of the subduction zone north of the Carnegie ridge (Fig. 8). For a comprehensive description of the NW Ecuador – SW Colombia 20<sup>th</sup> century large earthquake sequence, please refer to Chlieh et al. (2014).

The  $M_w$  8.8 1906 earthquake defines the Esmeraldas SMT-1 interface megathrust source zone. To look for possible boundaries for the southern limit of the 1906 rupture, several studies have been reviewed. Based upon so-called “*marginal evidence*”, Kelleher (1972) drew the southern termination of the great 1906 megathrust event at latitude 0°. Kanamori and McNally (1982), quoting

Rudolph and Szirtes (1911), suggested that the rupture zone did not extend farther south beyond Kelleher's limit, based on the intensity distribution.

F7

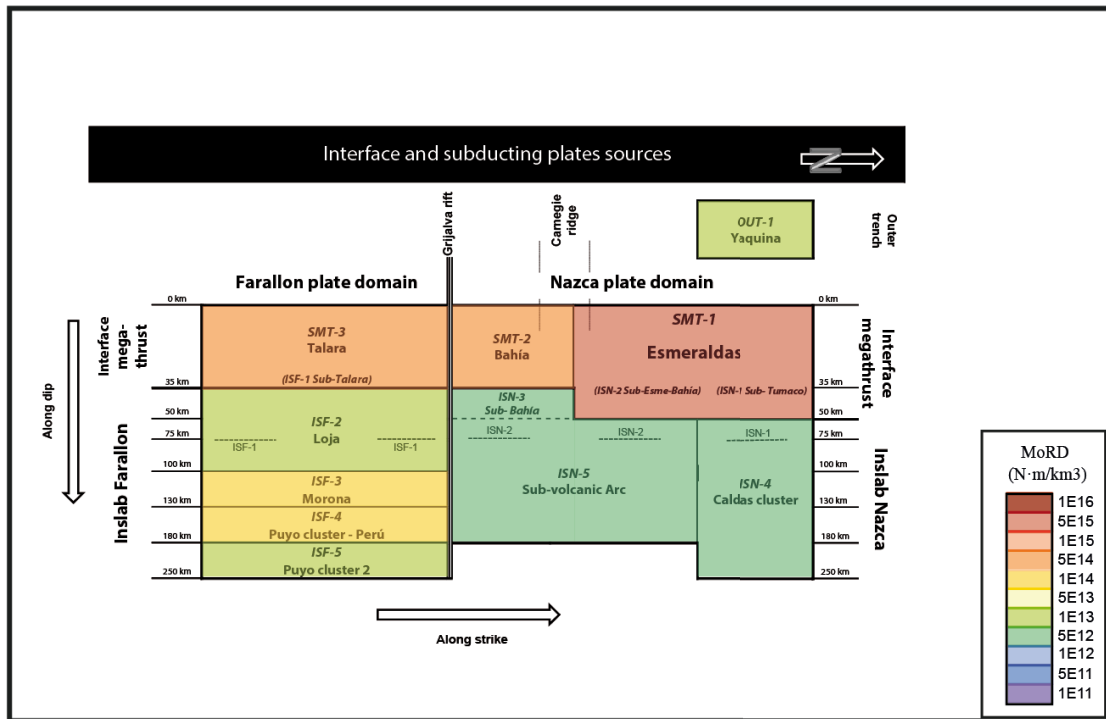


**Fig. 7. Schematic representation of interface and in-slab SSZs.** Along-dip and along-strike domains have been defined for interface and in-slab sources. Along-dip, the deeper portion of the megathrust seismogenic zone defines interface segments and separate them from in-slab sources. Along-strike, sources are defined by distinguishable intermediate depth seismicity distribution and earthquake focal mechanisms constrained by rheological conditions of the subducting plates. Older Farallon and younger Nazca plate domains are adopted, with the Grijalva rifted margin marking the separation between the two. SSZs are colored according to their Mo release density (MoRD).

Again, based on the relocation of aftershocks by Mendoza and Dewey (1984), Swenson and Beck (1996) suggested that it was unlikely that the 1906 rupture propagated south of  $0^\circ$ , by observing the 1942  $M_w$  7.8 aftershock zone and taking into account the presence of the Carnegie Ridge. Collot et al. (2004) proposed a different southern termination of the 1906 and 1942 earthquake rupture zones, coinciding with the offshore extension of the ancient Jama-Quininde fault and with the probable inland location of the Carnegie Ridge crest (approximately at Latitude  $0.5^\circ$ S). This limit is  $\sim 50$  km south of the previously

assumed limit (Fig. 8). From this review, it is clear that the 200 km wide Carnegie ridge constitutes a barrier for large Ecuadorian earthquakes to propagate southwards, similar to other subducting bathymetric features along the South American subduction zone (Bilek, 2010).

F8

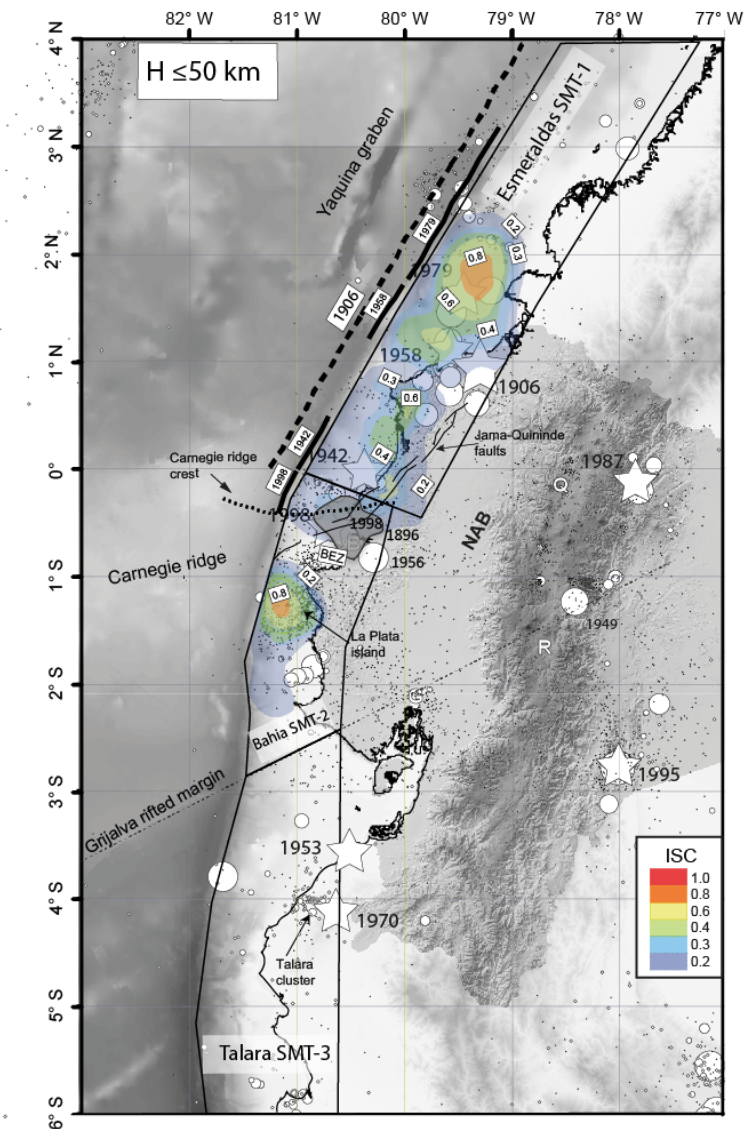


**Fig. 8. Interface seismogenic source zones.** The three sources are the outlined polygons. Continuous thick lines off the Esmeraldas trench represent the rupture length of  $M_w \geq 7$  earthquakes; the dashed line is for the 1906 earthquake rupture. Colored contours show distribution of the interseismic coupling –ISC– modified from Chlieh (2014). ISC values vary from 0 to 1. The dotted line is the proposed inland location of Carnegie ridge crest; thin lines are the traces of the ancient Jama-Quininde fault, both after Collot et al. (2004). BEZ=Bahía earthquakes zone comprising 1998, 1956 and 1896 events; the shadowed area corresponds to well located aftershocks for the 1998 earthquake. Circles and stars correspond to seismicity presented in Fig. 2a.

Let us further explore along the Carnegie ridge interface. There are three  $M_w \sim 7$  epicenters south of the 1906 and 1942 rupture zones, referred to hereafter as the Bahía earthquake zone (BEZ): the 1998  $M_w$  7.1; the 1956  $M_w$  6.95; and the 1896  $M \sim 7$  (assumed magnitude based on similarities with the other two events; this earthquake happened 10 years before the 1906 earthquake). Keller (2014) analyzed the intensity distribution of the 1896 earthquake applying the Bakun (2005) method, however it was not possible to provide an accurate location for the event due to shortcomings in the input data. Since the intensities of the 1896 event are distributed in a pattern similar to those of the 1998 event, including liquefaction, the rupture plane of this earthquake is assumed to belong to the BEZ. The BEZ as shown in Fig. 8 is defined by the well-located aftershocks from the 1998 main shock (Font et al., 2013). The southern limit of the 1906 rupture zone proposed by Collot (2004) falls in the middle of the 1998 event rupture plane. Considering the three earthquakes, the BEZ asperity is showing a characteristic behavior with a  $M \sim 7$  event every  $50 \pm 10$  years. Since the BEZ source seems to behave independently of the northern megathrust, the southern boundary of Esmeraldas SMT-1 is herein defined as the northern boundary of the BEZ (Fig. 8). South of the BEZ asperity the coupling model proposed by Chlieh et al. (2014) predicts a 50 km wide creeping corridor that could also have marked the southern limit of the 1906 rupture. In such a case the BEZ asperity would have also failed, and our interpretation would require a second scenario for the SMT-1 southern boundary.

With regard to the northern limit of SMT-1 ( $\sim 4^\circ\text{N}$ ), the Colombia trench abruptly changes its azimuth from NE-SW to  $\sim$ N-S. Buenaventura, a sea port at  $3.9^\circ\text{N}$  (Fig.1), still experienced 1.6 m of subsidence as a result of the 1906 rupture (Herd et al., 1981). However the rupture probably did not propagate north of the trench's sharp bend. At this same latitude, the Malpelo ridge rifting scarp could be projected inland (Lonsdale, 2005), which means that an across-strike discontinuity in the Nazca subducting slab could have stopped the northern propagation of the 1906 rupture. Therefore, we set the boundary at the discontinuity.

Up-dip and down-dip limits of the seismogenic part of the megathrust interface define the thickness of the EMS-1 seismic source zone. The 50 km boundary is defining the down-dip limit of the Esmeraldas SMT-1 zone. We consider that the up-dip limit reaches the trench, since all of the large and great earthquakes of the zone, except the 1942 event, have generated tsunamis.

The quality of the hypocentral solutions in the catalog does not help us to clearly differentiate between intraplate and overriding plate events. In an offshore and onshore passive seismic experiment, Manchuel et al. (2011) showed that at the Ecuadorian fore-arc region hypocentral depths reach at least 40 km but do not cluster along crustal active structures. On the other hand, it has not been possible to distinguish between offshore splay faults seismicity and interplate seismicity either, although Collot et al. (2004) proposed that the  $M_w$  7.6 1958 earthquake ruptured along one of these splay-fault structures and not at the interface. Therefore, for practical reasons, all the 0-50 km depth seismicity in the fore-arc is incorporated in SMT-1 and will be modeled as interface seismicity.

### ***Bahía SMT-2 and Talara SMT-3***

The SMT-2 Bahía source zone includes the BEZ and the highly coupled asperity of La Plata island (Chlieh et al., 2014; Vallee et al., 2012, Fig. 8). It is considered a transition zone linking the strongly locked SMT-1 with the SMT-3 Talara zone that shows weak to negligible interplate coupling. A 1000 km along-strike segment of the plate interface, comprising southern Ecuador and northern Peru, slips predominantly aseismically from the Gulf of Guayaquil to the Mendaña fracture zone at 10°S (Nocquet et al., 2014). The northern boundary of the Talara SMT-3 zone coincides with the inland prolongation of the Grijalva rifted margin (which separates the Farallon and Nazca domains) (Fig. 7, 8). The Talara SMT-3 zone could extend south at least until the prolongation of the Viru fracture zone in the continent (7.5°S, Lonsdale, 2005, Fig. 1), however it is artificially closed at 6°S, southern limit of our zoning.

The Talara SMT-3 could be considered a tsunami earthquake source due to its low coupling and to the occurrence of the rare 1960  $M_w$  7.8 tsunamigenic event (Fig. 2a). A second tsunami earthquake occurred in 1996 just north of Mendaña (Bilek, 2010) (Fig. 5), implying that ruptures in this segment could start at shallow depths and proceed up-dip, generating large slips but rather low frequencies, as described by Lay et al. (2012). In addition, two  $M_w > 7$  earthquakes belong to the Talara cluster's area ( $M_w$  7.6 1953,  $M_w$  7.2 1970, Fig. 8). The origin and precise depth distribution of the cluster is not well resolved. These large events could have ruptured the subduction megathrust (Suarez et al., 1983) or continental slope detachments in the Gulf of Guayaquil (Bourgois, 2013).

## **2.2 Inslab sources**

Inslab SSZs border intermediate depth seismicity. Notwithstanding that the seismic catalog used for this study contains the best available hypocentral locations, the seismicity is far from showing clear, neat Wadati-Benioff zones to define the shapes of individual segments in the Farallon plate. On the other hand, the Nazca plate is not prolific in generating intermediate depth earthquakes and the dipping slab can not be recognized solely from seismicity.

### ***Farallon ISF sources***

As hypocentral depth distribution and moment release vary along-dip inside the Farallon plate (Fig. 2b), four horizontal volumetric source zones of the inslab Farallon have been defined. The zones correspond to layers of seismicity of increasing depth towards the east and northeast (Figs. 7, 9). According to our model, apart from contortion, the plate is dipping gently ( $12^\circ$  on average) and is traceable eastwards for over 600 km from the trench (Fig. 4). Therefore, there is an overlap of the modeled sources, as observed on the map view of Figure 9.

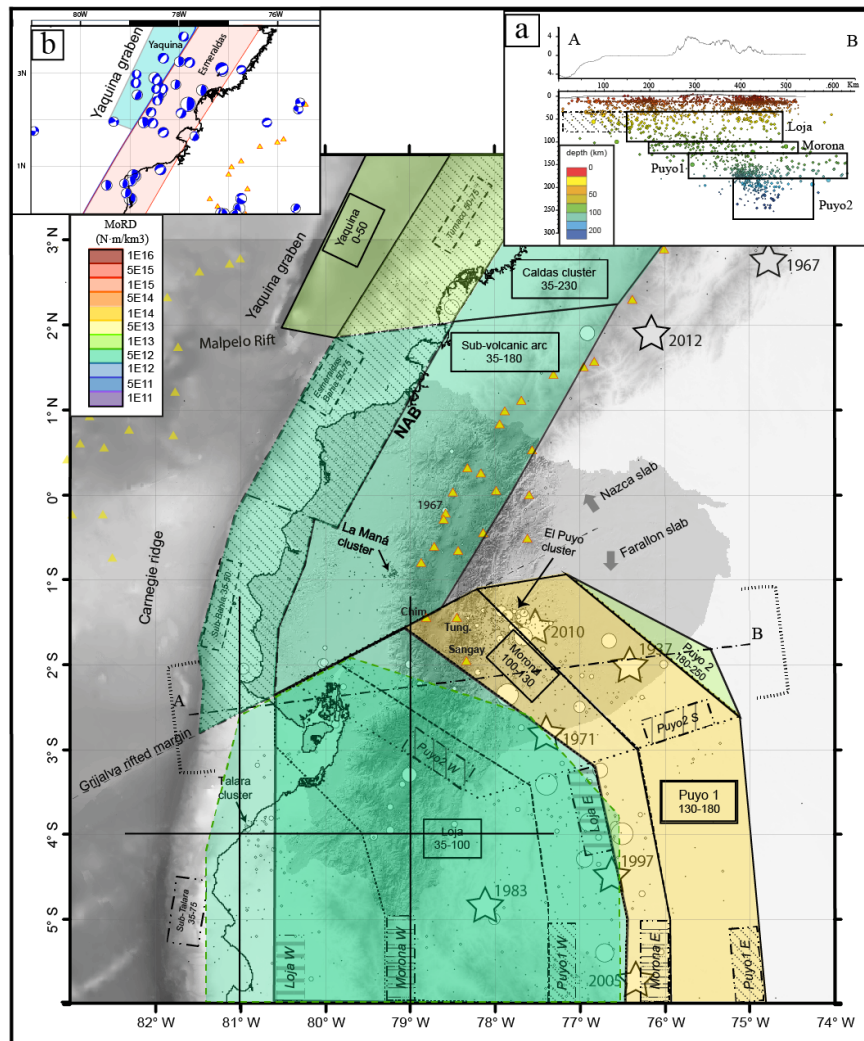


**Fig. 9. Inslab seismogenic source zones.** Seven in-slab SSZs have been defined along with four complementary sources (see the text for explanation). SSZs are colored according to their  $M_0$  release density (MoRD). Farallon slab zones are overlapped as seen in 9a. Only colors in the “visible” part of the plate in plan view are shown. They are identified by three labels: source zone name and depth range, western boundary (W) and eastern boundary (E). In the Puyo2 source, the southern boundary is shown. Nazca plate SSZs are not overlapped. Complementary zones below the interface SSZs are hatched. Yellow triangles are active late Holocene volcanoes. Circles and stars correspond to seismicity presented in Fig. 2b. **a.** A-B 150 km wide cross section in Farallon domain to show how plates overlap. **b.** Normal-faulting, shallow ( $Z \leq 50$  km) focal mechanisms related to the Yaquina graben extracted from the Harvard Global Centroid Moment Tensor catalog Dziewonski et al. (1981) from 1976 to 2013. Focal mechanisms correspond mainly to internal tearing. Outer trench bending is ruled out as the cause for normal faulting since dilatational focal mechanisms are obviously present east of the trench, where the slab is already plunging with normal angles and is not subjected to bending forces.

Most of the seismic moment is being released within two zones: a thin, 30 km thick layer –Morona ISF-3– at depths from 100 to 130 km due to slab flexuring as mentioned before, and at the El Puyo cluster –Puyo 2 ISF-5– (Figs.

2b, 9). By modeling Farallon subduction with thin horizontal sources, the total source volume has been reduced in comparison to modeling a 600 km wide and 200 km thick single body, thus aiming for a better representation of seismic distribution for upcoming PSHA calculations. A second possibility was to model this seismicity as single dipping parallelepiped, in which case all the details worked out in the first part of this paper would have been absorbed in one single volume. In any case, the impact of our decision to model horizontal sources can be weighted during the hazard calculations.

### ***Nazca ISN sources***

North of the Grijalva rifted margin, intermediate depth seismic moment release is very small in comparison to that of Farallon plate's (Figs. 2b, 3). The Sub-Volcanic Arc source, ISN-5, has been defined to include events located east of the interface megathrust and below the volcanic arc, although very little seismicity is generated in this warmer part of the subducting slab.

Intermediate depth seismicity is somehow more energetic north of  $\sim 2^{\circ}\text{N}$  (Fig. 2b) where it could be related to the normal dipping segment of the Nazca plate south of the Caldas tear ( $\sim 5^{\circ}\text{N}$ , Vargas and Mann, 2013). A second source ISN-4 is modeled, separated from the ISN-5 Sub-volcanic arc by the inland projection of the Malpelo paleo-rift (Fig. 10 in Lonsdale, 2005) (Figs. 1, 9).

A very conspicuous shallow seismicity is present between the Yaquina graben crest and the trench (Fig. 2a). Its seaward-trench location is anomalous and unique along the South American trench. The normal faulting focal mechanisms that characterize this seismicity are also anomalous, appearing west of the trench as well as in the interface megathrust source zone (Fig. 9b). This unusual seismicity is modeled as the OUT-1 Yaquina source zone (Figs. 7, 9).

## 2.3 Crustal sources

According to the description given for oblique convergence tectonics, crustal sources have been classified in three main domains: (a) the NAB east boundary domain that encompasses strike-slip and reverse faulting (accounting for the sliver's NNE movement); (b) the Romeral – Cauca-Patía domain (Fig.6) including the western Colombian Andes and the Ecuadorian Western Cordillera down to 1.5°S; and (c) the Andean back arc domain where east-verging fold belts on top of blind thrusts absorb shortening. A schematic representation and the geographical location of crustal source zones are shown in Figs. 10 and 11. In Table 1 greater detail about individual sources is presented and is complementary to the description below.

F10

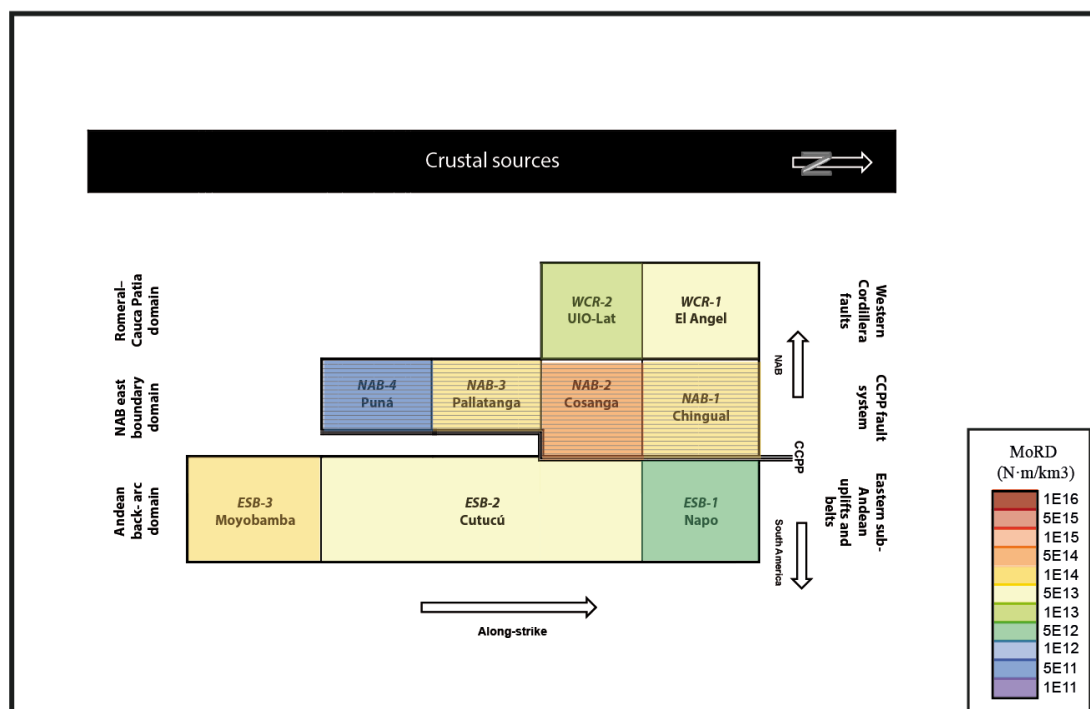


**Fig. 10. Schematic representation of crustal SSZs.** The North Andean Block (NAB) and South American Plate boundary is shown as the CCPP faults system. Shaded sources represent the boundary sources. SSZ are colored according to their Mo release density (MoRD).

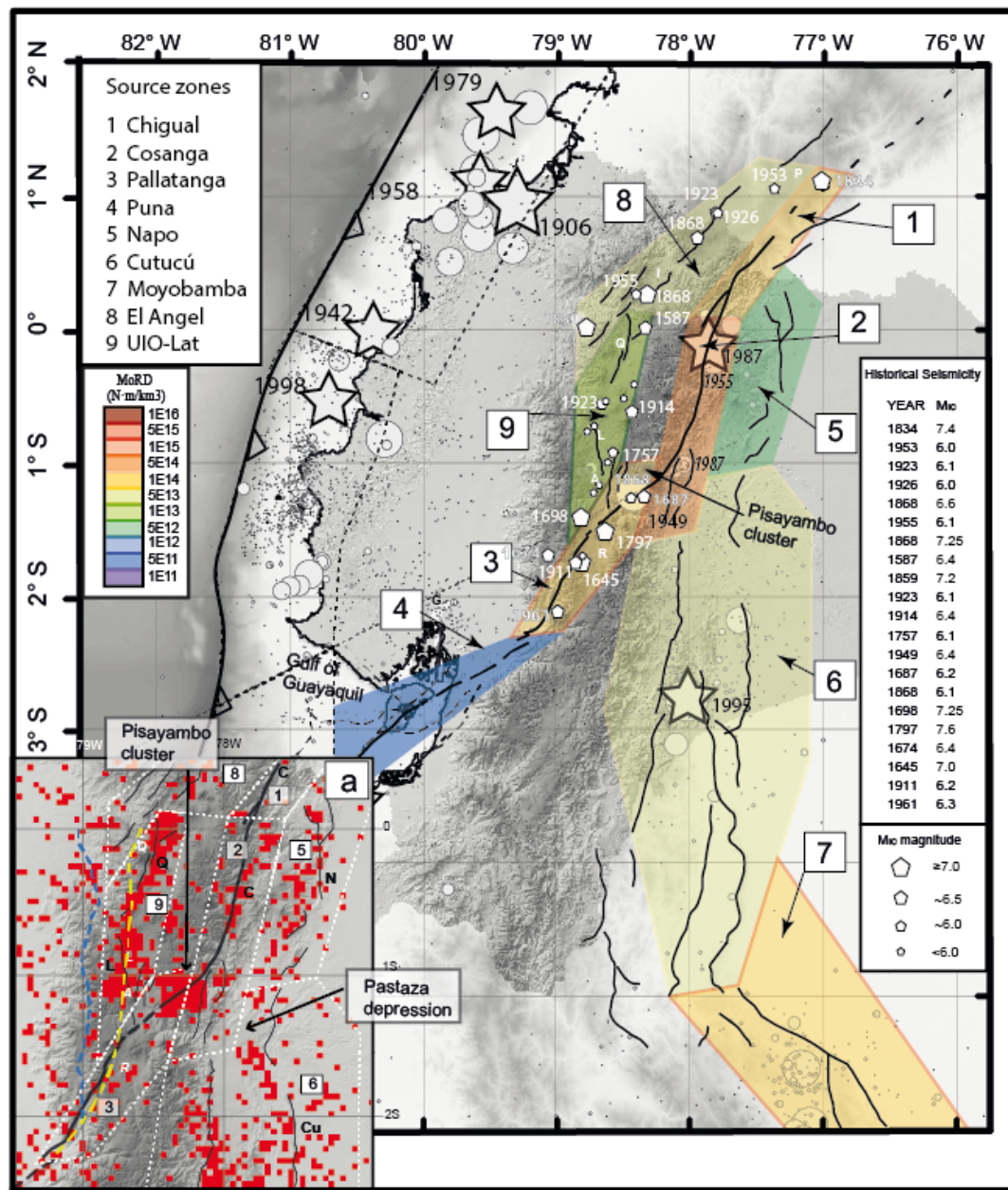


**Fig. 11. Crustal seismogenic source zones.** Nine crustal SSZs are defined. Polygons are colored according to the seismic moment release density MoRD for each source. Interface SSZs (hachured lines) have been included to show spatial relationship with crustal sources. The black continuous lines are main crustal fault systems shown in Fig. 6. Pentagons represent historical epicenters relocated by Beauval et al. (2010). Their sizes reflect magnitude classes.  $M_{ic}$  is the magnitude determined at the Intensity Center and is equivalent to  $M_w$ . White numbers are years when historical events occurred. Letters are main cities: I=Ibarra; Q=Quito; L=Latacunga; A=Ambato; R=Riobamba. **a.** Shallow seismicity ( $Z \leq 35$  km) moment release per unit area in the Interandean Depression. The instrumental catalog (1900-2009) is used (Beauval et al. 2013). The unit area is a  $5 \times 5$  km pixel, approximately equivalent to the rupture area of a  $M_w$  5.0 earthquake. Pixels are colored with a “saturation color” if the sum of all the seismic moments from events with epicentral location within the pixel reaches  $Mo \geq 10^{14} N \cdot m$ , which is close to  $M_w$  3.25. By this artifice it is possible to highlight the areas where microseismicity is occurring. The white-dotted polygons in **11a** are the SSZ. The yellow and blue lines are Pujili and Chimbo-Toachi sutures modified from Hughes and Pilatasig (2002). Numbers refer to the source zones listed in the upper left-hand corner.

### ***CCPP fault system***

The NAB east boundary includes four segments (Chingual, Cosanga, Pallatanga and Puná, Alvarado et al., 2015) and has been defined as the CCPP fault system (Figs. 6, 11). The CCPP shows general displacement rates on the order of  $7 \pm 2$  mm/a from published GPS results and 7.6 mm/a as an estimated mean geologic slip rate for the final part of the Pleistocene (Egbue and Kellogg, 2010). According to other authors (Tibaldi et al., 2007), those estimates could peak to  $11.9 \pm 0.7$  mm/a in the northernmost segment, also from geologic indicators.

The Chingual NAB-1 source has a NNE orientation and therefore is considered to be mostly of strike-slip nature (Fig. 11). We have placed its northern limit at the Sibundoy pull-apart (Soulas et al., 1991), but the fault system continues further north along the east Andean front (Ego et al., 1995; Tibaldi et al., 2007). In 1834 a  $M_{IC}$  7.4 earthquake (Beauval et al., 2013) destroyed the Sibundoy area, but very little seismic activity is recognizable along NAB-1 at present times (Figs. 2a, 11). The southern limit abuts with the next segment (NAB-2) at the zone where the CCPP fault system changes direction and runs parallel to the Andean chain

The Cosanga NAB-2 source is aligned  $N10^\circ$  (Fig. 11). The tectonic structures show mainly transpressive behavior. Its northern portion has experienced two  $M_w \sim 7$  earthquakes during the last 60 years (1955, 1987). The southern end has been drawn to include the southern termination of the Cosanga thrust (Bès de Berc et al., 2005) as well as  $M_w > 5$  earthquakes that show transpressive focal mechanisms (e.g. Sept 1987  $M_w$  6.3 event and March 1987 shock, both most likely on the same fault system). The Pisayambo seismic cluster (Fig. 11a) is not included in NAB-2.

The Pallatanga NAB-3 source contains both the Pallatanga fault and the Pisayambo cluster. The Pisayambo seismic cluster is a  $\sim 30 \times 30$  km zone where almost 35% of the instrumental seismic activity in the country is registered by the RENSIG (Segovia and Alvarado, 2009). Pallatanga is a

prominent strike-slip structure that diagonally crosses Ecuador's Western Cordillera, cuts the Interandean Depression, and then continues to the NE through the Eastern Cordillera reaching the Pisayambo area (Fi. 11). The Pallatanga fault is the locus of 4-5 Holocene  $M_w \sim 7.5$  great earthquakes with recurrence time between 1300 to 3000 years defined by paleoseismology (Baize et al., 2014). The latest event occurred in 1797 and the magnitude ( $M_{ic}$ ) evaluated from the intensities is 7.6 (67% confidence range: 7.5-7.9, Beauval et al., 2010). According to Leonard (2010), a M 7.6 strike slip earthquake can rupture a fault segment more than 100 km long; therefore the rupture may have diagonally crossed throughout the entire Interandean Depression.

Little is known about the Puná NAB-4 source zone. Active fault traces and strike slip geomorphic markers define a flower structure in the Puná island and a pull-apart basin has been identified including this and the Santa Clara islands in the Gulf of Guayaquil area (Dumont et al., 2005). The northeastward continuity of the fault trace from the Gulf shore across the flood plain to the Cordillera foothills is not observed (Fig. 11). The presence of en échelon faults suggested by Lavenu et al. transferring the deformation across the plain to the Cordillera (1995) is not clear either. Dumont et al. (2005) calculated a geological slip rate of 5.5 to 6.6 mm/a, which is consistent with the general slip rate along the NAB east boundary domain, even though historical earthquakes have not been recorded in the NAB-4 zone and instrumental seismicity is low (Fig. 11).

Around the same Gulf of Guayaquil area and further west to NAB-4, normal faults have been described by several authors (Deniaud et al., 1999; Witt et al., 2006) (Fig. 11). They are associated to E-W major detachments at the continental margin-to-shelf break that become vertical towards the surface and respond to the Gulf opening. These listric structures may not be capable of generating major seismic events due to their limited lateral and vertical extension. Their potential seismicity is included in the interface source SMT-3 as discussed previously and not modeled as part of the Puná NAB-4 source.

### ***Eastern sub-Andean uplifts, thrust faults and folds***

The Andean back arc domain has been subdivided in three sources: the Napo ESB-1, the Cutucú ESB-2, and the Moyobamba ESB-3 (Figs. 10, 11). There are two main structural uplifts –Napo and Cutucú– that characterize the N-S trending sub-Andean thrust-and-fold belt in Ecuador, both converging toward the Pastaza depression (Fig. 6). The axes of the two uplifts are deflected by the depression, so it is used as a source limit. The deflection is also noticeable from the small-energy seismicity that bends towards the Pastaza depression (Fig. 11a). No large earthquakes are reported for the Napo ESB-1 source. To the contrary, the Cutucú ESB-2 includes the 1995  $M_w$  7.0 event and the obvious seismicity in the central part of the source is probably related to the present-day active part of the Cutucú uplift (Figs. 2a, 6).

The Moyobamba ESB-3 source is located outside of Ecuadorian territory. We include it in our modeling because of its noticeable seismicity. Several interpretations are possible for the junction of the NW-SE trending Peruvian Andes, part of the Central Andes domain, with the N-S trending Cutucú uplift (ESB-2). We decide to extend the ESB-2 down to Lat  $-5^\circ$  so that it includes all the N-S thrust-and-fold belts. The ESB-3 seismicity is clustered around  $6^\circ\text{S}$ ,  $77^\circ\text{W}$  where several destructive earthquakes occurred at the beginning of the 1990's (Figs. 2a, 11).

### ***Western Cordillera faults***

The Romeral – Cauca-Patía domain is defined by two sources: the El Angel WCR-1 and the Quito-Latacunga WCR-2 (Figs. 10, 11). The WCR-1 faults are the southernmost expression of NNE-trending structures that are clearly recognizable along the western slopes of the Cordillera Central in Colombia, all the way to Pasto city (Fig. 1), defined as the Romeral Fault system (París et al., 2000) (Fig. 6). The WCR-1 is drawn to include several geomorphic lineaments that show a northeastern trend with a right-lateral strike-slip movement. In 1868 one of these segments, that is not well identified, ruptured in two consecutive  $M_C$  6.6 and 7.2 earthquakes. The 7.2 event is

considered to be the most destructive event in Ecuadorean Northern Andes in historical times (Beauval et al., 2010) (Fig. 11).

The WCR-1 is drawn to also include the 1859  $M_{IC}$  7.2 earthquake (Fig. 11). The magnitude and location were estimated assuming that the earthquake is shallow. However, on the basis of the wide spatial distribution of intensities VII, Beauval et al. (2010) suggested that, it could also be an inslab event. In the present study we have shown that north of the Grijalva rifted margin, intermediate depth seismic moment release is very small, especially between latitudes  $1^{\circ}S$  to  $2^{\circ}N$ . Consequently, it is reasonable to assume that the 1859 event is indeed shallow and might have ruptured one of the NE-SW lineaments west of Quito.

At the equator the NE-SW trending faults experience a sharp rotation in strike towards a N-S direction. These N-S tectonic structures are modeled as the UIO-Lat WCR-2 source. The Quito and Latacunga compressive structures are characterized by blind reverse faults and by folds and flexures at the surface. Along the Quito reverse fault system –a N-S, 60 km long complex structure– five sub-segments capable of rupturing individually or simultaneously in a single event have been identified, with magnitudes from  $M$  5.7 to 7.1 (Alvarado et al., 2014). A large historical earthquake occurred in 1587 at the northern termination of the source ( $M_{IC}$  6.4, Beauval et al., 2010), (Fig. 11). It is possibly related either to the Tangahuila segment of Alvarado et al. (2014) or to the strike-slip Guayllabamba fault system (Fig. 11). Two more historical earthquakes (1914 and 1923) have the same order of magnitude but may be better correlated with ENE-WSW right-lateral strike-slip faults obliquely crossing WCR-2. Such faults have not yet been well recognized in the field.

The Latacunga fault system shows compressive structures both west and east of the Interandean Depression with fault planes dipping towards the respective Cordilleras. A series of at least six historical earthquakes in the magnitude range  $M_{IC}$  5.0-6.0 have been relocated along the western slopes of the Depression (Beauval et al., 2010). The historical catalog mentions three more events (1703, 1800, 1944) that could have ruptured the same segment,

but these events have not been properly analyzed due to the paucity of intensity data. The great 1698  $M_{IC}$  7.3 Ambato earthquake was located by Beauval et al. (2010) at the foot of the Carihuairazo volcano, south of those moderate earthquakes. Baize et al. (2014) have recently shown that part of the Pallatanga fault deformation is being partitioned when the structure enters the Interandean Depression. One of the branches has a N-S trend, running between Chimborazo and Carihuairazo volcanoes, and could be the 1698 event causative fault. The 1698 earthquake location is on the limit separating the NAB-2 and the Pallatanga NAB-3 (Fig. 11).

### 3. DISCUSSION

Our new interpretation of Ecuador's complex geodynamics places emphasis on two aspects of the plates interaction on the continental scale: a) the convergence obliquity resulting from the convex shape of South America's northwestern continental margin and b) the differences in rheology between the Farallon and Nazca plates linked to their different ages. These two major features contrast with the overestimated role that the Carnegie ridge was given in controlling the slab's geometry, dip, and boundaries, and in conditioning the crustal and interface earthquake generation. Now we will discuss some of the features described in the first part of this paper and used in the second part for outlining the seismic sources in the Ecuadorian territory.

#### ***Subducting slabs***

The convex shape of the northwestern South American margin and the long-lived oblique collision have effectively imprinted a clear signature on the down-going slabs.

The 60° trench curvature acts as a concave lens for convergence. This has the effect of deflecting earthquake slippage along the megathrust and focusing the slab's down-dip deformation towards a focal point, i.e. to a hypothetical center of curvature at some depth inland. The contortion of the Farallon plate as seen at the El Puyo seismic cluster and the almost 100 km

deepening of hypocenters within a small volume (a cube 100 km long per side, Figs. 2b, 3) might be linked to the adjustment of the Farallon to a smaller available space at depth as it approaches the focusing point. The El Puyo cluster is one of the most severe contortions yet recognized in an intermediate-depth Benioff Zone (Bevis and Isacks, 1984b) and it is releasing a considerable amount of the seismic moment of the inslab Farallon source.

It is noteworthy that the Pastaza sub-Andean depression is located directly above the El Puyo cluster (Figs. 2b, 6). The Pastaza depression is the locus of one of the world's largest tropical alluvial megafans –the Pastaza megafan– that has been active since the Pliocene (Bès de Berc et al., 2005). The close geographical link suggests that the sharp plunge of the Farallon plate lying 150 km below locally removes support to the continental lithosphere provoking its subsidence through viscoelastic adjustment.

The NNW-SSE alignment of intermediate depth earthquakes with  $M_w$  up to  $\sim 7.5$  and lying approximately 600 km inland from the trench (Fig. 2b) concentrates the great majority of the largest earthquakes upon the Farallon plate. This high seismic moment release zone might be related to the hinge where the Farallon plate bends downward to sink deeper towards a focus of  $\sim 600$  km deep earthquakes located 500 km to the east (Hayes et al., 2012). A deflection of the  $\sim$ N-S alignment to the NNE towards the El Puyo contortion is also noticeable, corroborating the along strike bending of the plate as shown in Fig. 3a.

It should be mentioned that Sangay volcano, the southernmost volcano of the Andean Northern Volcanic Zone (NVZ), lies around 70 km south of the projected Grijalva rifted margin (Fig. 2b, 9), upon continental crust that overrides the Farallon plate. Further north, Chimborazo and Tungurahua volcanoes are located approximately above the transition between Farallon and Nazca while the remainder of the NVZ volcanoes grow above the Nazca slab. A possible explanation for Sangay's unusually eastward location (Monzier et al., 1999a) could be related to the discussed contortion towards the El Puyo cluster. The volcano is located  $\sim 80$  km to the SW of the center of the cluster. A rapid

northeastward deepening of the shallow dipping Farallon slab opens room for the presence of a mantle wedge above the slab flexure. A mantle wedge does not exist below the flat or gentle dipping slabs to the south, thus no volcanism is present further south.

Chimborazo, Tungurahua and Sangay are part of the so-called Riobamba volcanoes (Monzier et al., 1999b) and are considered as the southern termination of the NVZ. The Riobamba volcanoes display a different geochemical signature than the rest of the NVZ: (a) the presence of basic rocks is more abundant here, and (b) they do not show a decrease in a number of rare earth elements frequently observed in differentiated volcanic rocks along the rest of the Ecuadorian arc (Monzier et al., 1999b). The geochemistry of the Riobamba volcanoes could be related to the unusual mantle wedge mentioned above. Therefore, a possible slab tear separating the Farallon and Nazca plates proposed by Gutscher et al., (1999) exposing this way deep mantle fluids to contaminate the primary magma is not needed to explain the geochemistry of the southern termination of the NVZ.

Focal mechanisms do not support a tearing mechanism along the rifted margin either (Fig. 3). As a consequence, we believe that the Farallon slab flexure along the subducted Grijalva rifted margin is more compatible with the characteristics of the southernmost volcanoes of NVZ.

By contrast, the inslab Nazca plate is not as earthquake-prone as the Farallon plate. The maximum recorded magnitude in the ~400 km segment stretching from its contact with the Farallon along the Grijalva rifted margin to ~2°N is Mw 5.8 (1967, Fig. 2b). This segment coincides with the section of the NVZ where the density of Quaternary volcanoes is the highest (Hall et al., 2008; Martin et al., 2014). We state that the lack of intermediate depth seismicity is related to the thermal condition of the subducted Nazca plate in this high heat flow environment, where young slabs are too hot and ductile to allow the generation of large earthquakes at depths beyond the seismogenic interface as seen elsewhere (Syracuse et al., 2010).

This statement is corroborated by a similar situation observed along the Costa Rican subduction zone where the Cocos plate converges against the Caribbean plate. There is no intermediate depth seismicity where the youngest segment of the Cocos is subducting along southern Costa Rica, but seismicity increases towards the NW as the subducted plate gets older (Protti et al., 1994). Both in Costa Rica and Ecuador where no intermediate depth seismicity is present, plate ages fluctuate between 15 and 18 Ma. These two segments of the Cocos and Nazca slabs have the same origin as they are conjugate pieces that originated along the same plate-splitting fracture during the final episode of Farallon splitting at the beginning of the Miocene (Lonsdale, 2005). Both plates are transporting aseismic ridges, the Cocos and Carnegie ridges, that are being subducted along with their plates, but the ridges do not have an obvious influence on the inslab seismicity.

#### ***Carnegie Ridge and the interface***

The Carnegie ridge seems to control earthquake propagation at the interface. The four 20<sup>th</sup> century,  $M_w \geq 7.6$  great interface earthquakes, including the 1906 giant megathrust event, are located between the northern slope of the Carnegie ridge and 2°N. This is also the segment where present day inter-seismic coupling is concentrated in five asperities, including the rupture area of the smaller 1998  $M_w$  7.1 event (Chlieh et al., 2014) (Fig. 8). The 1906 event ruptured all four asperities north of BEZ and maybe also the 1998 earthquake coupling zone. Kanamori & McNally (1982) and Mendoza & Dewey (1984) have also shown that all the ruptures propagated to the NNE, away from the Carnegie ridge. From Fig. 5 it is apparent that convergence obliquity reaches its maximum along the trench segment where the four great earthquakes are located. These observations may indicate that the high convergence obliquity is forcing earthquake ruptures to propagate northeastward and that the role of the Carnegie as a barrier for the southward rupture propagation is also linked to this factor.

There is a notable along-strike heterogeneity in the inter-seismic coupling throughout the already-subducted portion of the Carnegie ridge (Chlieh et al.,

2014; Nocquet et al., 2014). Coupling changes from weak at the northern edge (BEZ) to non-existent along the ridge axis to being locally strong at the southern half (La Plata slow-slip event region). Further south, the Carnegie platform is bounded by the Grijalva rifted margin, where Nocquet et al. (2014) report weak coupling. Carena (2011) maintains that an oceanic fracture zone –the Grijalva rifted margin has similar bathymetry than a fracture zone but has a different origin–, once subducted, controls the lateral extent of great and giant earthquakes ruptures more effectively than seamounts or discontinuous ridges. This is because fracture zones constitute coherent topographic steps that require the rupture to climb up or descend a ramp for the entire width of the seismogenic zone before continuing to the next segment of the thrust. The Grijalva rifted margin represents a sustained step in the lower plate topography that can not be circumvented by the propagating rupture as smaller asperities might be.

Consequently, the Carnegie ridge's three interseismic coupling regions – the freely creeping, the slow slip, or the frequently discharged BSZ–, or ultimately the topographic step at the platform's southern boundary, constitute an effective series of barriers against rupture propagation from the northern mega-earthquakes. However, the Carnegie ridge itself could still generate large earthquakes along its complex interface contact with the NAB as implied or shown by the BEZ. PSHA modeling should take into account this complex segmentation in the Ecuadorian–southern Colombian subduction zone as well as its heterogeneous rupture timing, with asperities rupturing several times individually, before jointly failing in supercycles that are responsible for  $M_w > 8.5$  earthquakes (Bilek, 2010; Chlieh et al., 2014).

#### ***Grijalva to Mendaña interface***

The approximately 1000 km long segment from the Carnegie ridge platform to the Mendaña fracture zone in central Peru, slips aseismically or has a greater than average repeat time for great earthquakes (Nocquet et al., 2014). Carena (2011) has also argued that this segment has similarities to the subduction segment broken during the giant 2004 northern Sumatra

earthquake. There are a couple of observations that could contribute to this discussion. The Viru fracture zone (Lonsdale, 2005) constitutes a topographic step that shortens the effective length of the seismic gap by ~400 km before reaching the Mendaña fracture zone (Fig. 1). North of Viru there are less than 500 km in distance to reach the Grijalva rifted margin. Neither of the two segments could generate earthquakes similar to the 2004 event independently, but we must accept that we cannot rule out infrequent mega-earthquakes in this subduction zone segment simply on the basis of its most easily observable physical properties (Okal, 2010).

Along the subduction segment located seawards from the Gulf of Guayaquil, the trench shows a landward deflection where the Grijalva rifted margin reaches the trench (Fig. 1). This is also the segment where the strikes of the trench's orientation and of fault planes do not coincide within  $\pm 10^\circ$ , to all of the thrust events throughout the rest of the interface (Fig. 5). Focal mechanisms reflect the occurrence of earthquakes with an important strike-slip component, thus denoting a distinct origin or interaction among plates that concur in the area. At the Gulf zone four different rheologies are found: two oceanic slabs – the 22 Ma old Nazca and the 32-34 Ma old Farallon–, and two continental overriding blocks –the NAB and the Inca sliver, both moving in divergent directions with respect to stable South America. The northeastward sliding of the NAB generates trench-parallel extensional strain and is responsible for the development of the Gulf of Guayaquil basin since the Pleistocene (Witt et al., 2006).

Nocquet et al. (2014) have modeled the interseismic coupling along the Gulf's subduction segment, which shows two results. One model predicts no coupling south of the Grijalva rifted margin, while the second one allows for mild coupling close to the trench to take into account the tsunami earthquakes that occurred further south. In any case, the occurrence of earthquakes like the Mw 7.6 1953 event (Fig. 2a) still needs to be understood in the perspective of a freely slipping interface or as a crustal earthquake related to the NAB's southern

boundary and its continuation to the Tumbes detachment system that shapes the southern edge of the Gulf of Guayaquil (Witt and Bourgois, 2010).

### ***Crustal structures***

The obliquity of plate convergence is controlling the movement of the NAB to the NNE (Nocquet et al., 2014) along the localized transpressive right-lateral CCPP fault system. CCPP is the most important crustal seismogenic structure in the country.

Out of the four CCPP sub-segments, the central one –Cosanga– has released a higher seismic moment per unit volume throughout the instrumental seismicity period of the catalog (Fig. 11). By contrast, during pre-instrumental time, historical seismicity has been mainly related to the Pallatanga source and to the active structures located along the Interandean Depression close to colonial-time settlements (Beauval et al., 2010). In our SSZ model, historical seismicity has been important to define most of the crustal sources. But short-spanned historical accounts or large areas with no population and other externalities on the one hand, or the lack of present-day seismicity on the other, open the possibility for underestimating the seismic potential of certain sources outside the populated areas. To overcome this, strain rate models as a proxy for earthquake potential are being tested elsewhere. The information that is being gathered by a newly deployed dense geodetic network in continental Ecuador will be used in the future for that purpose.

The latest great earthquake to rupture the Pallatanga fault was the 1797  $M_{IC}$  7.5-7.9 event (Beauval et al., 2010). Beauval et al. (2013) have located a second historical  $M_w \sim 7$  earthquake that occurred in 1645, about 50 km SSW of the 1797 event on the same structure (Fig. 11). The occurrence of two  $M_w > 7$  within a short time span is in conflict with paleoseismological studies (Baize et al., 2014), because the recurrence time is too short for the segment. Therefore, it is plausible that a neighboring active structure could have failed during the 1645 earthquake, since the Pallatanga fault is moving at  $\sim 50\%$  of the overall velocity established for NAB (Baize et al., 2014; Winter et al., 1993). This is an

important aspect to take into consideration when modeling fault sources in the region.

At the northern end of this segment the 1949 Mw 6.5 earthquake rupture may have stopped at the Pisayambo seismic cluster (Troncoso, 2009) (Figs. 2a, 11a). The high rate of activity at the cluster could be related to creeping and may constitute a barrier to rupture propagation between the Pallatanga and Cosanga segments.

The compressive N-S trending Quito-Latacunga fault system shows different behavior in its two sub-segments. Alvarado et al. (2014) using GPS measurements with observation periods of at least 10 years report that Quito's Illumbisí segment is shortening at velocities ranging from 4.3 to 5.3 mm/a. They satisfactorily modeled the data with a fault plane dipping 40° that is weakly locked at 3 km depth. There are no measurements for the other four segments. The shortening value is surprisingly high and, if ratified, implies a worrisome seismic moment deficit along this fault located directly below Ecuador's capital city. Moreover, recent analyses about the probabilistic seismic hazard in Quito (Beauval et al., 2014) show that the Quito fault system is controlling the city's hazard level at 475 year return period, and that there is a great need for further, in-depth studies to ratify or modify the peak ground acceleration reference value of 0.4 g that they propose.

The Latacunga fault system is deforming at lower rates in the range from 1.4-2.1 mm/a (Ego and Sébrier, 1996; Lavenu et al., 1995) but has a seismicity rate higher than that of the Quito segment. Moderate earthquakes that characterize the Latacunga system faults have consistent magnitudes of Mw  $5.7 \pm 0.2$  (see Table 1 for the details), suggesting a very regular fault segmentation. The exception is the 1698 great  $M_{IC}$  7.3 earthquake that could have ruptured several small segments at the same time, from SW Latacunga southward to the contact with the CCPP fault system (Fig. 11) following a N-S branch of the Pallatanga fault. Both, the present-day microseismicity distribution and the epicentral location of the 1698 event confirm that Pallatanga deformation partitioning in the N-S direction at Riobamba might be channeled

by an old structure known as the Pujili fault bounding the Pujili mélange to the east (Hughes and Pilatasig, 2002). The Pujili mélange is the contact zone between the early Mesozoic continental basement to the east with early to late Cretaceous oceanic plateau fragments accreted in late Cretaceous times (Hughes and Pilatasig, 2002) as shown in Fig. 11a. This is the only clear evidence of a rejuvenated suture in the Ecuadorian Andes.

### ***Outer-trench seismicity***

The anomalous concentration of normal earthquakes along the Nazca plate's outer-trench segment from  $\sim 1.8^{\circ}\text{N}$  to  $4^{\circ}\text{N}$  (Fig. 9b) also merits an interpretation. No other segment west of the trench shows a similar clustering of events, given that a total of 155 events with magnitudes from  $M_w$  4.0 to 6.2 are reported in the catalog. This number represents a four-fold increase in the total number of earthquakes located in the outer-trench along the rest of the subduction zone examined in this study. Although this seismicity could be explained as relaxation aftershocks related to the 1979  $M_w$  8.1 or even to the 1906  $M_w$  8.8 megathrust earthquakes, normal faulting focal mechanism solutions could also result from internal, along-fabric tearing of an isolated platelet that originated along the Yaquina graben. In that case the topographic feature known as the Yaquina graben could be interpreted as a rifted microplate margin that marks the locus of another spreading ridge that created ocean floor in the complicated history that characterizes the splitting off of the Cocos plate. East of the Yaquina graben the platelet is being strained by slab pull forces related to its plunging portion and normal shallow inslab earthquakes would be produced mostly in the range from 35-50 km deep.

### **Conclusions**

This new model of Ecuador's complex geodynamics puts emphasis on two aspects of the plates' interactions at a continental scale: (a) the differences in rheology between the Farallon and Nazca plates and (b) the convergence obliquity resulting from the convex shape of the South American northwestern

continental margin. Both conditions satisfactorily explain several characteristics of the observed seismicity, as well as the interseismic coupling.

The Grijalva rifted margin sharply marks the difference in existing rheological conditions between the Farallon and Nazca plates related to their different ages. Intermediate depth seismicity reveals a severe flexure in the Farallon slab as it dips and converges towards a focal point that represents the center of curvature of the convex continental margin. The El Puyo cluster contortion is taking place in a reduced space at its northeastern tip within the contact zone with the Nazca slab. Nazca may be experiencing a similar type of flexuring at depth, but its aseismic penetration probably related to the thermal characteristic of this young plate precludes any type of visualization by seismicity. The two slabs positions and geometry below continental Ecuador show clear correlation with surface expressions in the local and regional geology and tectonics.

The Grijalva rifted margin highlights a sharp difference in the subducting plate topography. The 500 m step between the Nazca and Farallon plates is a formidable barrier for earthquake propagation involving the whole down-dip width of the plates, but it could also act as a stress concentrator for nucleation of great earthquakes (Carena, 2011). The Carnegie ridge plays an important role as a barrier in the propagation of interface earthquakes too, but its capacity to influence Nazca plate geometry and coherence remains unclear.

Interseismic coupling is influenced by the rheological differences in the two plates as well. Coupling is weak and shallow south of the Grijalva rifted margin and increases northward, with a heterogeneous pattern at the interface where the Carnegie ridge enters the subduction region. Higher levels of coupling occur north of Carnegie and are well correlated with the segments ruptured by great earthquakes in northern Ecuador. Strong persisting coupling and high convergence obliquity are complementary factors responsible for the NAB's northeastward movement along localized fault systems. The Cosanga and Pallatanga segments of the CCPP fault system concentrate most of the seismic moment release in continental Ecuador. The faults located along the western

border of the Interandean Depression also show a high rate of moderate size earthquake production.

A total of nineteen seismic source zones were designed according to this geodynamic and neotectonic scheme. The selected boundaries have some physical significance as barriers to rupture propagation or enclose intermediate depth seismicity that reveals the same type of seismic behavior within a geometrical volume. The next step is to model seismic recurrence in each source zone and calculate a new generation of probabilistic seismic hazard maps for Ecuador.

## References

- Alvarado, A.: Néotectonique et cinématique de la déformation continentale en Équateur, These, Université de Grenoble, Grenoble. 2012.
- Alvarado, A., Audin, L., Nocquet, J.-M., Lagreulet, S., Segovia, M., Font, Y., Lamarque, G., Yepes, H., Mothes, P. and Rolandone, F.: Active tectonics in Quito, Ecuador, assessed by geomorphological studies, GPS data, and crustal seismicity, *tectonics*, 33(2), 67–83, doi:10.1002/(ISSN)1944-9194, 2014.
- Alvarado, A. Audin, L., Nocquet, J. M., jaillard, E., Mothes, P., Jarrin, P., Segovia, M., Rolandone, F. and Cisneros, D.: Migration and localization of a continental plate boundary in Ecuador: present-day active faulting delimiting the North Andean Sliver to the East. *Tectonics in revision*, 2015.
- Baize, S., Audin, L., Winter, T., Alvarado, A., Pilatasig Moreno, L., Taipe, M., Reyes, P., Kauffman, P. and Yepes, H.: Paleoseismology and tectonic geomorphology of the Pallatanga fault (Central Ecuador), a major structure of the South-American crust, *Geomorphology*, 1–15, doi:10.1016/j.geomorph.2014.02.030, 2014.
- Baize, S., Cushing, E. M., Lemeille, F. and Jomard, H.: Updated seismotectonic zoning scheme of Metropolitan France, with reference to geologic and seismotectonic data, *Bulletin de la Societe Geologique de France*, 184(3), 225–259, 2013.
- Bakun, W. H.: Magnitude and location of historical earthquakes in Japan and implications for the 1855 Ansei Edo earthquake, *J. Geophys. Res.*, 110(B2), B02304, doi:10.1029/2004JB003329, 2005.
- Bakun, W. H. and Wentworth, C. M.: Estimating earthquake location and magnitude from seismic intensity data, *Bulletin of the Seismological Society of America*, 87(6), 1502–1521, 1997.
- Barazangi, M. and Isacks, B.: Spatial distribution of earthquakes and subduction of the Nazca plate beneath South America, *Geology*, 4(11), 686–692, 1976.

Barnes, J. B. and Ehlers, T. A.: End member models for Andean Plateau uplift, *Earth-Science Reviews*, 97(1-4), 105–132, doi:10.1016/j.earscirev.2009.08.003, 2009.

Beauval, C., Yepes, H., Audin, L., Alvarado, A., Nocquet, J. M., Monelli, D. and Danciu, L.: Probabilistic Seismic-Hazard Assessment in Quito, Estimates and Uncertainties, *Seismological Research Letters*, 85(6), 1316–1327, doi:10.1785/0220140036, 2014.

Beauval, C., Yepes, H., Bakun, W. H., Egred, J., Alvarado, A. and Singaicho, J.-C.: Locations and magnitudes of historical earthquakes in the Sierra of Ecuador (1587-1996), *Geophysical Journal International*, doi:10.1111/j.1365-246X.2010.04569.x, 2010.

Beauval, C., Yepes, H., Palacios, P., Segovia, M., Alvarado, A., Font, Y., Aguilar, J., Troncoso, L. and Vaca, S.: An Earthquake Catalog for Seismic Hazard Assessment in Ecuador, *Bulletin of the Seismological Society of America*, 103(2A), 773–786, doi:10.1785/0120120270, 2013.

Beck, S. L. and Ruff, L. J.: The rupture process of the great 1979 Colombia earthquake: Evidence for the asperity model, *Journal of Geophysical Research: Solid Earth* (1978–2012), 89(B11), 9281–9291, 1984.

Bevis, M.: The curvature of Wadati-Benioff zones and the torsional rigidity of subducting plates, *Nature*, 323(6083), 52–53, 1986.

Bevis, M. and Isacks, B.: Hypocentral trend surface analysis: Probing the geometry of Benioff zones, *Journal of Geophysical Research: Solid Earth* (1978–2012), 89(B7), 6153–6170, 1984a.

Bevis, M. and Isacks, B. L.: Correction to “Hypocentral trend surface analysis: Probing the geometry of Benioff Zones” by M. Bevis and BL Isacks, *Journal of Geophysical Research: Solid ...*, 1984b.

Bès de Berc, S., Soula, J. C., Baby, P., Souris, M., Christophoul, F. and Rosero, J.: Geomorphic evidence of active deformation and uplift in a modern continental wedge-top–foredeep transition: Example of the eastern Ecuadorian Andes, *Tectonophysics*, 399(1-4), 351–380, doi:10.1016/j.tecto.2004.12.030, 2005.

Bilek, S. L.: Invited review paper: Seismicity along the South American subduction zone: Review of large earthquakes, tsunamis, and subduction zone complexity, *Tectonophysics*, 495(1-2), 2–14, doi:10.1016/j.tecto.2009.02.037, 2010.

Bonilla, L. F., Ruiz, M. C. and Yepes, H.: Evaluation of seismic hazard in Ecuador, *Memoirs, Simposio Internacional sobre Prevención de Desastres Sísmicos*, 118–125, 1992.

Bonnardot, M. A., Hassani, R., Tric, E., Ruellan, E. and Régnier, M.: Effect of margin curvature on plate deformation in a 3-D numerical model of subduction zones, *Geophysical Journal International*, 173(3), 1084–1094, doi:10.1111/j.1365-246X.2008.03752.x, 2008.

Bourdon, E., Eissen, J.-P., Gutscher, M. A., Monzier, M., Hall, M. L. and Cotten, J.: Magmatic response to early aseismic ridge subduction: the Ecuadorian margin case (South America), *Earth and Planetary Science Letters*, 205(3), 123–138, 2003.

Bourgeois, J.: A Review on Tectonic Record of Strain Buildup and Stress Release across the Andean Forearc along the Gulf of Guayaquil-Tumbes Basin (GGTB) near Ecuador-Peru Border, *IJG*, 04(03), 618–635, doi:10.4236/ijg.2013.43057, 2013.

- Cahill, T. and Isacks, B.: Seismicity and shape of the subducted Nazca plate, *J. Geophys. Res.*, 97(B12), 17503–17529, 1992.
- Caputo, R., Chatzipetros, A., Pavlides, S. and Sboras, S.: The Greek Database of Seismogenic Sources (GreDaSS): state-of-the-art for northern Greece, *Annals of Geophysics*, 55(5), doi:10.4401/ag-5168, 2013.
- Carena, S.: Subducting-plate Topography and Nucleation of Great and Giant Earthquakes along the South American Trench, *Seismological Research Letters*, 82(5), 629–637, doi:10.1785/gssrl.82.5.629, 2011.
- CEC: Requisitos generales de diseño: Peligro sísmico, espectros de diseño y requisitos mínimos de cálculo para diseño sismo-resistente, edited by INEN, Instituto Ecuatoriano de Normalización, 1–32, 2001.
- Cediél, F., Shaw, R. P. and Cáceres, C.: Tectonic Assembly of the Northern Andean Block, edited by C. Bartolini, R. T. Buffler, and J. Blickwede, *AAPG Memoir*, 79, 815–848, 2004.
- Chen, P.-F., Bina, C. R. and Okal, E. A.: Variations in slab dip along the subducting Nazca Plate, as related to stress patterns and moment release of intermediate-depth seismicity and to surface volcanism, *Geochem. Geophys. Geosyst.*, 2(12), n/a–n/a, doi:10.1029/2001GC000153, 2008.
- Chlieh, M., Mothes, P. A., Nocquet, J. M., Jarrin, P., Charvis, P., Cisneros, D., Font, Y., Collot, J.-Y., Villegas-Lanza, J. C., Rolandone, F., Vallee, M., et al.: Distribution of discrete seismic asperities and aseismic slip along the Ecuadorian megathrust, *Earth and Planetary Science Letters*, 400(C), 292–301, doi:10.1016/j.epsl.2014.05.027, 2014.
- Cloos, M.: Lithospheric buoyancy and collisional orogenesis: Subduction of oceanic plateaus, continental margins, island arcs, spreading ridges, and seamounts, *Geological Society of America Bulletin*, 105(6), 715–737, 1993.
- Collot, J.-Y., Marcaillou, B., Sage, F., Michaud, F., Agudelo, W., Charvis, P., Graindorge, D., Gutscher, M. A. and Spence, G.: Are rupture zone limits of great subduction earthquakes controlled by upper plate structures? Evidence from multichannel seismic reflection data acquired across the northern Ecuador–southwest Colombia margin, *Journal of Geophysical Research: Solid Earth* (1978–2012), 109(B11), 2004.
- Daly, M. C.: Correlations between Nazca/Farallon plate kinematics and forearc basin evolution in Ecuador, *tectonics*, 8(4), 769–790, 1989.
- Davies, J. H. and Stevenson, D. J.: Physical model of source region of subduction zone volcanics, *J. Geophys. Res.*, 97(B2), 2037, doi:10.1029/91JB02571, 1992.
- Deniaud, Y., Baby, P., Basile, C., Ordóñez, M., Montenegro, G. and Mascle, G.: Opening and tectonic and sedimentary evolution of the Gulf of Guayaquil: Neogene and Quaternary fore-arc basin of the south Ecuadorian Andes, *Comptes Rendus de l'Academie des Sciences Series IIA Earth and Planetary Science*, 328(3), 181–187, 1999.
- Dorbath, L., Cisternas, A. and Dorbath, C.: Assessment of the size of large and great historical earthquakes in Peru, *Bulletin of the Seismological Society of America*, 80(3), 551–576, 1990.
- Dumont, J. F., Santana, E., Vilema, W., Pedoja, K., Ordóñez, M., Cruz, M., Jiménez, N. and Zambrano, I.: Morphological and microtectonic analysis of Quaternary deformation from

Puná and Santa Clara Islands, Gulf of Guayaquil, Ecuador (South America), *Tectonophysics*, 399(1-4), 331–350, doi:10.1016/j.tecto.2004.12.029, 2005.

Dziewonski, A. M., Chou, T. A. and Woodhouse, J. H.: Determination of earthquake source parameters from waveform data for studies of global and regional seismicity, *Journal of Geophysical Research: Solid Earth* (1978–2012), 86(B4), 2825–2852, 1981.

Egbue, O. and Kellogg, J.: Pleistocene to Present North Andean “escape,” *Tectonophysics*, 489(1-4), 248–257, doi:10.1016/j.tecto.2010.04.021, 2010.

Ego, F. and Sébrier, M.: The Ecuadorian Inter-Andean Valley: a Major and Complex restraining bend and Compressive Graben since Late Miocene Time, *Annales Tectonicae*, 10(1-2), 31–59–29, 1996.

Ego, F., Sébrier, M. and Yepes, H.: Is the Cauca-Patia and Romeral Fault System left or rightlateral? *Geophys. Res. Lett.*, 22(1), 33–36, 1995.

Ego, F., Sébrier, M., Carey-Gailhardis, E. and Insergueix, D.: Les phénomènes naturels générateurs de dommages, *Bull Inst fr études andines*, 1996a.

Ego, F., Sébrier, M., Lavenu, A., Yepes, H. and Egues, A.: Quaternary state of stress in the Northern Andes and the restraining bend model for the Ecuadorian Andes, *Tectonophysics*, 259(1), 101–116, 1996b.

Egred, J.: *El terremoto de Riobamba, Abya Yala, Quito. 2000.*

Fiorini, E. and Tibaldi, A.: Quaternary tectonics in the central Interandean Valley, Ecuador: Fault-propagation folds, transfer faults and the Cotopaxi Volcano, *Global and Planetary Change*, 90-91, 87–103, doi:10.1016/j.gloplacha.2011.06.002, 2012.

Font, Y., Segovia, M., Vaca, S. and Theunissen, T.: Seismicity patterns along the Ecuadorian subduction zone: new constraints from earthquake location in a 3-D a priori velocity model, *Geophysical Journal International*, 193(1), 263–286, doi:10.1093/gji/ggs083, 2013.

Frey Mueller, J. T., Kellogg, J. N. and Vega, V.: Plate Motions in the north Andean region, *J. Geophys. Res.*, 98(B12), 21853, doi:10.1029/93JB00520, 1993.

Gajardo, E., Yepes, H., Ramón, P., Hall, M., Mothes, P. and Aguilar, J.: Evaluación del peligro sísmico para la ruta del OCP y evaluación complementaria del peligro volcánico, *Internal Report, Instituto Geofísico-Escuela Politécnica Nacional*, 1–81, 2001.

Giesecke, A. A.: A Program for the Mitigation Of Earthquake Effects in the Andean Region (Project Sisra), in *Natural and Man-Made Hazards*, pp. 781–786, Springer Netherlands, Dordrecht. 1988.

Giesecke, A., Capera, A. G., Leschiutta, I., Migliorini, E. and Valverde, L. R.: The CERESIS earthquake catalogue and database of the Andean Region: background, characteristics and examples of use, *Annals of Geophysics*, 47(2-3), 2004.

Guillier, B., Chatelain, J. L., Jaillard, E., Yepes, H., Poupinet, G. and Fels, J. F.: Seismological evidence on the geometry of the Orogenic System in central-northern Ecuador (South America), *Geophys. Res. Lett.*, 28(19), 3749–3752, doi:10.1029/2001GL013257, 2001.

Gutscher, M.-A., Malavieille, J., Lallemand, S. and Collot, J.-Y.: Tectonic segmentation of the North Andean margin: impact of the Carnegie Ridge collision, *Earth and Planetary Science*

Letters, 168(3), 255–270, 1999.

Hall, M. L. and Wood, C. A.: Volcano-tectonic segmentation of the northern Andes, *Geology*, 13(3), 203–207, 1985.

Hasegawa, A. and Sacks, I. S.: Subduction of the Nazca Plate beneath Peru as determined from seismic observations, *J. Geophys. Res.*, 86(B6), 4971, doi:10.1029/JB086iB06p04971, 1981.

Hayes, G. P., Wald, D. J. and Johnson, R. L.: Slab1.0: A three-dimensional model of global subduction zone geometries, *J. Geophys. Res.*, 117(B01302), 15 p., doi:10.1029/2011JB008524, 2012.

Herd, D. G., Youd, T. L., Meyer, H., Arango, J. L., Pearson, W. J. and Mendoza, C.: The Great Tumaco, Colombia Earthquake of 12 December 1979, *Science*, 211(4481), 441–445, doi:10.1126/science.211.4481.441, 1981.

Heuret, A., Funiciello, F., Faccenna, C. and Lallemand, S.: Plate kinematics, slab shape and back-arc stress: A comparison between laboratory models and current subduction zones, *Earth and Planetary Science Letters*, 256(3-4), 473–483, doi:10.1016/j.epsl.2007.02.004, 2007.

Hey, R.: Tectonic evolution of the Cocos-Nazca spreading center, *Geological Society of America Bulletin*, 88(10), 1404–1420, 1977.

Hughes, R. A. and Pilatasig, L. F.: Cretaceous and Tertiary terrane accretion in the Cordillera Occidental of the Andes of Ecuador, *Tectonophysics*, 345(1), 29–48, 2002.

Isacks, B. and Barazangi, M.: Geometry of Benioff zones: lateral segmentation and downwards bending of the subducted lithosphere, *Maurice Ewing Series*, 1, 99–114, 1977.

Jaillard, E., Lapierre, H., Ordóñez, M., Alava, J. T., Amortegui, A. and Vanmelle, J.: Accreted oceanic terranes in Ecuador: southern edge of the Caribbean Plate? *Geological Society, London, Special Publications*, 328(1), 469–485, doi:10.1144/SP328.19, 2009.

Jordan, T. E., Isacks, B., Allmendinger, R. W., Brewer, J., Ramos, V. and and, C.: Andean tectonics related to geometry of subducted Nazca plate, *Geological Society of America Bulletin*, 94(3), 341–361, 1983.

Kanamori, H.: The energy release in great earthquakes, *Journal of Geophysical Research: Solid Earth* (1978–2012), 82(20), 2981–2987, 1977.

Kanamori, H. and McNally, K. C.: Variable rupture mode of the subduction zone along the Ecuador-Colombia coast, *Bulletin of the Seismological Society of America*, 72(4), 1241–1253, 1982.

Kelleher, J. A.: Rupture zones of large South American earthquakes and some predictions, *Journal of Geophysical Research: Solid Earth* (1978–2012), 77(11), 2087–2103, 1972.

Keller, E.: Caractérisation de séismes historiques. Application sur un grand séisme de subduction en Équateur,, 1–42, 2014.

Kendrick, E., Bevis, M., Smalley, R., Jr., Brooks, B., Vargas, R. B., Lauría, E. and Fortes, L. P. S.: The Nazca–South America Euler vector and its rate of change, *Journal of South American Earth Sciences*, 16(2), 125–131, doi:10.1016/S0895-9811(03)00028-2, 2003.

- Lavenu, A., Winter, T. and Dávila, F.: A Pliocene–Quaternary compressional basin in the Interandean Depression, Central Ecuador, *Geophysical Journal International*, 121(1), 279–300, 1995.
- Lay, T., Kanamori, H., Ammon, C. J., Koper, K. D., Hutko, A. R., Ye, L., Yue, H. and Rushing, T. M.: Depth-varying rupture properties of subduction zone megathrust faults, *J. Geophys. Res.*, 117(B4), B04311, doi:10.1029/2011JB009133, 2012.
- Leonard, M.: Earthquake Fault Scaling: Self-Consistent Relating of Rupture Length, Width, Average Displacement, and Moment Release, *Bulletin of the Seismological Society of America*, 100(5A), 1971–1988, doi:10.1785/0120090189, 2010.
- Lonsdale, P.: Creation of the Cocos and Nazca plates by fission of the Farallon plate, *Tectonophysics*, 404(3-4), 237–264, doi:10.1016/j.tecto.2005.05.011, 2005.
- Lonsdale, P. and Klitgord, K. D.: Structure and tectonic history of the eastern Panama Basin, *Geological Society of America Bulletin*, 89(7), 981–999, 1978.
- MacMillan, I., Gans, P. B. and Alvarado, G.: Middle Miocene to present plate tectonic history of the southern Central American Volcanic Arc, *Tectonophysics*, 392(1-4), 325–348, doi:10.1016/j.tecto.2004.04.014, 2004.
- Manchuel, K., Régnier, M., Béthoux, N., Font, Y., Sallarès, V., Díaz, J. and Yepes, H.: New insights on the interseismic active deformation along the North Ecuadorian–South Colombian (NESC) margin, *tectonics*, 30(4), n–a–n–a, doi:10.1029/2010TC002757, 2011.
- McCaffrey, R.: On the role of the upper plate in great subduction zone earthquakes, *J. Geophys. Res.*, 98(B7), 11953–11–966, 1993.
- Meletti, C., Galadini, F., Valensise, G., Stucchi, M., Basili, R., Barba, S., Vannucci, G. and Boschi, E.: A seismic source zone model for the seismic hazard assessment of the Italian territory, *Tectonophysics*, 450(1-4), 85–108, doi:10.1016/j.tecto.2008.01.003, 2008.
- Mendoza, C. and Dewey, J. W.: Seismicity associated with the great Colombia-Ecuador earthquakes of 1942, 1958, and 1979: Implications for barrier models of earthquake rupture, *Bulletin of the Seismological Society of America*, 74(2), 577–593, 1984.
- Michaud, F., Witt, C. and Royer, J. Y.: Influence of the subduction of the Carnegie volcanic ridge on Ecuadorian geology: Reality and fiction, *Geological Society of America Memoirs*, 204(0), 217–228, doi:10.1130/2009.1204(10), 2009.
- Monzier, M., Robin, C., Samaniego, P., Hall, M. L., Cotten, J., Mothes, P. and Arnaud, N.: Sangay volcano, Ecuador: structural development, present activity and petrology, *Journal of Volcanology and Geothermal Research*, 90(1), 49–79, 1999a.
- Monzier, M., Robin, C., Hall, M., Cotten, J. and Samaniego, P.: Geochemistry and tectonics at the southern termination of the northern volcanic zone (Riobamba volcanoes, Ecuador); preliminary results, 4th International Symposium on Andean Geodynamics -extended abstracts, 516–518, 1999b.
- Muir-Wood, R.: From global seismotectonics to global seismic hazard, *Annali di Geofisica*, 36(3-4), 153–168, 1993.
- NEC: CARGAS SÍSMICAS - DISEÑO SISMO RESISTENTE, Ministerio de Desarrollo Urbano y Vivienda, 1–139, 2014.

Nishenko, S. P.: Circum-Pacific seismic potential: 1989–1999, *Pure Appl. Geophys.*, 135(2), 169–259, 1991.

Nocquet, J. M., Villegas-Lanza, J. C., Chlieh, M., Mothes, P. A., Rolandone, F., Jarrin, P., Cisneros, D., Alvarado, A., Audin, L., Bondoux, F., Martin, X., et al.: Motion of continental slivers and creeping subduction in the northern Andes, *Nature Geosci.*, (7), 287–291, doi:DOI: 10.1038/NCEO2099, 2014.

Nocquet, J.-M.: Subduction Earthquake Cycle in Ecuador : Observation, Modelling, and Associated Seismic Hazard Assessment,, 1–57, 2009.

Okal, E. A.: Tsunamigenic Earthquakes: Past and Present Milestones, *Pure Appl. Geophys.*, 168(6-7), 969–995, doi:10.1007/s00024-010-0215-9, 2010.

París, G., Machette, M., Dart, R. and Haller, K.: Map and database of quaternary faults and folds in Colombia and its offshore regions, USGS Open file Report 00-0284, 2000.

Pedraza, P., Vargas, C. and Monsalve, H.: Geometric Model of the Nazca Plate Subduction in Southwest Colombia, *Earth Sciences Research Journal*, 11(2), 117–130, 2007.

Pennington, W. D.: Subduction of the Eastern Panama Basin and seismotectonics of northwestern South America, *J. Geophys. Res.*, 86(B11), 10753–10770, 1981.

Pindell, J. L. and Kennan, L.: Tectonic evolution of the Gulf of Mexico, Caribbean and northern South America in the mantle reference frame: an update, Geological Society, London, Special Publications, 328(1), 1–55, doi:10.1144/SP328.1, 2009.

Pontoise, B. and Monfret, T.: Shallow seismogenic zone detected from an offshore-onshore temporary seismic network in the Esmeraldas area (northern Ecuador), *Geochem. Geophys. Geosyst.*, 5(2), n/a–n/a, doi:10.1029/2003GC000561, 2004.

Protti, M., Güendel, F. and McNally, K.: The geometry of the Wadati-Benioff zone under southern Central America and its tectonic significance: results from a high-resolution local seismographic network, *Physics of the Earth and Planetary Interiors*, 84(1), 271–287, 1994.

Rudolph, E. and Szirtes, S.: Das Kolumbianische Erdbeben am 31 Januar 1906, *Gerlands Beitrage zur Geophysik*, XI(1), 1–34 [online] Available from: [http://www.osso.org.co/docu/especiales/Traduccion\\_TERREMOTO\\_1906.pdf](http://www.osso.org.co/docu/especiales/Traduccion_TERREMOTO_1906.pdf), 1911.

Segovia, M. and Alvarado, A.: Breve análisis de la sismicidad y del campo de esfuerzos en el Ecuador, Comisión Nacional de Derechos del Mar. 2009.

Soulas, J.-P., Egüez, A., Yepes, H. and Perez, V. H.: Tectónica activa y riesgo sísmico en los Andes Ecuatorianos y en el extremo Sur de Colombia, *Boletín Geológico Ecuatoriano*, 2(1), 3–11, 1991.

Stauder, W.: Subduction of the Nazca plate under Peru as evidenced by focal mechanisms and by seismicity, *J. Geophys. Res.*, 80(8), 1053–1064, 1975.

Stirling, M., McVerry, G., Gerstenberger, M., Litchfield, N., Van Dissen, R., Berryman, K., Barnes, P., Wallace, L., Villamor, P., Langridge, R., Lamarche, G., et al.: National Seismic Hazard Model for New Zealand: 2010 Update, *Bulletin of the Seismological Society of America*, 102(4), 1514–1542, doi:10.1785/0120110170, 2012.

- Suarez, G., Molnar, P. and Burchfiel, B. C.: Seismicity, fault plane solutions, depth of faulting, and active tectonics of the Andes of Peru, Ecuador, and southern Colombia, *J. Geophys. Res.*, 88(B12), 10403, doi:10.1029/JB088iB12p10403, 1983.
- Swenson, J. L. and Beck, S. L.: Historical 1942 Ecuador and 1942 Peru subduction earthquakes and earthquake cycles along Colombia-Ecuador and Peru subduction segments, *Pure Appl. Geophys.*, 146(1), 67–101, 1996.
- Syracuse, E. M. and Abers, G. A.: Global compilation of variations in slab depth beneath arc volcanoes and implications, *Geochem. Geophys. Geosyst.*, 7(5), n/a–n/a, doi:10.1029/2005GC001045, 2006.
- Syracuse, E. M., van Keken, P. E. and Abers, G. A.: The global range of subduction zone thermal models, *Physics of the Earth and Planetary Interiors*, 183(1-2), 73–90, doi:10.1016/j.pepi.2010.02.004, 2010.
- Taboada, A., Rivera, L. A., Fuenzalida, A., Cisternas, A., Philip, H., Bijwaard, H., Olaya, J. and Rivera, C.: Geodynamic of the northern Andes: Subductions and intracontinental deformation (Colombia), *tectonics*, 19(5), 787–813, 2000.
- Tavera, H. and Buforn, E.: Source mechanism of earthquakes in Perú, *Journal of Seismology*, 5(4), 519–540, 2001.
- Tavera, H., Vilca, R. and Marin, G.: Inferences on the geometry of the Nazca Plate in northwestern Perú based on data collected by a local seismograph network, *Earth Sciences Research Journal*, 10(1), 15–24, 2006.
- Tibaldi, A., Rovida, A. and Corazzato, C.: Late Quaternary kinematics, slip-rate and segmentation of a major Cordillera-parallel transcurrent fault: The Cayambe-Afiladores-Sibundoy system, NW South America, *Journal of Structural Geology*, 29(4), 664–680, doi:10.1016/j.jsg.2006.11.008, 2007.
- Toro, J.: Enregistrement des surrections liees aux accretions de terrains oceaniques: les sediments cretace-paleogenes de Andes d'Equateur, *Geologie Alpine*, 1–236, 2007.
- Trenkamp, R., Kellogg, J., Freymueller, J. and Mora, H.: Wide plate margin deformation, southern Central America and northwestern South America, CASA GPS observations, *Journal of South American Earth Sciences*, 157–171, 2002.
- Troncoso, L.: Estudio sismológico del nido sísmico de Pisayambo, Université de Nice - Sophia Antipolis, 1–68, 2009.
- Vallee, M., Nocquet, J. M., Battaglia, J., Font, Y., Segovia, M., Régnier, M., Mothes, P., Jarrin, P., Cisneros, D., Chlieh, M., Vaca, S., et al.: Intense interface seismicity triggered by a shallow slow-slip event in the Central-Ecuador subduction zone,, 1–27, 2012.
- Vallée, M., Nocquet, J.-M., Battaglia, J., Font, Y., Segovia, M., Régnier, M., Mothes, P., Jarrin, P., Cisneros, D., Vaca, S., Yepes, H., et al.: Intense interface seismicity triggered by a shallow slow slip event in the Central Ecuador subduction zone, *J. Geophys. Res. Solid Earth*, n/a–n/a, doi:10.1002/jgrb.50216, 2013.
- Vargas, C. A. and Mann, P.: Tearing and Breaking Off of Subducted Slabs as the Result of Collision of the Panama Arc-Indenter with Northwestern South America, *Bulletin of the Seismological Society of America*, 103(3), 2025–2046, doi:10.1785/0120120328, 2013.

White, S. M., Trenkamp, R. and Kellogg, J. N.: Recent crustal deformation and the earthquake cycle along the Ecuador–Colombia subduction zone, *Earth and Planetary Science Letters*, 216(3), 231–242, doi:10.1016/S0012-821X(03)00535-1, 2003.

Winter, T., Avouac, J.-P. and Lavenu, A.: Late Quaternary kinematics of the Pallatanga strike-slip fault (Central Ecuador) from topographic measurements of displaced morphological features, *Geophysical Journal International*, 115(3), 905–920, 1993.

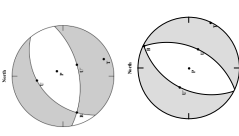
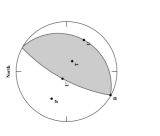
Witt, C. and Bourgois, J.: Forearc basin formation in the tectonic wake of a collision-driven, coastwise migrating crustal block: The example of the North Andean block and the extensional Gulf of Guayaquil-Tumbes Basin (Ecuador-Peru border area), *Geological Society of America Bulletin*, 122(1-2), 89–108, doi:10.1130/B26386.1, 2010.

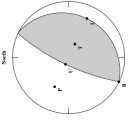
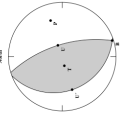
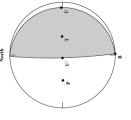
Witt, C., Bourgois, J., Michaud, F., Ordoñez, M., Jiménez, N. and Sosson, M.: Development of the Gulf of Guayaquil (Ecuador) during the Quaternary as an effect of the North Andean block tectonic escape, *tectonics*, 25(3), n/a–n/a, doi:10.1029/2004TC001723, 2006.

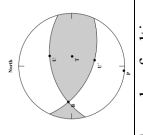
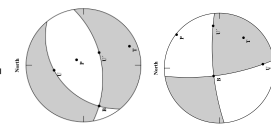
Yepes, H., Chatelain, J.-L., Guillier, B., Alvarado, A., Egred, J., Ruiz, M. and Segovia, M.: The Mw 6.8 Macas earthquake in the sub-Andean zone of Ecuador, October 3, 1995, *Seismological Research Letters*, 67(6), 27–32, 1996.

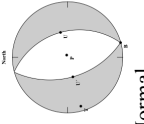
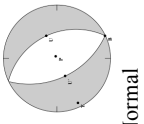
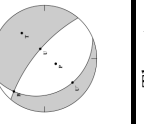
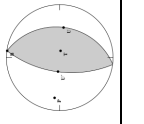
Yepes, H., Gajardo, E., Ramón, P. and Aguilar, J.: Evaluación Del Peligro Sísmico Para El Sitio Del Nuevo Aeropuerto Internacional De Quito, Internal Report, Instituto Geofísico-Escuela Politécnica Nacional, 1–236, 2006.

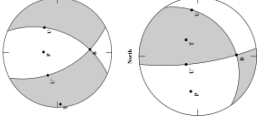
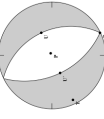
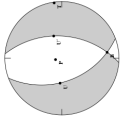
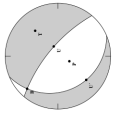
Table 1: Source zones features and description of the potential boundaries.

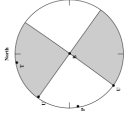
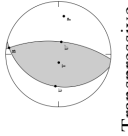
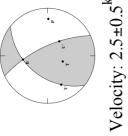
Zone ID	Morphotectonic features Structural/neotectonic evidence	Geophys./geodet./paleo - seism. evidences	Fault type focal mechanisms <sup>5</sup>	Significant earthquakes $M_w^1$ or $M_{TC}^2$ - $M_0$ density ( $N \cdot m$ )	hypocentral data: <sup>3</sup> range/mean/Std. dev (km) N events - Reported <sup>1</sup> /Suggested depth for largest events	Description of the zone boundaries	Observations - notes
<b>OUTER-TRENCH</b>							
OUT-1 Yaquina OUTER TRENCH	-Yaquina peleo-rift	-Ongoing seismicity	Normal Strike=N25 Dip>45° 	6.7 (2007) 6.1 (1991) - 6.74E+12	0-50 km/26 km /10.7/ 155 - 30 20-35 <sup>4</sup>	W: Yaquina graben E: Trench S: Malpelo rift fossil spreading center N: Lithospheric rifting site projection to 4°N <sup>a</sup>	Extensional seismicity continues below the interface in Esmeraldas SSZ
<b>INTERFACE MEGATHRUSTS</b>							
INTERFACE MEGATHRUST SMT-1 Esmeraldas	Trench, trench strike changes, interface megathrust faults, Carnegie Ridge crest, Jama fault zone <sup>b</sup> , Yaquina paleorift	Historical seismicity; ongoing seismicity Locked asperities and creeping corridor <sup>c</sup> 1998 aftershock zone	Thrust Strike=N30 Dip= 17-20° 	8.8 (1906) (range from 8.3s-8.8) 7.8 (1942) 7.6 (1958) 8.1 (1979) - 2.29E+15	0-50 km/19.5 km/ 11.16/ 854 - 30-37 <sup>4</sup> 20-27 <sup>f</sup> 30 <sup>d</sup>	W: trench N: N limit of Yaquina graben; sharp change in coastal strike (no trench morphology) S: S boundary of 1942 earthquake rupture and abutment with 1998 earthquake rupture; Carnegie ridge crest's inland projection <sup>b</sup> , low coupling strip <sup>c</sup> . E: 45-55 km megathrust earthquakes rupture maximum depth <sup>3</sup>	Three sub-segments could be identified corresponding to the 20 <sup>th</sup> Century seismic sequence <sup>c</sup> : Bahía- Atacames; Esmeraldas- Manglares; Southern Colombia trench.

SMT-2 Bahia	Trench, interface megathrust faults, Carnegie Ridge, Jama fault zone <sup>b</sup> , Grijalva rifted margin	Historical seismicity: ongoing seismicity; earthquake swarms; Locked shallow small asperity <sup>c</sup> ; creeping corridor <sup>c</sup> ; weakly coupling zones; slow slip events <sup>e</sup>	Thrust Strike=N27 Dip= 15° 	7.1 (1998) 7.0 (1956) ~7.0 (1896) potential to generate Mw~7.0-7.7 <sup>c</sup> 1.34E+14	0-35 km/1.6 km/ 8.46/ 1039 - 35 <sup>4</sup> 20 <sup>f</sup>	W: trench N: SMT-1 Esmeraldas S: Grijalva rift projection E: 35 km large thrust earthquakes rupture depth and modeled coupling <sup>c,g</sup>	Transitional segment from highly locked North to weakly locked South Müller 2012. Volcanic Ridges have fragile heterogeneous internal structure and a detachment interface → weak coupling
SMT-3 Talara	Trench, interface megathrust faults, Grijalva rifted margin, Viru fracture zone	Historical and Ongoing seismicity: earthquake cluster; tsunami earthquakes; weakly coupling zones <sup>g</sup> ,	Thrust (1970) Strike=N343 Dip= 65°  --- Strike=N340 Dip= 18° --- Thrust (1960) <sup>h</sup> Strike=0° Dip= 6° 	7.6 (1953) 7.6 (1960) 7.2 (1970) - 1.86E+14	0-35 km/25.6 km/ 9.02/ 129 - 19-25 <sup>4</sup> 15 <sup>6</sup>	W: trench N: SMT-2 Bahia S: Viru fracture zone projection (for practical purposes this study stops at 6°S) E: 15 (35?) km deep seismogenic zone <sup>6</sup> . The N-S azimuth of the boundary tries to account for the variation in dip as Farallon plate approaches Grijalva scarp	1970 earthquake is not an interface (IF) event but could be very close to the IF; hard to differentiate crustal from IF earthquakes This could be considered to be a tsunami earthquakes source zone implying that rupture could start at shallow depths but no strong damaging high frequency waves are generated.
INTRAPLATE							
INSLAB-NAZCA	Grijalva rifted margin; East Malpelo paleorift, trench,	Dipping seismicity; earthquake clusters;	Despite the few number of faulting mechanisms, there is a great variety of them but not enough number to characterize each subzone. Normal (2010) Strike=N65 Dip= 45°	7.2 (2012) 7.0 (2013) to the northeast of the modeled zones;	From 50 to 130 km.	North: artificial boundary East: magma generating conditions' depth South: Grijalva rift projection West: SMT-1 Esmeraldas/SMT-2 Bahia	The seismic catalog used in this study stops in 2009. Nevertheless, the 2012 Mw 7.2 and 2013 Mw 7.0 earthquake, have been used to define the zones. No earthquakes ≥6 were reported between ~1°S and ~2°N prior to 2012.

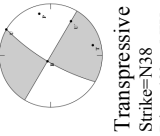
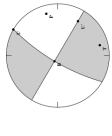
ISN-NAZCA						
ISN-1 Sub-Tumaco (aux)		Scarce seismicity		6.5 - 9.27E+12	50-75/61.2/7.37/ 39	Part of this seismicity could be related to Yaquima source zone
ISN-2 Sub-Esme-Bahia (aux)		Scarce seismicity	thrust Strike=N30 Dip= 20°	6.3 - 2.97E+12	50-75/60.5/7.07/ 63	
ISN-3 Sub-Bahia (aux)		Ongoing seismicity		5.3 - 1.23E+12	35-50/42.1/4.17/ 117	Small zone to permit incorporating all the seismicity in the model. To be added to ISN-2
ISN-4 Caldas cluster		Scarce seismicity	Complex faulting 	6.7 (1997) - 2.32E+12	50-230/122.3/45.65/ 62	
ISN-5 Sub-Volcanic arc		Ongoing seismicity	Complex faulting 	7.2 (2012) 7.0 (2013) - 1.56E+12	35 (50)-180/95/21.84/ 458 - 170-210 <sup>f</sup>	The upper surface of this subzone could reach up to 120 km below the Cordillera Real in the magma generation zone

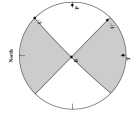
INSLAB FARALLON	Grijalva rifted margin	Dipping seismicity; earthquake clusters;	<p>From South to North:</p> <p>Normal Strike=N345 Dip= 40° </p> <p>Normal Strike=N335 Dip= 40° </p> <p>Normal Strike=N310 Dip= 70° </p>	<p>7.5 (2005) 7.4 (1971) 7.2 (1997) 7.1 (2010)</p>	<p>Progressively dipping from west to east starting at 35 km; maximum depth= 250 km</p>	<p>North: Grijalva rift projection East: intermediate depth seismicity South: artificial boundary West: SMT-3 Talara</p>	<p>Dip from focal mechanisms do not show the dipping slab. They represent detachments/tears inside the plunging slab. Rough slab dip estimates vary from very shallow (13°) South of 3°S to normal 20°-100 km north and plunges to &gt;30° at the El Puyo cluster. Due to seismicity distribution there is room for defining sub-segments as consecutively deeper volumes to the NE</p>
ISF - FARALLON			<p>Thrust Strike=N 0-10 Dip= 20-45° </p>	<p>5.8 (1997, 2000) 5.64E+12</p>	<p>35-75/50/10.88/ 156</p>		
Sub-Talara (aux)							

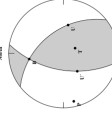
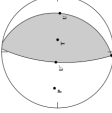
	ISF-2 Loja			<p>Transpressive or transpressive Strike=N30-50 Dip= 60-75° Normal Strike=N 30° Dip= 30-45°</p> 	6.0 (1982) - 2.84E+12	35-100/63.7/20.29/ 506		There is a variety of focal mechanisms. The zone is probably subjected to different stress regimes
ISF-3	Morona			<p>Normal Strike=N335-345 Dip= 40°</p> 	7.5 (2005) 7.4 (1971) 7.2 (1997) - 6.02E+13	100-130/114/8.26/ 260		
ISF-4	Puyo 1			<p>Normal Strike=N301 Dip= 68° Normal Strike=N310 Dip= 70°</p> 	6.5 (1982) 7.1 (2010) - 5.74E+13	100-130/114/8.26/ 260		
ISF-5	Puyo2 cluster - Peru			<p>Normal Strike=N301 Dip= 68° Normal Strike=N310 Dip= 70°</p> 	6.5 (1982) 7.1 (2010) - 6.79+12	130-180/157.1/14.28/ 511		

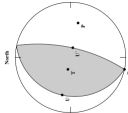
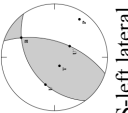
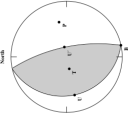
Zone ID	Morphotectonic features Structural/neotectonic evidence	Geophys./geodet./paleo - seism. evidences	Fault type focal <sup>s</sup> mechanisms	Significant earthquakes $M_w$ <sup>1</sup> or $M_C$ <sup>2</sup> - $M_0$ density ( $N \cdot m$ )	hypo-central data: <sup>3</sup> range/mean/Std. dev (km) N events - Reported <sup>d</sup> /Suggested depth for largest events	Description of the zone boundaries (by hierarchy)	Observations - notes
CRUSTAL CCPP							
NAB-1 Chingual	Regional fresh lineaments 270 km long <sup>1</sup> , strong drainage control; spurs and shutter ridges <sup>1</sup> and pull apart basin; displaced lava and debris flows	Historical seismicity; Geological markers such as lava flows displaced during the Holocene <sup>1</sup>	Right lateral- strike slip Strike=N35 Dip= 90°  Velocity: $7 \pm 3$ <sup>f</sup> - 11.9 $\pm$ 0.7 <sup>f</sup> mm/a	7.2-7.6 (1834) <sup>2</sup> - 7.58+12	0-33/8.1/7.88/ 18 -	N35° 150 km long 30 km wide segment from E of Cayambe volcano to Sibundoy pull apart. Seven small sub-segments have been detailed by Tibaldi <sup>1</sup> .	The fault's length could be as much as 240 km in Ecuador and Colombia <sup>1</sup> . Any of the seven sub- segments could produce a $M$ 7.0 $\pm$ 0.1
NAB-2 Cosanga	Regional fresh lineaments, strong drainage control, upthrown alluvial deposits <sup>1</sup>	Thrust fault mechanisms along the N10 trending segment of the boundary; $M_w$ >6 instrumental earthquakes	Thrust (N) Strike=N15 Dip= 25° to E  Transpressive (S) Strike=N38 Dip= 42° to NW  Velocity: $2.5 \pm 0.5$ <sup>k</sup> mm/a	6.8 (1955) North 7.1 (1987) North 6.3 (1987) South - 2.91+14	0-35/9.1/7.38/ 414 - 12 <sup>4</sup> 10 <sup>f</sup>	N-S (N12°) 160 km long and 40 km wide zone including Baeza- Reventador and Cosanga-Jatunyacu faults <sup>1</sup> . North and south limits are related to changes in strike of the megastructure. The segment is also limited by instrumental seismicity $M > 6$	The transition zone around Pisayambo cluster allows at least three different ways of modeling: the two segments: including the sept. 22 <sup>nd</sup> , 1987 earthquakes in either segment or defining one single segment that comprises N12° and N30° shorter segments.

NAB East Boundary

NAB-3 Pallatanga	Offset ridges and valleys, linear pressure ridges, fluvial terrace raisers <sup>m</sup> in Rio Pangor zone, fault plane outcrops <sup>m</sup>	South: repetitive surface rupture from paleoseismic studies <sup>m</sup> North: Pisayambo seismic cluster; Repetitive M>6 historical earthquakes	<p>Right lateral-strike slip (paleo) Strike=N30 Dip= 75° to NW<sup>b</sup> Velocity: 2.5<sup>m</sup> – 3.0<sup>c</sup>-4.6<sup>n</sup> mm/a</p> <p>Right lateral-strike slip Strike=N35 Dip= 75° to NW<sup>n</sup></p>  <p>Transpressive Strike=N38 Dip= 42° to NW</p>	7.5 (paleoseismic) 7.6 (1797) 7.0 (1645) - 9.58+13	0-35/9.73/5.37/ 931 -	NNE-SSW, ~40 km wide zone including Bucay-Rio Chimbo and Pallatanga-Rumipamba segments <sup>a</sup> to the south Pucará-Pisayambo <sup>n</sup> (Llanganates) faults to the north. North and south limits are related to changes in strike of the megastucture. The segment is also limited by historical and instrumental seismicity with M>6	The 1698 earthquake is located <sup>2</sup> close to the limit between Pisayambo and UJO-Latacunga sources. It has either ruptured a different fault and not Pallatanga or is a reverse fault of the Western Cordillera, Romeral-Caupa-Patia domain. It is not included here.
NAB-4 Puna	Uplifted Quaternary dome along a positive flower structure <sup>b</sup> ; beach morphology control, pull apart basin <sup>p</sup>	Paleo-evidences: Repetitive drainage offset. Low seismicity rate	<p>Right lateral-strike slip (paleo) Strike=N30</p>  <p>Velocity: 5.8 – 8.0<sup>p</sup> mm/a (up to 80% of the total slip rate)</p>	- - 5.25+11	0-35/17.37/9.48/ 104 -	N60°, ~200 km corridor that widens in the GGYE zone, abutting SMT-3 Talara to the west and NAB-3 Pallatanga to the east. The Zambapala fault zone <sup>k</sup> and the Santa Clara fault <sup>p</sup> are recognized structures.	Normal faults have been described in the GGYE area. They are detachment surfaces that verticalize towards the surface <sup>q</sup> . They are limited in extension and are not modeled here.

CRUSTAL WESTERN CORDILLERA					
Romeral – Cauca Patía WCR-1 El Angel	Offset of Quaternary moraines, drainage control, strike slip neotectonic morphology with dextral movement pattern <sup>k</sup> ,	Historical Seismicity, scattered microseismicity	Right lateral-strike slip.  Velocity: 1.2 – 1.5 <sup>f</sup> mm/a defined for the Buesaco fault in Colombia	7.2 (1859) 7.2 (1868) 6.6 (1868) - 2.56+11	0-29/10.06/5.73/ 130 -
				NE-SW ~200 km long, 80 km wide zone including San Isidro-Guachuca, El Angel, Otavalo, Huayrapungo, Apuela, and Nanegalito, faults or lineaments, all having NE-SW trend and right lateral movement. To the East it butts against NAB-1 Chingual. It is part of the Romeral Fault System that's apparently comes very close to the CCPP System at that region. To the south it engulfs WCR-2. There are local structures showing thrust movement.	The Buesaco-Aranda faults in Colombia are excluded because microseismicity is not defining it in the catalog and is too far to be influential for Ecuador PSHA. Borderline sources have to be worked in conjunction with neighbor countries' scientists. Large historical earthquakes tend to align with El Angel-Otavalo faults. The "deep" 1859 earthquake <sup>2</sup> is included here due to lack of intermediate depth seismicity north of Grijalva rift (this study). The 1994-05-11 m <sub>b</sub> 5.2 earthquake to the west is excluded from the zone since it shows thrust faulting <sup>5</sup>

<p>WCR-2 UIO-Latacunga</p>	<p>150 km long series of discontinuous Quaternary folds and piggy back basins related to blind reverse faults with evidences of tilted young volcanoclastic deposits. Quito Fault System (QFS)<sup>1</sup>: N-S, ~60 km long en echelon folds, five subsegments, tilted outcrops, controlled drainage pattern. Up-thrown block ~400 m above original surface since the Q<sup>k</sup> Latacunga Fault System (LFS)<sup>2</sup>: N-S ~80 km long folds both sides of the Interandean Depression and transversally cutting it; five well defined main structures<sup>3,u</sup>, divergently dipping faults in both sides of the Interandean Depression</p>	<p>Microseismicity, historical seismicity, GPS measured deformation (transect in QFS), paleoseismic deformation sequence in paleo-lakes<sup>w</sup> for QFS</p> <p>QFS: N-S reverse dip ~45° W<sup>1</sup> Strike=N10 Dip= 55° to W<sup>5</sup> Dip= 30°-55° to W<sup>1</sup></p>  <p>Velocity:<sup>1</sup> 4.3 – 5.3<sup>1</sup> mm/a from GPS modeling</p> <p>LFS: reverse, W structures: dip ~28°<sup>o,k,x</sup> Strike=N-S Dip= 70° to W<sup>d</sup></p>  <p>Velocity: 1.4±0.3<sup>1</sup>– 2.1±0.5<sup>k</sup> mm/a E structures: dip ~28°<sup>o,k,y</sup> (theo) Strike=N-S Dip= 80° to E<sup>x</sup></p>	<p>QFS: 6.4 (1587) 6.4 (1914)? 5.8 (1938) &gt;6.0 (1923) LFS: 5.9 (1996) 5.7 (1976) 5.8-6.0 (1962) 5.6-5.7 (1960) 5.9-6.4 (1757) 5.7-6.2 (1736)</p> <p>- 8.80±12</p>	<p>0-35/12.42/8.41/ 704 - 5<sup>4</sup> QFS: Latacunga: 15<sup>4</sup></p>	<p>N-S to N15° ~40 km wide zone including Quito Fault System and Guayllabamba Fault to the north and Latacunga Fault System to the south. Machachi strike slip fault lays between the two. Latacunga FS contains La Victoria, Latacunga, Yanayacu, Poaló and Nagsiche faults and folds<sup>v</sup> (Mollepamba-Guambalo, Jachahuangu, are alternative names for some of the structures<sup>y</sup>). To the north this zone abuts WCR-1 El Angel zone reflecting the strike rotation and faulting type; to the south it butts against NAB-3 Pallatanga including the 1698 earthquake. The eastern boundary is drawn to include the 1914 event which could be related to NNE-SSW strike slips faults north of Cotopaxi Volcano<sup>x</sup></p>	<p>These are reverse structures divergently dipping to the west and east along the western and eastern slopes respectively of the Interandean Depression, a push-down feature<sup>u</sup> North of Cotopaxi Volcano Transpressive minor faults have also been described<sup>7,a</sup>. The structures define the N-S portion of a restraining bend<sup>7</sup>. For including hanging wall effects in PSIA, individual fault segments will have to be considered. Since he 1587 and 1914 historical earthquakes are just east of the main structures, they could belong to ENE transversal structures<sup>1</sup>. Historical seismicity has been extensively listed to show recurrence of moderate shallow earthquakes.</p>
--------------------------------	---	--	--	--	---	--

CRUSTAL EASTERN SUBANDEAN BELTS AND UPLIFTS							
ESB-1 Napó	East verging folds on top of blind thrusts dipping west. Right lateral strike slip faults <sup>z</sup> , NNW-SSE positive flower structure <sup>aa</sup>	Microseismicity, medium size magnitude instrumental earthquakes	Thrust faults Velocity: 3 <sup>gg</sup> mm/a 	- - 1.66+12	0-33/13.64/7.39/ 201 -	N-S to NNE-SSW 150 km long, 70 km wide uplift north of Pastaza depression. Main faults are Cascales, Payamino, Sumaco, Pusuno, Puyo and Mera faults <sup>y</sup> .	There are two main uplifts composing the sub-Andean Belts: Napo and Cutucu, both converging to the Pastaza depression. Basement thrusts are underlying both uplifts <sup>bb</sup> . They are overthrust in the west by rocks of the Cordillera Real <sup>cc</sup> .
ESB-2 Cutucu	Fold-and-thrust belt; rivers diversion in Pastaza depression <sup>dd</sup> ; complex reverse-transpressive faults system in Cutucu uplift <sup>cc</sup> ; deformed alluvial terraces by thrust belts in Upano river <sup>dd</sup>	Large earthquakes, persistent microseismicity.	Reverse E-NE faults <sup>cc</sup> ; Strike=N45 Dip=40° to W <sup>5</sup>  SS-left lateral N-NW faults <sup>cc</sup> Strike=N165 Dip=75° to W <sup>5</sup> Thrust faults <sup>dd</sup> Velocity: 10-28 mm/a <sup>dd</sup> of uplift at the Pastaza depression	7.0 (1995) - 3.42+13	0-35/13.81/8.35/ 1009 - 13 <sup>4</sup> 30 <sup>f</sup>	N-S to NNW-SSE 250+ km long, ~100 km wide uplift south of Pastaza depression. Main faults are <sup>y</sup> Pastaza, Santiago-Upano, Taisha and Morona <sup>cc</sup> faults in Ecuador and Shitari fault in Peru. It includes the Macas fault system to the west.	The rapid uplift of the Mera plateau <sup>dd</sup> in the Pastaza Depression may be caused by regional-scale low angle thrust ramp <sup>dd</sup> . The Mw 7.0 earthquake may be located at the Morona thrust if a deep hypocentral depth is accepted <sup>cc</sup> . The Macas fault system is included although no present day seismic activity has been confirmed.
ESB-3 Moyobamba	Thin-skinned thrust-and-fold belt; folds and high angle thrusts <sup>ee</sup>	Moderate to large earthquakes; persistent microseismicity.	Thrust faults <sup>dd</sup> Reverse E-NE faults <sup>cc</sup> ; Strike=N170 Dip=20-25° to W <sup>5</sup> 	6.5 (1990) 6.4 (1991) - 7.16+13	0-35/25.93/7.53/ 95 -	NW-SE zone that continues to the SE as part of the central Andes sub-Andean zone.	This is part of the Huallaga-Santiago foreland segment <sup>bb</sup> , is characterized by the Salt-related thin-skinned Santiago thrust belt <sup>bb</sup> . This source zone has to be constructed with neighboring countries' scientists.

Andean Back-Arc

**Table 1: Source zones features and description of the potential boundaries.** We have subdivided the table according to the plate environments and the domains presented in Figs. 7 and 10. Seismicity information and hypocentral statistics are obtained from the Ecuadorian PSHA seismic catalog. Focal mechanism solutions are meant to graphically describe the general fault source mechanism in the Table. When available, they come from the Harvard Global Centroid Moment Tensor catalog<sup>5</sup> and correspond to the most significant earthquakes occurred from 1976 on, as listed in the next column. If more than one type of focal mechanisms are found for significant earthquakes, both are displayed. The moment density is calculated by adding all the seismic moments released by the cataloged earthquakes in the source volume and dividing by the total source volume. The reference to numbers and letters is described below.

<sup>1</sup> Beauval et al. (2013); <sup>2</sup> Beauval et al. (2010); <sup>3</sup> Brittle limit of seismogenic layers in the crust is defined by local seismicity relocated by Font et al. (2013), seismogenic zone bottom limits for underthrusting large earthquakes is taken as reported in the literature (Lay et al., 2012); <sup>4</sup> Focal depths from reported megathrust or large crustal hypocenters taken from the catalog (Beauval et al., 2013); <sup>5</sup> Focal mechanisms from the GCMT data base (Dziwonski et al., 1981); <sup>6</sup> Nucleation depths of rare tsunami earthquakes that propagate updip.

<sup>a</sup>Lonsdale, 2005; <sup>b</sup>Collot et al., 2004; <sup>c</sup>Chlieh et al., 2014; <sup>d</sup>Manchuel et al., 2011; <sup>e</sup>Vallee et al., 2012; <sup>f</sup>Storchak et al., 2013; <sup>g</sup>Nocquet et al., 2014; <sup>h</sup>Pelayo and Wiens, 1990; <sup>i</sup>Tibaldi et al., 2007; <sup>j</sup>Ego et al., 1996; <sup>k</sup>Ego and Sébrier, 1996; <sup>l</sup>Alvarado et al., 2015; <sup>m</sup>Baize et al., 2014; <sup>n</sup>Winter et al., 1993; <sup>p</sup>Dumont et al., 2005; <sup>q</sup>Witt et al., 2006; <sup>r</sup>Tibaldi and Romero, 2000; <sup>s</sup>Alvarado, 2012; <sup>t</sup>Alvarado et al., 2014; <sup>u</sup>Lavenue et al., 1995; <sup>v</sup>Egüez et al., 2003; <sup>w</sup>Hibsch et al., 1997; <sup>x</sup>Fiorini and Tibaldi, 2012; <sup>y</sup>Soulas et al., 1991; <sup>z</sup>Balseca et al., 1993; <sup>aa</sup>Barragan et al., 2005; <sup>bb</sup>Kley et al., 1999; <sup>cc</sup>Legrand et al., 2005; <sup>dd</sup>Bès de Berc et al., 2005; <sup>ee</sup>Alva-Hurtado et al., 1992.

## References

- Alva-Hurtado, J. E., J. F. Meneses, L. Chang, and J. L. Lara (1992), Ground effects caused by the Alto-Mayo earthquakes in Peru, *Tenth World Conference on Earthquake Engineering*.
- Alvarado, A. (2012), *Néotectonique et cinématique de la déformation continentale en Équateur*, Thèse, Université de Grenoble, Grenoble.
- Alvarado, A., L. Audin, J. M. Nocquet, E. Jaillard, P. Mothes, P. Jarrin, M. Segovia, F. Rolandone, and D. Cisneros (2015), Migration and localization of a continental plate boundary in Ecuador: present-day active faulting delimiting the North Andean Sliver to the East (in revision), *Tectonics*, 1–40.
- Alvarado, A., L. Audin, J.-M. Nocquet, S. Lagreulet, M. Segovia, Y. Font, G. Lamarque, H. Yepes, P. Mothes, and F. Rolandone (2014), Active tectonics in Quito, Ecuador, assessed by geomorphological studies, GPS data, and crustal seismicity, *tectonics*, 33(2), 67–83, doi:10.1002/(ISSN)1944-9194.
- Baize, S., E. M. Cushing, F. Lemeille, and H. Jomard (2013), Updated seismotectonic zoning scheme of Metropolitan France, with reference to geologic and seismotectonic data, *Bulletin de la Société Géologique de France*, 184(3), 225–259.
- Baize, S., L. Audin, T. Winter, A. Alvarado, L. Pilatasig Moreno, M. Taïpe, P. Reyes, P.

- Kauffman, and H. Yepes (2014), Paleoseismology and tectonic geomorphology of the Pallatanga fault (Central Ecuador), a major structure of the South-American crust, *Geomorphology*, 1–15, doi:10.1016/j.geomorph.2014.02.030.
- Balseca, W., L. Ferrari, G. Pasquare, and A. Tibaldi (1993), *Structural evolution of the Northern sub-Andes of Ecuador : the Napo uplift*, Second ISAG, Oxford.
- Barragan, R., P. Baby, and R. DUNCAN (2005), Cretaceous alkaline intra-plate magmatism in the Ecuadorian Oriente Basin: Geochemical, geochronological and tectonic evidence, *Earth and Planetary Science Letters*, 236(3-4), 670–690, doi:10.1016/j.epsl.2005.03.016.
- Beauval, C., H. Yepes, P. Palacios, M. Segovia, A. Alvarado, Y. Font, J. Aguilar, L. Troncoso, and S. Vaca (2013), An Earthquake Catalog for Seismic Hazard Assessment in Ecuador, *Bulletin of the Seismological Society of America*, 103(2A), 773–786, doi:10.1785/0120120270.
- Beauval, C., H. Yepes, W. H. Bakun, J. Egred, A. Alvarado, and J.-C. Singaicho (2010), Locations and magnitudes of historical earthquakes in the Sierra of Ecuador (1587-1996), *Geophysical Journal International*, doi:10.1111/j.1365-246X.2010.04569.x.
- Bès de Berc, S., J. C. Soula, P. Baby, M. Souris, F. Christophoul, and J. Rosero (2005), Geomorphic evidence of active deformation and uplift in a modern continental wedge-top–foredeep transition: Example of the eastern Ecuadorian Andes, *Tectonophysics*, 399(1-4), 351–380, doi:10.1016/j.tecto.2004.12.030.
- Chlieh, M. et al. (2014), Distribution of discrete seismic asperities and aseismic slip along the Ecuadorian megathrust, *Earth and Planetary Science Letters*, 400(C), 292–301, doi:10.1016/j.epsl.2014.05.027.
- Collot, J.-Y., B. Marcaillou, F. Sage, F. Michaud, W. Agudelo, P. Charvis, D. Graindorge, M. A. Gutscher, and G. Spence (2004), Are rupture zone limits of great subduction earthquakes controlled by upper plate structures? Evidence from multichannel seismic reflection data acquired across the northern Ecuador–southwest Colombia margin, *Journal of Geophysical Research: Solid Earth (1978–2012)*, 109(B11).
- Dumont, J. F., E. Santana, and W. Vilema (2005), Morphologic evidence of active motion of the Zambapala Fault, Gulf of Guayaquil (Ecuador), *Geomorphology*, 65(3-4), 223–239, doi:10.1016/j.geomorph.2004.09.003.
- Dziewonski, A. M., T. A. Chou, and J. H. Woodhouse (1981), Determination of earthquake source parameters from waveform data for studies of global and regional seismicity, *Journal of Geophysical Research: Solid Earth (1978–2012)*, 86(B4), 2825–2852.
- Ego, F., and M. Sébrier (1996), The Ecuadorian Inter-Andean Valley: a Major and Complex restraining bend and Compressive Graben since Late Miocene Time, *Annales Tectonicae*, 10(1-2), 31–59–29.
- Ego, F., M. Sébrier, E. Carey-Gailhardis, and D. Insergueix (1996), Les phénomènes naturels générateurs de dommages, *Bull Inst fr études andines*.
- Egüez, A., A. Alvarado, H. Yepes, M. Machette, C. Costa, and R. Dart (2003), Database and Map of Quaternary faults and folds of Ecuador and its offshore regions, *USGS Open file Report 03-289*, 1–77.
- Fiorini, E., and A. Tibaldi (2012), Quaternary tectonics in the central Interandean Valley, Ecuador: Fault-propagation folds, transfer faults and the Cotopaxi Volcano, *Global and Planetary Change*, 90-91, 87–103, doi:10.1016/j.gloplacha.2011.06.002.
- Font, Y., M. Segovia, S. Vaca, and T. Theunissen (2013), Seismicity patterns along the Ecuadorian subduction zone: new constraints from earthquake location in a 3-D a priori velocity model, *Geophysical Journal International*, 193(1), 263–286, doi:10.1093/gji/ggs083.
- Hibsch, C., A. Alvarado, H. Yepes, V. H. Perez, and M. Sébrier (1997), Holocene liquefaction and soft-sediment deformation in Quito (Ecuador): A paleoseismic history recorded in lacustrine sediments, *Journal of Geodynamics*, 24(1-4), 259–280, doi:10.1016/S0264-

3707(97)00010-0.

- Kley, J., C. R. Monaldi, and J. A. Salfity (1999), Along-strike segmentation of the Andean foreland: causes and consequences, *Tectonophysics*, 301(1), 75–94.
- Lavenu, A., T. Winter, and F. Dávila (1995), A Pliocene–Quaternary compressional basin in the Interandean Depression, Central Ecuador, *Geophysical Journal International*, 121(1), 279–300.
- Lay, T., H. Kanamori, C. J. Ammon, K. D. Koper, A. R. Hutko, L. Ye, H. Yue, and T. M. Rushing (2012), Depth-varying rupture properties of subduction zone megathrust faults, *J. Geophys. Res.*, 117(B4), B04311, doi:10.1029/2011JB009133.
- Legrand, D., P. Baby, F. Bondoux, C. Dorbath, S. Bès de Berc, and M. Rivadeneira (2005), The 1999–2000 seismic experiment of Macas swarm (Ecuador) in relation with rift inversion in Subandean foothills, *Tectonophysics*, 395(1-2), 67–80, doi:10.1016/j.tecto.2004.09.008.
- Lonsdale, P. (2005), Creation of the Cocos and Nazca plates by fission of the Farallon plate, *Tectonophysics*, 404(3-4), 237–264, doi:10.1016/j.tecto.2005.05.011.
- Manchuel, K., M. Régnier, N. Béthoux, Y. Font, V. Sallarès, J. Díaz, and H. Yepes (2011), New insights on the interseismic active deformation along the North Ecuadorian–South Colombian (NESC) margin, *tectonics*, 30(4), n/a–n/a, doi:10.1029/2010TC002757.
- Nocquet, J. M. et al. (2014), Motion of continental slivers and creeping subduction in the northern Andes, *Nature Geosci.*, (7), 287–291, doi:DOI: 10.1038/NGEO2099.
- Pelayo, A. M., and D. A. Wiens (1990), The November 20, 1960 Peru tsunami earthquake: Source mechanism of a slow event, *Geophys. Res. Lett.*, 17(6), 661–664.
- Soulas, J.-P., A. Egüez, H. Yepes, and V. H. Perez (1991), Tectónica activa y riesgo sísmico en los Andes Ecuatorianos y en el extremo Sur de Colombia, *Boletín Geológico Ecuatoriano*, 2(1), 3–11.
- Storchak, D.A., D. Di Giacomo, I. Bondár, E. R. Engdahl, J. Harris, W.H.K. Lee, A. Villaseñor and P. Bormann, 2013. Public Release of the ISC-GEM Global Instrumental Earthquake Catalogue (1900-2009). *Seism. Res. Lett.*, 84, 5, 810-815, doi: 10.1785/0220130034.
- Tibaldi, A., A. Rovida, and C. Corazzato (2007), Late Quaternary kinematics, slip-rate and segmentation of a major Cordillera-parallel transcurrent fault: The Cayambe-Afiladores-Sibundoy system, NW South America, *Journal of Structural Geology*, 29(4), 664–680, doi:10.1016/j.jsg.2006.11.008.
- Tibaldi, A., and J. Romero (2000), Morphometry of Late Pleistocene-Holocene faulting in the southern Andes of Colombia and volcano-tectonic relationships, *tectonics*, 19(2), 358–377.
- Vallee, M. et al. (2012), Intense interface seismicity triggered by a shallow slow-slip event in the Central-Ecuador subduction zone,, 1–27.
- Winter, T., J.-P. Avouac, and A. Lavenu (1993), Late Quaternary kinematics of the Pallatanga strike-slip fault (Central Ecuador) from topographic measurements of displaced morphological features, *Geophysical Journal International*, 115(3), 905–920.
- Witt, C., J. Bourgois, F. Michaud, M. Ordoñez, N. Jiménez, and M. Sosson (2006), Development of the Gulf of Guayaquil (Ecuador) during the Quaternary as an effect of the North Andean block tectonic escape, *tectonics*, 25(3), n/a–n/a, doi:10.1029/2004TC001723.

# Probabilistic Seismic-Hazard Assessment in Quito, Estimates and Uncertainties

by Céline Beauval, Hugo Yepes, Laurence Audin, Alexandra Alvarado, Jean-Mathieu Nocquet, Damiano Monelli, and Laurentiu Danciu

*Online Material:* National earthquake catalog for Ecuador.

## INTRODUCTION

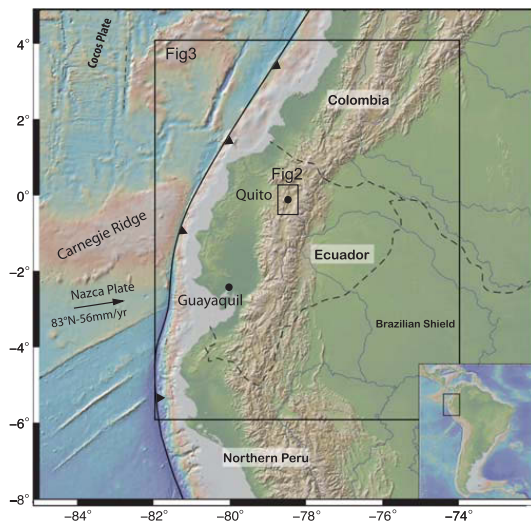
The present study is focused on estimating the probabilistic seismic hazard for the capital city of Ecuador, Quito, the population of which currently exceeds 2 million inhabitants at present. Quito is located at 2800 meters above sea level within the Interandean Depression, bounded by the equatorial line to the north, in an earthquake-prone environment (Chatelain *et al.*, 1999; Fig. 1). The city and its suburbs have developed in a piggy-back basin on the hanging wall of a reverse fault system (Fig. 2) that has been recognized as seismically active in historical, geomorphologic, geologic, and geodetic studies (Soulas *et al.*, 1991; Ego and Sebrier, 1996; Hibschi *et al.*, 1997; Egred, 2009; Champenois *et al.*, 2013; Alvarado *et al.*, 2014).

The historical record, spanning five centuries, shows that the city experienced MSK intensities (Medvedev *et al.*, 1963) in the VII–VIII range at least five times, with damages reported in churches and houses (Pino and Yepes, 1990; Egred, 2009). The most destructive earthquake was the 1859 event ( $I_{\max}$  VII–VIII). Analyzing its intensity dataset, Beauval *et al.* (2010) proposed a mean magnitude  $M_I$  7.2 (fig. 12 of their paper,  $M_I$  is an intensity magnitude equivalent to moment magnitude) and a location at an intermediate depth in the slab; a location on a shallow crustal fault cannot, however, be excluded. The 1797 Riobamba earthquake ( $M_I$  7.6), 160 km south of Quito, produced an intensity VII in the city. A similar shaking level was experienced during another large earthquake, the 1868 Ibarra event, probably generated on the Otavalo fault located 50 km north of Quito ( $M_I$  7.2, fig. 13 in Beauval *et al.*, 2010). Two more earthquakes, described by a sparse set of intensities and therefore difficult to characterize, could have been produced by one of the Quito fault segments. These events occurred in 1587 ( $I_{\max}$  VIII,  $M_I$  6.3–6.5, fig. 15 in Beauval *et al.*, 2010) and 1755 (observations available only in Quito, corresponding to intensity VII). In the last 150 years, no major earthquake hit Quito. The most recent significant earthquakes on the city fault system were in 1990 ( $M_w$  5.3), and in 2014 (12 August,  $M_w$  5.1); in both cases three inhab-

itants were killed in the northern suburb of Pomasqui (location indicated in Fig. 2). In an attempt to extend the observation time window, Hibschi *et al.* (1997) analyzed earthquake-induced deformation phenomena in lacustrine sediments in the northern part of the Quito basin. They studied approximately a 1500-year time span prior to the historical record. One major event was identified (intensity evaluated to X, greater than the maximum intensity in the historical record) between the tenth and the sixteenth centuries, which they believed could have ruptured the entire Quito fault reaching a magnitude 6.5–7.0. This is the unique evidence for such a large earthquake on the fault system. More recently, the seismic potential of the Quito fault was confirmed on the basis of observations covering a much shorter time window. Analyzing Global Positioning System (GPS) measurements at sites with 10–15 years of recordings, east–west horizontal shortening rates were estimated in the 4.3–5.3 mm/yr range across this blind thrust (Alvarado *et al.*, 2014).

Since 2007, a joint collaboration between France and Ecuador has been in place to prepare all the necessary inputs for computing PSH for Ecuador. The research laboratories involved are the Geophysical Institute (IG) in Quito, ISTERre in Grenoble, and Géozur in Nice. The IG has a governmental mandate to monitor earthquakes and provide national seismic-hazard estimations. PSH maps are the basis for establishing seismic building codes. A PSH assessment requires a seismicity model, a description of the probability of occurrence of future earthquakes, and a ground-motion prediction equation (GMPE), which gives the probability of occurrence of accelerations as a function of magnitude and distance. As the Ecuadorian strong-motion network is very young, GMPEs established elsewhere in the world must be imported.

By analyzing seismicity distribution, active faults and plate margins, as well as geodetic measurements, Alvarado (2012, Fig. 3) subdivided the region into seismic sources. This seismotectonic zoning is the one used in our 2011 PSH calculations that we provided to the Ecuadorian committee in charge of establishing the new Ecuadorian building code (MIDUVI-CCQ, 2011). Beauval *et al.* (2010, 2013) created a unified and homogeneous earthquake catalog for Ecuador and borders covering five centuries and integrating instrumental and historical events (Ⓔ see Tables S1 and S2, available in the

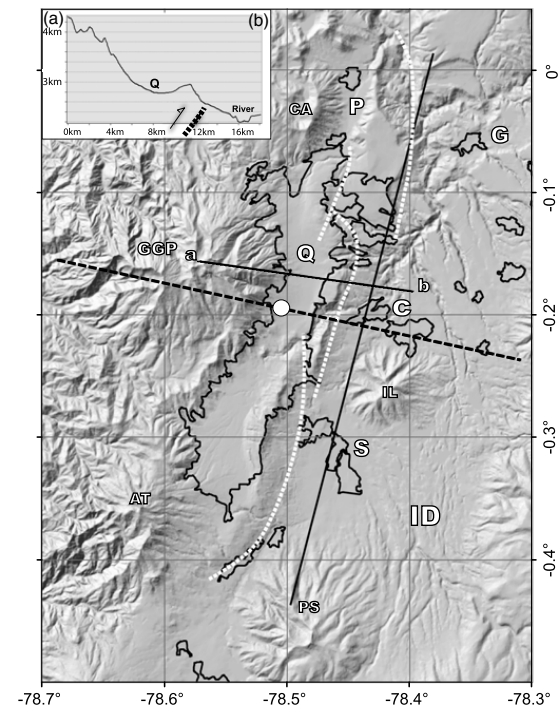


▲ **Figure 1.** Regional map of the study, rectangles define the areas displayed in Figures 2 and 3. Inset shows South America with the plotting region marked.

electronic supplement to this paper). The present study proposes to estimate PSH in Quito based on the Alvarado (2012) zoning coupled with the newly published earthquake catalog. The OpenQuake engine is used for all PSH calculations (Global Earthquake Model, [www.globalquakemodel.org/](http://www.globalquakemodel.org/) (last accessed October 2014); Crowley *et al.*, 2013; Pagani *et al.*, 2014). We focus on hazard estimate at 475 years return period, corresponding to a 10% probability of exceedance over 50 years. Our approach is first to identify the controlling parameters and then to evaluate the uncertainties on these parameters and the corresponding impact on the hazard levels.

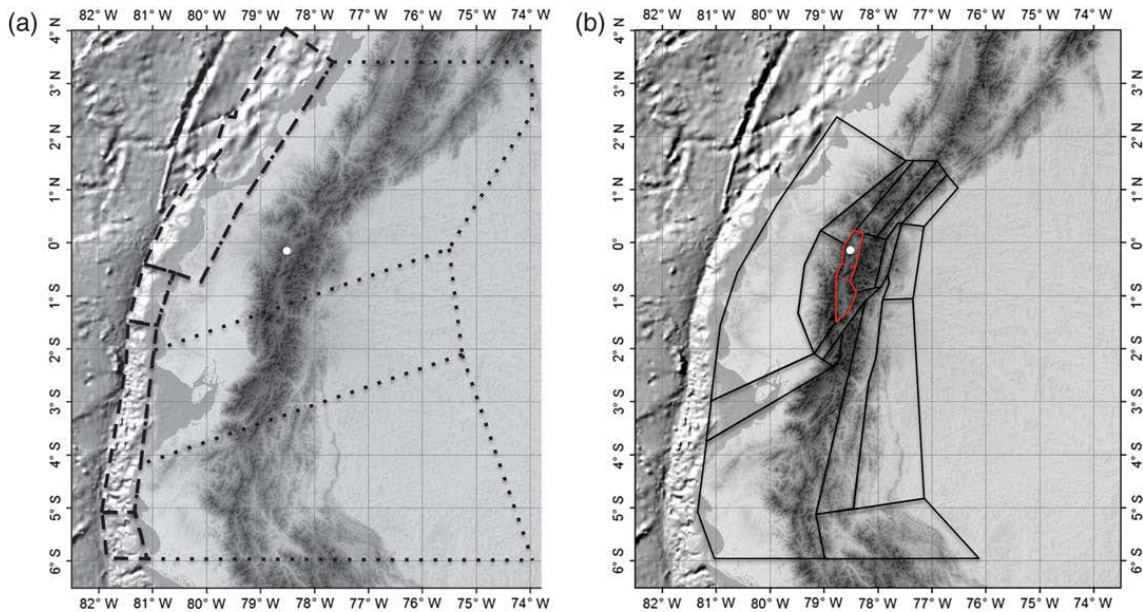
### PROBABILISTIC SEISMIC HAZARD IN QUITO: THE HOST ZONE IS CONTROLLING THE HAZARD

The territory of Ecuador has been subdivided into seismic sources, producing a seismotectonic model with 26 source zones. The criteria used for deriving this model are described in Alvarado (2012). Crustal sources enclose fault systems or zones of diffuse seismicity. Recurrence curves are modeled based on the observed seismicity rates using the earthquake catalog (see Tables S1 and S2) and the time windows of completeness published in Beauval *et al.* (2013) and reported in Table 1. Different complete time periods have been determined for shallow earthquakes occurring in the Cordillera and for subduction earthquakes. For example, all earthquakes with magnitudes  $M_w \geq 4.5$  are considered complete since 1963, whereas earthquakes with magnitudes  $M_w \geq 6.0$  are complete since 1860 in the Cordillera and since 1900 for the plate margins (interface events) and at depth (inslab events). Recurrence rates are estimated for magnitudes 4.5 and above, together with



▲ **Figure 2.** Geomorphology and tectonic setting of the Quito basin. The city has grown on a 50 km long piggy-back basin generated by the permanent activity of the Quito reverse fault dipping west. Northeast-southwest-trending hills bordering Quito to the east: folds are produced by the thrust movement of the blind fault. White dashed lines: detailed fault segments identified in Alvarado *et al.* (2014). North-south black segment indicates the projection of the Quito fault top edge to the surface (simplified model, dip 50°). Altitude difference between the basin and the Interandean Depression (ID) is 600 m (see the a-b cross section, inset, vertical axis denotes altitude above sea level in kilometers). Contours indicate city and neighboring suburbs (Q, Quito; P, Pomasqui; S, Sangolqui; G, Guayllabamba; C, Cumbaya). Neighboring volcanoes: GGP, Pichincha; AT, Atacazo; PS, Pasochoa; IL, Ilaló; CA, Casitagua. White dot indicates rock site considered in the study; dashed black segment indicates profile studied in Figure 10.

the  $b$ -value (applying Weichert, 1980; see, e.g., Beauval and Scotti, 2003). All crustal sources are modeled as a real zones, with seismicity rates distributed over depth according to the observed depth distribution of instrumental earthquakes in each zone (up to 35 km in the Cordillera). Based on selected earthquake focal mechanisms and tectonic analysis (Alvarado, 2012), predominant focal mechanisms are identified and further taken into account in the prediction of ground motions. The subduction interfaces are modeled as dipping fault planes, the segmentation along the trench relies on the rupture zone estimated from past megathrust earthquakes (Esmeraldas zone,



▲ **Figure 3.** Seismotectonic sources for probabilistic seismic-hazard assessment in Ecuador (Alvarado, 2012). (a) Interface subduction planes (dashed lines) and inslab volumes (dotted lines); (b) shallow crustal source zones (continuous black lines); Quito, Machachi, and Latacunga source zones highlighted in red (see Fig. 5). White dot: the rock site in Quito considered in the study.

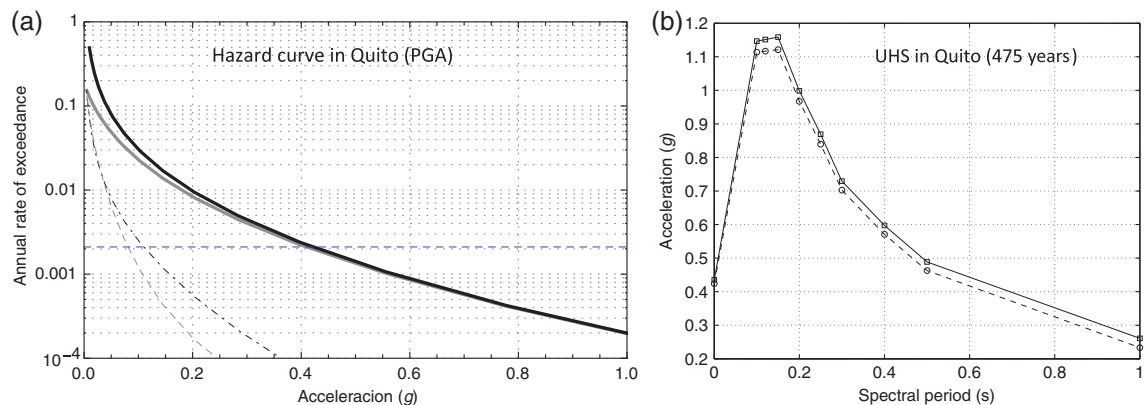
corresponding to the rupture plane of the 1906  $M_w$  8.8 event) or on the seismicity pattern observed along the interface zone. The subduction inslab zones are modeled as volumes, with seismicity distributed between 35 and 200 km. Maximum magnitudes in each source zones are based on the maximum length of fault segments identified as active using the magnitude–length equations published in Leonard (2010) and Strasser *et al.* (2010). We checked that these magnitudes inferred from active tectonics are always higher or equal to the maximum historical magnitudes recorded in the zones.

The first hazard calculations identify the contributions to the hazard in Quito of crustal sources, inslab volumes, and interface planes. Calculations are performed for a rock site located in Quito (coordinates  $-78.51$  in longitude and  $-0.2$  in latitude, Figs. 2 and 3), applying the GMPE for a  $V_{S30}$  of 760 m/s (shear-wave velocity in the top 30 m). To begin with, the GMPE Zhao *et al.* (2006) is used for the three tectonic regimes to predict the ground motions produced by earthquakes. Zhao *et al.* (2006) is based on the rupture distance (closest distance to the fault plane,  $R_{rup}$ ). The minimum mag-

nitude considered in the probabilistic calculation is  $M_w$  5.0; Gaussian distributions predicted by GMPEs are truncated at  $\pm 3\sigma$ . Hazard curves are calculated taking into account all source zones and then considering separately the crustal source zones, the inslab sources, and the interface sources (Fig. 4a, for peak ground acceleration [PGA]). Using the GMPE Zhao *et al.* (2006) for the three tectonic regimes, an acceleration of  $0.41g$  is obtained at 475 years, when either all sources or only the crustal host zone is considered. These results show that, for a site on rock ( $V_{S30}$  760 m/s), there is only one source zone—the host crustal zone—that contributes significantly to the seismic hazard in Quito (PGA) for 475 years return period. The same calculations, using other GMPEs (for crustal sources: Boore and Atkinson, 2008; Akkar and Bommer, 2010, both based on Joyner and Boore distance  $R_{JB}$ ; for subduction sources: Youngs *et al.*, 1997), indicate that the host source always controls the hazard in Quito at 475 years. This result is also valid for spectral frequencies over the 0.1–1 s range. The uniform hazard spectra displayed in Figure 4b show that the spectral accelerations at 475 years based on the full seismicity

**Table 1**  
Completeness Time Windows Used in the Modeling of Earthquake Recurrence in the Source Zones

Magnitude interval	4.0–4.5	4.5–5.0	5.0–5.5	5.5–6.0	6.0–6.5	6.5–7.0	7.0–7.5
Time period of completeness: crustal sources	1997	1963	1957	1920	1860	1860	1587
Time period of completeness: subduction sources	1997	1963	1963	1963	1900	1900	1900



▲ **Figure 4.** (a) Hazard curves for a site located at rock in Quito (peak ground acceleration [PGA]). Total hazard curve including contributions from all sources (black solid curve), hazard curves including only the contribution from the crustal host zone (solid gray curve), the interface sources (dotted dashed curve), and the inslab sources (dashed curve). (b) Contribution of the host crustal zone to the total hazard in Quito: Uniform Hazard Spectrum (UHS) including contributions from all source zones (solid line) and UHS including only the contribution from the host zone (dashed line). Zhao *et al.* (2006) model used for the three source zone types.

model are very close to the accelerations relying only on the host zone contribution.

For the hazard at 475 years return period in Quito (0.41g for the PGA), the interface contribution is negligible with respect to the contribution of the crustal host zone. Nonetheless, considering the interface sources alone, an acceleration of 0.12g is obtained in Quito at 475 years return period (Fig. 4a). The interface contributing is the Esmeraldas zone, modeled as a dipping plane (20°) between 4 and 44 km depth, extending over the rupture area of the 1906 event (from latitude -0.5° to +4°, approximately 500 km long, Fig. 3a), with maximum magnitude 8.8 ( $M_w$ ). The Gutenberg–Richter recurrence curve established from the seismic catalog predicts one earthquake with magnitude  $\geq 7.0$  on average every 25 years in this source zone, and one earthquake with magnitude  $\geq 8.0$  on average every 110 years. However, this interface is located at 200 km from Quito, and its contribution to the annual exceedance rate for an acceleration of 0.41g is negligible (calculations at rock).

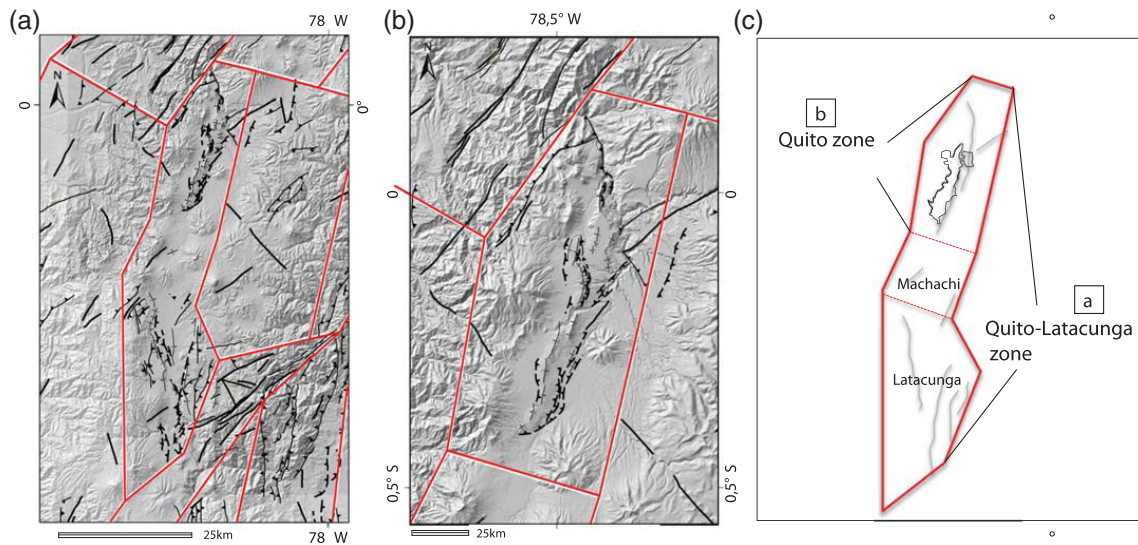
## VARIABILITY OF THE UNIFORM HAZARD SPECTRUM AT 475 YEARS

### Host Zone: Frequency–Magnitude Distributions

We now focus on the host zone controlling the seismic hazard in Quito. The characterization of the Quito reverse fault system has improved significantly with the use of Interferometric Synthetic Aperture Radar (InSAR) by Champenois *et al.* (2013) and the use of geomorphology, tectonics, and GPS by Alvarado *et al.* (2014). However, the information available does not yet permit to propose a recurrence model for each fault segment. Rather than considering individual segments in the PSH calculations, an areal seismic source has been delin-

eated enclosing the whole reverse fault system (Figs. 3b and 5a, c). The prolongation of the Quito fault system to the south is the reverse Latacunga system (see e.g., fig. 16 in Beauval *et al.*, 2010, named Poalo-Saquisilí-Yambo fault), both dipping to the west. Between these systems (between latitudes -0.4° and -0.7°), no fault trace has been clearly identified, although historical earthquakes, for example in 1923, have occurred there (Beauval *et al.*, 2013). Following Alvarado (2012), two options are proposed for delineating the source zone enclosing Quito (host zone). The first one (option S1, Fig. 5a) is a large area enclosing both fault systems, extending from latitude -1.15° to +0.5° (Quito–Latacunga zone). This option has been used in the previous calculations (see Probabilistic Seismic Hazard in Quito: The Host Zone is Controlling the Hazard section). As Alvarado *et al.* (2014) note, the north–south-trending Quito and Latacunga reverse faulting systems are geodynamically similar because they form the western boundary of the “Quito–Latacunga microblock” (~150 km long). The fault systems located to the north and to the south of this microblock trend northeast–southwest and have right-lateral strike-slip mechanism. The microblock is characterized by discontinuous Quaternary folds and piggy-back basins related to blind thrusts with evidences of tilted young volcanoclastic deposits (Lavenue *et al.*, 1995; Alvarado *et al.*, 2014). Available focal mechanisms for  $M_w \geq 5.0$  earthquakes suggest a common present day behavior along strike. The second option isolates each fault system and divides the large zone into three smaller ones (Quito, Machachi, and Latacunga zones, Fig. 5b,c). As the Latacunga source zone contains more earthquakes than the Quito source zone, the hazard evaluated in Quito will be higher for the large host zone option (S1) than for the small Quito host zone option (S2).

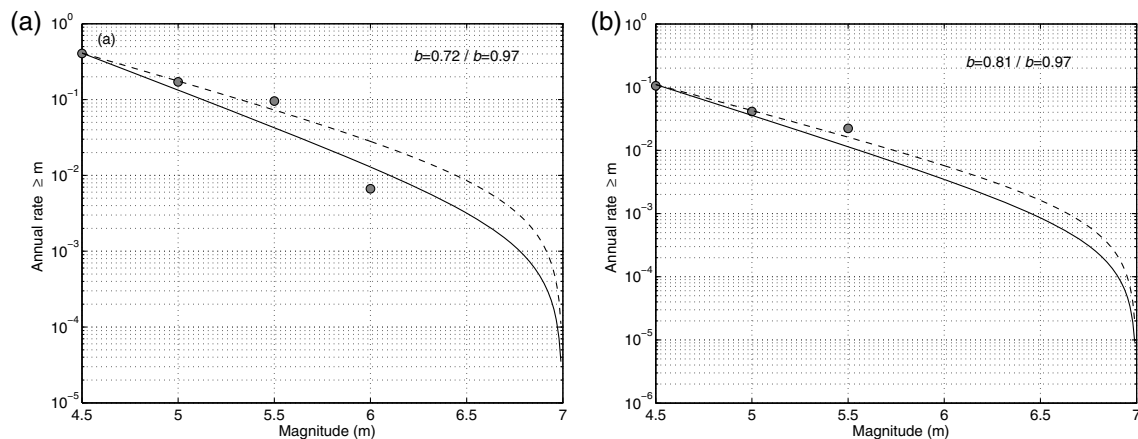
The recurrence curve corresponding to the Quito zone relies on very few events (Fig. 6b). Seven events with magnitudes



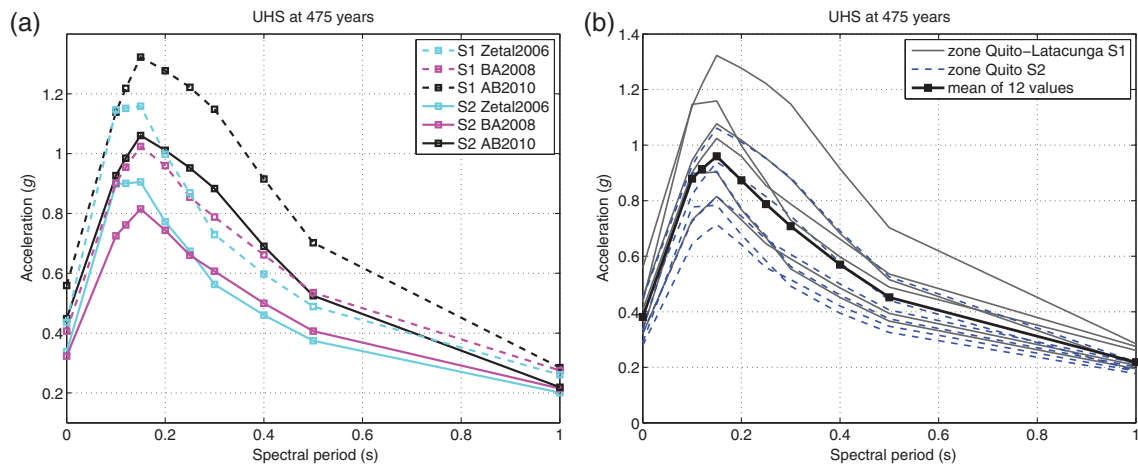
▲ **Figure 5.** Two crustal host zone definitions. (a) The Quito–Latacunga zone enclosing both the Quito fault system and the Latacunga reverse fault system (Poalo-Saquisilí-Yambo fault system in [Beauval et al., 2010](#)), option S1. (b) The Quito zone enclosing the Quito reverse fault system (option S2). (c) Scheme displaying the two options for the crustal host zone. See [Figure 3b](#) for the location of these zones in a regional perspective.

$M_w \geq 4.5$  belong to the source zone; the greatest magnitudes are  $M_1$  5.8 (10 August 1938, Sangolquí event, [Beauval et al., 2010](#)) and  $M_1$  6.4 (31 August 1587, Guayllabamba event, [Beauval et al., 2010](#)). Six events fall inside the completeness time windows

( $4.5 \leq M_w \leq 5.8$ ). One option is to work with the rate and  $b$ -value inferred from this scarce catalog ( $b = 0.81$ ). Around 0.11/year events with  $M_w \geq 4.5$  occur within this source zone, equivalent to 1 event  $M_w \geq 4.5$  every 9 years. Another option is



▲ **Figure 6.** Recurrence curves for the host zone, superimposed to the observed rates (completeness time windows in [Table 1](#)). (a) The host zone is the Quito–Latacunga zone enclosing both the Quito and the Latacunga fault system (see [Fig. 5a](#)): dashed line, recurrence based on 27 events with  $M_w \geq 4.5$  and depth lower than 35 km,  $a = 2.42$  and  $b = 0.72$  ([Gutenberg–Richter, 1944](#) parameters); solid line, recurrence curve based on the observed rate for  $M_w$  4.5+ and on the  $b$ -value from the Cordillera region. (b) The host zone is the Quito zone enclosing only the Quito fault system (S2, [Fig. 5b](#)): dashed line, recurrence curve based on 7 events with  $M_w \geq 4.5$  and depth lower than 35 km,  $a = 2.69$  and  $b = 0.81$ ; solid line, recurrence curve based on the observed rate for  $M_w$  4.5+ and on the  $b$ -value from the Cordillera region.



▲ **Figure 7.** Uniform hazard spectra for a rock site in Quito, at 475 years return period. (a) Testing two geometries for the host source zone, S1 and S2 (see [Variability of the Uniform Hazard Spectrum \(UHS\)](#) section), and three ground-motion prediction equations (GMPEs) for crustal events (AB2010: [Akkar and Bommer, 2010](#); BA2008: [Boore and Atkinson, 2008](#); Zetal2006: [Zhao et al., 2006](#)). (b) UHS resulting from the final logic tree including two geometries for the host zone, two optional  $b$ -values, and three GMPEs. Black indicates host source zone option S1 and blue indicates host source zone option S2. All source zones are taken into account in the calculations (crustal, interface, inslab), although interface/inslab contributions are negligible at this return period.

to use only the observed rate for magnitudes  $M_w \geq 4.5$  and associate this rate with the more robust  $b$ -value calculated considering the whole Cordillera ( $b = 0.97$ , [Beauval et al., 2013](#)). As for the larger Quito–Latacunga source zone, 27 events with  $M_w \geq 4.5$  belong to this spatial zone. The recurrence parameters are retrieved from a catalog of 24 events falling in the completeness time windows (yielding  $b = 0.72$ , Fig. 6a). The earthquake catalog of this zone includes several events  $M_w \geq 5.5$ , which are linked to the Latacunga fault system, mostly in the twentieth century (1736, 1944, 1960, 1962, 1976, and 1996), with maximum observed magnitude 6.1 in 1757 ([Beauval et al., 2010, 2013](#)). Two further events in 1923 ( $M_{IC}$  5.8–6.5) and 1929 (Murco event,  $M_{IC}$  5.9) fall in this zone, in the area where no fault trace has been evidenced. The Gutenberg–Richter model predicts 0.41 events per year with  $M_w \geq 4.5$  within this source zone, corresponding to 1 event every  $\sim 2.5$  years. These recurrence curves need to be bounded in the upper range. All the segments of the Quito fault system breaking at once would produce an earthquake with approximately 50 km subsurface length rupture (Fig. 2). Applying the [Wells and Coppersmith \(1994\)](#) magnitude–length relationship for this fault gives a magnitude  $\sim 7.0$ :  $M = 4.49 + 1.49 \times \log_{10}(L)$  with  $L = 50$  km. The relationship from [Leonard \(2010\)](#) gives similar results.

#### Variability of the Uniform Hazard Spectrum (UHS)

To begin with, three equations are selected to explore the epistemic uncertainty of the ground-motion predictions from crustal earthquakes: [Zhao et al. \(2006\)](#), established from Japanese data; [Akkar and Bommer \(2010\)](#), based on European and Middle East data; and [Boore and Atkinson \(2008\)](#), using

western United States strong motions. Tested against diverse strong-motion datasets, these equations proved to be robust and stable models over the full frequency range (e.g., [Delavaud et al., 2012](#); [Beauval, Tazan, et al., 2012](#)). As inslab and interface sources have a negligible contribution to the hazard at 475 years, only one GMPE is considered for these sources, namely, [Zhao et al. \(2006\)](#), which was identified among best-fitting subduction models for South America in [Arango et al. \(2012\)](#) and [Beauval, Cotton, et al. \(2012\)](#). We confirmed that the present results are similar if [Youngs et al. \(1997\)](#) is used.

We estimated PSH using two definitions for the host zone contour (S1 or S2, seismic rates for  $M \geq 4.5$  and  $b$ -values based on the zone dataset), and the three selected GMPEs. The six combinations of source zones and GMPEs result in six uniform hazard spectra at 475 years (Fig. 7a). As expected, using the zoning S2 provides lower hazard estimates in Quito than when using the zoning S1. For the PGA, results vary between 0.32g and 0.55g, depending on the zonation used and on the GMPE selected. Based on [Akkar and Bommer \(2010\)](#), the PGA increases from 0.46g (S2) to 0.55g (S1); whereas in the case of [Boore and Atkinson \(2008\)](#), the PGA increases from 0.32g to 0.41g. Keeping the zoning fixed (S2), the PGA increases from 0.32g to 0.46g if using [Akkar and Bommer \(2010\)](#) instead of [Boore and Atkinson \(2008\)](#) (0.41g–0.55g in the case of S1). These calculations show that the hazard in Quito at 475 years is controlled both by the definition of the areal host zone ( $\sim 20\%$ – $30\%$  variability at the PGA,  $\sim 30\%$ – $35\%$  variability at 0.5 s) and by the choice of the GMPE selected for this zone ( $\sim 35\%$ – $45\%$  variability at the PGA,  $\sim 30\%$ – $35\%$  variability at 0.5 s), for all spectral periods up to 0.5 s (Fig. 7a). At the spec-

tral period of 1 s, the impact of the choice of the host zone is much higher than the impact of the GMPE choice.

The recurrence model in the source zone S2 is not well constrained. The rate for events with  $M_w \geq 4.5$  and the  $b$ -value, used for extrapolating this rate to higher magnitudes, rely on very few events (see [Host Zone: Frequency–Magnitude Distributions](#) section). To take into account the uncertainty on the recurrence model, two more recurrence models are included in the analysis. Gutenberg–Richter curves based on the rates of  $M \geq 4.5$  coupled with the well-constrained 0.97  $b$ -value of the Sierra region (Fig. 6) are now considered. This  $b$ -value is larger than the  $b$ -values estimated from the zone dataset, producing lower seismic rates over the magnitude range [4.5–7.0]. The uncertainty in the predicted recurrence of earthquakes with magnitudes 6 and larger is significant. The mean recurrence time in the Quito–Latacunga zone S1 varies between 33 and 90 years, depending on the  $b$ -value selected. In the case of the smaller Quito zone S2, the recurrence time for an earthquake  $M \geq 6.0$  varies between 166 and 285 years. Results for this simple logic tree, obtained from the combination of four seismicity models for the host zone and three crustal GMPEs, are displayed in Figure 7b. The PGA in Quito at 475 years varies between 0.28g and 0.55g, with the mean value around 0.39g. At 0.2 s (5 Hz), accelerations vary between 0.63g and 1.28g, with a mean around 0.88g, whereas at 0.5 s (2 Hz), accelerations vary between 0.32g and 0.7g, with a mean value around 0.45g.

#### Frequency–Magnitude Distributions Based on the Slip Rate and Corresponding Hazard

Recent development of geodetic (GPS) networks in Ecuador provided the first present-day estimates of crustal deformation and slip rates on major faults (Nocquet *et al.*, 2014). In the Quito area, GPS results spanning a period of ~15 years show a horizontal shortening rate at ~4 mm/yr between sites located west and east of the Quito fault system (Alvarado *et al.*, 2014). Alvarado *et al.* (2014) further show that GPS data are well modeled by a single fault with an associated slip rate ranging from 4.3 to 5.3 mm/year. Moreover, a sharp velocity gradient observed across the Quito fault system indicates that only a fraction of the fault plane is presently accumulating elastic stress, available for future earthquakes. More precisely, Alvarado *et al.* (2014) found that the depth over which elastic stress is presently accumulated is in the range of 3–7 km.

The average slip-rate estimates can be used to propose alternative earthquake occurrence relations independent of the earthquake catalog (see e.g., Anderson and Luco, 1983; Youngs and Coppersmith, 1985; Bungum, 2007). Under the assumption that deformation remains steady in time, geodetically derived fault slip rates can be used to propose earthquake frequency–magnitude distributions consistent with the annual rate of moment deficit accumulation. The Quito zone is an area of approximately 70 km × 40 km, which encloses the Quito fault. Most of the seismicity in the zone is related to the Quito fault system. This fault system is composed of several blind thrust segments, the exact geometries and extensions in depth of which are yet to

be defined (Alvarado *et al.*, 2014). For the purpose of the calculation, a simplified geometry is considered. The fault is modeled as a single segment of 50 km (subsurface length, latitudes 0.0275° to –0.423° and longitudes –78.385° to –78.50°, Fig. 2).

Although the fault slip rate constrains the seismic moment rate to be released on the fault, a model is required to distribute it through earthquakes of various magnitudes. Anderson and Luco (1983) propose a frequency–magnitude distribution constrained by the slip rate, the  $b$ -value, and the maximum magnitude  $M_{\max}$  on the fault. They have reviewed several forms of recurrence relationships that have been developed using slip-rate constraints. Following the work achieved in the SHARE project (Woessner *et al.*, 2012), the model number 2 providing the activity rate  $N_2$  is selected (table 3 in Anderson and Luco, 1983; equation 7 in Bungum, 2007). The cumulative number of earthquakes with magnitude greater than  $M$  is modeled by an exponential function truncated at  $M_{\max}$ . The density function decreases continuously to zero as  $M$  approaches  $M_{\max}$ . The number of earthquakes  $N$  above magnitude 5.0 ( $M_{\min}$  in the PSH calculation) is calculated as follows:

$$N(m \geq 5.0) = \frac{d \ln(10) - b \ln(10) S}{b \ln(10)} \frac{S}{\beta} \left[ e^{b \ln(10) \times (M_{\max} - M)} - 1 \right] \times e^{-\frac{d \ln(10) M_{\max}}{2}},$$

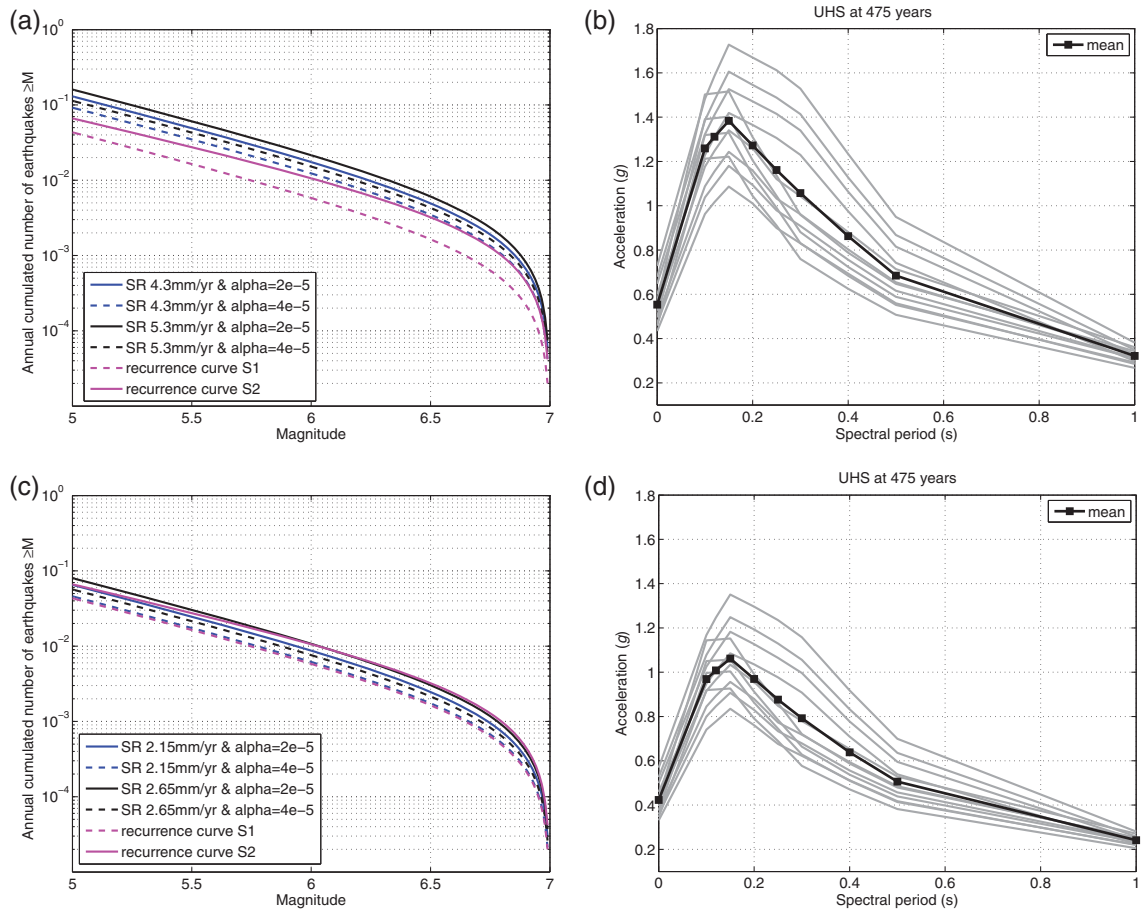
in which

$$\beta = \sqrt{\frac{\alpha M_0(0)}{\mu W}}; \quad \alpha = \frac{D}{L};$$

$$\log M_0 = c + dM (c = 160.5, d = 1.5)$$

$S$  is the slip rate. The  $b$ -value is assumed equal to the  $b$ -value from the Quito zone dataset (0.81, Fig. 6b). The well-known log–linear relation between the seismic moment  $M_0$  and moment magnitude is used (Kanamori and Anderson, 1975). The rigidity modulus is fixed to  $3.0 \times 10^{11}$  dyn/cm<sup>2</sup>. The parameter  $\alpha$  is the ratio of the average displacement  $D$  in the largest earthquake rupturing the total width to the fault length  $L$ . This parameter bears large uncertainties. Considering an average displacement from 1 to 2m (earthquake with magnitude ~7.0, Wells and Coppersmith, 1994), and assuming a length equal to 50 km, yields the range  $2 \times 10^{-5}$  to  $4 \times 10^{-5}$  for  $\alpha$ . These values are in accordance with  $\alpha = 2 \times 10^{-5}$  recommended for thrust faults in Anderson and Luco (1983). The equation is applied using both  $\alpha$  values.

Here, we present two sets of calculations. The first set directly uses the geodetically derived slip rate for the Quito fault, and four calculations are then performed based on the minimum (4.3 mm/yr) and maximum (5.3 mm/yr) slip-rate bounds, combined with two  $\alpha$  values. This calculation implicitly assumes that the fault is locked over the entire seismogenic thickness. The second set accounts for aseismic slip on the Quito fault. Assuming that  $\epsilon\%$  of the fault surface is creeping, the annual seismic moment rate deficit is



▲ **Figure 8.** (a) Recurrence curves inferred from average slip rates on the Quito fault system (blue and black lines, four optional curves, combination of two slip rates and two  $\alpha$  parameters (see [Frequency–Magnitude Distributions Based on the Slip Rate and Corresponding Hazard](#)), superimposed on the frequency–magnitude distributions based on earthquake data (S1 resized to the Quito zone area and S2). (b) Uniform hazard spectra in Quito, resulting from the application of the slip rate-based recurrence curves to describe earthquake occurrence in the Quito zone (S2). The 12 uniform hazard spectra correspond to the combinations of four optional recurrence curves and three optional GMPEs ([Akkar and Bommer, 2010](#); [Zhao et al., 2006](#); [Boore and Atkinson, 2008](#)). (c) and (d) Same as (a) and (b) with a slip rate reduced by 50% (consistent with a partially locked fault).

$$\dot{M}_0 = \mu A(1 - \epsilon)S,$$

in which  $A$  is the surface of the fault. It is therefore equivalent to divide  $A$  or  $S$  to obtain the same annual moment rate deficit. Most faults on continents are locked over the whole seismogenic upper crust that is  $\sim 15$  km. The locking depth of 7 km indicated by the GPS results therefore suggests that  $\epsilon$  is close to  $\sim 50\%$ . We therefore perform the calculation using 50% of the slip rate ( $S/2$ ) to derive a frequency–magnitude distribution for the case of the partially locked Quito fault.

The first set of calculations provides frequency–magnitude distributions with many more earthquakes than has been observed in the past (Fig. 8a). As a consequence, the resulting

recurrence models are predicting higher rates than those inferred from the earthquake catalogs. This trend, that is, modeled rates based on fault slip rates higher than rates based on past seismicity, has been observed in other seismic-hazard studies using GPS strain rates, for example, [Mazzotti et al. \(2011\)](#) or in the SHARE project ([Woessner et al., 2012](#)). If one divides the measured slip rates into an aseismic and a seismic release, the predicted rates are lower and in agreement with the recurrence inferred from past seismicity (Fig. 8c).

The UHS at 475 years is calculated considering four seismicity models (Quito zone S2, minimum and maximum slip rates, two optional  $\alpha$  values) and the three selected crustal GMPEs. Assuming  $\epsilon$  equal to 0 (Fig. 8b), the acceleration levels

are significantly higher than those relying on the catalog-based recurrence curves (Fig. 7). Accelerations at the PGA vary between  $0.43g$  and  $0.73g$ , at 475 years, with a mean close to  $0.55g$ . Assuming  $\epsilon$  equal to 50% (Fig. 8d), the accelerations are close to those relying on the catalog-based recurrence curves. Accelerations at the PGA vary between  $0.32g$  and  $0.58g$ , with a mean around  $0.42g$ .

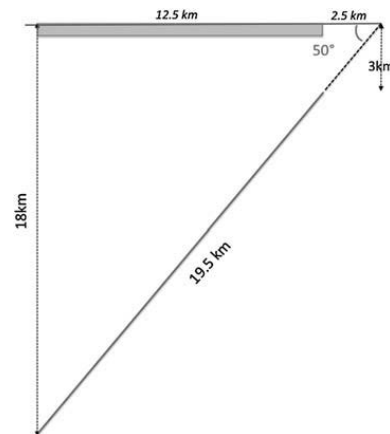
## RESTRICTING LARGE EARTHQUAKES TO THE QUITO FAULT AND HANGING-WALL EFFECT

### PGA at 475 Years: Profile Perpendicular to the Fault

When modeling the seismicity with areal sources in the probabilistic calculations, the hanging-wall effect cannot be taken into account properly. The city is lying over the hanging wall of the Quito reverse fault system, and in case of a large earthquake below the city, ground motions are expected to be much higher in Quito than in the suburbs at the foot of the hills (footwall, see Fig. 2). There are several past examples of this effect, for example, during the Chi-Chi  $M_w$  7.1 earthquake in Taiwan (Chang *et al.*, 2004). As an attempt to include hanging-wall amplifications, two more GMPEs for crustal earthquakes are included, the Abrahamson and Silva (2008) and Chiou and Youngs (2008) models.

Within the Quito areal zone, all large earthquakes (e.g.,  $M \geq 6.0$ ) are expected to occur on the identified segments of the reverse fault system. Rather than distributing all seismicity rates ( $M$  5–7) homogeneously over the Quito areal zone, an alternative is to distribute the seismicity rates of magnitudes 5–6 over the zone (as background seismicity) and assign the rates of magnitudes 6–7 on the Quito fault plane. To perform this exercise, the simplified fault geometry described in the Frequency–Magnitude Distributions Based on the Slip Rate and Corresponding Hazard section is used. The reverse fault is dipping to the west with an angle of  $50^\circ$ , extending from 3 to 18 km depth (Fig. 9, corresponding to a width around 19–20 km, compatible with an earthquake magnitude around 7.0, Wells and Coppersmith, 1994). There is a significant uncertainty in this geometry, however, the dip and extension in depth are compatible with the distribution of microseismicity and with geomorphological characteristics (relocations of tectonic events by Lamarque [2011] and Font *et al.* [2013], analysis of local microseismicity by Alvarado *et al.* [2014]). Each segment of the fault system has a main compressional and secondary dextral strike-slip component, confirmed by the available focal mechanisms (Segovia and Alvarado, 2009; Alvarado *et al.*, 2014).

At first, calculations are performed applying the frequency–magnitude distribution based on the Quito zone dataset ( $b = 0.81$  and rates of  $M \geq 4.5$  equal to 0.11, Fig. 6b). Four GMPEs are applied: Akkar and Bommer (2010), Boore and Atkinson (2008), Abrahamson and Silva (2008), and Chiou and Youngs (2008) (distance measures  $R_{JB}$ ,  $R_{JB}$ ,  $R_{rup}$ , and  $R_{rup}$ , respectively). The PGA obtained at 475 years, for sites located on a profile perpendicular to the fault, is displayed in Figure 10a (profile in Fig. 2). For comparison, accelerations obtained distributing all the seismicity over the areal source zone case are

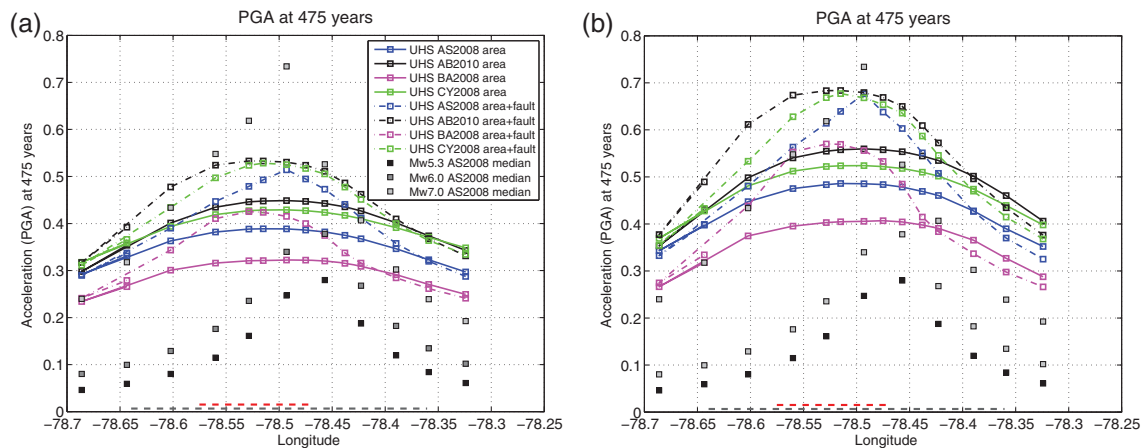


▲ **Figure 9.** Geometry of the simplified fault at depth. Black: dipping fault; gray: surface projection of the fault, as shown by the red dashed line in Figures 10a,b.

also superimposed (see Variability of the Uniform Hazard Spectrum (UHS) section). Concentrating the occurrence of magnitudes 6–7 on the fault plane produces an increase of acceleration levels at sites located above the fault plane ( $R_{JB} = 0$ ). Applying the models Akkar and Bommer (2010) and Boore and Atkinson (2008) (no hanging-wall coefficient) or Chiou and Youngs (2008) (with hanging-wall coefficient) at the sites located above the fault plane results in an increase in accelerations up to 20%–30%. Maximum accelerations of  $0.53g$  at 475 years are obtained applying the Akkar and Bommer (2010) ground-motion equation. Applying the equation by Abrahamson and Silva (2008) produces a greater acceleration increase (35% at maximum) with respect to the areal zone case. If using the larger host zone option (S1 zone Quito–Latacunga), the hazard obtained in Quito is higher than when using the smaller Quito host zone. Restricting magnitudes 6–7 to the fault plane (rates proportionated to the Quito zone area) increases accelerations at 475 years by 20%–40% (Fig. 10b), reaching a maximum of  $0.68g$  (Akkar and Bommer, 2010 or Abrahamson and Silva, 2008 models).

### Scenarios and Hazard Values at 475 Years

The acceleration at 475 years is a threshold, corresponding to the acceleration at the site with a 10% probability of being exceeded at least once over 50 years. All earthquakes included in the model, with low-to-high magnitudes, close or far from the site, with a nonzero probability of producing an acceleration greater than this threshold, contribute to this hazard calculation. It can be interesting, although requires care, to compare these accelerations at 475 years with acceleration levels corresponding to different earthquake scenarios. We believe that such exercises can be helpful to better grasp the meaning of the probabilistic output. The median acceleration to expect in case of a given earthquake on the Quito fault is superimposed on the previous profiles, applying the Abrahamson and Silva



▲ **Figure 10.** PSH in Quito city: PGA acceleration at 475 years, at sites located along a profile perpendicular to the fault (west to east, see Fig. 2); as well as median accelerations predicted for three given earthquake scenarios. Solid line: the frequency–magnitude distribution ( $5 \leq M_w \leq 7$ ) is homogeneously distributed over the areal zone; dashed line: large magnitudes ( $6 \leq M_w \leq 7$ ) are restricted to the fault plane. Surface projections of the source zone (dashed black segment) and of the fault plane (red dashed segment) indicated at the bottom. (a)  $b$ -value and annual rate of  $M \geq 4.5$  inferred from the seismicity in the Quito zone (S2,  $b = 0.81$ ,  $\lambda_{M \geq 4.5} = 0.11$ ). (b)  $b$ -value and annual rate of  $M \geq 4.5$  inferred from the seismicity in the Latacunga–Quito zone (S1,  $b = 0.72$ ,  $\lambda_{M \geq 4.5} = 0.15$ ). Gray squares: median accelerations predicted for  $M_w$  5.3, 6.0, and 7.0, using the GMPE model AS2008. AS2008: Abrahamson and Silva (2008); AB2010: Akkar and Bommer (2010); BA2008: Boore and Atkinson (2008); and CY2008: Chiou and Youngs (2008).

(2008) equation. The accelerations correspond to an earthquake occurring on the segment of the fault intersecting the profile. The smallest magnitude considered is 5.3 ( $M_w$ ), similar to that of an earthquake that occurred in 1990 on a northern segment of the fault (Pomasqui, 11 August 1990, Fig. 2), which could be repeated anywhere on the fault. Two larger events are considered: an earthquake with  $M_w$  6.0, which probably occurred at least once in the last five centuries (Beauval *et al.*, 2010, 2013), and an earthquake with  $M_w$  7.0 corresponding to the complete rupture of the fault (for which there is evidence of only one, from paleoseismology, 500–1000 years ago, Hibschi *et al.*, 1997). Results displayed in Figure 10a,b show that, whatever the decision on the seismicity model or the GMPE, the acceleration levels at 475 years are greater than the acceleration corresponding to the  $M_w$  5.3 scenario. Considering the worst scenario in our seismicity model,  $M_w$  7.0, the maximum acceleration to expect (if considering only the median) exceeds the maximum acceleration at 475 years, whatever the combination of models chosen.

## CONCLUSIONS

In the present study, PSH estimates at 475 years return period for Quito, capital city of Ecuador, show that the crustal host zone is the only source zone that determines the city's hazard levels for such return period. Therefore, the emphasis is put on identifying the uncertainties characterizing the host zone, that is, uncertainties in the recurrence of earthquakes expected in the zone and uncertainties on the ground motions that these

earthquakes may produce. As the number of local strong ground motions is still scant, GMPEs are imported from other regions. Rather than sampling a complex logic tree, several plausible models are considered and associated with the corresponding uniform hazard spectra.

Exploring recurrence models for the host zone based on different observations and assumptions, and including three GMPE candidates (Zhao *et al.*, 2006; Boore and Atkinson, 2008; Akkar and Bommer, 2010), we obtain a significant variability on the estimated acceleration at 475 years (site coordinates:  $-78.51^\circ$  in longitude and  $-0.2^\circ$  in latitude,  $V_{S30} 760$  m/s):

- Considering historical earthquake catalogs, and relying on frequency–magnitude distributions where rates for magnitudes 6–7 are extrapolated from statistics of magnitudes 4.5–6.0 mostly in the twentieth century, the acceleration at the PGA varies between  $0.28g$  and  $0.55g$  with a mean value around  $0.4g$ . The results show that both the uncertainties in the GMPE choice and in the seismicity model are responsible for this variability.
- Considering slip rates inferred from geodetic measurements across the Quito fault system, and assuming that most of the deformation occurs seismically (conservative hypothesis), leads to a much greater range of accelerations,  $0.43g$ – $0.73g$  for the PGA (with a mean of  $0.55g$ ).
- Considering slip rates inferred from geodetic measurements, and assuming that 50% only of the deformation is released in earthquakes (partially locked fault, model based on 15 years of GPS data), leads to a range of accelerations  $0.32g$ – $0.58g$  for the PGA, with a mean of  $0.42g$ .

These accelerations are in agreement with the catalog-based hazard estimates.

- Restricting the occurrence of magnitudes 6–7 to the Quito fault (a simplified geometry), applying the three initial GMPEs (Akkar and Bommer, 2010; Zhao *et al.*, 2006; Boore and Atkinson, 2008) or GMPEs including a hanging-wall coefficient (Abrahamson and Silva, 2008; Chiou and Youngs, 2008), increases the hazard by 20%–40% at sites located above the fault plane (range 0.42g–0.68g at the considered site). Strong hypotheses are required to define a simple fault plane and to define the recurrence of earthquakes on this fault plane; therefore, these results must be taken with great caution. However, they demonstrate that taking into account faults in hazard calculations can have a major impact.

Modeling the recurrence based on the past earthquake catalog, and relying on an areal source zone model, gives a mean value around 0.4g for the PGA at 475 years in Quito. This mean value is for a site on rock, and site effects need to be further taken into account. These results are in accordance with the acceleration level recently adopted by the new Ecuadorian Building Code (MIDUVI-CCQ, 2011). The seismic provisions of this Building Code are based on our 2011 national PSH map at rock, based on a single best-estimate model (no logic tree and no exploration of uncertainties). Nonetheless, based on various exercises, we show that if taking into account the fault itself in the hazard calculations, much higher values can be obtained for sites located above the fault. Interdisciplinary studies must be pursued to better understand paleoseismicity and fault kinematics around Quito. Soon there will be enough recordings available from the recently installed strong-motion stations, so that imported GMPEs can be tested to refine the selection. Future research should also focus on understanding better how to include source–site geometry effects such as the hanging wall, as these effects will certainly have direct consequences on the damage distribution in case of a large destructive earthquake. ☒

## ACKNOWLEDGMENTS

The authors thank Editor Zhigang Peng and two anonymous reviewers for their helpful and constructive reviews of the manuscript, as well as Brian E. Tucker (Geohazards International) for careful proofreading of the manuscript and for improving the English. In addition, we thank Fabrice Cotton for insightful comments on the manuscript, which led to significant improvements. This work was partially supported by the laboratory IS-Terre, by the Agence Nationale de la Recherche through the project Andes du Nord (Contract Number ANR-07-BLAN-143-01), and by the Institut de Recherche pour le Développement (IRD). Hugo Yepes' stays in Grenoble also benefited from a LabEx OSUG@2020 Grant Number (ANR10 LABX56), as well as from the MEEES Erasmus Mundus program ([www.meees.org/](http://www.meees.org/); last accessed October 2014). On the Ecuadorian side, additional support was available from the Secretaría Nacional de Educación Superior, Ciencia y Tecnología SENESCYT (LAE-5 y Proyecto PIN\_08-EPNGEO-00001). This work has been carried out in the frame of the Joint International Laboratory "Seismes &

Volcans dans les Andes du Nord" (IRD LMI SVAN). Finally, we are grateful to the Global Earthquake Model (GEM) Modeling Facility for constant support on the handling of the OpenQuake software since 2010 ([www.globalquakemodel.org](http://www.globalquakemodel.org); last accessed October 2014).

## REFERENCES

- Abrahamson, N., and W. Silva (2008). Summary of the Abrahamson & Silva NGA ground-motion relations, *Earthq. Spectra* **24**, no. 1, 67–97.
- Akkar, S., and J. J. Bommer (2010). Empirical equations for the prediction of PGA, PGV and spectral accelerations in Europe, the Mediterranean and the Middle East, *Seismol. Res. Lett.* **81**, no. 2, 195–206.
- Anderson, J. G., and J. E. Luco (1983). Consequences of slip rate constraints on earthquake occurrence relations, *Bull. Seismol. Soc. Am.* **73**, no. 2, 471–496.
- Alvarado, A. (2012). Néotectonique et cinématique de la déformation continentale en Equateur, *Thèse de doctorat (Ph.D.)*, Université de Grenoble, France, 259 pp.
- Alvarado, A., L. Audin, J. M. Nocquet, M. Segovia, Y. Font, G. Lamarque, H. Yepes, P. Mothes, F. Rolandone, and P. Jarrin (2014). Active tectonics in Quito, Ecuador, assessed by geomorphological studies, GPS data, and crustal seismicity, *Tectonics*, doi: [10.1002/2012TC003224](https://doi.org/10.1002/2012TC003224).
- Arango, M., F. Strasser, J. Bommer, J. Cepeda, R. Boroschek, D. Hernandez, and H. Tavera (2012). An evaluation of the applicability of current ground-motion models to the south and central American subduction zones, *Bull. Seismol. Soc. Am.* **102**, 143–168.
- Beauval, C., and O. Scotti (2003). Mapping b-values in France using two different magnitude ranges: Possible non power-law behavior, *Geophys. Res. Lett.* **30**, no. 17, 1892, doi: [10.1029/2003GL017576](https://doi.org/10.1029/2003GL017576).
- Beauval, C., F. Cotton, N. Abrahamson, N. Theodulidis, E. Delavaud, L. Rodriguez, F. Scherbaum, and A. Haendel (2012). Regional differences in subduction ground motions, *World Conference on Earthquake Engineering*, Lisboa, Portugal, 24–28 September, 10 pp.
- Beauval, C., H. Tasan, A. Laurendeau, E. Delavaud, F. Cotton, Ph. Guéguen, and N. Kuehn (2012). On the testing of ground-motion prediction equations against small magnitude data, *Bull. Seismol. Soc. Am.* **102**, no. 5, 1994–2007.
- Beauval, C., H. Yepes, W. Bakun, J. Egred, A. Alvarado, and J.-C. Singaicho (2010). Locations and magnitudes of historical earthquakes in the Sierra of Ecuador (1587–1996), *Geophys. J. Int.*, doi: [10.1111/j.1365-246X.2010.04569.x](https://doi.org/10.1111/j.1365-246X.2010.04569.x).
- Beauval, C., H. Yepes, P. Palacios, M. Segovia, A. Alvarado, Y. Font, J. Aguilar, L. Troncoso, and S. Vaca (2013). An earthquake catalog for seismic hazard assessment in Ecuador, *Bull. Seismol. Soc. Am.* **103**, 773–786, doi: [10.1785/0120120270](https://doi.org/10.1785/0120120270).
- Boore, D., and G. Atkinson (2008). Ground motion prediction equations for the average horizontal component of PGA, PGV, and 5%-damped PSA at spectral periods between 0.01 s and 10.0 s, *Earthq. Spectra* **24**, 99–138.
- Bungum, H. (2007). Numerical modelling of fault activities, *Comput. Geosci.* **33**, 808–820.
- Champenois, J., L. Audin, S. Baize, J.-M. Nocquet, and A. Alvarado (2013). Interseismic deformations along Ecuador active fault systems: Contribution of space-borne SAR interferometry, *AGU Meeting of the Americas*, Mexico, Cancun, 14–17 May.
- Chang, T.-Y., F. Cotton, Y.-B. Tsai, and J. Angelier (2004). Quantification of hanging-wall effects on ground motion: some insights from the 1999 Chi-Chi earthquake, *Bull. Seismol. Soc. Am.* **94**, no. 6, 2186–2197.
- Chatelain, J. L., B. Tucker, B. Guillier, F. Kaneko, H. Yepes, F. Fernandez, J. Valverde, G. Hoefler, M. Souris, E. Dupérier, T. Yamada, G. Bustamante, and C. Villacis (1999). Earthquake risk management pilot project in Quito, Ecuador, *Geojournal* **49**, 185–196.
- Chiou, B. S.-J., and R. R. Youngs (2008). An NGA model for the average horizontal component of peak ground motion and response spectra, *Earthq. Spectra* **24**, 173–215.

- Crowley, H., D. Monelli, M. Pagani, V. Silva, and G. Weatherill (2013). Hands-on-instructions on the different types of calculations you can carry out with the OpenQuake Engine Software, *Openquake Engine, User Instruction Manual, Version 1.0.0*, Global Earthquake Model, 154 pp.
- Delavaud, E., F. Cotton, S. Akkar, F. Scherbaum, L. Danciu, C. Beauval, S. Drouet, J. Douglas, R. Basili, M. A. Sandikkaya, M. Segou, E. Faccioli, and N. Theodoulidis (2012). Toward a ground-motion logic tree for probabilistic seismic hazard assessment in Europe, *J. Seismol.*, doi: [10.1007/s10950-012-9281-z](https://doi.org/10.1007/s10950-012-9281-z).
- Ego, J., and M. Sebrier (1996). The Ecuadorian inter-Andean valley: A major and complex restraining bend a compressive graben since late Miocene time, *Annales Tectonicae* **X**, 31–59.
- Egred, J. (2009). Catalogo de terremotos del Ecuador 1541–2009, Escuela Politecnica Nacional, Instituto Geofisico, *Internal Report*.
- Font, Y., S. Segovia, S. Vaca, and T. Theunissen (2013). Seismicity pattern along the Ecuadorian subduction zone: New constraints from earthquake location in a 3D a priori velocity model, *Geophys. J. Int.*, doi: [10.1093/gji/ggs083](https://doi.org/10.1093/gji/ggs083).
- Gutenberg, B., and F. Richter (1944). Frequency of earthquakes in California, *Bull. Seismol. Soc. Am.* **34**, 185–188.
- Hibsch, C., A. Alvarado, H. Yepes, V. H. Perez, and M. Sébrier (1997). Holocene liquefaction and soft-sediment deformation in Quito (Ecuador): A paleoseismic history recorded in lacustrine sediments, *J. Geodyn.* **24**, 259–280.
- Kanamori, H., and D. L. Anderson (1975). Theoretical basis of some empirical relations in seismology, *Bull. Seismol. Soc. Am.* **65**, 1073–1095.
- Lamarque, G. (2011). Analyse méthodologique pour la localisation de séismes dans la zone de Quito et corrélation avec les failles actives, Mémoire M1, Université de Nice Sophia-Antipolis, 33 pp.
- Lavenu, A., T. Winter, and F. Dávila (1995). A Pliocene-Quaternary compressional 899 basin in the Interandean depression, central Ecuador, *Geophys. J. Int.* **121**, 279–300.
- Leonard, M. (2010). Earthquake fault scaling: Self-consistent relating of rupture length, width, average displacement, and moment release, *Bull. Seismol. Soc. Am.* **100**, no. 5A, 1971–1988, doi: [10.1785/0120090189](https://doi.org/10.1785/0120090189).
- Mazzotti, S., L. J. Leonard, J. F. Cassidy, G. C. Rogers, and S. Halchuk (2011). Seismic hazard in western Canada from GPS strain rates versus earthquake catalog, *J. Geophys. Res.* **116**, B12310 doi: [10.1029/2011JB008213](https://doi.org/10.1029/2011JB008213).
- Medvedev, S. V., W. Sponheuer, and V. Karnik (1963). Seismische Scala, Inst für Bodendynamik und Erdbebenforschung, Jena, 6 pp.
- MIDUVI-CCQ (2011). Norma Ecuatoriana de la Construcción NEC-11, Cap. 2: Peligro Sísmico, y Requisitos de Diseño Sismo Resistente, Cámara de la Construcción de Quito, <http://www.normaconstruccion.ec/> (last accessed October 2014).
- Nocquet, J.-M., J. C. Villegas-Lanza, M. Chlieh, P. A. Mothes, F. Rolandone, P. Jarrin, D. Cisneros, A. Alvarado, L. Audin, F. Bondoux, X. Martin, Y. Font, M. Régnier, M. Vallée, T. Tran, C. Beauval, J. M. Maguina Mendoza, W. Martinez, H. Tavera, and H. Yepes (2014). Continental deformation and creeping subduction in the Northern Andes, *Nature Geosci.* **7**, 287–291.
- Pagani, M., D. Monelli, G. Weatherill, L. Danciu, H. Crowley, V. Silva, P. Henshaw, L. Butler, M. Nastasi, L. Panzeri, M. Sionato, and D. Vigano (2014). OpenQuake-engine: An open hazard (and risk) software for the global earthquake model, *Seismol. Res. Lett.* **85**, 692–702.
- Pino, D., and H. Yepes (1990). « Apuntes para una historia sísmica de Quito. Centro Histórico de Quito. Problemática y perspectivas », Dirección de planificación, Ilustre Municipio de Quito, Ecuador.
- Segovia, M., and A. Alvarado (2009). Breve análisis de la sismicidad y del campo de esfuerzos en el Ecuador, in *Geología y geofísica marina y terrestre del Ecuador: Desde la costa continental hasta las Islas Galápagos*, J.-Y. Collot, V. Sallares, and N. Pazmiño (Editors), Comisión Nacional Del Derecho del Mar (CNDM), Guayaquil-Ecuador, 131–150, ISBN: 978-9978-92-737-3.
- Soulas, J.-P., A. Egüez, H. Yepes, and V. H. Perez (1991). Tectónica activa y riesgo sísmico en los Andes Ecuatorianos y en el extremo Sur de Colombia, *Boletín Geológico Ecuatoriano* **2**, no. 1, 3–11.
- Strasser, F., M. C. Arango, and J. J. Bommer (2010). Scaling of the source dimensions of interface and intraslab subduction-zone earthquakes with moment magnitude, *Seismol. Res. Lett.* **81**, no. 6, 941–950.
- Weichert, D. H. (1980). Estimation of the earthquake recurrence parameters for unequal observation periods for different magnitudes, *Bull. Seismol. Soc. Am.* **70**, no. 4, 1337–1346.
- Wells, D. L., and K. J. Coppersmith (1994). New empirical relationships among magnitude, rupture length, rupture width, rupture area, and surface displacement, *Bull. Seismol. Soc. Am.* **84**, no. 4, 974–1002.
- Woessner, J., D. Giardini, and The SHARE Consortium (2012). Seismic hazard estimates for the Euro-Mediterranean region: A community-based probabilistic seismic hazard assessment, *Proceedings of the 15th World Conference of Earthquake Engineering*, Lisbon, Portugal, 24–28 September, Paper No. 4337.
- Youngs, R., and K. Coppersmith (1985). Implications of fault slip rates and earthquake recurrence models to probabilistic seismic hazard estimates, *Bull. Seismol. Soc. Am.* **75**, 939–964.
- Youngs, R. R., S. J. Chiou, W. J. Silva, and J. R. Humphrey (1997). Strong ground motion attenuation relationships for subduction zone earthquakes, *Seismol. Res. Lett.* **68**, no. 1, 58–73.
- Zhao, J. X., J. Zhang, A. Asano, Y. Ohno, T. Oouchi, T. Takahashi, H. Ogawa, K. Irikura, H. K. Thio, P. G. Somerville, Y. Fukushima, and Y. Fukushima (2006). Attenuation relations of strong ground motion in Japan using site classifications based on predominant period, *Bull. Seismol. Soc. Am.* **96**, no. 3, 898–913.

Céline Beauval  
 Laurence Audin  
 ISTERre  
 Univ. Grenoble Alpes-CNRS-IRD  
 F-38041 Grenoble, France  
 celine.beauval@ujf-grenoble.fr

Hugo Yepes  
 Alexandra Alvarado  
 Instituto Geofisico  
 Escuela Politécnica Nacional  
 Ladrón de Guevara  
 2759 Quito, Ecuador

Jean-Mathieu Nocquet  
 Geoazur  
 IRD, Université de Nice Sophia-Antipolis  
 Observatoire de la Côte d'Azur, CNRS  
 250, Rue A. Einstein  
 06560 Valbonne, France

Damiano Monelli  
 Laurentiu Danciu  
 GEM Hazard Team  
 SED-ETHZ  
 Sonneggstrasse 5  
 8092 Zurich, Switzerland

Published Online 22 October 2014

<sup>1</sup> Also at ISTERre, Univ. Grenoble Alpes-CNRS-IRD, F-38041 Grenoble, France.

## 6 Communicating the hazard

*“At the start, I only knew them [the scientists] through telephone calls, through the radio, but then more so in the meetings and training events. We have become better friends through the reunions because they are people who we can talk to and this shows a growth in trust and we now know what they think, what they do, not only talking about the eruptive process but also about our lives and how we live. Sometimes we can have a laugh based on the trust we have gained” Vigía at Tungurahua Volcano, in Stone et al., (2014)*

### 6.1 Introduction

Humanity is constantly exposed to the occurrence of natural phenomena related to the dynamic activity of the Earth System; earthquakes are among the most feared ones. Their dramatic consequences both in human lives and economic losses may have long-lasting impacts in the social and economic growth of a region or a country. From an earth scientists/engineer perspective, in order to reduce their effects it is fundamental to:

- understand the physics behind both hazard and physical vulnerability, which implies to be able to
  - anticipate the occurrence of a defined level of ground shaking in a specific site and time frame
  - decipher the capacity of constructions and human systems to absorb shaking and damage
- promote resilience, i.e. to reduce vulnerability and exposure, to built up coping capacities in human systems to absorb the impact of the natural phenomenon and to rebound to the previous condition without remaining with permanent distortions.

More and more, modern societies and individuals make decisions through knowledge instead of through faith or intuition. Therefore, that scientific knowledge generated by earth scientists on the physics and probabilities of earthquake occurrence, shaking and damage has to be transmitted to the people for them to decide (a) the level of risk they are willing to accept and (b) the actions they need to implement for making it bearable.

But people gather around political systems where decisions are taken by their representatives, the decision-makers. Therefore, decision-makers both in the public and private sectors need to receive earthquake-related, critical information so that they can also make informed decisions for the benefit of all.

Not every scientist has the ability or the willingness to communicate his or her findings outside academic channels, i.e. published articles in scientific journals or conferences in scientific meetings. Researchers are very often reluctant to discuss complex, sensitive matters with decision-makers or the media and it is rather difficult to build a relationship among them based on trust.

As the scientist in charge of the Instituto Geofísico in Quito (IGEPN) for almost 15 years I had to interact with authorities, media, citizens and very diverse and uninformed audiences during different and sometimes difficult moments of my duties. I learned a lot from that relationship. As a result, I am convinced that some of us in the scientific community have to make the effort not only to convey to society the knowledge we acquire but also to cross the line and feel ourselves as part of the public we want to serve. This means that the paradigm of working **for** the community that is commonly used in outreach programs is replaced by a new one of working **with** the community, with all the implications this has.

In Chapter 6 I present my own experience related to communicating the hazard. I refer to the case of Tungurahua volcano's long-lasting 1999-2015 eruption in the central Andes of Ecuador. My reflections are based on three papers: (a) Mothes, Yepes, et al. (2015) that factually describes the eruption and several circumstances around the relationship between IGEPN scientists and the endangered community throughout the eruption period; (b) the social sciences more structured paper (*the research proposal underwent institutional ethical review and was conducted according to UK Economic and Social Research Council ethical guidelines*, p.3, Stone et al., 2014), written by Stone et al. (2014) related to the role played by local observers/farmers –vigías– in a successful community-based monitoring at Tungurahua; and (c) the Bartel (2014) paper that better describes the active role that IGEPN has taken in building and strengthening the vigías network, and the way this relationship has engenders trust in scientists and

risk management personnel. Paper (a) was written during my doctoral work and is included in *Appendix 2*.

The objective in this Chapter is to propose a potential strategy for earthquake risk community-based monitoring in Quito built on the experienced in Tungurahua rural communities. It is clear that both phenomena as well as both communities are completely different, but some of the learned lessons in Tungurahua could prove to be relevant for reducing the earthquake risk in Quito.

## **6.2 Lessons learned in communicating hazard and risk during the Tungurahua volcano eruption**

Tungurahua is a dangerous volcano that threatens the populated northern and western slopes where the touristic town of Baños and small agricultural villages flourish. The volcano was dormant for over 80 years until 1999 when it reawakened, changing the lives of around 25000 people settled at the base of the cone at the time (Fig. 1).

The main threat for the population and infrastructure in the volcano's area-of-influence are the pyroclastic flows or pyroclastic density currents –PDC– which are fast *nuée ardents* that in seconds could obliterate whatever they found in their paths downslope. The consequences of being impacted by PDCs have been made clear in the case of Plymouth, the capital city of the Caribbean island of Montserrat (Fig. 1). Plymouth was destroyed during the long-lasting eruption of La Soufrière volcano, that started impacting the city in August 1997 (Kokelaar 2002). With the understanding that both volcanoes are capable of generating PDCs, it is pretty evident Baños' high exposure due to its geographic location (Fig. 1). The hazard was depicted by the publication of several volcanic hazard maps of Tungurahua prior to and after the onset of the eruption, but before the first PDCs flowed down (e.g. Samaniego et al. 2008).

F1

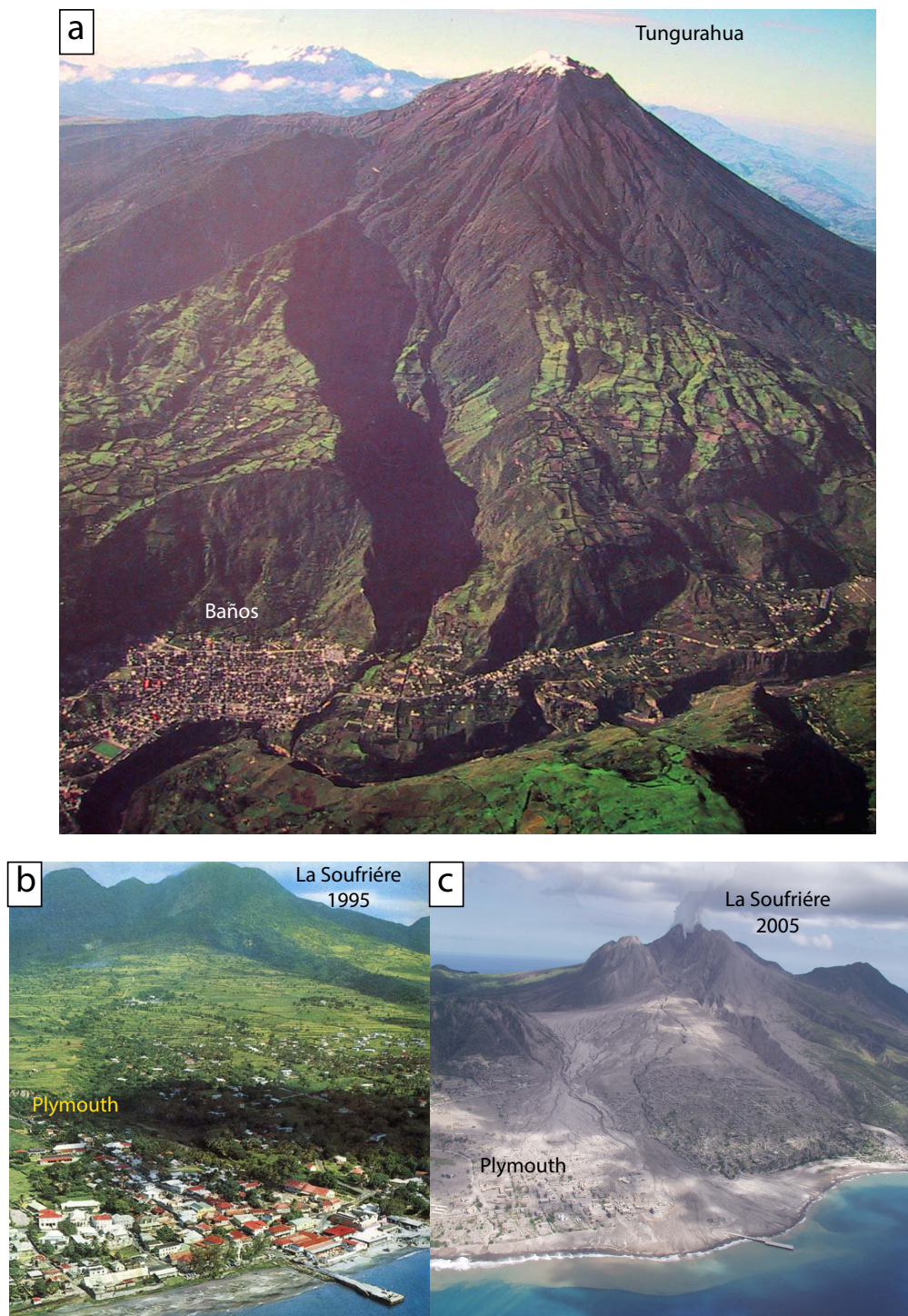


Fig. 1. **a** Tungurahua volcano (5023 m above sea level) and the touristic town of Baños (1900 m a.s.l.). The horizontal distance from the summit to the town is ~8 km. **b** Plymouth, capital city of the island of Montserrat before the eruption of La Soufrière volcano in 1995. **c** Plymouth after ten years of eruption and repeated impacts of pyroclastic flows or PDFs coming from the volcano's summit (915 m a.s.l.) located at 5 km horizontal distance. No human construction can resist to the energy and temperature of PDCs. Photos courtesy of: Tungurahua: Jorge Anhalzer; Plymouth: Peter Dunkley.

### 6.2.1 *The scientific–community interface over the fifteen-year eruptive episode of Tungurahua Volcano, Ecuador (Appendix 2)*

The IGEPN has continuously monitored Tungurahua volcano since the early 90's. A synthesis of the eruptive activity and some of the monitored parameters is presented in Fig. 2.

At least six major eruptive phases can be identified during the ongoing eruption in a chronological sequence:

- 1998-1999 – precursory signals; vent opening explosions (1999);
- 1999-beginning of 2005 – steady state Strombolian eruptions (episodic, starting with the onset of the eruption in November 1999, observable throughout the present eruptive episode) punctuated by energetic ash-rich VEI 1-2 eruptions at the rate of one per year (VEI = volcanic explosivity index, a scale to measure the size of eruptions);
- 2005 – relative quiescence;
- 2006-July-August – paroxysmal phase (VEI 3) with the generation of the first PDCs and the destruction of populated areas;
- 2006-May 2010 – strombolian eruptions with months-long quiescence periods;
- May 2010-present – sudden onset of Vulcanian-style eruptions intermixed with Strombolian activity (characterizing the present-day style of eruption). During strong Vulcanian activity large PDCs have also been generated.

From Fig. 2 it is apparent that the volcano's eruptive style has shifted a number of times. It has to be highlighted that (a) the vent-opening process did not culminated with high VEI eruptions generating harmful PDCs as feared on the basis of the volcano's history and global statistics (Le Pennec et al. 2008); (b) the first PDCs came after almost seven years of continuous, steady-state Strombolian-type eruptions, when the erupting volcano already was “part of the landscape”, i.e. the local population had already forgotten that Tungurahua was **not** erupting less than a decade ago and thought that it will stay with mild eruptions forever; (c) after the paroxysmal VEI 3 eruption of August 16<sup>th</sup> 2006

F2

# Tungurahua's Eruption History

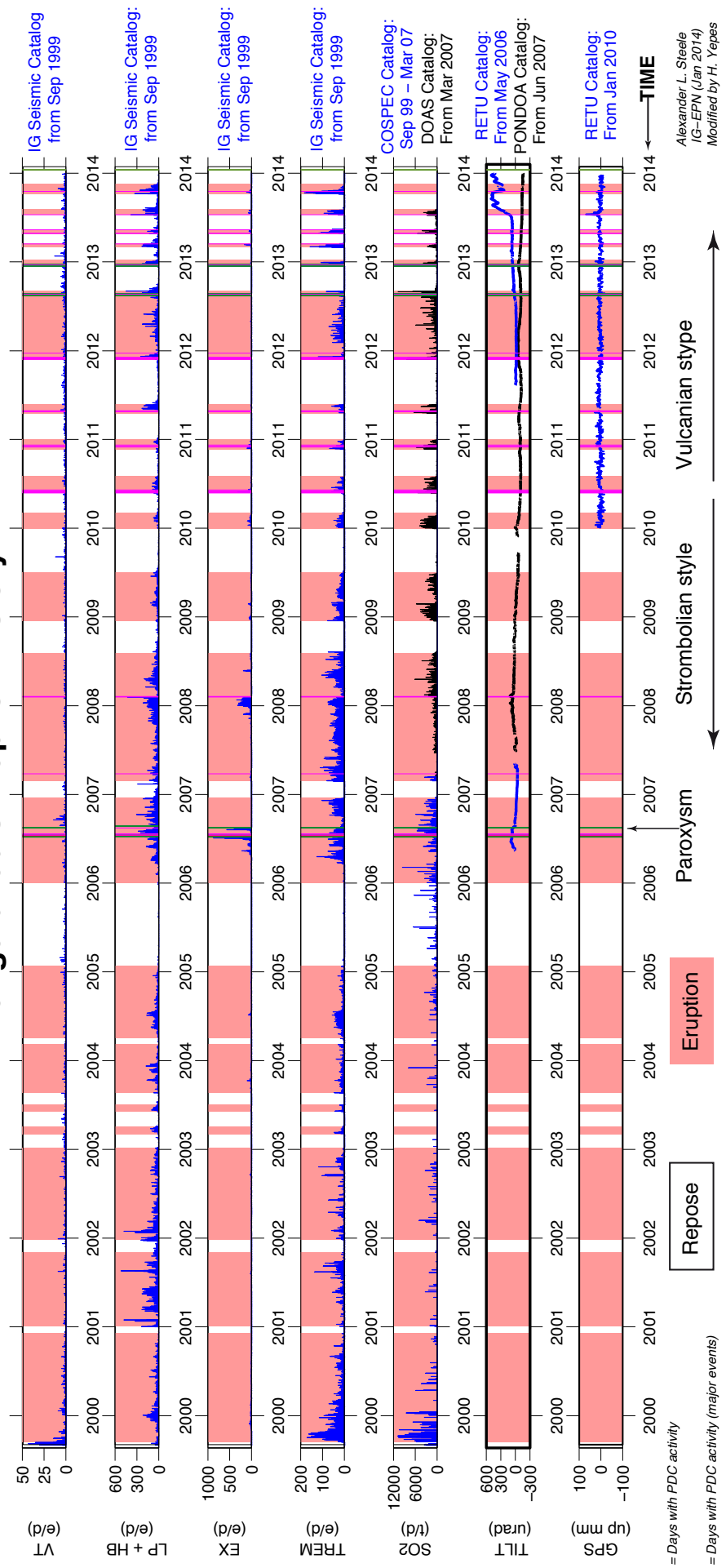


Fig. 2. A timeline of Tungurahua's eruptive activity 1999-2014. Shown on the left margins are the geophysical parameters that are monitored in the volcano. From top to bottom: Vt=volcano-tectonic seismicity; Lp+HB= long period and hybrid seismicity; EX=volcanic explosions;TREM=volcanic tremor; these four seismicity parameters are presented in number of events/day. SO2=measured volcanic gas in ton per day; TILT=electronic inclinometer tilt values in micro-radians; GPS=geodetic GPS corrected measurements in mm. On the right margin the data source is presented. Eruptive activity is presented in pink, while repose is represented by white. The activity was predominantly Strombolian-style through 2010. Vulcanian-style activity started in 2010 and is intermixed with Strombolian-style. Episodes of pyroclastic flows (PDC) are represented by vertical lines: green lines are for major PDC events; magenta lines are mild PDC events. The August 16<sup>th</sup> 2006 paroxysmal eruption is marked. Modified from Mothes, Yepes, et al. (2015).

and the ensuing deposit of one lava flow, the volcanic activity did not start declining, as certain possibility for some (C. Robin, pers. Comm., 2008); (d) ten years after the onset of the volcanic activity, the general pattern of Strombolian-type explosions shifted to sudden, Vulcanian-type more powerful eruptions preceded by completely different and sometimes minor precursory activity, in comparison with the already well documented and well observed Strombolian ones.

It is not difficult to understand that during this extended eruption and numerous changes in the volcanic behavior, the citizens' credibility in appraisals made by IGEPN scientists about the eruption process and its changes was sometimes very low. There was a general feeling that the scientific message was contradicting the people's expectations or empirical knowledge acquired throughout the eruptive process. There were many moments when scientists had to face difficult situations. Some of them are related in Mothes et al. (2015) and summarized here in order to frame the evolution of the community/scientists relationships.

#### *6.2.1.1 Initial eruptions and difficulties in the relationship between scientists and the community*

At the onset of the eruption it was clear that neither Baños nor the villages along the western slopes were prepared for the reactivation of the volcano in 1999. The whole country's emergency management system proved also to be in

deficit. Since the probability of an initial explosive eruption including far-reaching PDCs was substantial (IGEPN internal documents), the Ecuadorian President (Dr. Jamil Mahuad, 1998-2000) himself decided a complete evacuation of the high exposure zones observing the high-risk limits defined in the volcanic hazard map published by IGEPN years before re renewal of the volcanic activity (Hall et al. 1988).

On October 16th, 1999, the populace were given 36 hours to completely evacuate the map's red zones and the Ecuadorian military handled all procedures. The highly complex socio/political circumstances of the country (the President was finally overthrown from power right after the end of the forceful evacuation in early January 2000) made much more complicated for the concerned authorities to manage the situation. As with all forecasting and warning decisions, there was a trade-off between the reducing risk exposure through evacuation and the concomitant increase in social, economic and political disruption (Tobin & Whiteford 2002).

The three months long mandatory evacuation removed all inhabitants from the high risk zone potentially preserving their lives but producing deep resentment in the affected citizens and huge economic losses. Once evacuated, communities were literally forgotten by a central government on the brink of a *coup d'état*. Even though we had not made the decisions to evacuate them or keep them away from their homes and livelihoods for 3 months and that we did not have the mandate to change those decisions, they fully blamed the IGEPN for the actions taken (Tobin & Whiteford 2002).

After an anarchic return to Baños, in early February 2000 several big hotels owners, facing the lack of tourist visitation to their facilities, proclaimed that excessive information about the volcano's behavior was given by IGEPN scientists to the media and that visitors were being scared away from the zone. At the most critical moment, the entrepreneurs threatened to violently chase OVT –the local IGEPN branch at Tungurahua volcano– scientists out and even to set the observatory on fire (Mothes et al. 2015). Some rural community leaders also showed their irritation and discomfort with our presence out in the surroundings of the volcano. It took years to overcome these accusations and part of the IGEPN's

response was to develop positive interactions with the local community (Leonard et al. 2005).

### *6.2.2 The vigías network, a fruitful initiative to establish effective communication between scientists and the community*

The local branch of IGEPN at Tugurahua volcano (OVT) was established at a prudent distance from the volcano (14 km) with three main purposes: (a) to serve as a hub for the transmission of instrumental data from the volcano; (b) to observe and correlate the summit visible volcanic activity with the recorded geophysical, geodetic and geochemical data acquired through the instrumental network; and (c) to serve as a source of scientific information to local authorities, the media and the population. The observatory has been permanently staffed by IGEPN scientists and works on a 24/7 basis. It has been maintained with international, public and private resources for 15 years now.

To fulfill objective (b), considering the cloudy weather conditions in the region and since the OVT only views one side of the volcano, the IGEPN and the National Civil Defense Office –NCDO (since 2008 the National Civil Defense is called the National Office for Risk Management –Secretaría de Gestión de Riesgos–SGR) initiated a system of voluntary volcano observers in 2000. The primary goal of the project was to report back to OVT visual observations from the different sites along the base of the cone where vigías were located. Information was sent via two-way radio transceivers provided by the NCDO. These radios constituted at the time the only technological means to communicate with the endangered communities.

The objective of disseminating scientific information about the status of the volcano was served by (a) daily morning contacts with the local radio station to give a technical report of the latest 24 hours of activity; (b) a weekly live radio program called “Having lunch with a volcanologist” with incoming calls from local citizens; and (c) sporadic local 1-2 hours TV shows to answer any type of questions related to the eruption. National mass media had open access to the scientific personnel at OVT and at IGEPN in Quito as well. We were also attending official meetings called by local and national authorities on a regular basis to inform/give advise about the status of the volcano and to issue/explain early warnings related

to sharp increases of internal activity. These forms of communication, while interactive, are still dominated by one-way communication, with the scientists as the source and the public as the recipient (Bartel 2014); one-way communication does not guarantee that the message will be significant for the public and that will effectively raise awareness about hazard and exposure or promote preparedness or protective actions. Moreover, in the prevailing atmosphere described in 6.2.1.1, our messages were at least suspicious if not taken as false for part of the population.

A turning point in the harsh scientists-community relationship resulted from the implementation of the European Community-funded DIPECHO project during 2003-2004, which at that time was involved in ameliorating social issues in the affected rural areas to the west of the cone (CRS-DIPECHO 2005). One of the strategies devised by us in the project was to have IGEPN scientists directly interact with the vigías, with the campesinos, with the community itself, instead of adopting the more standard approach of training the trainers in the basics of volcanic eruptions, typical of this type of NGOs social projects (V. Zambrano, per. comm., 2015). The scientific members of IGEPN and young students on their weekly shift at OVT got thoroughly involved with these rural communities and very little reluctance to tackle these non-monitoring, non-research activities was expressed.

This strategy proved to be very effective for easing personal relationships among individuals and groups that did not trust each other as a result of the management of the eruption during the vent-opening phase. During the training workshops the community got to know their scientists as normal people, as individuals who do not know all the answers, who could also be wrong, make mistakes, but have a genuine concern about the safety of the community. On the other hand, scientists grasped a view about people's relationship and interaction with their land, with the environment, with the volcano, and learned to respect them (Fig. 3).



Fig. 3. Vigias training workshop organized by IGEPN in Nov. 2008 at Baños

A strong cooperation relationship developed between scientists, the vigías network and the community that was mutually beneficial. On the one hand IGEPN was able to receive visual information to correlate with the instrumental data, was getting help from some community members to maintain remote field stations (mainly to dust the volcanic ash away from solar panels and to carry batteries up the slopes for maintenance) and was relying on them for security of the field stations. In latter stages of the relationship, some vigías participated –and still do it– in monitoring the volcano by collecting ash samples and reporting on ash falls (Bernard 2013).

On the other hand, the vigías and their communities were being trained by the IGEPN scientists themselves about the internal volcanic processes, volcanic products and the associated hazards. Via the two-way radio system, they were receiving daily updates of the volcanic activity, permanent feedbacks to their questions, and plain-language scientific explanations to their observations. During pre-crisis times, they were warned immediately if the internal activity would increase beyond observed fluctuations in instrumental data’s time series and would receive full attention and priority during crises. In contrast to the one-way communication described above, this two-way communication has been strongly

reciprocal (Bartel 2014), greatly enhancing the significance of the conveyed information to the community and helping it to better understand the visible phenomena they were observing at any particular moment in the volcano and to make decisions about their lives and livelihoods.

The 2006 paroxysmal eruptive phase (Fig. 2) is linked to a definitive change in attitude from the population at risk towards the scientific information and to us, the messengers. This shift was probably related to two main factors: (a) people were finally able to have a personal experience with and therefore a mental representation of the life-threatening volcanic hazards that had been listening about for seven years; and (b) since two successful early warnings were issued by the IGEPN before the July and August, 2006 eruptive episodes that saved lives, people were able to better appreciate the value of scientific information about the status of the volcano and about their own exposure to volcanic hazards.

Social research (Stone et al. 2014; Bartel 2014) shows that years after the 2006 eruptions the vigías network is still active and resilient, strengthened by reciprocal trust. The vigías attribute the trust in the scientists to their communities being able to see over time that the information provided by the IGEPN is consistent with the behavior of the volcano. While most vigías put confidence in religious figures to help them in times of crisis, their faith does not appear to dissuade them from taking practical measures toward preparedness (Bartel 2014).

In its current state, with a lack of direction from the SGR, the network is based on the relationships between the vigías, key scientists and individuals in fire services of nearby localities. The vigías network demonstrates the enhanced communication capacity fostered by strong trust-based relationships built by sustained contact between the public and scientists, allowing communities to adaptively respond to risk in a resilient way (Stone et al. 2014).

### **6.2.3 Discussion**

Altogether social sciences researchers (Tobin & Whiteford 2002; Stone et al. 2014; Bartel 2014) recognize that this community-based monitoring network, originated and based on communication of scientific information related to ongoing threatening eruption and driven by trust, performs multiple functions that

effectively reduce the volcanic risk. Community-based monitoring directly contributes to risk reduction by contributing observations of on-going phenomena and their evolution, enhancing risk communication, facilitating community preparedness, serving as an early warning system for civil protection and mediating relationships between scientists and the general public (Stone et al. 2014).

Bartel (2014) summarizes the multiple best practices –as described in the literature regarding risk communication– that are addressed through the vigías network. Her list is presented here including bibliographic references for informative purposes, although this literature was not reviewed in Chapter 6 and is not cited in the References:

- making the scientist a communicator (*Haynes, Barclay, & Pidgeon, 2008a*)
- direct communication from the scientists in order to control information (*Newhall et al., 1999*)
- building scientist recognition and credibility among those who will receive warnings (*Newhall, 1999*)
- persisting in scientist-public engagement between crises as well as during volcanic activity (*Campbell, 2011*)
- utilizing both scientists and community members (friends, family, and neighbors) as communicators (*Haynes, Barclay, & Pidgeon, 2008a*)
- involving the target audience and bypassing news media as a principle source of information dissemination (*Campbell, 2011*)
- communicating via community leaders (*Scanlon, 2007*)
- working off simple, redundant technology (*Voight, 1990*)

Now, looking back to the early years around the onset of Tungurahua eruption, when the idea in town was to kill the messenger (Mothes et al. 2015) as in ancient Greek times instead of looking at one’s own exposure and vulnerability, I feel that we have walked a long and fruitful journey in terms of communicating the hazard. Profiting from my experience and the freshly written literature on the vigías network, there are three central ideas I do want to highlight about our role as disseminators of scientific knowledge:

1. it is not easy to communicate (the French word 'vulgariser' is much more appropriate for the task) complicated physical processes driving natural phenomena that we as scientists do not fully understand and that are crossed by uncertainties, but our knowledge is of extreme importance for the security and well being of society. The objective of hazard/risk communication has to be seen by hazard/risk scientists as an opportunity to educate and to promote risk-reducing behavior in the community.
2. Communication is a two-way road. In the one direction we provide society with knowledge about hazards, exposure, vulnerability and risks related to its own, immediate environment. In the other direction we receive information about people's relationship and interaction with Mother Nature (for them the Pacha Mama), about their ways of life and their daily pressures. We should listen to their concerns and questions and learn from their feedbacks to our messages.
3. Our message should have three main characteristics (Feuerstein et al. 1988): (a) intentionality, (b) significance, and (c) effectiveness for people to take ownership of their situation and to successfully change the risk (*I include some naïve examples using earthquakes*):
  - a. A scientist's **intentionality** [*for instance to explain the physical process by which seismic energy is stored and released, profiting from the opportunity of a felt earthquake in the area*] should be linked to reciprocity from the audience; once reciprocity is present, it means that the message was understood and appropriated by some or all.
  - b. The message is **significant** when it has a specific (valid) meaning for the audience so that it is valuable and remains latter as part of everyone's knowledge [*following with the above example: the seismic energy released during the latest, felt earthquake is only a small fraction of the energy that has been stored along the fault from the last great earthquake on; therefore I, the scientists in charge, can not rule out a major one within the foreseeable future*].
  - c. The message is **effective** when it produces a change as a result of the new knowledge, i.e. messages –and concepts behind them– are applied for the individual or common good [*since there is a real*

*possibility of a greater earthquake I will retrofit and insure my home; authorities will prepare the community for a potential next event]. It is not information that you know as part of your general culture, it is knowledge that becomes part of your new way of facing life, in this case a new attitude towards your seismic risk.*

We as scientists have the opportunity to add these three main characteristics to our message by tuning ourselves into the needs, feedbacks and beliefs of the community.

There is a fourth idea that has not been discussed in this Chapter but comes from years of my own experience with the media and is worth mentioning:

- d. The media are still the most effective way to convey the message even in today's era of the internet and the so called social networks (which actually are virtual networks). Media reporters, interviewers and producers are a scientist's allies, not the enemies. If the three characteristics mentioned above are also used by scientists for passing the message to the media people, then there is a much greater possibility that the original scientific message will be correctly delivered producing the desired effect.

The Tungurahua case may be unique, but there are general lines that we could identify to propose a comparable approach for enhancing earthquake risk communication, facilitating preparedness and fostering community empowerment to reduce the seismic risk in Quito.

## **6.3 A strategy for earthquake risk community-based risk management in Quito**

### **6.3.1 Theoretical grounds**

To promote risk-reducing behavior inextricably links hazard risk communication to risk management strategies and encourages a more inclusive approach involving many stakeholders. Robust methods must be developed for allowing dialogue between the community, authorities and the scientists at a number of levels to address risk reduction effectively (Barclay et al. 2008).

Several forms of participatory initiatives, e.g. community-based disaster risk management (CBDRM), community-based monitoring (CBM) and more, have been suggested by the social science community when conditions of uncertainty related to natural phenomena make it more difficult to communicate hazard and risk to the population (Maskrey 2011). CBDRM places greater value on local knowledge, local ownership, vulnerability and capacity assessments, and on participatory methods. CBDRM allows calculations about risk and uncertainty to be left to communities, who are expected to make choices about risk management decisions based on their own knowledge of the environment in which they live and the livelihood options available to them (Barclay et al. 2008).

Our evidence from rural communities in Tungurahua shows that strong interactions between scientists and citizens can built relationships that ultimately contribute to volcanic risk reduction at a local level. If one of the by-products of community-based monitoring –CBM–, which is based on good scientists-citizens relationships, is people’s empowerment to take ownership of their problems and solve them as in the Tungurahua experience, then it is a valid exercise to explore these possibilities for reducing the seismic risk in Quito.

### **6.3.2 Outline for a CBDRM strategy in Quito**

While in Baños and along the western slopes of the volcano the hazard is related to the ongoing eruption of Tungurahua, in Quito the threat is coming from the probability of experiencing strong ground motions due to earthquakes generated by the Quito fault system and other sources, as described in Chapter 5. Both phenomena are completely different and, generally speaking, the concurrent risk has different causes at both sites too. At Tungurahua risk is related to the geographical location of settlements (exposure) while in Quito, acknowledging that exposure is permanent and soil response will play a role, risk is mostly coming from the condition of the structures (physical vulnerability).

In Table 1 an overview of the differences between the two situation is presented. The Table try to capture the generalities of each case and by no means it pretends to be inclusive.

Table 1: General characteristics of volcanic and earthquake hazards/risk for CBDRM purposes

Hazard	Volcanic eruption	Earthquake
Characteristic		
Precursory activity	Weeks to months	Not identifiable
Susceptibility of being forecasted	yes	no
Onset	Gradual	Sudden
Duration	Months to years, Intermittent episodes	Seconds to minutes, Decaying aftershocks
Reach	Govern by volume, topography. Driven by gravity	Govern by magnitude, focal mechanism and distance to the source
Damaging agent	Momentum, heat, mass (weight): Density currents, i.e. pyroclastic, debris, lava. Ash	Acceleration: Ground shaking Secondary phenomena, i.e. landslides, tsunami, soil subsidence
Modifiers	Internal: % of SiO <sub>2</sub> , water, External: water, wind	Attenuation Ground condition (soil type)
Potential damage related to:	Exposure to any of the volcanic products	Physical condition of the elements at risk
Hazard assessment	Deterministic Scenario type Maps	Probabilistic Maps, hazard curves
Uncertainties	Not included	Quantified

From Table 1 it is possible to obtain important differences to help define how CBDRM could be effectively proposed for Quito.

During Tungurahua's eruptive long-lasting process the community has been able to observe the eruptive activity at the crater and beyond, from premonitory to steady state to paroxysmal. This is one of the main motivations for the vigías and local campesinos to get involved in CBM and to stay doing it, as stated in Section 6.2.2. In the case of earthquakes no premonitory activity –identifiable by the community or by scientists– is expected and the event will only last seconds; therefore, since the natural event will be sudden and short-lived, a possible CBM initiative in Quito can not be centered on observing it.

People in the two locations are completely different as well. In Quito the community is urban. The citizens of Quito have a different interpretation of Mother Nature; they are not as attached to the land as the campesinos are; their tempo of the daily life is frantic and very little time is dedicated to observe nature or to interact with neighbors; their ambitions in life are different. Then, what would be the motivation for these urban individuals to interact with seismologists about a potential earthquake that they do not see coming or that may have not even heard about? What type of information can we scientists provide that is significant, is needed and could get the community interested in CBDRM to produce a permanent change in the present-day high vulnerability? How is it possible to have the risk from earthquakes be viewed not as an isolated phenomenon but within the broader contexts of economic and social development?

I summarize some major characteristics of the city and of the citizens of Quito:

- Quito is the Capital City of Ecuador:
  - The Ecuadorian presidency and the vast majority of the ministries and governmental offices are based in Quito
  - Quito is the second largest consumption pole and the largest tax-payer in the country
  - The city is a crowded communications and business hub
  - UNESCO declared the city World Cultural Heritage of Humanity 25 years ago
- Quito is a, large, complex and vulnerable city (2.5 M):
  - 20% of the Ecuadorian population lives in Quito
  - >60% of total buildings were built without municipal permits (d'Ercole & Metzger 2004)
  - Application of the Ecuadorian Building Code is not mandatory
  - There is no control of seismic designs by municipal bodies or it is very recent
  - Poor construction practices that includes lack of professional advise, use of substandard materials and assembly methods, and inappropriate sitting of buildings are very common

- The most important economic sectors where people work at are services, commerce, education and public.

With all these in mind, some valid questions for the citizens of Quito and for city managers are:

- What does it mean for buildings that the ground would shake at 0.4-0.5 g – or more – with a probability of exceedance of 10% in 50 years as described in Chapter 5? What does it mean for the city's infrastructure, for the continuation of normal life, for keeping doing business as usual to have such a strong shaking due to an earthquake below the city? What would be the cost for the city? What would be the toll in human lives? What does it mean in terms of governability for the entire country?

Nobody knows the answer yet, but any answer will not be nice. Even worse, no public official in the city, no emergency manager, no economist, no politician, no development planner, no businessman, no normal citizen has the slightest idea of the various dimensions of a potential earthquake-related disaster in the Quito. There is no earthquake risk awareness in the collective imaginary despite the obvious exposure, obvious at least for seismologists, earth scientists, vulnerability science researchers, and to some local civil engineers too (Fig. 4, (GEM foundation 2012)).

As described in Section 6.3.1 CBDRM is one possible answer to foster risk mitigation. Integrating risk management and community development activities in ways that develop competencies (e.g. discussion of hazards, problem solving activities) and relationships (e.g. empowering) will increase the degree of preparedness. When communities and concerned public officials (e.g. development planners, emergency management agencies) play complementary roles in the risk management process, community members levels of trust, satisfaction with communication, risk acceptance, willingness to take responsibility for their own safety, and commitment to prepare for hazards will increase (Paton et al. 2008).

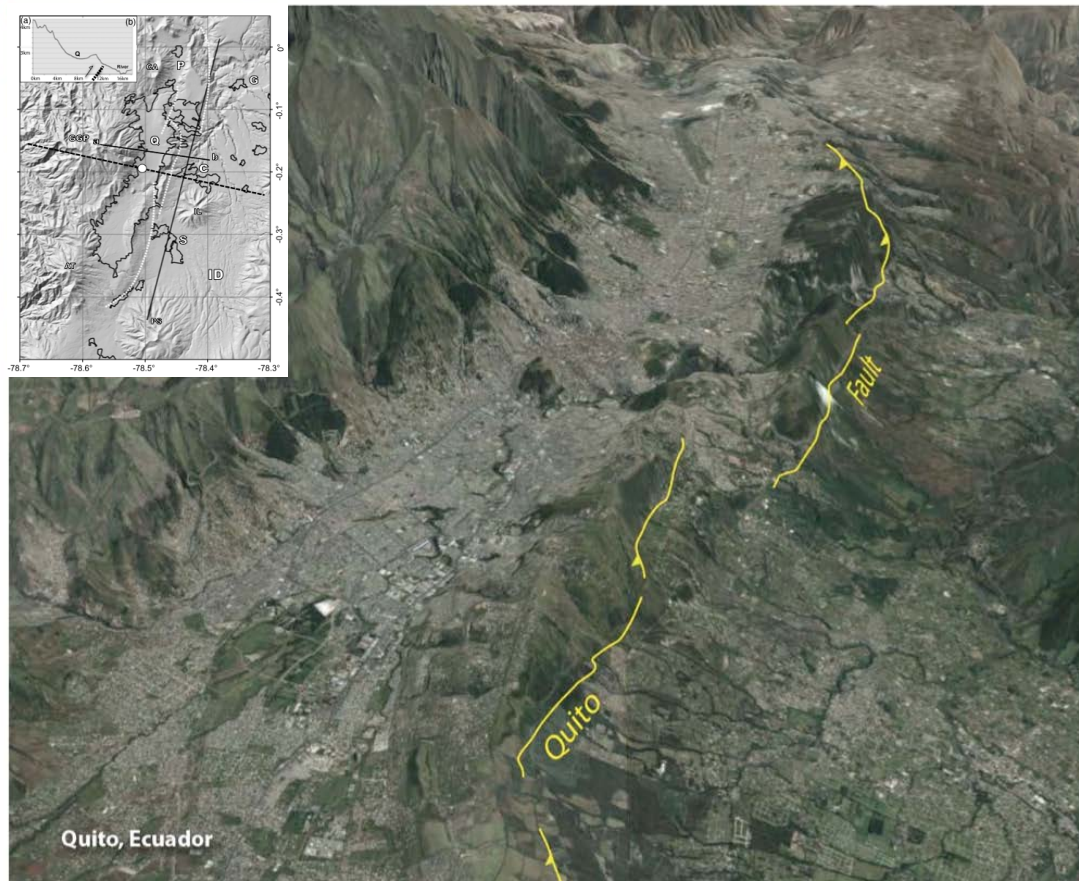


Fig. 4. Google Earth view of the setting of Quito and the Quito Fault (Photo courtesy of GEM Foundation). The fault is dipping to the west. The elevation difference between the Quito Plateau and the bottom of the Interandean Depression is almost 600 m accumulated during tens of thousands of years of thrusting activity . The inset shows the modeled fault used to calculate the PSH in Quito, as described in Chapter 5. For more information refer to Fig. 2 in Chapter 5.

Consequently, I propose to start building up knowledge about the various dimensions of the earthquake risk in Quito in a participatory fashion, in the same way we started building up local knowledge with the rural communities in the western flanks of Tungurahua volcano 15 years ago. In view of the notorious differences between the two populations, this collective construction could take the form of a citizens observatory<sup>1</sup> for seismic risk awareness and reduction, for

---

<sup>1</sup> The concept of a citizens observatory –CO– comes from the social and political sciences and is related to the participation of the so-called “civil society” in processes aiming at understanding specific realities of social phenomena and at proposing solutions for the problems arising from those realities. A CO is an autonomous, technical and interdisciplinary participatory space formed by groups of citizens or civil organizations where a reality or the circumstances, conditions and factors around a social situation

instance the “*Quito Earthquake and Urban Risk Observatory*”, a citizens initiative where key actors of the very complex city’s life will start understanding the significance of strong ground shakings for themselves and for their social or economic sectors. With our leading guide based on our knowledge about both the physical phenomenon and the physical performance of man-built structures, those who are at risk – the citizens–, will have their own diagnoses of the seismic problem that matters to them and will propose solutions tailored to their own realities. In a way the eternal question posed to me regarding a close by earthquake that may occurs in the near future (in general related to a seismic catastrophe hitting somewhere else) will be turned back to them taking the form of ‘what will happen TO YOU if that earthquake happens’. The participatory construction of knowledge and this shift in rhetoric will make the citizen to own the problem, will lead to their empowerment. Thus, the combination of scientific, community and local expertise, integrated into national and regional disaster reduction policies and the people’s will and urgencies could result in an effective approach to a disaster risk reduction management.

For instance, issues about the potential outcome for businesses of a strong earthquake in Quito regarding their continuation, direct costs, lost markets, time for recovery, and so on, would be addressed by the city’s Chamber of Commerce; or school buildings performance during the shaking by an interdisciplinary group of parents, school districts representatives, the Municipality and the civil engineers local association, for example; and so on.

---

are observed, analyzed, processed and theorized (Consejo de participación ciudadana y control social – Ecuador, <http://www.cpcs.gob.ec/?mod=observatoriociudadano>). A CO is permanent, durative, not punctual and, its life and vitality depend on its members’ involvement and activity. Central to the concept of a CO is its autonomy and independency from the governmental sector and the voluntary condition of the membership. There are no fix structural schemes for COs but some of those that have effectively influenced public policies have two components: political and technical. The technical component might gather and analyze data and information about the specific issue and generate diagnoses and proposals, while the political part might use them to raise public opinion and lobby for implementing or for changing public policies (Observatorio de los derechos de la niñez y adolescencia -Ecuador, <http://www.odna.org.ec/>).

These are only a couple of examples of a myriad of issues and possibilities that should be addressed by such an earthquake risk observatory if we want to responsibly answer to questions that would rise around this topic in Quito. The force to keep moving the initiative –as is the permanent and palpable activity of the volcano for the vigía network at Tungurahua– will be the growing realization of the extremely large impacts of a potential earthquake. The idea is to promote local ownership of the knowledge and appropriation of the problem by a few individuals who would champion a particular dimension of the risk. Our intentionality as scientists will be to give significance to both, the hazard and the physical vulnerability with specific information for each of those dimensions. This information aims to be used for sector-specific risk appraisals obtained by the sector actors. Once a committed group of people start generating sectorial information more sectors would get involved and the program would achieve sustainability.

Quito city officials, as elected representatives of the general public, are one of the key actors in this process, but they are not indispensable for the work to be done; moreover, a citizens observatory has to be independent from the current political authority. The permanent shift in public policies and the high mobility of public officials precludes institutional appropriation of the knowledge, as I have seen throughout the short history of risk management in the country. Therefore this CBDRM initiative –the observatory– different actors will demand the authority to take action and implement policies and activities to reduce the seismic risk. The observatory would play a key role in monitoring the authority's compliancy. The observatory will exceed the authority regular term since it will be a citizens' voluntary effort, enduring in time with the active participation of motivated individuals in the businesses community, construction industry, insurance, tourism and other industries, as well as professionals from civil engineering, architecture, educators, NGOs working in risk reduction issues, and more.

### **6.3.3 Conclusion**

After the L'Aquila trial there is a vivid debate among earth scientists about the role of scientific experts during seismic crises and the protocols that would frame their actions. Some arguments go in the line that scientific conclusions, in

spite of their potential difficulty and intricacy, once delivered to decision makers, are not under the responsibility of the scientific experts that originated them. Decisions are taken by decision makers, not by experts or scientists, not only based on scientific conclusions but on a set of information where the expert's opinion is only one element (COMETS 2013).

On the other hand, social scientist challenge the ability of the one-way communication described above to effectively transmit the message and see that difficulties in the management and communication of uncertainty, common to almost all fields of risk communication, largely govern the [bad] outcome of a natural crisis situation (e.g. Barclay et al. 2008). Thus the challenge to the value of science under conditions of uncertainty has been answered by the social science and development community with participatory approaches like CBM or CBDRM. One of the key lessons learned in the three-way relationship volcano-scientists-community during the long-lasting Tungurahua eruption was that if scientists want to effectively influence in reducing the hazard and risk, the paradigm of communicating scientific knowledge to the community should be replaced by a shared construction of knowledge within the community.

Earthquake communication is different. In locations like Quito, situated right above an active fault, there are no chances for issuing early warnings, and monitoring of the natural phenomenon by the community is out of the question. But earthquake scientists can probabilistically quantify the hazard and more and more efforts are being done to probabilistically quantify the risk. Uncertainties play now a very important role in this type of quantifications and should also be communicated. Following the practices of the social sciences and the Tungurahua experience, a participatory approach is outlined to start effectively managing the earthquake risk in Quito.

## 6.4 References

Barclay, J. et al., 2008. Framing volcanic risk communication within disaster risk reduction: finding ways for the social and physical sciences to work together. *Geological Society, London, Special Publications*, 305(1), pp.163–177.

- Bartel, B., 2014. Citizen empowerment in volcano monitoring, communication and decision- making at Tungurahua volcano, Ecuador. *University of Colorado - Boulder*, pp.1–44.
- Bernard, B., 2013. Homemade ashmeter: a low-cost, high-efficiency solution to improve tephra field-data collection for contemporary explosive eruptions. *Journal of Applied Volcanology*, 2(1), pp.1–9.
- COMETS, 2013. Risques naturels, expertise et situation de crise. *Avis du Comité d'éthique du CNRS*, pp.1–4.
- CRS-DIPECHO, 2005. Communities affected by Tungurahua: Mitigating the Risk of Living near an active volcano. *DIPECHO-QUITO*, pp.1–67.
- d'Ercole, R. & Metzger, P., 2004. *La vulnerabilidad del distrito metropolitano de Quito*, Quito: Dirección Metropolitana de Territorio y Vivienda. Municipio del Distrito Metropolitano de Quito; Institut de Recherche pour le Développement (IRD).
- Feuerstein, R., Rand, Y. & Rynders, J.E., 1988. *Don't accept me as I am: Helping 'retarded' people to excel*, Plenum Press.
- GEM foundation, 2012. *An integrated and collaborative assessment of seismic risk in South America*, Pavia, Italy: GEM.
- Hall, M., Beate, B. & Hillebrandt, von, C., 1988. *Mapa de los Peligros Volcánicos Potenciales asociados con el volcán Tungurahua, Provincia de Tungurahua, Escala 1:50.000*, Quito: Instituto Geofísico, Escuela Politécnica Nacional.
- Kokelaar, B.P., 2002. *Setting, chronology and consequences of the Eruption of Soufrière Hills Volcano, Montserrat (1995- 1999)* T. H. Druitt & B. P. Kokelaar, eds., Geological Society of London.
- Le Pennec, J.L. et al., 2008. The AD 1300–1700 eruptive periods at Tungurahua volcano, Ecuador, revealed by historical narratives, stratigraphy and radiocarbon dating. *Journal of Volcanology and Geothermal Research*, 176(1), pp.70–81.
- Leonard, G.S. et al., 2005. Impacts and management of recent volcanic eruptions in Ecuador: lessons for New Zealand. *Institute of Geological & Nuclear Sciences science report 2005/20*, pp.1–51.
- Maskrey, A., 2011. Revisiting community-based disaster risk management. *Environmental Hazards*, 10(1), pp.42–52.
- Mothes, P.A. et al., 2015. The scientific–community interface over the fifteen-year eruptive episode of Tungurahua Volcano, Ecuador. *Journal of Applied Volcanology*, 4(9), p.15 p.
- Paton, D. et al., 2008. Risk perception and volcanic hazard mitigation: Individual and social perspectives. *Journal of Volcanology and Geothermal Research*,

172(3-4), pp.179–188.

Samaniego, P. et al., 2008. Mapa de los peligros potenciales del volcán Tungurahua. *Instituto Geofísico - EPN*, pp.1–1.

Stone, J. et al., 2014. Risk reduction through community-based monitoring: the vigías of Tungurahua, Ecuador. *Journal of Applied Volcanology*, 3(1), pp.1–14.

Tobin, G.A. & Whiteford, L.M., 2002. Community resilience and volcano hazard: the eruption of Tungurahua and evacuation of the faldas in Ecuador. *Disasters*, 26(1), pp.28–48.

## 7 Summary and perspectives

### 7.1 Summary

Ecuador is a country where seismic hazard and risk are substantial. The death toll due to earthquakes during the country's history is high and notable events during previous centuries have hampered sustained development in cities or entire regions. Although there have been several initiatives to develop a culture of seismic prevention (e.g. EPN et al. 1994, EPN-GHI 1995) it is evident that the public interest on this most important issue fades as quickly as the time goes by since the last damaging earthquake, or much faster. This lack of seismic culture results in a permanent and ever-growing construction of vulnerability which inexorably will be evidenced by the impact of the next sizable earthquake close to populated areas or important infrastructure. Unless the country starts shifting this dangerous trend with a sustained effort to procure better knowledge about seismic hazard, exposure, vulnerability and risk for making more and more informed decisions aiming at risk reduction, our seismic future looks dark.

As a contribution to revert this condition a systematic approach to carry out PSHA at the country level, observing up-to-date international practices in every step of the analysis, started in Ecuador seven years ago. This endeavor was not born under the shadow of a damaging earthquake, as is frequently observed elsewhere when seismic provisions for an emergency building code are needed; it results from the academic cooperation between French and Ecuadorian scientists. This dissertation is one of the products of this cooperation.

For PSHA, all possible contributing earthquakes and their resulting ground motion should be considered, along with the uncertainties related to the occurrence, location, size and wave propagation of these natural events. The first step towards PSHA was to construct the Ecuadorian earthquake catalog. The final catalog includes 10.823 independent seismic events from 1587 to

2009 and with a magnitude range from 3.0 to 8.8. The catalog proved to be very important for the formulation of the seismic source zones SSZ model because a sharper picture of the geodynamic and seismotectonic processes in the country was able to be depicted with the depurated seismicity.

One of the major contributions of this doctoral work has to do precisely with the new view of Ecuador's geodynamic scheme proposed here and with its ability to explain the earthquake occurrence in the country. This new model is based on two main ideas. On the one hand, it is a fact that two different plates, Nazca and Farallon, are being subducted below northern and southern Ecuador, respectively. The two plates are in contact along the Grijalva "suture", which is a plate margin relict of the final episode of Farallon plate fragmentation. Plate rheology to the north and south of Grijalva is different due to the differences in age of both plates. On the other hand, the convex shape of the northwestern corner of South America's plate margin is responsible for a very rapid change of the convergence obliquity angle that shifts from positive in Ecuador to negative in northern Peru. This variation in obliquity deviates the trench-perpendicular shear stresses at the interface in a convergent manner. These stresses, the plate's inherited fabric and the differences in rheology at depth underneath Ecuador, may explain the contortion of Farallon's northeastern corner along the Grijalva rifted-margin. This model satisfactorily explains several characteristics of the observed inslab seismicity and allows a clearer definition of the inslab sources.

The inter-seismic coupling at the interface may also be conditioned by the presence of the two rheologically different plates. The coupling models show that south of Grijalva the Nazca plate (Farallon in our interpretation) is practically sliding aseismically. The catalog shows that no historical  $M_w \geq 8$  earthquake has been located between Grijalva and Mendaña fracture zone in Central Peru. To the north, the  $M_w \geq 8$  ruptures did not completely break the interface where Carnegie ridge is subducting, and today's interseismic coupling north of Carnegie reveals the rupture zones of the 20<sup>th</sup> century's great events. The highly coupled small area below La Plata island, where slow earthquakes

have been detected, and the Bahía zone, where characteristic  $M \sim 7$  earthquakes have recurred during the 20<sup>th</sup> century, is considered as a transition zone. Interface seismic sources were modeled accordingly.

The model also endorses the postulate that the oblique Nazca/South America convergence and the high coupling along the northern Ecuador subduction interface are responsible for the divergent northeastern motion of the NAB. The NAB – South America shearing contact diagonally extends across Ecuador from SW to NE. This faulted boundary is the locus of the larger crustal earthquakes described in the catalog. The Andean back-arc domain and internal deformation inside the NAB are also responsible for large to great earthquakes. These earthquakes are located much closer to populated areas than the interface events and have triggered the major earthquake disasters in Ecuador's history, i.e. in 1797 and 1868, as was illustrated in Fig. 2 of Chapter 1.

A natural first target for using the preparatory work to compute PSH for Ecuador was Quito and its fault system. The study was conducted with the objectives of identifying the parameters controlling the target acceleration and evaluating the uncertainties on these parameters. The catalog and earlier versions of the SSZ model (Alvarado 2012) were used. It was found that for 475 years return period the seismic hazard is controlled by the Quito crustal SSZ. This source zone basically models the Quito fault system. A mean PGA value around 0.4 g for a rock site at 475 years in Quito was obtained by modeling the earthquake recurrence based on the catalog.

The different combinations of options for the local SSZ, of GMPEs, the ways of defining the seismic recurrence, the modeling of the source as a fault source and the inclusion of the hanging wall effect, result in a variability from 0.28g to 0.73g for the same site conditions. It is well established that acceleration is not a good descriptor of damage (Elenas & Meskouris 2001). Therefore uniform hazard spectra UHS for a generic rock site in Quito taking into account all source zones were also calculated, since spectral seismic

intensity parameters are better correlated with damage. The overall qualitative interpretation is that Quito is exposed to a notably large seismic hazard.

## 7.2 Perspectives

The immediate next step is to calculate a new generation of probabilistic seismic hazard maps for Ecuador using the PSHA-ready seismic catalog discussed in Chapter 3 and the new seismic source model developed in Chapter 4. The update will supersede the probabilistic seismic hazard estimates obtained during the last years (MIDUVI-CCQ 2011; Beauval et al. 2014; NEC 2015). For this calculation the detailed description of the sources made in Chapter 4 will let the modeler propose alternatives in order to quantify the epistemic uncertainties related to the sources. Since no GMPEs have been derived for the country yet, and even less for the different tectonic environments that characterize our geological setting, existing GMPEs relying on large global or regional databases must be applied for the calculation (e.g. equations selected in the Global Earthquake Model –GEM project). Several GMPEs will have to be selected to capture the uncertainty on the prediction of strong ground motion as well.

Probabilistic seismic hazard calculations contain two types of uncertainty, and both will have to be quantified: epistemic uncertainty coming from lack of knowledge (inability to identify the correct model), and aleatory uncertainty arising from an inherent variability in nature (Senior Seismic Hazard Analysis Committee 1997). Epistemic uncertainties will be included in PSHA by comprehensive logic tree exercises. The sources of highest uncertainties and highest impact on hazard should be identified, to understand where efforts should be put to reduce the lack of knowledge on hazard estimates in the future.

There are present-day efforts to harmonize the current practices in PSHA in South America. The GEM initiative is supporting the South America Risk Assessment (SARA) project ([www.globalquakemodel.org/what/regions/south-america/](http://www.globalquakemodel.org/what/regions/south-america/)) which aims to calculate hazard and risk involving local experts and institutions from the region. Data sharing and integration is central for this endeavor. A common and standardized catalog, a unique database with

shallow active faults and subduction sources where country borders are transparent, GPS data, and regional GMPEs evaluated and tested are the goals of SARA. A state-of-the-art seismic hazard model for the region consisting of the individual countries' share will come out, replacing previous versions described in Section 1.3 and hopefully improving in a great deal the local capacities. The work presented in this manuscript is already being used by SARA in its different components.

Seismic hazard models are always dynamic since new results from seismology, paleoseismology, historical seismicity, microseismicity, earthquake geology, geodesy, strong ground motions, etc., will render more and better information regarding crustal faults, earthquake recurrence, strain accumulation and release, local attenuation, site response, and so on. This information has to be periodically included in PSHA in order to improve the reliability of the model and to reduce epistemic uncertainties. Thus, PSH assessments will have to be updated every 3-5 years, once the availability of new information make it worth doing it.

One of the short to medium-term objectives in PSHA practice in Ecuador should be to model more fault sources, as was done in Chapter 5. The fault source model requires a complete, viable representation of the known active faults (fault trace, average dip, average upper/lower seismogenic depth, average long-term slip rate, average seismic/aseismic slip factor, focal mechanism, and uncertainties attached). There are several fault candidates for targeting immediate research in this direction

- Pallatanga FS -fault system-, with several branches, responsible for the 1797 M7.6 earthquake. The faults trace location has a direct influence on the probabilistic seismic hazard assessment (Mariniere 2014). The N-S branch running into Riobamba city deserves especial interest. A pioneer work with paleoseismological trenching and the use of satellite technologies is already underway in this FS (Baize et al. 2014).

- Cosanga FS shows very clear neotectonic activity that may let defining the fault characteristics for fault source modeling. It will be a challenge to figure out the slip rate and paleoseismology could provide some answers.
- Puna FS is located in flat lands and shows very sparse seismicity. Current-deformation modeling using GPS data could provide slip rates for fault source definition.
- Chingual FS has enough published information but little recorded seismicity, so modeling would depend on geological slip rates (the above four FS are part of the NAB-South America boundary)
- Quito-Latacunga FS. The target would be the Latacunga segment. The 1698 M7.2 earthquake could have originated in this FS but there is no fault trace assigned to it. It is important for understanding the partitioning of the deformation along the NAB boundary –CCPP and internal faults.
- El Angel FS, with little recorded seismicity but several branches with clear neotectonic characteristics. The most damaging historical earthquake for Quito (1859) could have originated in this FS but the causative structure has not been identified yet. It is also the generator of the catastrophic 1868 Ibarra earthquake.

Regarding the interface seismic source zones, results from ongoing studies in the weakly-coupled segment of the Ecuadorian subduction zone south of the Grijalva rifted margin will give insight about the seismic potential of single or multiple segments in which the interface could be divided and modeled for PSHA. Researchers (e.g. Vallée et al. 2013) are looking now at the possibility that the stress accumulation around asperities at the interface varies with time. If demonstrated and quantified, in the future hazard analysis will have to consider this time variation since it has implications in the related seismic hazard. Finally, with improved maps of the spatial distribution of the interseismic coupling along the interface and local tomography studies, it will be possible to improve the modeling of the interface SSZs and better quantify the epistemic uncertainties analysis.

Since 2012 the Geophysical Institute in Quito –IGEPN– has implemented a permanent, real-time, dense network of seismological and geodetic instrumentation consisting in BB seismometers, accelerometers and GPS receivers installed at a spacing of less than 50 km in the tectonically active part of the territory. The instrumental network is part of the national seismological service in charge of IGEPN (Servicio Nacional de Sismología y Vulcanología – SENASV). The database that is building up will give researches a great potentiality to address the above-mentioned issues and to improve PSHA practice in Ecuador. The use of this new information is implicit in the discussion below.

In the short term, more accurate earthquake locations will improve the quality and reliability of the seismic catalog. Our seismic catalog could serve as a basis for integrating the catalogs from neighboring Peru and Colombia under the same standards for PSHA and other purposes. Moreover, the rapid development of the national seismic networks asks for real-time data integration in order to produce combined hypocentral solutions and earthquake parameters in the Northern Andes.

Once that national seismic networks have been modernized, there have been some discussions about the need to develop a South American tsunami early warning system where the earthquake component could be well served by a regional distributed processing Center. This is a very important initiative not only for tsunami but for every large earthquakes since we know from experience that major events such as the 2010  $M_w$  8.8 in Maule, Chile will render the national seismic services inoperative. If there is a regional distributed center in place, emergency roles, such as defining the tsunamigenic condition of an interface great earthquake, would be taken by the center still using local data of the disabled local processing facility.

A second straightforward application to be implemented in such an integrated center and/or in local processing facilities is earthquake early warning capabilities for earthquake crisis management. There is an ongoing initiative to develop a near-real time unified system for earthquakes analysis

and shake maps production (REMAKE project –Seismic Risk in Ecuador : Mitigation, Anticipation and Knowledge of Earthquakes– a French-Ecuadorian proposal submitted to the Agence Nationale de la Recherche, ANR; France, in April 2015). The aim will be to automatically obtain, within minutes, moment magnitudes, focal mechanisms, and first estimates of rupture properties such as rupture length and directivity. The results can be used (1) to obtain a rapid assessment about the size and characteristics of the event, providing information required for earthquake response and damage scenarios, and (2) to build a database of earthquake source parameters needed for the seismotectonic analysis (Charvis et al., 2015).

In the medium-long term perspective, we should aim at testing the existing GMPEs on the local data and latter at developing local equations, once enough strong motion data are collected through the SENASV instrumentation. A campaign for recording seismic noise is underway for more than 100 installed instruments to get a first estimation of the amplification at the instrumented sites. Every effort should be made to characterize each site so that both the instrumental data and the site metadata are valid under international standards and can be used for GMP purposes.

There are some distinctive characteristics in the Ecuadorian Andes' geologic and tectonic settings, especially in the Interandean Depression, that make this region of great research interest for understanding strong ground motions under special conditions. As described in Section 1.1 of Chapter 4, both the active volcanic arc and the Interandean Depression are closely related to the NAB –CCPP– boundary and to the Western Cordillera faults. Therefore large earthquakes and strong ground motions should be expected in the Interandean Depression, home for over one third of the Ecuadorian population. More research in the fields of source mechanisms in a warmer crust, near field attenuation related to shallow magma chambers, and site conditions of young and thick volcanic soil would be useful for characterizing the Ecuadorian Sierra GMPEs and other volcanic zones where similar attenuation relationships may be valid. A special effort will have to be done in understanding the Quito thrust

fault system. A better knowledge of the hanging-wall effect physics, basin and soil response would be crucial for the specific case of Quito, as was suggested in Chapter 5.

The REMAKE proposal is also aiming at performing a detailed evaluation of both hazard and vulnerability in Quito, based on earthquakes scenarios. The proposition includes the study of the seismic response of the Quito basin using broadband noise correlation obtained in stations located within the basin and inter-stations Green functions, as well as ground motion simulations by means of numerical and empirical methods. In this way the seismic response variability expected in the basin will be taken into account. The ground motion simulations will be converted into seismic intensities according to Shake-Map™ procedures and will be used as an input for seismic damage scenarios, through city-wide or building-specific approaches. The business quarter in northern Quito will deserve especial attention due to its location on lacustrine sediments and for socio-economical risk considerations.

Regardless of the realization or not of the aforementioned proposal, for a city like Quito it is of extreme importance for a better quantification of the hazard including uncertainties— to keep on building up scientific knowledge about its fault, and the physical constraints and effects of future earthquakes. Therefore this must be a long term objective for the IGEPN and more groups in or outside the country that would be willing to study this unique environment. The capacity to estimate the physical damage to human-built structures under predefined seismic scenarios is also of utmost importance since society is provided with a tool to visualize several dimensions of the potential earthquake impacts and to make decisions to revert vulnerability conditions. Earthquake damage scenarios are, at the same time, powerful communication tools for risk reduction by raising earthquake risk awareness. It should be one more of the IGEPN objectives to promote these type of tools and to convene the engineering community around the hazard for them to produce adequate damage assessments, including uncertainties.

Increased hazard and physical vulnerability knowledge does not necessarily lead to risk reduction. This important wealth of information should not remain only in the scientific literature or revolve around international scientific colloquia, but should have an impact in the day-to-day life of citizens and society. A participatory approach has been outlined for the citizens themselves to start building up knowledge about the various dimensions of the earthquake risk in Quito that has significance for their own security (the present) and for their growth and development (the future). This collective construction could take the form of an observatory for seismic risk awareness and reduction the –“*Quito Earthquake and Urban Risk Observatory*”– as was presented in Section 6.3.2. and should be implemented immediately. The combination of scientific, community and local expertise, integrated into national and regional disaster reduction policies might result in an effective approach to good disaster risk reduction management practices and results.

We as scientists should become more aware of our role in disaster risk reduction and start thinking about treating hazard and risk communication, planning and education with comparable importance as gathering ‘baseline data’ (Barclay et al. 2008). Our compromise as liaisons between science and society must go much further than the production of reports and maps delivered to appropriate government institutions. It should include our meaningful participation at all levels, where the participatory construction of earthquake risk knowledge within the community is lead by our understanding of the physical phenomenon and the physical vulnerability of man-made structures and our positive presence working with the community, and not only unilaterally for the community, building this way the new paradigm.

### 7.3 References

- Alvarado, A., 2012. *Néotectonique et cinématique de la déformation continentale en Équateur*, Grenoble: Université de Grenoble.
- Barclay, J. et al., 2008. Framing volcanic risk communication within disaster risk reduction: finding ways for the social and physical sciences to work together. *Geological Society, London, Special Publications*, 305(1), pp.163–177.

- Baize, S., L. Audin, T. Winter, A. Alvarado, L. Pilatasig Moreno, M. Taipei, P. Reyes, P. Kauffman, and H. Yepes, 2014, Paleoseismology and tectonic geomorphology of the Pallatanga fault (Central Ecuador), a major structure of the South-American crust, *Geomorphology*, 1–15, doi:10.1016/j.geomorph.2014.02.030.
- Beauval, C. et al., 2014. Probabilistic Seismic-Hazard Assessment in Quito, Estimates and Uncertainties. *Seismological Research Letters*, 85(6), pp.1316–1327.
- Charvis, P., et al. 2015. REMAKE –Seismic Risk in Ecuador : Mitigation, Anticipation and Knowledge of Earthquakes. Research proposal presented to ANR, pp.1–30.
- Elenas, A. & Meskouris, K., 2001. Correlation study between seismic acceleration parameters and damage indices of structures. *Engineering Structures*, 23(6), pp.698–704.
- EPN et al., 1994. *The Quito, Ecuador, Earthquake Risk Management Project*, San Francisco: GeoHazards International.
- EPN-GHI, 1995. Invirtiendo en el Futuro de Quito, Proyecto de seguridad sísmica para las construcciones escolares de Quito, Ecuador. GeoHazards International, pp.1–22.
- Mariniere, J., 2014. Estimation de l'aléa sismique probabiliste dans la Cordillère équatorienne, le cas de la ville de Riobamba. *Stage Master 2, Université de Strasbourg - ISTerre*, pp.1–33.
- MIDUVI-CCQ, 2011. Norma Ecuatoriana de la Construcción NEC-11 Capítulo 2: Peligro sísmico y requisitos de diseño sismo resistente. *Cámara de la Construcción de Quito*, pp.1–78. Available at: <http://www.normaconstruccion.ec/>.
- NEC, 2015. CARGAS SÍSMICAS - DISEÑO SISMO RESISTENTE. *Ministerio de Desarrollo Urbano y Vivienda*, pp.1–139.
- Senior Seismic Hazard Analysis Committee, 1997. Recommendations for probabilistic seismic hazard analysis: guidance on uncertainty and use of experts. *Lawrence Livermore National Laboratory*.
- Vallée, M. et al., 2013. Intense interface seismicity triggered by a shallow slow slip event in the Central Ecuador subduction zone. *Journal of Geophysical Research: Solid Earth*, 17 p.



## Locations and magnitudes of historical earthquakes in the Sierra of Ecuador (1587–1996)

Céline Beauval,<sup>1</sup> Hugo Yepes,<sup>2</sup> William H. Bakun,<sup>3</sup> José Egred,<sup>2</sup> Alexandra Alvarado<sup>2</sup> and Juan-Carlos Singaicho<sup>2</sup>

<sup>1</sup>LGIT, IRD-UJF-CNRS, BP 53, 38041 Grenoble Cedex 9, France. E-mail: celine.beauval@obs.ujf-grenoble.fr

<sup>2</sup>Instituto Geofísico, Escuela Politécnica Nacional, Ladrón de Guevara E11-253, Apartado 2759 – Quito, Ecuador

<sup>3</sup>USGS, Menlo Park, CA, USA

Accepted 2010 February 16. Received 2010 February 16; in original form 2009 September 4

### SUMMARY

The whole territory of Ecuador is exposed to seismic hazard. Great earthquakes can occur in the subduction zone (e.g. Esmeraldas, 1906,  $M_w$  8.8), whereas lower magnitude but shallower and potentially more destructive earthquakes can occur in the highlands. This study focuses on the historical crustal earthquakes of the Andean Cordillera. Several large cities are located in the Interandean Valley, among them Quito, the capital (~2.5 millions inhabitants). A total population of ~6 millions inhabitants currently live in the highlands, raising the seismic risk. At present, precise instrumental data for the Ecuadorian territory is not available for periods earlier than 1990 (beginning date of the revised instrumental Ecuadorian seismic catalogue); therefore historical data are of utmost importance for assessing seismic hazard. In this study, the Bakun & Wentworth method is applied in order to determine magnitudes, locations, and associated uncertainties for historical earthquakes of the Sierra over the period 1587–1976. An intensity-magnitude equation is derived from the four most reliable instrumental earthquakes ( $M_w$  between 5.3 and 7.1). Intensity data available per historical earthquake vary between 10 (Quito, 1587, Intensity  $\geq$ VI) and 117 (Riobamba, 1797, Intensity  $\geq$ III). The bootstrap resampling technique is coupled to the B&W method for deriving geographical confidence contours for the intensity centre depending on the data set of each earthquake, as well as confidence intervals for the magnitude. The extension of the area delineating the intensity centre location at the 67 per cent confidence level ( $\pm 1\sigma$ ) depends on the amount of intensity data, on their internal coherence, on the number of intensity degrees available, and on their spatial distribution. Special attention is dedicated to the few earthquakes described by intensities reaching IX, X and XI degrees. Twenty-five events are studied, and nineteen new epicentral locations are obtained, yielding equivalent moment magnitudes between 5.0 and 7.6. Large earthquakes seem to be related to strike slip faults between the North Andean Block and stable South America to the east, while moderate earthquakes ( $M_w \leq 6$ ) seem to be associated with thrust faults located on the western internal slopes of the Interandean Valley.

**Key words:** Seismicity and tectonics; Seismic attenuation; South America.

### INTRODUCTION

In any region, the essential elements for estimating seismic hazard are seismic catalogues, localization and characterization of active faults (or definition of seismic source zones), and ground-motion prediction models adapted to the region under study (Esteve 1968; Beauval & Scotti 2003, 2004; McGuire 2008). The present work deals with the first element, the seismic catalogue, which is the basis for characterizing potential seismic source zones, especially in a country where a lot of work is still to be done for identifying potential active faults. The Ecuadorian seismic network

(RENSIG), maintained by the Geophysical Institute in Quito (IG, part of the Escuela Politécnica Nacional, EPN), provides instrumental locations and magnitudes for the period 1990–present. For earlier periods, international catalogues can provide instrumental solutions for earthquakes with significant magnitude (EHB Centennial catalogue, Engdahl & Villaseñor (2002); USGS/NEIC PDE catalogue (2009) or CMT/HRV catalogue (2009)). However, as will be shown, very few moderate magnitudes have an instrumental characterization. They correspond to shallow but damaging events that occurred before 1976, originating on faults cutting the two Andean ranges in Central Ecuador. Nonetheless, much work has been done over the

last 40 yr to gather information on Ecuadorian past events and assign MSK intensity to the available observations (CERESIS 1985; Egred 2009a,b). This intensity catalogue covers the last 470 yr with the earliest events reported dating back to the XVIth century, a few years after the arrival of the Spaniards in Ecuador. Earthquakes are reported if the maximum intensity reached at least the degree V. Based on the intensity distribution in space, isoseismal maps have been drawn for the most significant earthquakes (e.g. Egred 2004), and epicentral locations have been determined based on these isoseismal maps. However, little work has been devoted to magnitude estimation. Until now, magnitude estimates were based solely on maximum intensity and the magnitude-intensity equation of Gutenberg & Richter (1956). Several methods have been proposed in the literature for determining locations and magnitudes of earthquakes, for example, methods by Gasperini *et al.* (1999), Musson & Jimenez (2008), Bakun & Wentworth (1997, henceforth B&W and further publications by Bakun). For this study, the B&W method is chosen. It makes use of individual intensity observations and uncertainties are quantified in an objective and reproducible way. This method has been applied in many different tectonic contexts using different data sets, and has proved its efficiency as well as its difficulties and limits (e.g. Germany: Hinzen & Oemisch 2001; Turkey: Parsons 2004; Japan: Bakun 2005; France: Bakun & Scotti 2006; Venezuela: Choy *et al.* 2010). After establishing the intensity attenuation model and checking the method on the calibration events, magnitude and locations are determined for nineteen historical events located in the Ecuadorian Andes.

## REGIONAL SETTINGS AND DATA

The Andes, the major physiographic feature of Western South America, is the result of the subduction of the Pacific oceanic lithosphere beneath the South American plate (e.g. Nieto 1991; Espinosa *et al.* 1991a). In Ecuador, three N–S trending geological and geomorphic zones can be distinguished (Fig. 1): (1) the coastal plain to the west (Costa), (2) the central Andean mountainous area and (3) the eastern lowlands (Oriente) which are part of the upper Amazon basin. This study focuses on the Andean range (also known as ‘Sierra’), 150 km wide on average, which includes three geological and geomorphic zones: the Western Cordillera, the Interandean Valley, and the Eastern Cordillera (Cordillera Real). The high Interandean Valley (2200–3000 m in elevation) is a geomorphic depression not wider than 30 km that is very well developed between the two cordilleras, and filled with Quaternary volcanoclastic and pyroclastic deposits north of latitude 1.7° S. South of 1.7° S, spacious intramountainous basins show sedimentary fillings lacking the fresh volcanic deposits of the Interandean Valley due to the absence of Quaternary volcanic activity. Almost half of the Ecuadorian population resides in the Sierra.

The B&W (1997) method requires an intensity attenuation model, which is best obtained from calibration events with both a reliable instrumental and a macroseismic determination. Analysing the intensity catalogue (Egred 2009a,b) with respect to the instrumental EPN catalogue, few events appear to meet this criteria in the Sierra. Three instrumental events described by a large set of intensities will be used (Table 1): Pujili (1996,  $M_w$  5.9), Pomasqui (1990,  $M_w$  5.3) and Salado-Reventador (1987,  $M_w$  7.1). A fourth event with magnitude and location available in the EHB Centennial catalogue is included in the calibration: the Pastocalle event (1976,  $M_b$  5.7). Unfortunately, there is no moment magnitude available for this earthquake. A few other Sierra events were analysed for

calibration purposes (Santa Rosa,  $M_w$  5.1, 2000 October 8; Vacas Galindo,  $M_b$  5.3, 1994 May 11), but their intensity distributions relative to epicentral distances display curious trends, probably due to incompleteness of observations in space for lower intensities (III and IV). Furthermore, the Tena earthquake (1987,  $M_w$  6.4) has an EHB solution close to the ISC solution; however the intensity distribution versus epicentral distance relation is counter-intuitive, for highest intensity degrees the median distances are increasing with increasing intensity degrees (from intensity V–VII). This may be due to a strong site effect in the Interandean Valley southwest of the epicentre, or to a directivity effect of the seismic waves related to the fault mechanism. We decided to discard these events and to establish the intensity-magnitude equation on few, but reliable, events. Ideally, the intensity-magnitude equation should be established with a first set of earthquakes, and then the B&W method should be applied on another reliable and independent set of instrumental earthquakes (e.g. Bakun & Hopper 2004). Obviously such a validation of the equation is not possible here. Nevertheless, three events with an EHB determination (Engdahl *et al.* 1998; Engdahl & Villaseñor 2002) can be partially used as test events (Table 1): Pelileo (1949), Due-Reventador (1955) and Pepinales (1961). The method is then applied to all earthquakes reported in the intensity catalogue (Egred 2009b) with a minimum of 10 intensity observations. The study covers an area approximately 300-km-long and 80-km-wide, the two mountain ranges of the Ecuadorian Andes and the Interandean Valley.

## METHODOLOGY

### Establishing the attenuation model from calibrating events

Intensity, like seismic energy, attenuates with increasing distance from the epicentre. The calibrating earthquakes provide a set of intensity degree/median distance couples that are used to linearly solve the following system (e.g. Bakun 2006)

$$I = a + bM_w + c\text{Log}\sqrt{(R^2 + h^2)} + d\sqrt{(R^2 + h^2)}, \quad (1)$$

where  $M_w$  is the moment magnitude,  $R$  the epicentral distance,  $h$  a generic depth and  $a$ ,  $b$ ,  $c$ ,  $d$ , the coefficients to be determined. Each earthquake provides a set of intensity degrees and associated median hypocentral distances (Fig. 2; Table 2). Not all low intensity levels (III, IV) are included; those shown to be incomplete in space are discarded. As the coefficient  $d$  we obtained is close to zero and has an associated uncertainty larger than its value, the linear dependence of intensity with hypocentral distance is abandoned and the system is solved for three parameters only ( $a$ ,  $b$ ,  $c$ ). The final attenuation model takes into account moment magnitude and geometrical spreading:

$$I = -(0.85 \pm 0.76) + (2.41 \pm 0.14) M_w - (5.39 \pm 0.35) \log \Delta_h, \quad (2)$$

where  $I$  is the intensity,  $\Delta_h$  is the slant distance. The depth of the instrumental events bears rather large uncertainties, therefore a fixed 10-km depth is used here for all crustal events. Uncertainty on the coefficient  $a$  is quite large, as found by other authors (e.g. Bakun 2005); there is also a trade-off between coefficients  $a$  and  $b$ . The attenuation model is superimposed to the intensity data versus distance (Fig. 2); the model is consistent with the assigned intensity values and median distances. This attenuation model is only valid for crustal earthquakes occurring within the Sierra, and preferably with magnitudes  $M_w$  between 5.3 and 7.1 (range of magnitude of calibration events). This model predicts higher attenuation

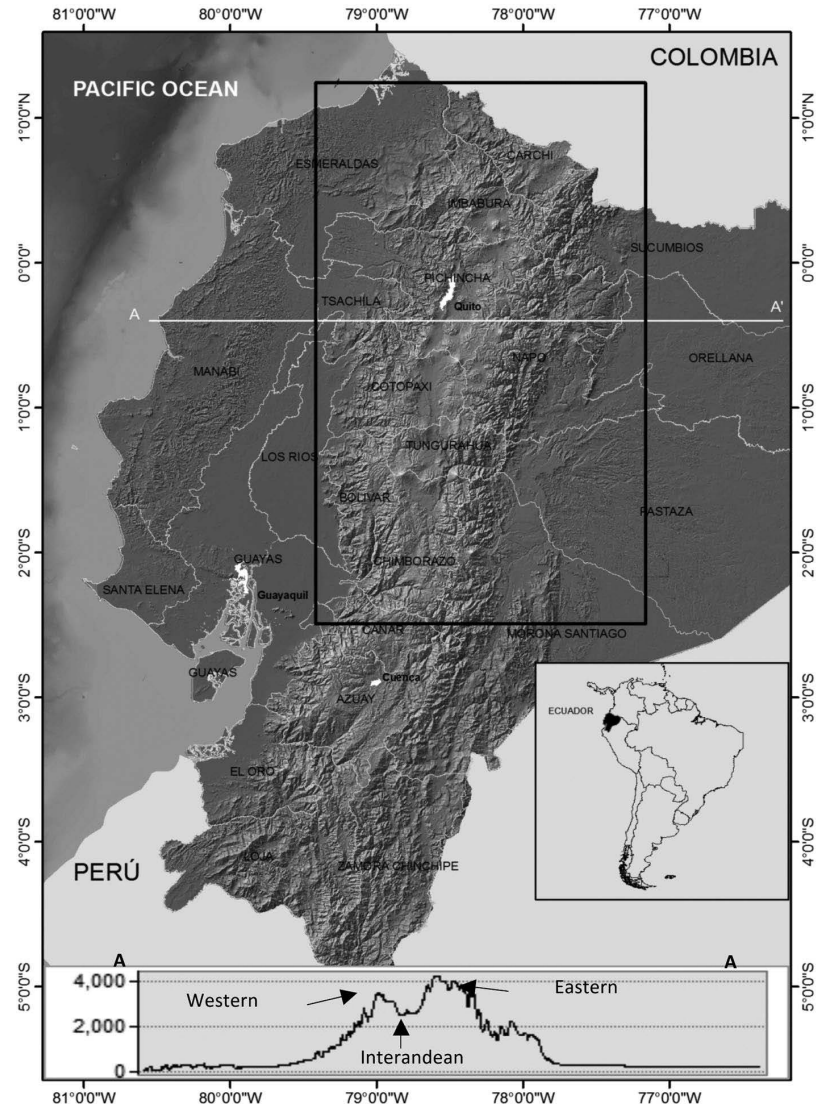


**Figure 1.** Ecuador and the region under study (rectangle). A-A' is a topographic profile showing the Interandean Valley and both bordering mountain ranges: the Western and Eastern Cordilleras. Province names mentioned through the paper are indicated.

**Table 1.** Calibration and test earthquakes.

Event no.	Event name	Year/Month/Day	Instr. Latitud	Instr. Longitud	Source	$M$	Source
1 <sup>a</sup>	Pujili	1996/3/28	-1.044	-78.724	EPN catalogue	5.9 $M_w$	CMT/HRV
2 <sup>a</sup>	Pomasqui	1990/8/11	-0.0392	-78.4274	EPN (EPN 1990)	5.3 $M_w$	CMT/HRV
3 <sup>a</sup>	Salado-Reventador	1987/3/6	-0.087	-77.814	EPN (Gajardo <i>et al.</i> 2001)	7.1 $M_w$	CMT/HRV
4 <sup>a</sup>	Pastocalle	1976/10/6	-0.727	-78.734	EHB	5.7 $M_b$	ISC
5	Due-Reventador	1955/5/11	-0.200	-77.800	EHB	6.8	UK
6	Pepinales	1961/4/8	-2.0890	-78.9680	EHB	-	-
7	Pelileo	1949/8/5	-1.23	-78.405	Woodward-Clyde 1981	6.8 $M_s$	UK GR (EHB)

Notes: EPN, determination by the Escuela Politecnica Nacional, Instituto Geofisico, Quito.

EHB: relocated by Engdahl & Villasenor (2002) using the method Engdahl *et al.* (1998).

<sup>a</sup>Calibration event; otherwise test event.

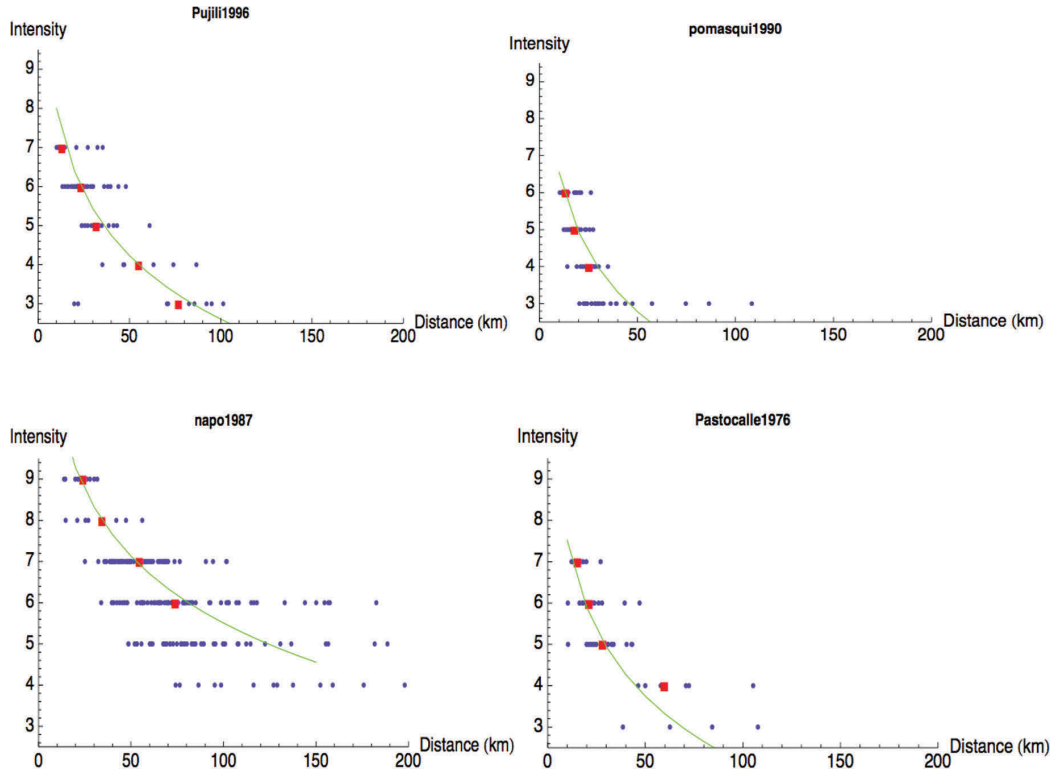


**Figure 2.** Intensity data for the calibrating events (Table 1). Blue dots: intensity observations. Red squares: median distances (see Table 2). Green curve: attenuation model (eq. 2). Distance is hypocentral, with a generic depth fixed to 10 km.

**Table 2.** Intensity data for calibration and test events: median hypocentral distances used in calibration.

Event no.	III	IV	V	VI	VII	VIII	IX	X	No. of MSKI $\geq$ III
1	76.9	55.1	31.8	23.5	13.1	–	–	–	87
2	–	25.3	17.9	13.4	–	–	–	–	66
3	–	–	–	73.8	54.5	34.3	24.1	–	228
4	–	59.8	28.1	21.2	15.3	–	–	–	72
5	Test event (magnitude determination only)								22
6	Test event (location determination only)								31
7	Test event								82

*Note:* Median distances are used only when there is no doubt on the spatial completeness of the intensity degree (and with a minimum of 7 intensity assignments).

with distance than models established in stable continental regions (e.g. Atkinson & Wald 2007), which is expected in a region that is geologically younger and dotted with volcanoes (e.g. Azzaro *et al.* 2006). Interestingly, Egred (2004) noted that for several large earthquakes, isoseismals are elongated in the north–south direction, which could indicate a lower attenuation of seismic waves along the axis of the Interandean Valley than in the east–west direction perpendicular to the mountain chains. Unfortunately, it is not possible to take into account differences in attenuation according to azimuth due to the few available calibrating events. Furthermore, note that directivity and extended sources are not represented in this simple point-source model. If using eq. (2) in the future for predicting intensities produced by a given magnitude earthquake in the Sierra, one cannot expect to correctly predict intensities at very close distance to the epicentre for earthquakes of magnitude higher than  $\sim 6.5$ .

Applying the intensity-magnitude equation for large earthquakes will require imposing saturation of the intensity at a given distance from the epicentre (e.g. at a distance equivalent to half of the fault length, applying Wells & Coppersmith 1994, magnitude-fault length equations).

#### Determination of magnitude and location from intensities

Following the B&W methodology, a grid is defined over the felt region including all intensity observations describing the studied event, with a grid step of 2.5–5 km depending on the desired precision. Each grid node is a potential location for the source. At each node, the intensity magnitude  $M_I$  and the associated root mean square  $\text{rms}[M_I]$  are calculated. The intensity magnitude  $M_I$  is

calibrated to equal moment magnitude  $M_w$ . Intensity magnitude is simply the mean value of all magnitude values inferred from the individual intensity assignments

$$M_I = \frac{1}{n} \sum_{i=1}^n M_i, \quad (3)$$

where  $M_i = [I_i + 0.85 + 5.39 \log \Delta_i] / 2.41$ ,  $I_i$  is the MSK intensity value at site  $i$ ,  $\Delta_i$  is the slant distance (in km) of observation  $i$  from the assumed gridpoint, and  $n$  the number of intensity assignments. Iso-contours of magnitude estimates can then be plotted.

The rms quantifies the error between observed and estimated intensities

$$\text{rms}[M_I] = \text{rms}[M_I - M_i] - \text{rms}_0[M_I - M_i], \quad (4)$$

with  $\text{rms}[M_I - M_i] = \{\sum [W_i^*(M_i - M_I)]^2 / \sum W_i^2\}^{1/2}$  and  $\text{rms}_0[M_I - M_i]$  the minimum  $\text{rms}[M_I - M_i]$  over the grid of assumed trial source locations, and  $W_i$  the following weighting function (B&W 1997)

$$W_i = 0.1 + \cos[(\Delta_i / 150) * \pi / 2], \quad \text{for } \Delta_i \leq 150 \text{ km}, \quad (5)$$

$$0.1, \quad \text{for } \Delta_i > 150 \text{ km}.$$

Observations located close to the assumed epicentre are therefore given a higher weight than observations at large distances. However, note that in general tests on Ecuadorian earthquakes showed that results are similar with or without using the weighting function (very few exceptions, as discussed later in the paper). The node corresponding to the minimum  $\text{rms}[M_I]$  is the intensity centre (IC); it is the point source where the error between observed and estimated intensities is lowest. The magnitudes at trial source locations within the confidence-level contour of interest (67 per cent) constitute the uncertainty distribution for the intensity magnitude of the earthquake (Bakun 1999). The intensity centre corresponds to the location on the fault plane where the energy release is highest (i.e. to the location of maximum fault displacement, or moment centroid); therefore the intensity centre does not always match the epicentre (Bakun 2006). Unfortunately, the moment centroid is not available for the calibrating events. In any case, if some candidate causative fault is located within the confidence contours, the earthquake epicentre might be preferably localized on the fault. This 'preferred' location might be different from the location of the intensity centre corresponding to the minimum rms.

Few historical earthquakes in the Sierra are described by intensity observations higher than IX (Table 4). Exceptions include the Pelileo earthquake (1949 August 5) with maximum intensities reaching X, and the Riobamba event (1797 February 4) with highest intensities of XI. Intensities higher than VIII in remote times have a high probability of being overestimated. The adobe houses of these periods are destroyed or damaged beyond repair for intensity levels of VII–VIII, thus discrimination between levels VIII, IX, X and XI is really difficult (Ambraseys 2001; Ambraseys & Bilham 2003; Parsons 2004). For these two Sierra events, location and magnitude are calculated taking into account intensities up to level VIII, then up to levels IX, X (and XI for Riobamba), in order to evaluate the influence on the results of highest intensity levels. Note that, unlike most intensity catalogues (e.g. the French catalogue, see Bakun & Scotti 2006), no information on the quality of the individual intensity observations is provided in the Ecuadorian catalogue. However, as will be shown later, testing the application of the method using different data sets extracted from the original data set gives indications of the stability of the results.

Site effects can influence intensity observations (e.g. Pasolini *et al.* 2008), and thus bias magnitude and intensity centre location

estimates. While establishing the attenuation model, the influence of site effects is reduced by calculating median distances after eliminating outliers (observations higher or lower than mean  $\pm 2\sigma$ ). Nonetheless, B&W (1997) proposed a method to take site effects into account through the calculation of site correction factors based on the calibrating events. To calculate such amplification factors, several observations must be available at a given site (B&W 1997). Relying only on four calibrating events prevents us from calculating reliable and meaningful correction factors. In this investigation site effects will not be taken into account. However, as already said, tests will be performed to check the influence of potentially overestimated higher intensity degrees.

### Determining confidence contours applying systematically bootstrap resampling

The intensity centre location corresponds to the node of the grid with highest probability, however other nodes of the grid have non-zero probability of being the intensity centre. Therefore, it is of importance to identify all potential locations together with the associated probability, in other words to define the confidence contours that delineate the areas containing given probability levels that the intensity centre lays within the contours. At first, the tables associating contours of rms values to different levels of confidence depending on the number of intensity assigned values, as published by Bakun & Wentworth (1999), were applied directly (results not shown in the paper). However results for the Sierra events showed that the location uncertainty resulting from a bootstrap resampling (Efron 1982) is always smaller than inferred from the appropriate California contours with similar numbers of intensity observations (as also found in France by Bakun & Scotti 2006). Therefore, the bootstrap statistical technique is coupled to the B&W (1997) method to determine confidence contours adapted to each earthquake (see e.g. Bakun 2006). The complete calculation is performed 1000 times, each time the intensity data set is resampled (random sampling with replacement, keeping the size of the original data set constant), and 1000 intensity centres are obtained together with 1000 intensity magnitude estimates. The results show that the spatial distribution of bootstrapped intensity centres always mimics the rms contours. Therefore, the 50 per cent confidence contour is the rms iso-contour containing 500 of these intensity centres, the 67 per cent contour is the rms iso-contours containing 670 of these intensity centres, and so on. The uncertainty based on bootstrap resampling can be considered as the uncertainty due to the use of only a sample of the population, assuming that the model is perfect. This should not be confused with the true epistemic uncertainty on the epicentre, which is not obtainable by any statistical means.

### Application to the calibration events

The minimum requirement for the validation of the method is to obtain satisfactory results for the calibrating events. Location and magnitude estimates derived from the application of the B&W (1997) method on the four instrumental events are reported in Table 3 and results are displayed in Figs 4 and 5. Note that the calculations were performed with and without the weighting function, and the results were similar. From now on, results are displayed for calculations with weights. The intensity centres and intensity magnitudes obtained are consistent with the instrumental estimations. There is little difference in magnitudes estimated for locations at the hypocentre or at the intensity centre.

**Table 3.** Calibration and test events—results from applying Bakun & Wentworth (1997) analysis.

Event no.	Event name	Year/Month/Day	$M$	Source	$M_I^b$	$M_I^c$	$\Delta^d$ (km)	FL (km)	Width (km)
1 <sup>a</sup>	Pujili	1996/3/28	5.9 $M_w$	CMT/HRV	5.85	5.97	8.4	11	7.5
2 <sup>a</sup>	Pomasqui	1990/8/11	5.3 $M_w$	CMT/HRV	5.28	5.4	7.1	4.9	4.8
3 <sup>a</sup>	Salado-Reventador	1987/3/6	7.1 $M_w$	CMT/HRV	6.96	7.0	4.2	56	18
4 <sup>a</sup>	Pastocalle	1976/10/6	5.7 $M_b$	ISC	5.8	5.89	5.9	8.4	6.5
5	Due-Reventador	1955/5/11	6.8	UK	7	6.9	5.9	37	14.7
6	Pelileo	1949/8/5	6.8 $M_s$	UK GR	6.6	6.3	21	37	14.7
7	Pepinales	1961/4/8	—	—	6.3	6.5	10	18.9	10.1

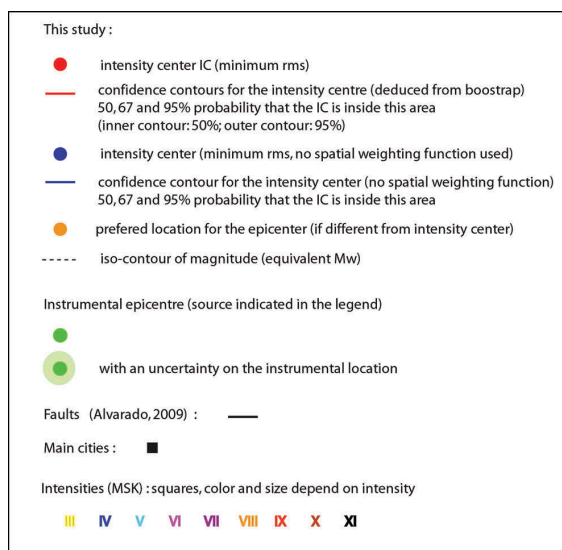
Note: FL is subsurface rupture length, FL and downdip rupture width are estimated from the instrumental magnitude (Wells & Coppersmith 1994, generic equation).

<sup>a</sup>Calibration event; otherwise test event.

<sup>b</sup>Evaluated at the epicentre.

<sup>c</sup>Evaluated at intensity centre.

<sup>d</sup>Distance from the epicentre to the intensity centre.

**Figure 3.** Detailed legend for Fig. 4 and Figs 6 to 15.

#### Pujili (1996, $M_w$ 5.9, Figs 4a and 5a)

This earthquake occurred in Cotopaxi province and affected mostly Pujili county, where the strongest damage was reported (many adobe houses partially collapsed; light damage in brick houses). Intensity observations are numerous, 87 between III and VII, and rather evenly distributed in space. As shown in Fig. 4(a), the intensity centre location is 8 km to the southwest of the instrumental epicentre, consistent with the hypothesis that the earthquake occurred on a N–S fault dipping to the west (La Victoria fault, Lavenu *et al.* 1995). Confidence contours corresponding to 50, 67 and 95 per cent are narrow (5 km  $\times$  5 km for 67 per cent). The intensity magnitude at the instrumental epicentre is 5.85, and 5.97 at the intensity centre (5.9–6.01 at the 67 per cent confidence level). Individual magnitudes inferred from all intensity observations higher than III are plotted versus slant distance. No bias is observed related to intensity degree: the trends corresponding to the different intensity degrees overlap as expected (see e.g. Bakun & Scotti 2006). A moving average mean for the intensity magnitude is calculated (every 10 km). Its value is more or less stable with distance (which means no bias, Fig. 5a).

#### Pomasqui (1990, $M_w$ 5.3, Figs 4b and 5b)

The earthquake occurred on one of the two northern segments that are part of the Quito thrust fault system (north–south trend), the San Juan de Calderon and Catequilla segments (Alvarado 2009). The intensity data set is made of 66 observations between IV and VI, distributed in a north–south direction following the main road. The intensity centre is located 7 km to the north of the epicentre, at the end of the Catequilla fault segment. The confidence contour 67 per cent covers an area of approximately 10 km  $\times$  5 km. The confidence contour at 95 per cent is elongated in the NW–SE direction, as there is no intensity data in this direction. Magnitude at the epicentre is 5.28 and 5.4 at the intensity centre (5.3–5.6 at the 67 per cent confidence level). The moving mean average for the intensity magnitude is stable over distance (no bias with distance, Fig. 5b).

#### Salado-Reventador (1987, $M_w$ 7.1, Figs 4c and 5c)

The earthquake occurred on the border between Napo and Sucumbios provinces, where highest damages were reported in buildings and natural settings. Other provinces were also heavily affected (Imbabura, Pichincha and east Carchi). The catastrophic debris flow triggered by this earthquake caused an estimated death toll of more than one thousand people and severe destruction of the Trans-Ecuador oil pipeline. The estimated economic loss reached about one billion U.S. dollars (Kawakatsu & Proaño 1991). An extensive intensity collection survey was led (228  $\geq$  III, Espinosa *et al.* 1991b; Egred 2009b). Intensity observations of IV are reported for distances up to 200 km. As shown in Fig. 4(c), the instrumental epicentre location is right on the potential causative thrust fault (Salado, see Soulas *et al.* 2001), with a probable extension on a fault segment to the north (Reventador segment, Soulas *et al.* 2001). The intensity centre is located 4 km away from the instrumental epicentre, which is located in between confidence contours 50 and 67 per cent. The 67 per cent confidence contour delineates an area of approximately 6 km  $\times$  6 km. Equivalent moment magnitude is 7.0 at the intensity centre, and 6.96 at the instrumental epicentre (Table 3). The moving average mean for the intensity magnitude is very stable over distance (Fig. 5c).

#### Pastocalle (1976, $M_b$ 5.7, Figs 4d and 5d)

This earthquake caused heavy damage in rural villages of Cotopaxi province (mainly adobe houses). The location of the causative fault

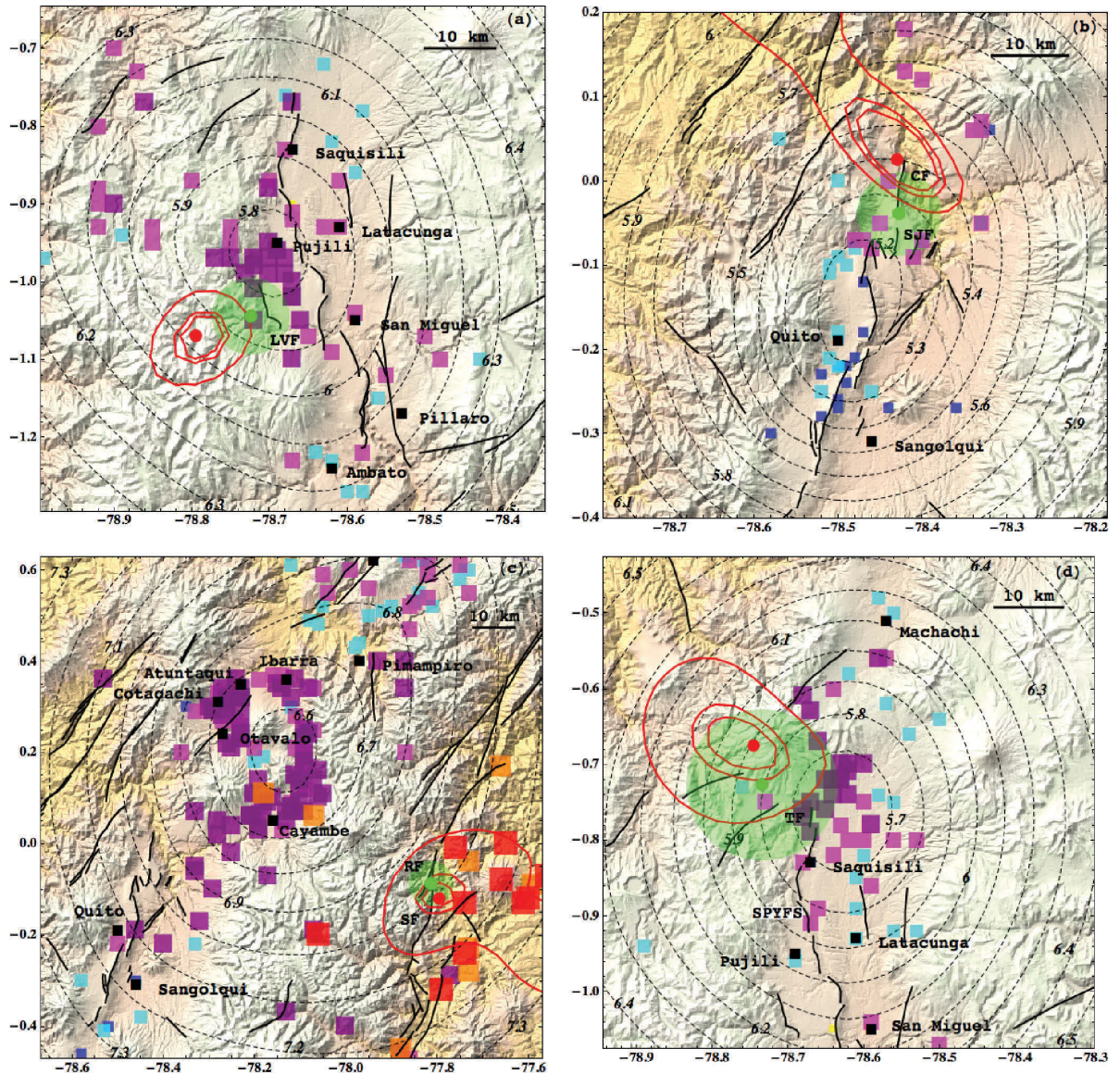


**Figure 4.** Determination of magnitude and location for calibrating events (Table 3): (a) Pujili ( $M_w$  5.9, 1996); (b) Pomasqui ( $M_w$  5.3, 1990); (c) Napo ( $M_w$  7.1, 1987); (d) Pastocalle ( $M_b$  5.7, 1976). LVF, CF, SJF, RF, SF, MF and TF are faults (Table 6). See legend in Fig. 3. Topography: SRTM data from <http://srtm.csi.cgiar.org/>

is not obvious. The instrumental epicentre and the intensity centre are  $\sim 6$  km apart. The instrumental location is located on the 67 per cent confidence contour. Taking into account the 95 per cent confidence area and up to a  $\sim 10$  km uncertainty on the instrumental epicentre, a location along a northwestern branch of the inverse Saquisili-Poalo-Yambo fault system (Toacazo segment: Alvarado 2009) is conceivable. The mean average magnitude is very stable with distance (Fig. 5d). The equivalent moment magnitude obtained (5.89 at intensity centre, 5.8 at epicentre) is slightly higher than the instrumental magnitude, which is possible if the  $M_b$  5.7 magnitude was slightly saturated.

#### Application on three instrumental events

Three events can be partially used as test events, that is, earthquakes that have instrumental determination and that do not take part in the calibration. These events are the Pelileo (1949, G-R  $M_s$  6.8), Due-Reventador (1955, UK  $M$  6.8) and Pepinales (1961) earthquakes. These events can be used only partially as test events, because the magnitudes are not moment magnitudes (no magnitude estimate for Pepinales) and instrumental locations bear uncertainties much higher than the calibrating events localized by the EPN. However, it is worth testing the application

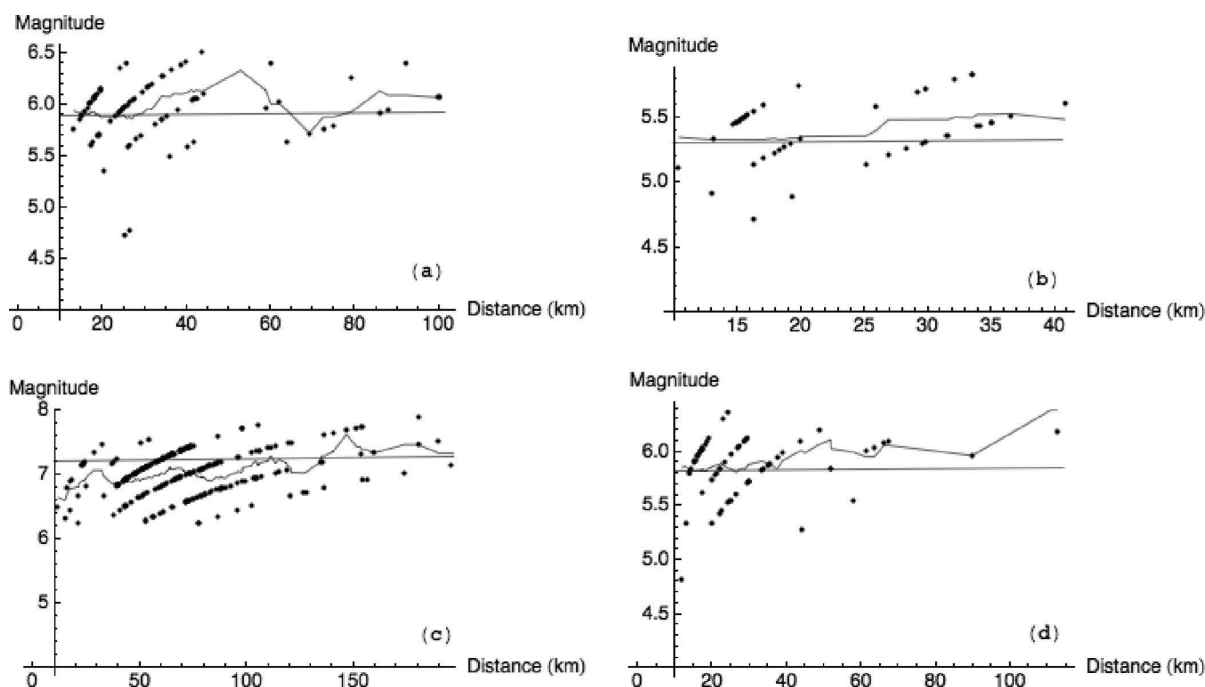


**Figure 5.** Calibrating events: magnitudes calculated from all intensity observations using eq. (1), versus hypocentral distances calculate based on the intensity centre. (a) Pujili; (b) Pomasqui; (c) Salado-Reventador; (d) Pastocalle. Curve: moving average over 10 km width distance intervals. Horizontal line: instrumental magnitude  $M_w$  (except for Pastocalle event,  $M_b$ ).

of the method on these events, which have partial instrumental determinations.

#### *Pelileo (1949, $M$ 6.8, Fig. 6)*

This earthquake was highly destructive in the Tungurahua and Cotopaxi provinces, and partially destructive in the Chimborazo and Bolívar provinces. In the epicentral zone, the Pelileo and Patate villages were destroyed, whereas most houses in Guano and Ambato collapsed (Ramirez 1951). Approximately 6000 deaths were reported. Intensities as high as X were assigned but these intensities are potentially overestimated and must be considered with caution. In Pelileo and its surroundings, the soil is apparently prone to site effects (Woodward-Clyde 1981), and furthermore, large landslides increased damages and casualties. Note that there is an EHB solution for this event (coordinates  $(-1.5; -78.25)$ ; Engdahl & Villaseñor 2002), but it is located more than 40 km to the southeast from the highest intensities and cannot be considered reliable. At first, calculations are performed based on intensity observations up to IX (Fig. 6a). The intensity centre is located close to the epicentre determined from isoseismals (Egred 2009b) and is well constrained (area of the 67 per cent contour:  $10 \text{ km} \times 8 \text{ km}$ ). Nonetheless, the instrumental location that is currently considered the most reliable (Woodward-Clyde 1981) is located 20 km to the northeast, within the 95 per cent confidence contour. The equivalent moment magnitude is 6.3 at the intensity centre, and close to 6.6 at the instrumental epicentre. Taking into account a probable 0.2 unit uncertainty on the G-R magnitude estimate (Bakun 1999), these results can still be considered consistent with a G-R 6.8 magnitude. The fault should extend a minimum of 20 km ( $M6.3$ , Wells & Coppersmith 1994).

According to the report by Woodward-Clyde (1981), the causative fault might be a SW-NE fault segment north of the instrumental epicentre (Pucara segment, Alvarado 2009). Considering both the instrumental and the intensity centre locations, the earthquake might have occurred on a SW-NE fault system made of the north-eastern prolongation of the Pallatanga fault system (which is very well identified to the southwest) joined with the Mundug and the Pucara faults. The intensity centre would then be located very close to the causative fault plane.

Several sensitivity tests were performed. Previous results are based on intensities up to degree IX. When intensities X, assigned at Pelileo and at locations within a 5 km radius from this town are included, calculations yield an identical epicentral location but the confidence contours enclose narrower areas (Fig. 6b). Woodward-Clyde *et al.* (1981) justified the high intensity reported at Pelileo arguing the existence of site effects. To eliminate the influence of potentially overestimated IX intensity assignments, the calculations were performed taking into account intensities up to VIII (Fig. 6c, see Supporting Information). The 67 and 95 per cent areas are extended, but the intensity centre remains identical and the associated magnitude is slightly lower (6.5 instead of 6.6 at the instrumental epicentre). Furthermore, as Singaicho (2009) provides a revision of intensity assignments for this earthquake, the calculations were performed based on the revisited 58 intensities (III to X) instead of the 82 original observations. Intensity observations are reduced because it was not possible to have access to all original documents; however the intensity centre location is still unchanged. Only future work, based on other kind of data (waveforms, neotectonics) will enable confirmation of the SW-NE orientation of the causative fault. However, in the zone of highest destruction (Patate and Pelileo villages) where the intensity centre is located, landslides triggered by

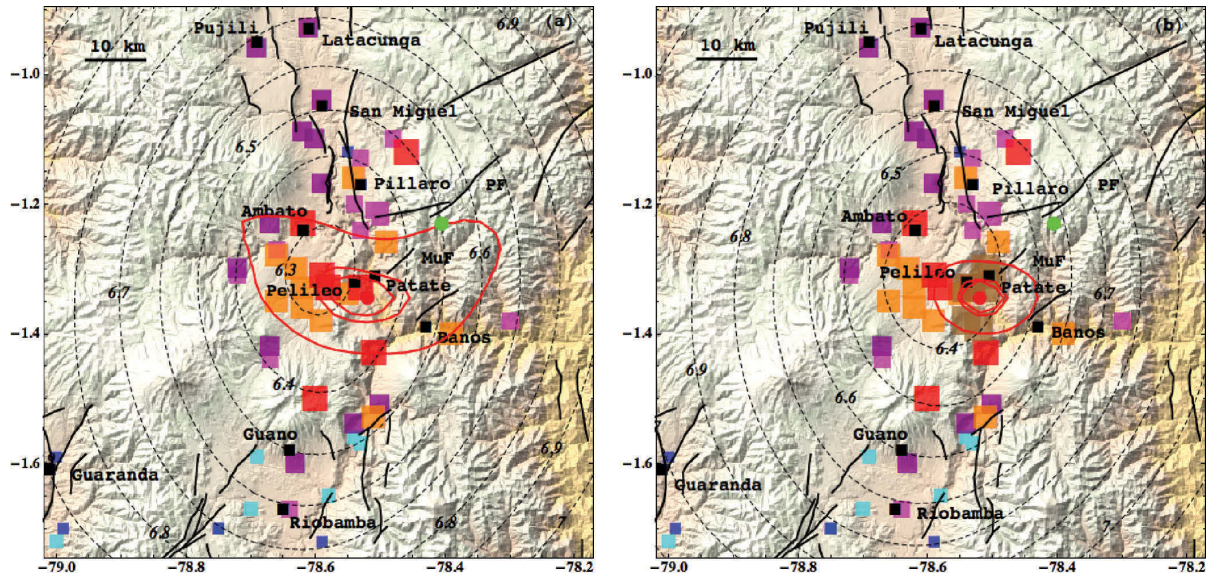


Figure 6. Determination of magnitude and location for Pelileo historical event (1949,  $M_{G-R}$  6.8): (a) using intensities up to IX; (b) including intensities X. Instrumental location from Woodward-Clyde (1981). The uncertainty on the instrumental location is not known. PF and MuF are Pucara and Mundug faults (Table 6). See legend in Fig. 3.

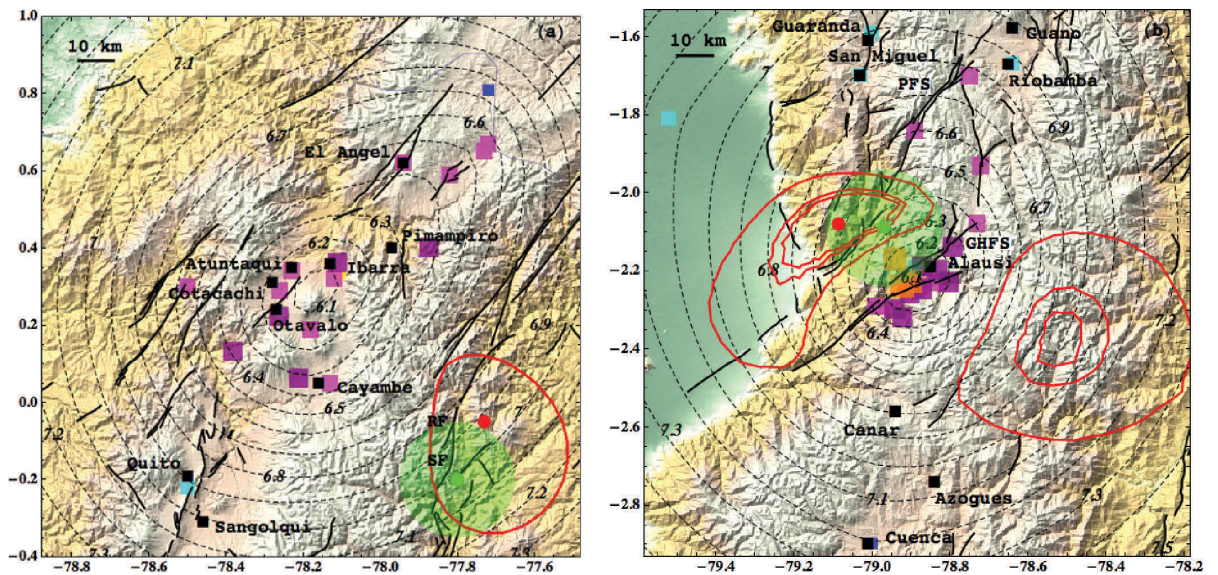


Figure 7. Determination of magnitude and location for (a) Due-Reventador (1955,  $M_{UK-PAS}$  6.8, EHB) and (b) Pepinales (1961, EHB, no instrumental magnitude). No reliable confidence contour can be obtained for Due-Reventador (red contour is 10 per cent). RF, SF, PFS and GHFS are faults (Table 6). See legend in Fig. 3. Results are reported in Table 5.

the earthquake covered a large area, making it difficult to presently identify evidence of surface rupture.

*Due-Reventador (1955, UK PAS magnitude 6.8, Fig. 7a)*

The intensity distribution does not enable us to localize the intensity centre with confidence, probably because the epicentre is far from

the observation ‘network’ (35–40 km). Therefore, only the intensity magnitude will be compared to the magnitude at the EHB instrumental location (Engdahl & Villaseñor 2002). Note that although the intensity centre is not well constrained, it is located close to the instrumental epicentre. Equivalent magnitude at the epicentre is 7.0, which is compatible with a UK magnitude 6.8 that might bear a 0.2 uncertainty. Taking into account a possible 15 km uncertainty on the instrumental epicentre, the equivalent moment magnitude

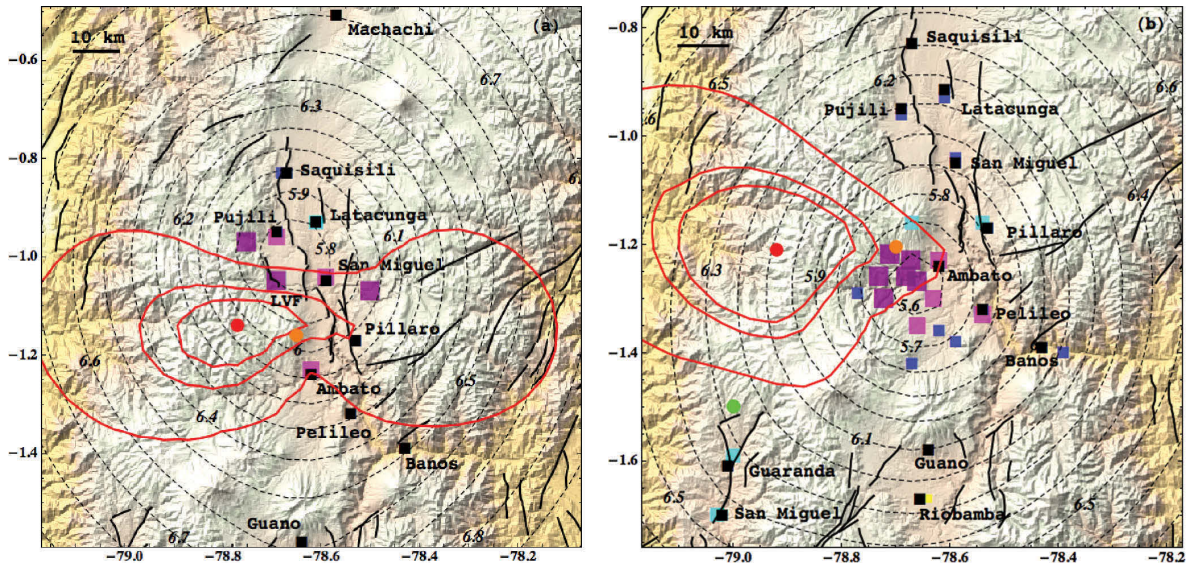


**Figure 8.** Determination of magnitude and location for historical events. (a) Cusubamba (1962). (b) Pasa (1960), instrumental epicentre from CGS (certainly bearing at least 30 km uncertainty). LVF is La Victoria fault (Table 6). See legend in Fig. 3. Results are reported in Table 5.

predicted by the intensity data set at these locations ranges from 6.8 to 7.2.

#### *Pepinales (1961, Fig. 7b)*

This earthquake was felt throughout the whole country, and produced extensive damage in the southern areas of Chimborazo province (collapsing of adobe constructions). There is an EHB instrumental location (Engdahl & Villaseñor 2002) that might bear some error (15km-uncertainty is assumed in Fig. 8b). The intensity centre obtained lies close to the instrumental epicentre (10 km), which is located on the 50 and 67 per cent confidence contours, to the north of Alausi town. Both the intensity centre and the instrumental epicentre are within the Pallatanga SW–NE strike-slip system (Winter 1990; Alvarado 2009). Equivalent moment magnitude at the intensity centre is 6.5 (6.3 at instrumental epicentre), and the 67 per cent confidence interval is 6.3–6.8. However note that the confidence contours also allow possible locations of the intensity centre southeast of Alausi. Moreover, the valley where the Pallatanga fault system lies, that would be the epicentral region according to the 67 per cent confidence contour, does not display high intensities (VII and VIII). This lack of high intensity observations is surprising, as this valley was already well populated at the time. Therefore, the actual data available do not enable us to provide a satisfactory solution for this earthquake. The Guamote-Huigra fault system (Alvarado 2009) lies in the valley where the nest of intensities VII and VIII is located. This could also be a potential candidate for this earthquake, yielding a lower magnitude (6.1–6.2). More work is required to clearly identify the responsible fault segment.

### DETERMINATION OF LOCATION AND MAGNITUDE OF HISTORICAL EVENTS

The method is applied to historical events for which no instrumental determination is available (Table 4). All events with a minimum

of 10 intensity observations higher or equal to III were considered, which results in more than 20 studied earthquakes. However locations cannot be obtained for all of them. Some events are described by a large intensity data set well distributed in space (various distances and azimuths), others are described by only 2 intensity degrees with unevenly distributed observations. When intensities reported are few or when the probable epicentre is far outside the ‘network’ of observations, locating the intensity centre is not possible. This is the case for the three events that occurred north of the Colombian border (1843, 1923, 1953). As these events are described both by intensities collected in Ecuador and in Colombia, the analysis of these earthquakes is left for future collaborative work between both countries. Bakun & Wentworth (1997) demonstrated that their method is particularly adapted to Californian historical earthquakes with very few observations (down to 5). This might be less true for earthquakes in the Sierra of Ecuador, as even for recent earthquakes the absence of observations in the mountain ranges to the east and to the west of the populated Interandean Valley represents a difficulty. In the following,  $M_{IC}$  is the intensity magnitude estimated at the intensity centre, equivalent to a moment magnitude. For all earthquakes, the uncertainty on magnitude, that is, 67 per cent probability intervals deduced from the magnitudes of the bootstrap intensity centres lying within the 67 per cent spatial confidence contour, are also reported (Table 5).  $M_{Preferred}$  is the magnitude obtained at a ‘preferred’ location for the epicentre, different from the intensity centre (the minimum rms location) but located within the confidence contours.

#### Earthquakes of the second half of the XXth century

The earthquakes studied are Aloasi (1976,  $I_{max\_obs}$  VII,  $M_{IC} = 5.$ ), Cusubamba (1962,  $I_{max\_obs}$  VII,  $M_{Preferred} = 5.8$ –6.0), Pasa (1960,  $I_{max\_obs}$  VII,  $M_{Preferred} = 5.6$ –5.7), Latacunga (1958,  $I_{max\_obs}$  VI,  $M_{IC} = 5.0$ ), and Atahualpa (1955,  $I_{max\_obs}$  VIII,  $M_{IC} = 6.14$ ). Magnitudes obtained for these earthquakes of the second half of the

**Table 4.** Historical earthquakes: number of data per intensity degree (II is not used in calculations) based on the intensity historical catalogue (Egred 2009b).

Year/Month/Day	Event Name	II	III	IV	V	VI	VII	VIII	IX	X	XI	Total
1955/5/11	Due-Reventador	4	1	1	1	10	5	–	–	–	–	22
1949/8/5	Pelileo	–	7	15	10	14	12	11	7	6	–	82
1976/11/29	Aloasi	4	6	4	5	9	6	–	–	–	–	34
1962/11/16	Cusubamba	–	2	2	1	3	3	–	–	–	–	11
1961/4/8	Pepinales	–	1	5	5	9	8	3	–	–	–	31
1960/7/30	Pasa	–	3	10	4	4	6	–	–	–	–	27
1958/1/24	Latacunga	1	7	1	1	4	–	–	–	–	–	14
1955/7/20	Atahualpa	–	4	3	–	10	23	5	–	–	–	45
1944/9/15	Toacazo	2	2	3	1	10	3	–	–	–	–	21
1938/8/10	Sangolqui	–	8	4	3	10	13	2	–	–	–	40
1929/7/25	Murco	2	3	2	4	1	9	1	–	–	–	24
1914/5/31	Antisana	–	11	10	6	3	9	6	–	–	–	45
1911/9/23	Cajabamba	1	2	1	–	4	9	1	–	–	–	18
1868/8/15	El Angel	–	1	1	–	–	3	8	–	–	–	15
1868/8/16	Ibarra	–	1	5	2	4	9	24	26	–	–	71
1859/3/22	Quito	–	5	2	1	2	18	1	–	–	–	30
1797/2/4	Riobamba	–	9	2	1	1	11	34	19	37	3	117
1698/6/20	Ambato	2	1	–	–	3	1	7	6	–	–	20
1587/8/31	Guayllabamba	–	–	–	–	1	6	3	–	–	–	10

**Table 5.** Historical earthquakes: results.

Year/Month/Day	Event Name	Lat. <sup>a</sup> of IC	Long. <sup>a</sup> of IC	$M_{IC}^b$	$M_{IC}$ : 67 per cent <sup>c</sup>	FL <sup>d</sup> (km)
1976/11/29	Aloasi	–0.52	–78.61	5.	5.0–5.2	3.2
1962/11/16	Cusubamba	–1.16 <sup>e</sup>	–78.65 <sup>e</sup>	5.8–6 <sup>e</sup>	–	13
1960/7/30	Pasa	–1.20 <sup>e</sup>	–78.7 <sup>e</sup>	5.6–5.7 <sup>e</sup>	–	7.3
1958/1/24	Latacunga	–0.98	–78.59	5.0	4.9–5.2	3.3
1955/7/20	Atahualpa	0.28	–78.39	6.14	6.1–6.3	15.2
1944/9/15	Toacazo	–0.71 <sup>e</sup>	–78.7 <sup>e</sup>	5.6–5.8 <sup>e</sup>	–	8.4
1938/8/10	Sangolqui	–0.4	–78.41	5.8	5.6–6.0	9.6
1929/7/25	Murco	–0.5	–78.48	5.88	5.8–6.1	10.7
1914/5/31	Antisana	–0.6	–78.42	6.44	6.4–6.5	22.9
1911/9/23	Cajabamba	–1.73 <sup>e</sup>	–78.8 <sup>e</sup>	6.1–6.3 <sup>e</sup>	–	16.5
1868/8/15	El Angel	0.7	–77.92	6.6	6.4–6.8	28.4
1868/8/16	Ibarra	0.38	–78.43	7.25	7.1–7.7	70.7
1859/3/22	Quito	0.02	–78.75	7.2	6.9–7.3	64
1797/2/4	Riobamba	–1.5	–78.6	7.6	7.5–7.9	110.7
1698/6/20	Ambato	–1.4 <sup>e</sup>	–78.8 <sup>e</sup>	7.2–7.3 <sup>e</sup>	–	64
1587/8/31	Guayllabamba	0.05	–78.33	6.4	6.35–6.55	21.7

<sup>a</sup>Note that the precision on the latitude and longitude is dependent on the spatial grid step (varying between 0.025° and 0.05°)

<sup>b</sup>Intensity magnitude obtained at the intensity centre.

<sup>c</sup>Intensity magnitude confidence range: range of magnitudes of epicentres contained within the 67 per cent confidence contour.

<sup>d</sup>FL: Subsurface rupture length according to magnitude at intensity centre (and generic equation from Wells & Coppersmith 1994).

<sup>e</sup>Intensity magnitude at a preferred location for the earthquake epicentre, which is not the intensity centre (see text).

XXth century are moderate (5–6), as expected, since these earthquakes are not reported in the international seismic catalogues.

The magnitude 5.0 Aloasi earthquake was felt in a narrow rural area between Pichincha and Cotopaxi provinces, its confidence contours are indeed narrow (67 per cent, 5 km × 5 km, Fig. 7c, Supporting Information). This earthquake might be related to the Pastocalle earthquake that occurred less than 2 months earlier 20 km to the south. The causative fault might be the northern continuation of La Victoria Fault (Lavenu *et al.* 1995) or the Machachi SW–NE fault (Soulas *et al.* 1991).

The Cusubamba earthquake (Fig. 8a) was strongly felt in the central region of Ecuador. The intensity centre falls in a zone where no fault has previously been identified, the 50 and 67 per cent confidence contours delineate quite large zones (only 11 intensity assignments, III–VII) and indicate an intensity centre on the west-

ern slope of the Interandean Valley. The 95 per cent contour extends in the direction corresponding to a lack of data, perpendicular to the valley, including the western and eastern slopes. This earthquake might have occurred on the north–south thrust fault system, preferably on the Western slope of the valley, which represents the southern continuation of La Victoria Fault (Lavenu *et al.* 1995).

The Pasa event (Fig. 8b) also occurred within the Western Cordillera and might be related to the same fault system as the Cusubamba event. The intensity centre, corresponding to the minimum rms, is located within the Western Cordillera where no fault has been identified. The preferred location for the epicentre is close to the 67 per cent confidence contour, on the western slope of the Valley, slightly south of the 1962 event.

The Latacunga earthquake is a small event probably generated by the north–south Alaquez fault (Alvarado 2009); the intensity centre

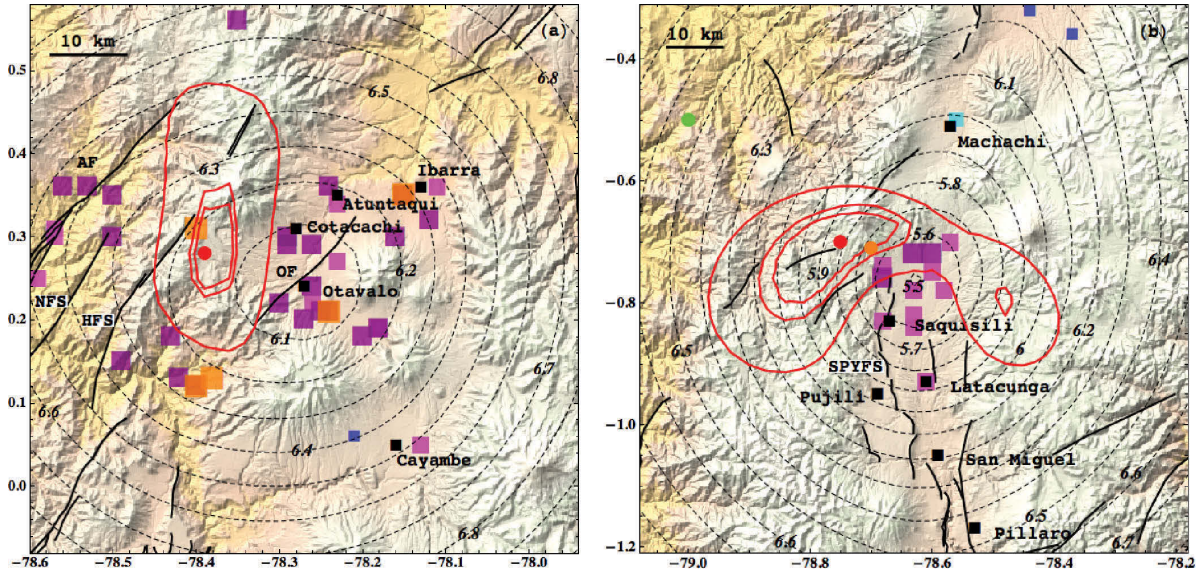


**Figure 9.** Determination of magnitude and location for historical events. (a) Atahualpa (1955). (b) Toacazo (1944), instrumental epicentre from CGS (certainly bearing at least 30 km uncertainty). AF, NFS, HFS, OF, SPYFS are faults (Table 6). See legend in Fig. 3. Results are reported in Table 5.

is located on the southern end of this fault (Fig. 8c, Supporting Information).

Finally, the Atahualpa event (Fig. 9a) was strongly felt in the Imbabura province, but also in the neighbouring Pichincha and Carchi provinces. Many rural adobe buildings collapsed in the epicentral area, and several large landslides cut main roads in Imbabura. This event is well described by 45 assigned intensity points from degree III to VII quite homogeneously distributed. The magnitude is 6.14 at the intensity centre, and 6.1–6.2 at the 67 per cent confidence level. Taking into account the extension of the 95 per cent contour ( $\approx 30 \text{ km} \times 15 \text{ km}$ ), several SW–NE fault segments might be considered as candidate: from west to east, the Apuela segment, the northern segment of the Nanegalito fault system, the northern segment of the Huayrapungo fault segment, or the Otavalo fault (Eguez *et al.* 2003).

#### Earthquakes of the first half of the XXth century

Earthquakes studied are Toacazo (1944,  $I_{\text{max,obs}}$  VII,  $M_{\text{Preferred}} = 5.6\text{--}5.7$ ), Sangolqui (1938,  $I_{\text{max,obs}}$  VII–VIII,  $M_{\text{IC}} = 5.8$ ), Murco (1929,  $I_{\text{max,obs}}$  VII–VIII,  $M_{\text{IC}} = 5.88$ ), Antisana (1914,  $I_{\text{max,obs}}$  VIII,  $M_{\text{IC}} = 6.44$ ), Cajabamba (1911,  $I_{\text{max,obs}}$  VII–VIII,  $M_{\text{Preferred}} = 6.1\text{--}6.3$ ).

The Toacazo earthquake (Fig. 9b) produced extensive destruction in rural areas and in the towns of Toacazo and Pastocalle. Fifty and 67 per cent confidence contours delineate quite large zones ( $25 \text{ km} \times 10 \text{ km}$  for 50 per cent). The intensity centre is located within the Western Cordillera, on geological folds that are not considered as seismically active (Alvarado 2009). The preferred location for the epicentre is slightly shifted to the east on the 50 per cent confidence contour, on the slope of the Interandean valley. The sources of the Pastocalle (1976) and Toacazo events might be the same: a segment on a northwestern branch of the inverse Saquisilí-Poalo-Yambo fault system (Alvarado 2009). Note that there is an instrumental location for this earthquake ( $-0.5, -79.0$ ) from CGS, but it is very likely that it bears an error of at least 30 or 40 km.

The Sangolqui earthquake (Fig. 10a) was strongly felt in a rather narrow area in a valley southeast of Quito (Los Chillos), many adobe houses collapsed. The 50 and 67 per cent confidence contours point at the Pintag NW–SE fault as the causative fault (Alvarado 2009). This fault is part of the lineament described by Hall & Wood (1985). The segment can accommodate a magnitude 5.8 earthquake ( $\sim 9\text{--}10 \text{ km}$  rupture length, Wells & Coppersmith 1994).

The Murco earthquake (Fig. 10b) destroyed the village of Murco and was partially destructive in some other villages in southern areas of Pichincha province. Confidence contours 50, 67 and 95 per cent are rather narrow, delineating a zone where no potentially active faulting has been reported. This earthquake might have occurred on a segment south of the Quito fault system that would be located within the 67 or 95 per cent confidence contours to the west of the intensity centre. Another option would be on the northeastern continuation of the Machachi fault (Soulas *et al.* 1991). This option is preferred since damages are localized in that direction.

The Antisana event ( $M_{\text{IC}} 6.44$ , Fig. 11a) was felt over a large region, from Cuenca to the south (Fig. 1) up to Ibarra to the north, with strongest damage in Pichincha province. It triggered several landslides on the slopes of Antisana volcano and surrounding hills. Several reported VIII intensities correspond to landslides and liquefaction effects. The intensity centre is quite well constrained, with rather narrow confidence contours; however within the 95 per cent contour no previous evidence of active faulting has been reported. As the historical documents for this event have been revised with reassessment of the intensity values and checking of the locations (Singaicho 2009), this earthquake is an opportunity for evaluating the impact on the estimations of potential ‘errors’ in the data. Some errors in locations were detected, some high intensities based on landslides/liquefaction were eliminated. Recent results have indeed shown that effects such as liquefaction can be poor indicators of overall shaking levels (e.g. Ambraseys & Douglas 2004). From the original 45 locations of observations, 34 remained (III–VII). The resulting intensity centre and confidence contours remain very stable;

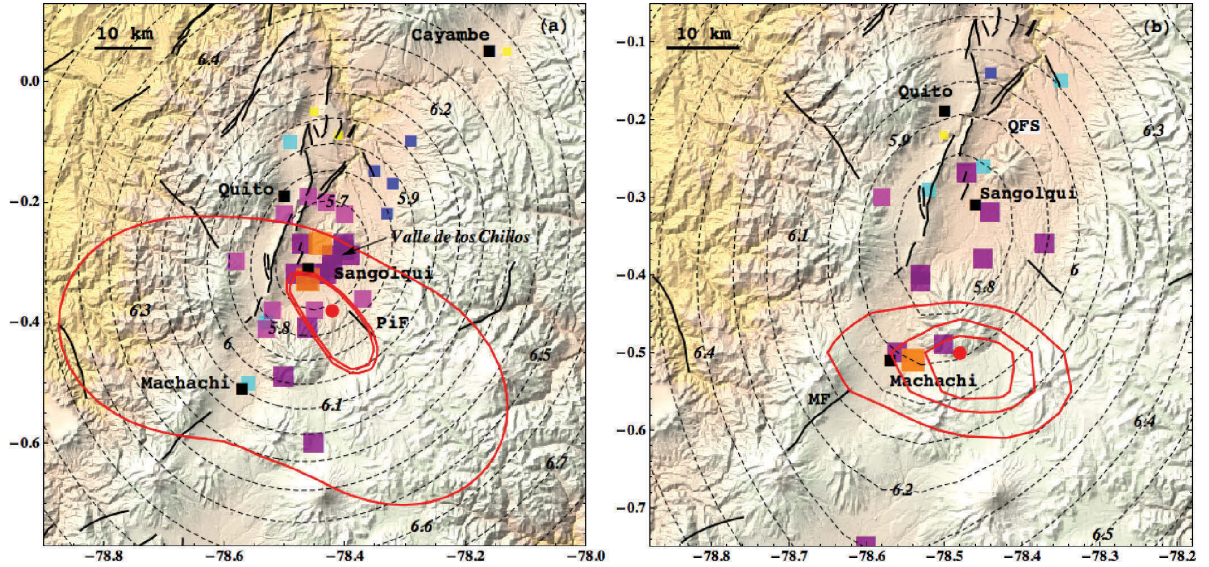


Figure 10. Determination of magnitude and location for historical events. (a) Sangolqui (1938). (b) Murco (1929). PiF and MF are Pintag and Machachi faults (Table 6). See legend in Fig. 3.

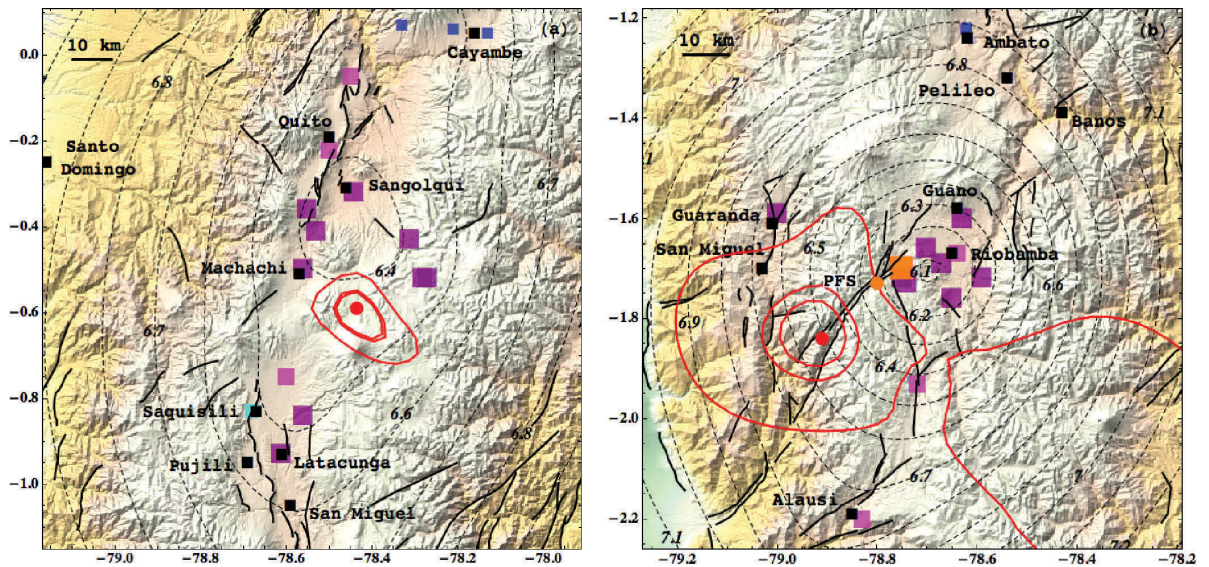
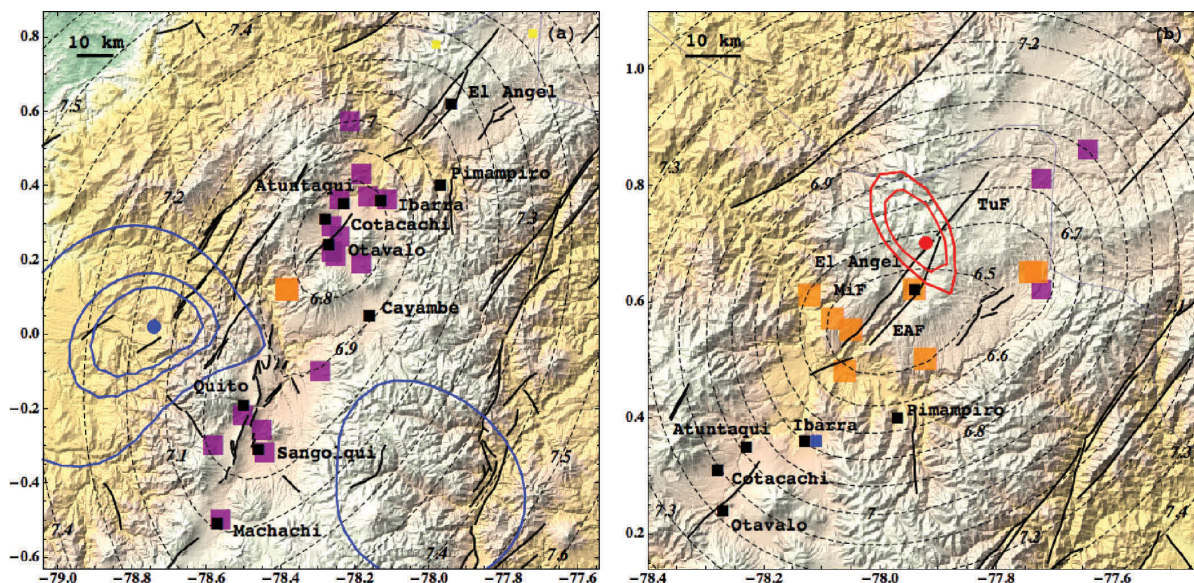


Figure 11. Determination of magnitude and location for historical events. (a) Antisana (1914) based on revised intensities (Singaicho 2009) (b) Cajabamba (1911). PFS is Pallatanga fault system (Table 6). See legend in Fig. 3.

only the equivalent moment magnitude slightly decreased from 6.56 to 6.44. Note that the Antisana lineament identified by Hall & Wood (1985) crosses the zone of high damage (intensities VII), 10 km to the northeast of the intensity centre; a fault segment belonging to this lineament could be a possible candidate for this earthquake. More fieldwork is required in this area to determine the causative fault.

The Cajabamba event (Fig. 11b) was strongly felt and produced heavy damage in several sectors of Chimborazo province. The inten-

sity centre and 50/67 per cent contours clearly identify one segment of the SW–NE Pallatanga strike-slip fault system as the source of the earthquake [Eguez *et al.* 2003; Alvarado 2009]. By shifting the intensity centre on the same fault segment to the northeast, to the 95 per cent confidence contour, the magnitude deduced from intensities decreases to 6.2. This location of the intensity centre is more in accordance with the lack of intensity observations in the Pallatanga valley to the southwest, a valley that was already well populated at the time.



**Figure 12.** Determination of magnitude and location for historical events. (a) Quito (1859). (b) El Angel (1868). For El Angel, the 95 per cent confidence contour is not drawn, as a very large region would be required. MiF, TuF and EAF are faults (Table 6). See legend in Fig. 3.

### Large earthquakes of the XVI–XVIIIth centuries

#### *Quito (1859 March 22)*

This earthquake (Fig. 12a) produced destruction in a large area; the Cotopaxi, Pichincha and Imbabura provinces, were equally struck (intensities VII). It was felt as far as Guayaquil on the coast (intensity IV ~300 km far from Quito, see Fig. 1). Analysing the pattern of the intensity distribution, mainly one intensity degree (VII, see Table 4) extending in a direction north–south over 150 km, one anticipates that the B&W method will not be able to localize a reliable intensity centre. Indeed, only a loose 50 per cent confidence contour can be plotted, indicating possible locations to the west and to the east of the intensity observations (figure not shown). One explanation is that this event is not crustal, but is a deep event within the subducting slab beneath the Andean Range. This would explain the large extension of the VII macroseismic area. Interestingly, this event is one exception regarding the influence of the weighting function on the location and magnitude estimates. If applying the method without the weighting function (all intensity assignments have equal weight whatever the distance to the assumed epicentre is), a different result is obtained (Fig. 12a): the intensity centre can be localized more reliably 15 km to the west of Quito. The intensity magnitude at intensity centre is 7.2, however this magnitude estimate cannot be considered reliable if the event is located in the slab as the attenuation model has been derived from crustal shallow earthquakes. As doubt remains, this event is kept in the crustal event list. More work is required to reliably identify its source.

#### *El Angel (1868 August 15)*

The El Angel earthquake (Fig. 12b) occurred 10 hr before the larger Ibarra event described below. It was strongly felt all over the Carchi province, causing damage to many houses and churches, and dozens of casualties. The damage increased with the following larger Ibarra event (40–50 km to the south), which implies that the magnitude

based on the intensity data set might be overestimated. Essentially two intensity degrees are described (VII and VIII); however the intensity centre and the confidence contours 50 and 67 per cent clearly identify three potential faults within the El Angel fault system (Eguez *et al.* 2003), all oriented SW–NE: Mira, Tufiño and El Angel (Alvarado 2009). The equivalent moment magnitude obtained at the intensity centre is 6.6, and the 67 per cent probability interval 6.4–6.8. It is likely that damage of the first event cannot be easily separated from damages of the second larger event and this magnitude estimate should be considered with caution.

#### *Ibarra (1868 August 16)*

The Ibarra earthquake (Fig. 13) is the most destructive earthquake to strike northern Andean Ecuador during historical times. Several cities, namely Atuntaqui, Cotacachi, Ibarra and Otavalo, were completely ruined, as well as many villages in their neighbourhood. Damages were also reported in churches and houses in Quito. In the Imbabura province, large landslides destroyed roads and haciendas. Several strong aftershocks were reported. Seventy-five intensity assignments ranging from III to IX are available for analysing this event, yielding a 7.27 equivalent moment magnitude at the intensity centre (Fig. 13a, 67 per cent confidence interval: 7.1–7.7). Note that this magnitude is higher than the maximum magnitude of the calibrating events (7.1). The distribution pattern of the intensities, with decreasing values from west (IX and VIII) to east (VI and V) parallel to the SW–NE trending fault system, favours a location of the intensity centre to the west. Wells & Coppersmith's (1994) generic equation predicts approximately a 70 km rupture for a  $M$  7.27 earthquake. Fault segments within the 95 per cent confidence contour include the Apuela fault to the west, and northern segment of the Huayrapungo fault (Eguez *et al.* 2003). The next SW–NE trending fault to the east is the Otavalo fault (Eguez *et al.* 2003). Assuming that the earthquake was generated on the Otavalo fault, the intensity observations would yield a  $M$  7.0 event (rupture length ~50 km).

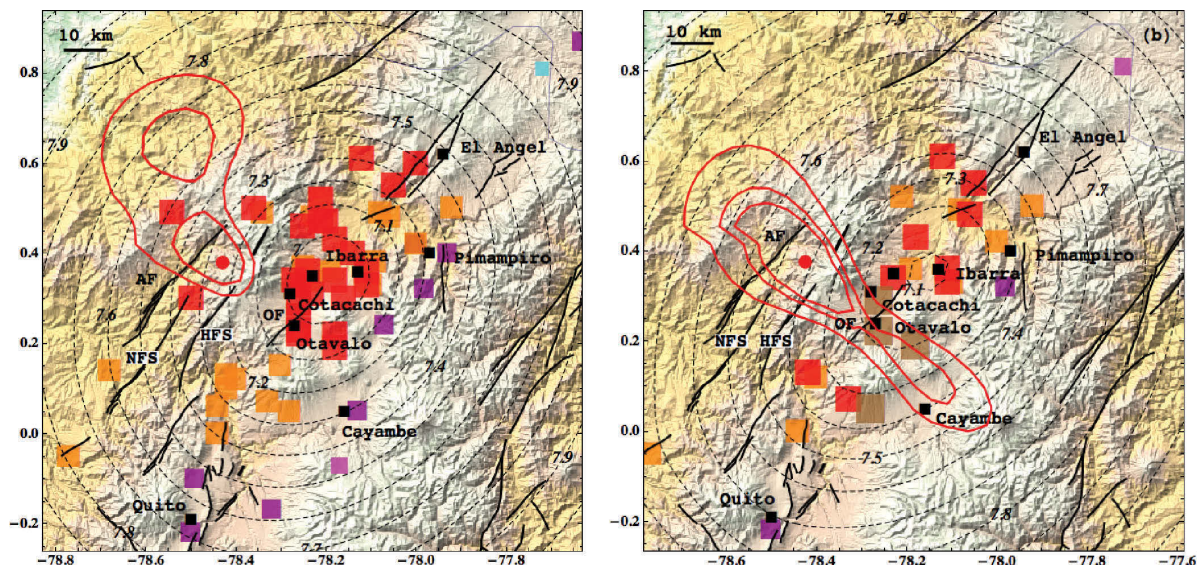


**Figure 13.** Determination of magnitude and location for the Ibarra historical event (1868): (a) original data; (b) revised intensity data set (Singaicho 2009). AF, NFS, HFS and OF are faults (Table 6). See legend in Fig. 3.

Furthermore, a new analysis of the intensity data set by Singaicho (2009) showed that some intensities reported are rather unreliable. These observations were eliminated in the revised data set. Unfortunately, Singaicho (2009) could not locate all original documents, and his work provides a set of 31 revised and reliable intensity values, free of geographical location errors and of intensities relying on effects in nature. The new intensity data set does not include any intensity assignment west or close to the Apuela and Huayrapungo segments (Fig. 13b). Maximum intensity now reaches degree X. The results remain stable (location of intensity centre and associated magnitude), however the confidence contours are extended in the NW–SE direction, with contours 95 and 67 per cent crossing the Otavalo fault. Only future work based on other type of data (tectonic, geology fieldwork) will enable confirmation or rejection of these findings.

#### *Riobamba (1797 February 4)*

The earthquake that razed Riobamba Antiguo to the ground is the most destructive earthquake in the written history of Ecuador (five centuries), causing at least 25 000 casualties (Egred 2000, 2004). The city of Riobamba was relocated after the tragedy. Many towns and villages were demolished in the provinces of Chimborazo, Tungurahua and Cotopaxi, but also in some parts of Pichincha and Bolívar. Many large cracks resulted in the topography and many liquefaction effects were observed. The earthquake triggered extensive landslides, covering entire districts of Riobamba city but also creating dams in rivers 50 km to the north. This earthquake was followed by months of aftershocks, some of them increased the destruction. The available intensity data set is large (Table 4) with 117 intensity values ranging from degree III to degrees X (at 37 locations) and XI (at three locations). Intensities X extend over approximately 100 km in a north–south direction (Fig. 14). The earthquake was felt in northern Peru (Piura, intensity III, ~400 km south of Riobamba). Taking into account all intensities up to IX results in an intensity centre located close to the city of Guano, and yields

a 7.6 equivalent moment magnitude (7.5–7.9 at the 67 per cent confidence level, Fig. 14a). The 67 per cent confidence area oriented NW–SE and extending over approximately 50 km is less constrained to the southeast as no intensity observation is available in that azimuth. Taking into account intensities X and XI yields results consistent with the previous one; however the confidence contours are much narrower (Fig. 14b). The weighting function is not taken into account in this case, in order not to give too much weight to observations that might be very close to the fault plane and for which the point source model is not adequate. Using only intensities up to VIII still yields comparable locations of the intensity centre (Fig. 14c, Supporting Information) as well as applying the method on the revised intensity data set provided by Singaicho (2009). A magnitude 7.6 earthquake can rupture over ~110 km (Wells & Coppersmith 1994). The only known fault system able to generate a magnitude 7.6 earthquake in the area is the SW–NE Pallatanga system (Winter 1990). The most probable fault plane for the Riobamba earthquake is therefore a segment of the Pallatanga fault system that ruptured to the northeast to join the Pucara fault segment (Alvarado 2009; the Pucara fault segment has been identified as the potential source of the 1949 Pelileo earthquake). The intensity centre would then be located somewhere in the middle of the fault plane. Directivity effects could explain the high intensity observations within the Interandean Valley, and the rather low intensities reported on the southwestern segment of the Pallatanga fault system (VII). More neotectonic fieldwork is required in this area to clearly identify the potential fault segments involved, although this task might be difficult as the recurrent activity of the active volcanoes in the area might have obscured superficial evidence.

Note that the point source hypothesis, which is the basis of the B&W (1997) method and the inherent hypothesis for using an intensity–magnitude relationship considering hypocentral distances, is obviously not fulfilled in this case. B&W have applied this method for earthquakes up to  $M$  7.8 (Bakun & Hopper 2004), using observations located at long distances from the source. For large extended sources, assuming that the energy comes from a

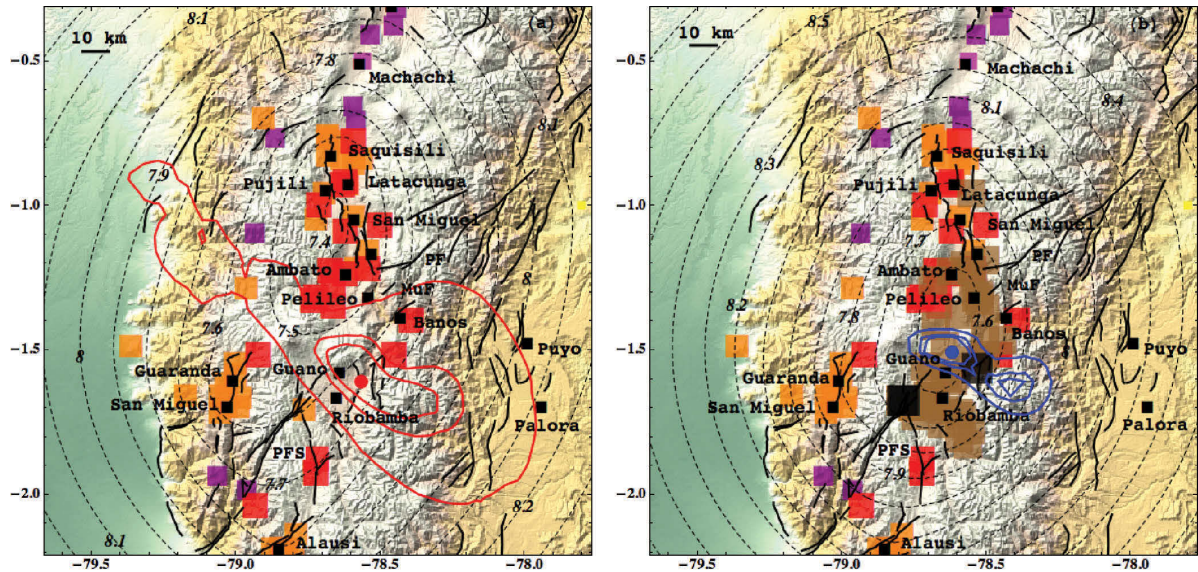


**Figure 14.** Determination of magnitude and location for the Riobamba historical event (1797); (a) using intensities up to IX; (b) using intensities up to XI. PFS is the Pallatanga fault system, PF is the Pucara fault, MuF is the Mundug fault (Table 6). See legend in Fig. 3.

point source might lead to an overestimation of intensity magnitude if using many intensity observations close to the rupture surface (Bakun 1999). We cannot ignore this fact, however we believe that in the case of the Riobamba event, using only intensities up to VIII and then up to IX reduces this effect. Far enough from the fault, rupture distances between an intensity observation site and any point along the rupture are quite similar. To correctly treat this problem, we would need to establish an intensity-magnitude equation with the nearest distance to the rupture plane (e.g. Ambraseys 2002), which is currently not possible considering the available calibrating events. In the near future, other methods relying on the individual intensity observations for estimating magnitude and location should be tested on the Riobamba intensity data set. For example, it will be interesting to test the method by Gasperini *et al.* (1999), which is intended for taking into account the extension of the fault plane.

#### Ambato (1698 June 20)

The Ambato earthquake (Fig. 15a) is one of the most destructive earthquakes of the colonial period. Damages were reported over an extended region, including the Tungurahua, Cotopaxi and Chimborazo provinces. The earthquake occurred at night and several thousands of casualties were reported. The cities of Ambato and Latacunga were totally razed to the ground, whereas Riobamba (Antiguo) was partially demolished. Ambato was relocated after the earthquake. The event triggered a giant debris flow on the slopes of Carihuairazo Mountain that buried Ambato downstream. Some damage was also reported in Pichincha and Bolivar provinces. Only 17 intensities higher than IV are available, with maximum intensities reaching IX (Table 4). The intensity centre is located on the western slope of the Interandean Valley, however both slopes are possible locations of the epicentre according to the confidence contours. The magnitude interval is 7.2–7.9 if considering all locations within the 67 per cent confidence contour. The large landslides at Carihuairazo favour a location of the epicentre on the western slope. A source close to Carihuairazo Mountain (on the 67 per cent con-

**Table 6.** Names and acronyms of faults mentioned in the text and displayed on the maps.

Acronym of the fault	Fault (or fault system) name
AL	Alaquez Fault
AF	Apuela Fault
CF	Catequilla Fault
EAF	El Angel fault
GHFS	Guamote-Huigra Fault System
HFS	Huayrapungo Fault System
LVF	La Victoria Fault
MF	Machachi Fault
MiF	Mira Fault
MuF	Mundug Fault
NFS	Nanegalito Fault System
NPF	Nono-Pululahua Fault
OF	Otavalo Fault
PF	Pucara Fault
PFS	Pallatanga Fault System
PiF	Pintag Fault
QFS	Quito Fault System
RP	Reventador Fault
SF	Salado Fault
SJF	San Juan de Calderon Fault
SPYFS	Poalo- Saquisili-Yambo Fault System
TF	Toacazo Fault
TuF	Tuñiño Fault

tour) would imply a  $M_I$  7.2 earthquake. No active fault has been previously identified in this area. The source of this earthquake might be the same fault system responsible for the much smaller Cusubamba (1962) and Pasa (1960) events, and may be part of the north–south thrust fault system. On the other hand, as the 67 per cent confidence contour extends to the east and crosses the Interandean valley, a location on the Pallatanga fault system (or its extension to the northeast) located on the eastern side of the Carihuairazo cannot be excluded (yielding a magnitude  $M_I$  7.2–7.3). More

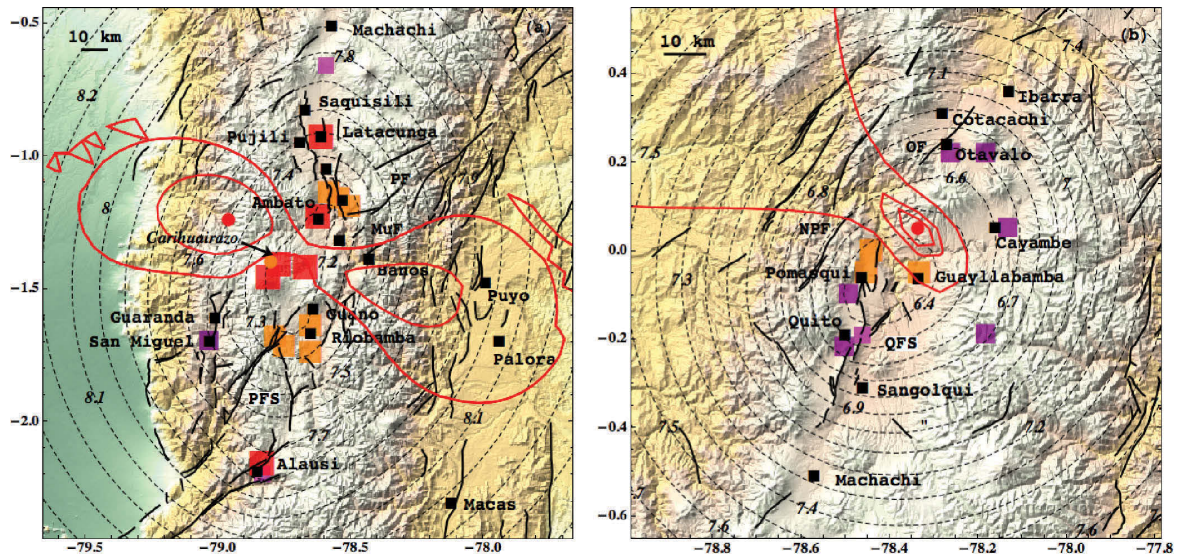


**Figure 15.** Determination of magnitude and location for (a) the Ambato event (1698)—only the 50 and 67 per cent contours are drawn—and for the (b) Guayllabamba event (1587). QFS is the Quito fault system; NPF is the Nono-Pululahua fault (see Table 6). The Carihuairazo is a volcano (see the text). See legend in Fig. 3.

multidisciplinary work (tectonic, paleoseismology, etc.) is required to identify the potential source of this destructive earthquake.

#### *Guayllabamba (1587 August 31)*

This earthquake struck northern areas of Pichincha province and southern towns of Imbabura province (Fig. 15b). The city of Quito was largely affected (churches and houses). Casualties and destruction were also reported in several villages north of Quito (Guayllabamba, Pomasqui), and extended all the way to Otavalo (intensity VII) in Imbabura. Although this earthquake is described by a few intensities (10 observations mainly within intensity degrees VII and VIII), the confidence contours are quite narrow (10 km × 10 km for contour 67 per cent). The intensity centre is located north of Quito, suggesting rupture on a segment of the Quito fault system as the causative seismic source: either the Catequilla fault, the San Juan de Calderon fault or its extension to the north, or an unknown branch of the Quito fault system to the east. The magnitude is 6.4 at the intensity centre, and 6.35–6.55 at the 67 per cent confidence level. Another possibility would be the Nono-Pululahua fault orientated NE–SW (same direction as the Otavalo fault) located west of the Quito fault system (intensity magnitude around 6.6) and crossing the 95 per cent confidence contour.

### STUDIED EVENTS WITHIN THE GENERAL GEODYNAMIC FRAMEWORK

For many years it has been recognized that the northwestern corner of South America is moving north–northeast as a block relative to the rest of the South American plate (Pennington 1981; Kellogg *et al.* 1985) along a system of faults following the piedmont of the Eastern Andean Cordillera in Colombia, but obliquely crossing the Andean Ranges in Ecuador. The geodynamics of the northern Andes have been interpreted either as resulting from the obliquity of convergence between the Nazca and South American plates, or from the collision of the Carnegie Ridge with Ecuadorian margin (Ego

*et al.* 1995), in any case with consequences that could be recognized along approximately 1400 km of escape tectonics (Trenkamp *et al.* 2002). The SW–NE trending right-lateral Pallatanga fault system (Fig. 16) probably constitutes the southern limit of the North Andean Block (NAB) which, starting from the Gulf of Guayaquil, crosses the Western Cordillera where the Interandean Valley can be first recognized (in the general area of the Riobamba basin). The Interandean Valley itself between Ambato and Quito appears to be a compressive N–S restraining bend (Lavenu *et al.* 1995; Ego *et al.* 1996), and constitutes a large left offset of the SW–NE strike-slip deformation. The right-lateral Chingual–Eastern Frontal and Romeral fault systems (Fig. 16, Romeral fault is in Colombia) constitute the deformation corridors further northeast of the Interandean Valley, the former being recognized as the eastern limit of the NAB further north (Tibaldi *et al.* 2007). For the Interandean Valley the concomitant E–W shortening proposed by Lavenu *et al.* (1995) is kinematically consistent with the right lateral movement of the aforementioned strike-slip systems in an oblique convergence regime. It has been suggested that in the central Ecuadorian Andes the eastern limit of the NAB could be identified as a deformation corridor that, including the SW–NE Pallatanga fault trend, obliquely cuts the Eastern Cordillera along the Pisayambo earthquake cluster (1°S, 78°W) and then turns northwards to meet the Chingual fault system 150 km to the north (Soulas *et al.* 1991). The N–S deformation corridor mostly shows a compressional regime with a small right lateral strike-slip component and is known as the Baeza-Reventador transpressive system (Gajardo *et al.* 2001).

Bearing in mind the depicted geodynamic framework for the Sierra, groups of earthquakes can be ascribed to different fault systems (Fig. 16). The Pepinales 1961, Cajabamba 1911, Riobamba 1797, Pelileo 1949 and the Tena 1987 (not examined in this study) earthquakes are distributed along the SW–NE Pallatanga-Pucara-Llanganates corridor. The Ambato 1698 earthquake could also have been generated along this corridor. All these events have intensity magnitudes larger than 6, with the largest being the large 1797 earthquake relocated at the southern edge of the Interandean Valley

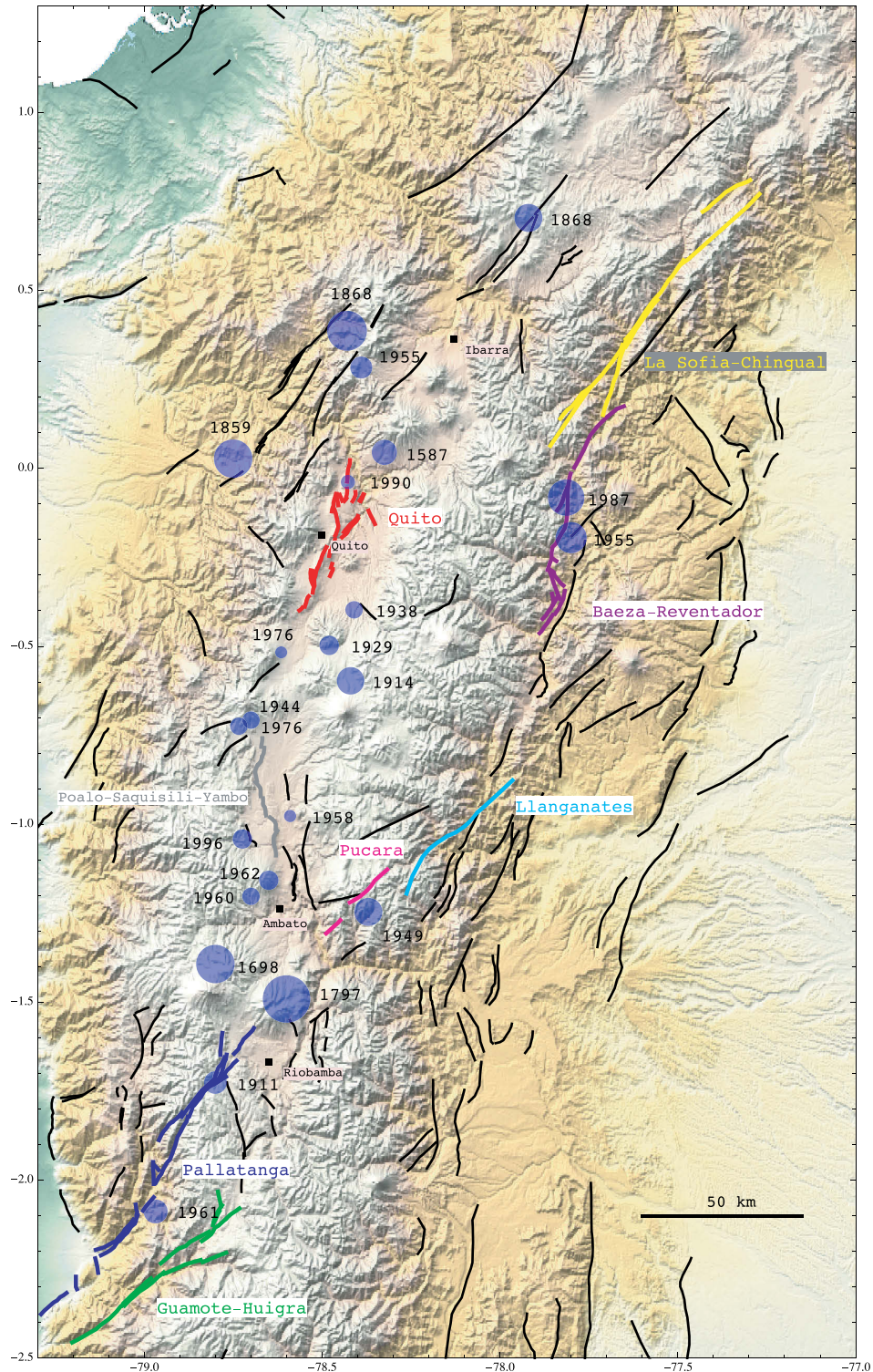


**Figure 16.** All events studied in this paper, located either in Interandean Valley or within the Cordilleras. The larger the magnitude, the larger the radius of the blue disc (see values in Tables 3 and 5). The year of the earthquake is indicated to the right of each disc. Black thick lines: fault segments (Alvarado 2009). Specific fault systems are also highlighted (see text).

within this study. Two events (Due-Reventador 1955 and Salado-Reventador 1987) are localized further north in the Baeza Reventador transpressive system and show magnitudes greater than 6.5. There is no event assigned to the faster right-lateral strike-slip Chingual fault system in Ecuador, which is the northeastern continuation of the transpressive faults. The great 1834 Sibundoy earthquake, not analysed in this study, is probably located on this fault system 100 km north of the border between Ecuador and Colombia.

Starting from the south, the Pasa 1960, Cusubamba 1962, Pujili 1996, Pastocalle 1976, Toacazo 1944 and Aloasi 1976 earthquakes are located on the internal slopes of the Western Cordillera, very close to high Andes indigenous villages. The Guayllabamba 1587, Murco 1929 and Pomasqui 1990 events might also be included in this group. Their spatial distribution shows a clear N–S trend; focal mechanisms for the Pastocalle 1976 and Pujili 1996 events show N–S planes dipping to the west as probable focal solutions. These directions coincide with the N–S trend of the western limit of the restraining bend and confirm the compressional tectonics prevalent in the Interandean Valley. It is noteworthy that all of these events (except Guayllabamba) show magnitudes around five to six, and a recurrence time of less than 15 yr during the XXth Century. The great 1698 Ambato earthquake could also be part of this group if located on the foot of the Western Cordillera, to the south of the Pasa epicentre. However, as indicated above, the small number of intensity points, their lack of good azimuthal coverage plus the event's very large intensity magnitude opens the possibility that the 1698 event may be related to the Pallatanga-Pucara-Llanganates group.

Both 1868 events (El Angel and Ibarra) and the 1955 Atahualpa event could be related to the southern prolongation of the Romeral Fault system or to a different set of faults running along the same SW–NE trend but located further west of the Romeral faults as suggested by Soulas *et al.* (1991). The 1587 Guayllabamba event could also be ascribed to this group. These earthquakes related to the strike-slip faults also show magnitudes greater than 6. Finally, a few historical events could be related to the eastern border of the restraining bend. This could be the case of the 1914 Antisana event ( $M_{IC}$  6.44); while the smaller 1938 Sangolquí and 1958 Latacunga (and 1929 Murco) events might be related to small structures that are localized in or enter obliquely in the Interandean Valley. The small 1990 Pomasqui earthquake could also fit in this category. These events have magnitudes in the range of five to six. At last, the 1859 earthquake might be a deep earthquake so no group is suggested for it.

## CONCLUSIONS

This is the first time an objective and reproducible method is applied for estimating the locations and magnitudes of historical earthquakes in the Sierra of Ecuador (covering the last 500 yr). The Bakun & Wentworth (1997) grid-search method is applied. Spatial confidence contours corresponding to different probability levels delineate the possible locations of the intensity centre (equivalent to moment centroid), and the uncertainty on magnitude can be obtained from the distribution of the magnitudes of potential epicentres lying within given confidence contours. These uncertainty estimates will be taken into account in future seismic hazard studies. Nineteen crustal events of the Sierra are relocated, yielding equivalent moment magnitudes between 5.0 and 7.6 (Table 5). Bakun & Wentworth (1997) show that the method can be applied down to five observations. However, due to some difficulties inherent to

the Ecuadorian data (mainly the spatial distribution), our study indicates that below 10 intensity assignments the results cannot be considered reliable. Furthermore, as shown in other applications of B&W (1997) technique (e.g. Bakun & Scotti 2006), the results show that the extension of the areas delineating the intensity centre location at different confidence levels is strongly dependent on the amount of intensity data, on their internal coherence, on the number of intensity degrees available, and on their spatial distribution in space.

To take into account the specificities of the Ecuadorian intensity data set, and to understand their influence on the magnitude and location estimates, different sensitivity tests were performed:

(1) The distribution of intensities in space can be rather uneven, due to the sparsely inhabited mountain ranges. Intensities are mainly distributed in a north-south direction, following the axes of the Interandean valley, the main roads and the localization of main cities and villages. One way of estimating the influence of this spatial distribution on the results is to use different spatial weighting. For all earthquakes, calculations were performed (1) without any weight and (2) with the weighting function initially proposed by B&W (1997) and used in nearly all applications of the method since then. This function gives higher weights to the points close to the assumed epicentre. In nearly all cases, the results are independent of the weighting chosen. The few exceptions concern very large magnitude events.

(2) Four large earthquakes display intensities higher or equal to IX (Pelileo 1949; Ibarra 1868; Riobamba 1797; Ambato 1698). Dealing with earthquakes of the XVIth, XVIIth and XVIIIth centuries, these intensities can be over-estimated, due to a possible saturation at intensity degree VIII–IX and to the difficulty of assigning intensities to effects on nature. For these earthquakes, calculations were performed using intensities up to VIII, then up to IX, and so on. The results on locations and magnitudes are quite stable. However, magnitudes usually increase when including intensity degrees higher than X, therefore magnitudes of reference (Table 5) are always estimated with intensities up to IX.

(3) For very large earthquakes (equivalent moment magnitudes higher than 7.0), the hypothesis of a point source is no longer fulfilled, with possible over-estimation of the magnitude from the points located close to the fault plane. Therefore, calculations were performed after removing highest intensity degrees, that is observations located close to the assumed epicentre. Influence on the results appears rather limited for the location determination, but proved to be quite high for the magnitude estimation.

Interestingly, in the Ecuadorian Sierra characterized by 'escape' compressional tectonics, where two major right-lateral strike-slip systems to the NE and SW are connected by a N–S trending restraining bend, large earthquakes seem to be related to the strike-slip faults, while the reverse faults of the western border of the restraining bend seem to produce only moderate earthquakes no larger than  $M_6$ . Large events  $M > 6.5$  have been generated along the transpressive system of the piedmont of the Eastern Cordillera.

Finally, this work aims at building a historical seismic catalogue homogeneous in magnitude, essential for any probabilistic seismic hazard assessment in Ecuador. We are currently working on a similar study for the coastal earthquakes. In the next years the on-going work on active tectonic faulting should provide new information on the potential active faults. Another important study will be to re-analyse the few earthquakes recorded by the international networks (in particular, the 1949, 1960, 1961 events); then more earthquakes would be available for the calibration. All these future findings

might confirm or contradict the present results relying mostly on macroseismic intensities, and it is likely that further macroseismic analyses will have to be carried out in the light of this new information, deriving updated intensity attenuation models. Other methods than the Bakun & Wentworth (1997) will be worth applying, for example, the method by Gasperini *et al.* (1999), and the different magnitude and location estimates obtained should be combined to determine the epistemic uncertainty (see Bakun 2010).

## ACKNOWLEDGMENTS

In charge of historical seismicity first at the Observatorio Astronómico and later at the Geophysical Institute in Quito since the early seventies, Jose Egred has contributed to this specific study and is naturally a co-author. Nonetheless, a special tribute must be paid for his long-lasting involvement in gathering and analysing historical documents, and building the intensity catalogue, which constitutes one of the fundamental foundations for all future seismic hazard studies led in Ecuador. Besides, we are grateful to R. Stein and W. Mooney who made interesting and stimulating comments on an earlier version of the manuscript. We thank the editor Andrew Curtis and two anonymous reviewers for insightful evaluations of the manuscript and constructive suggestions. Programs and figures rely on Mathematica (<http://www.wolfram.com/>). J. Aguilar, E. Pathier and C. Lasserre kindly helped us for producing some of the figures. This work has been partially supported by the ADN project (Andes du Nord) from the Agence Nationale de la Recherche under the Contract Number ANR-07-BLAN-143.

## REFERENCES

- Alvarado, A., 2009. Mapa de fallas y pliegues cuaternarios del Ecuador, database, Instituto Geofísico, Escuela Politécnica Nacional, Internal Report.
- Ambraseys, N.N., 2001. Reassessment of earthquakes, 1900–1999, in the Eastern Mediterranean and the Middle East, *Geophys. J. Int.*, **145**, 471–485.
- Ambraseys, N.N., 2002. The Seismic Activity of the Marmara Sea Region over the Last 2000 Years, *Bull. seism. Soc. Am.*, **92**(1), 1–18.
- Ambraseys, N.N. & Bilham, R., 2003. Reevaluated intensities for the great Assam earthquake of 12 June 1897, Shillong, India, *Bull. seism. Soc. Am.*, **93**, 665–673.
- Ambraseys, N. & Douglas, J., 2004. Magnitude calibration of Northern Indian earthquakes, *Geophys. J. Int.*, **159**, 165–206.
- Atkinson, G.M. & Wald, D.J., 2007. “Did you feel it?” Intensity data: a surprisingly good measure of earthquake ground motion, *Seismol. Res. Lett.*, **78**(3), 362–368.
- Azzaro, R., Barbano, M.S., D’Amico S. & Tuve, T., 2006. The attenuation of seismic intensity in the Etna region and comparison with other Italian volcanic districts, *Ann. Geophys.*, **49**(4/5), 1003–1005.
- Bakun, W.H., 1999. Seismic activity of the San Francisco Bay Region, *Bull. seism. Soc. Am.*, **89**(3), 764–784.
- Bakun, W.H., 2005. Magnitude and location of historical earthquakes in Japan and implications for the 1855 Ansei Edo Earthquake, *J. geophys. Res.*, **110**, B02304, doi:10.1029/2004JB003329.
- Bakun, W.H., 2006. Estimating locations and magnitudes of earthquakes in Southern California from modified Mercalli intensities, *Bull. seism. Soc. Am.*, **96**, 1278–1295.
- Bakun, W.H., 2010. Estimating epistemic uncertainty for historical earthquakes, in *Proceedings of the Seismological Society of America, Annual Meeting*, Portland, Oregon, 21–23 April, abstract, in press.
- Bakun, W.H. & Hopper, M.G., 2004. Magnitudes and locations of the 1811–1812 New Madrid, Missouri, and the 1886 Charleston, South Carolina, earthquakes, *Bull. seism. Soc. Am.*, **94**, 64–75.
- Bakun, W.H. & Scotti, O., 2006. Regional intensity attenuation models for France and the estimation of magnitude and location of historical earthquakes, *Geophys. J. Int.*, **164**, 596–610.
- Bakun, W.H. & Wentworth, C.M., 1997. Estimating earthquake location and magnitude from seismic intensity data, *Bull. seism. Soc. Am.*, **87**(6), 1502–1521.
- Bakun, W.H. & Wentworth, C.M., 1999. Erratum to Estimating earthquake location and magnitude from seismic intensity data, *Bull. seism. Soc. Am.*, **89**, 557.
- Beauval, C. & Scotti, O., 2003. Mapping b-values in France using two different magnitude ranges: possible non power-law behavior, *Geophys. Res. Lett.*, **30**(17), 1892, doi: 10.1029/2003GL017576.
- Beauval, C. & Scotti, O., 2004. Quantifying sensitivities of Probabilistic Seismic Hazard Assessment for France to earthquake catalogue uncertainties, truncation of ground-motion variability and magnitude limits, *Bull. seism. Soc. Am.*, **94**(5), 1579–1594.
- Centro Regional de Sismología para America del Sur (CERESIS), 1985. Proyecto SISRA (Programa para la mitigación de efectos de los Terremotos en la Región Andina)—Ecuador, *datos de hipocentros e intensidades*, **6**, 175.
- CMT (Global Centroid Moment tensor database) catalogue search, 2009. <http://www.seismology.harvard.edu/>, last accessed 2009 August.
- Choy, J.E., Palme, C., Guada, C., Morandi, M. & Klarica, S., 2010. Macro-seismic interpretation of the 1812 earthquakes in Venezuela using intensity uncertainties and a priori fault-strike information, *Bull. seism. Soc. Am.*, **100**(1), 241–255.
- Efron, B., 1982. The jackknife, the bootstrap and other resampling plans, in *Proceedings of the CBMS-NSF Regional Conference Series in Applied Mathematics*, Society for Industrial and Applied Mathematics, Philadelphia, 92 pp.
- Ego, F., Sébrier, M. & Yepes, H., 1995. Is the Cauca-Patia and Romeral Fault System left or rightlateral? *Geophys. Res. Lett.*, **22**(1), 33–36.
- Ego, F., Sébrier, M., Lavenu, A., Yepes H. & Egúez, A., 1996. Quaternary state of stress in the Northern Andes and the restraining bend model for the Ecuadorian Andes, *Tectonophysics*, **259**, 101–116.
- Egred, J., 2000. El terremoto de Riobamba, Ediciones Abya-Yala, Tomo 2, 107 pp.
- Egred, J., 2004. Terremoto de Riobamba del 4 de Febrero de 1797, in *Investigaciones en Geociencias*, Vol. 1, pp. 67–86, eds Alvarado, A., Garcia-Aristizabal, A., Mothes, P., Segovia, M., IRD, IG, Corporación Editora Nacional, Municipio del Distrito Metropolitano de Quito.
- Egred, J., 2009a. Terremotos del Ecuador, dos volumen, Escuela Politécnica Nacional, Instituto Geofísico, Internal Report.
- Egred, J., 2009b. Catalogo de terremotos del Ecuador 1541–2009, Escuela Politécnica Nacional, Instituto Geofísico, Internal Report.
- Egúez, A., Alvarado, A., Yepes, H., Machette, M.N., Costa, C. & Dart, R.L., 2003. Database and map of quaternary faults and folds of Ecuador and its offshore regions, USGS Open-File Report 03–289.
- Engdahl, E.R. & Villaseñor, A., 2002. Global Seismicity: 1900–1999, in *International Handbook of Earthquake and Engineering Seismology, Part A*, Chapter 41, pp. 665–690, eds Lee, W.H.K., Kanamori, H., Jennings, P.C. & Kisslinger, C., Academic Press.
- Engdahl, E.R., Van Der Hilst, R. & Buland, R., 1998. Global teleseismic earthquake relocation with improved travel times and procedures for depth determination, *Bull. seism. Soc. Am.*, **88**, 722–743.
- EPN, 1990. *Informe de actividades 1989–1990*, Instituto Geofísico, Quito, 92 pp.
- Espinosa, A.F., Hall, M.L. & Yepes, H., 1991a. Tectonics and seismicity, in *The March 5, 1987, Ecuador Earthquakes—Mass Wasting and Socioeconomic Effects. Natural Disaster Studies, National Academy of Sciences*, Vol. 5, pp. 29–41, ed. Schuster, R.L., National Academy Press, Washington, DC.
- Espinosa, A.F., Egred, J., García-López, M. & Crespo, E., 1991b. Intensity and damage distribution, in *The March 5, 1987, Ecuador Earthquakes—Mass Wasting and Socioeconomic Effects. Natural Disaster Studies, National Academy of Sciences*, Vol. 5, pp. 42–50, ed. Schuster, R.L., National Academy Press, Washington, DC.

- Esteve, L., 1968. Regionalización sísmica de México para fines de Ingeniería, *PhD thesis*. School of Engineering, National Autonomous University of Mexico (UNAM).
- Gajardo, E., Yepes, H., Ramon, P., Hall, P., Mothes P. & Aguilar, J., 2001. Evaluación del peligro sísmico para la ruta del OCP y evaluación complementaria del peligro volcánico, Escuela Politécnica Nacional, Instituto Geofísico, Internal Report.
- Gasparini, P., Bernardini, F., Valensise G. & Boschi, E., 1999. Defining seismic sources from historical earthquake felt reports, *Bull. seism. Soc. Am.*, **89**, 94–110.
- Gutenberg, B. & Richter, C.F., 1956. Earthquake magnitude, intensity, energy and acceleration, *Bull. seism. Soc. Am.*, **46**, 105–145.
- Hall, M.L. & Wood, C.A., 1985. Volcano-tectonic segmentation of the northern Andes, *Geology*, **13**, 203–207.
- Hinzen, K.-G. & Oemisch, M., 2001. Location and magnitude from seismic intensity data of recent and historic earthquakes in the Northern Rhine area, central Europe, *Bull. seism. Soc. Am.*, **91**, 40–56.
- Kawakatsu, H. & Proaño Cadena, G., 1991. Focal mechanisms of the March 6, 1987 Ecuador Earthquakes—CMT Inversion with a First Motion Constraint, *J. Phys. Earth.*, **39**, 589–597.
- Kellogg, J.N., Ogujiofor, I.J. & Kansaka, D.R., 1985. Cenozoic tectonics of the Panama and North Andes blocks, *Memorias—Congreso Latinoamericano de Geología* **6**, 34–49.
- Lavenu, A., Winter, T. & Dávila, F., 1995. A Plio-Quaternary compressional basin in the Interandean Depression, Central Ecuador, *Geophys. J. Int.*, **121**, 279–300.
- Musson, R.M.W. & Jiménez, M.-J., 2008. Macroseismic estimation of earthquake parameters. NERIES project report, Module NA4, Deliverable D3.
- McGuire, R.K., 2008. Probabilistic seismic hazard analysis: early history (a Review), *Earthq. Engng. Struct. Dyn.*, **37**, 329–338.
- Nieto, A.S., 1991. Mass wasting and flooding, in *The March 5, 1987, Ecuador Earthquakes—Mass Wasting and Socioeconomic Effects. Natural Disaster Studies, National Academy of Sciences*, Vol. 5, pp. 23–28, ed. Schuster, R.L., National Academy Press, Washington, DC.
- Parsons, T., 2004. Recalculated probability of  $M \geq 7$  earthquakes beneath the Sea of Marmara, Turkey, *J. geophys. Res.*, **109**, B05304, doi:10.1029/2003JB002667.
- Pasolini, C., Gasparini, P., Albarello, D., Lolli, B. & D'Amico, V., 2008. The attenuation of seismic intensity in Italy. Part I: theoretical and empirical backgrounds, *Bull. seism. Soc. Am.*, **98**, 682–691.
- Pennington, W.D., 1981. Subduction of the Eastern Panama Basin and Seismotectonics of Northwestern South America, *J. geophys. Res.*, **86**(B11), 10 753–10 770.
- Ramírez, E., 1951. El gran terremoto ecuatoriano de Pelileo, *Revista Academia Colombiana, Ciencias exactas, Físicas y naturales*, **8**, 126–136.
- Singaucho, J.-C., 2009. Mapa de máximas intensidades sísmicas del Ecuador. Criterios estructurales para mejorar la estimación de intensidades. Proyecto de Titulación, Facultad de Ingeniería Civil y Ambiental, Escuela Politécnica Nacional, 219 pp.
- Soulas, J-P., Ramón, P., Eguez, A., Alvarado, A., Yepes, H. & Gajardo, E., 2001. Evaluación de las fallas activas que cruzan el trazado del OCP, Instituto Geofísico, Escuela Politécnica Nacional, Internal Report (TECHINT LTD).
- Soulas, J.-P., Eguez, A., Yepes, H. & Perez, H., 1991. Tectónica activa y riesgo sísmico en los Andes Ecuatorianos y el extremo Sur de Colombia, *Bol. Geol. Ecuat.*, **2**(1), 3–11.
- Tibaldi, A., Rovida, A. & Corozzato, C., 2007. Late Quaternary kinematics, slip-rate and segmentation of a major Cordillera-Parallel transcurrent fault: the Cayambe-Afiladores-Sibundoy system, NW south America, *J. Struct. Geol.*, **29**(4), 664–680.
- Trenkamp, R., Kellogg, J.N., Freymueller, J.T. & Mora, H.P., 2002. Wide plate margin deformation, southern Central America and northwestern South America, CASA GPS observations, *J. S. Am. Earth Sci.*, **15**, 157–171.
- USGS/NEIC (United States Geological Survey/National Earthquake Information Center), 2009. Preliminary Determination of Epicentres (PDE) catalogue search, <http://earthquake.usgs.gov/regional/neck/>, last accessed August 2009.
- Wells, D.L. & Coppersmith, K.J., 1994. New empirical relationships among magnitude, rupture length, rupture width, rupture area, and surface displacement, *Bull. seism. Soc. Am.*, **84**, 974–1002.
- Winter, T., 1990. *Mécanismes des déformations récentes dans les Andes équatoriennes*, These Univ. Paris-Sud, Orsay, 205 pp.
- Woodward-Clyde Consultants, 1981. Investigations for the studies of seismic risk for the Agoyan dam site, Report for the Agoyan Hydroelectric project of the Instituto Ecuatoriano de Electrificación (INECEL), 85 pp.

#### SUPPORTING INFORMATION

Additional Supporting Information may be found in the online version of this article:

**Figure 6(c)**. Determination of magnitude and location for Pelileo historical event (1949,  $M_{G-R}$  6.8): (c) using intensities up to VIII. Instrumental location from Woodward-Clyde (1981). The uncertainty on the instrumental location is not known. PF and MuF are Pucara and Mundug faults (Table 6). See legend in Fig. 3.

**Figure 7(c)**. Determination of magnitude and location of Aloasi historical event (1976,  $M_{IC}$  = 5). See legend in Fig. 3.

**Figure 8(c)**. Determination of magnitude and location of Latacunga historical event (1958, MIC = 5). See legend in Fig. 3.

**Figure 14(c)**. Determination of magnitude and location for the Riobamba historical event (1797); (c) using intensities up to VIII. PFS is the Pallatanga fault system, PF is the Pucara fault, MuF is the Mundug fault (Table 6). See legend in Fig. 3.

Please note: Wiley-Blackwell are not responsible for the content or functionality of any supporting materials supplied by the authors. Any queries (other than missing material) should be directed to the corresponding author for the article.

## Appendix 2-Chapter 6: The scientific–community interface over the fifteen-year eruptive episode of Tungurahua Volcano, Ecuador

Mothes et al. *Journal of Applied Volcanology* (2015) 4:9  
DOI 10.1186/s13617-015-0025-y

 Journal of Applied Volcanology  
a SpringerOpen Journal

RESEARCH

Open Access

# The scientific–community interface over the fifteen-year eruptive episode of Tungurahua Volcano, Ecuador

Patricia A Mothes\*, Hugo A Yepes, Minard L Hall, Patricio A Ramón, Alexander L Steele and Mario C Ruiz

### Abstract

The successful handling of Tungurahua's frequent eruptions during 15 years via permanent instrumental monitoring and good community relations by the Instituto Geofísico of the Escuela Politécnica Nacional (IGEPN) is due to these factors: 1./ Instrumental monitoring of Tungurahua volcano by the IGEPN started a decade before the 1999 reactivation. In early 1999 increased background seismicity and high SO<sub>2</sub> readings suggested that magma was stirring. 2./ The long-term participation of IGEPN scientists in both monitoring and volcanic studies has fostered an institutional memory and a knowledge base that is referential for providing early warnings and in aiding the authorities to make critical decisions in anticipation of dangerous volcanic behavior. 3./ The permanent presence of IGEPN scientists at Tungurahua's Volcano Observatory (OVT) who oversee the monitoring operations and maintain close contact with the threatened community. 4./ Participation of volunteer volcano observers from the community (*vigías*) who convey their observations 24 hours/day via a pan-volcano UHF radio system.

Challenges to the operation's success include: identifying precursor geophysical signals before volcanic eruptions begin; financing OVT's operations and real-time instrumental surveillance; assuring active involvement of experienced scientists at OVT; instructing new rotating public officials in volcanic hazards and volcano crisis management, as well as working alongside them during critical moments; maintaining positive working relations with the community.

Here we report on volcano monitoring and risk reduction strategies that have served the IGEPN in a semi-rural environment, where ~30,000 people reside in high-risk zones. On reflection, we believe that our "bottom-up" approach has been effective and has merit. This approach developed gradually; our actions were in response to our instrumental monitoring activity of Tungurahua, providing credible information to the public and authorities and overcoming negative perceptions by the population. If there is a recipe, it is conditioned on good monitoring results and interpretation that is adequately and frequently communicated to those concerned, and over many years fostering a mutual trust among the actors. Some strategies described herein may not be pertinent at a volcano whose eruptive activity is short-lived.

**Keywords:** Tungurahua volcano; Early warnings before eruption; Volcano observatory; Scientific-community relations; Vulcanian eruptions; *Vigías*

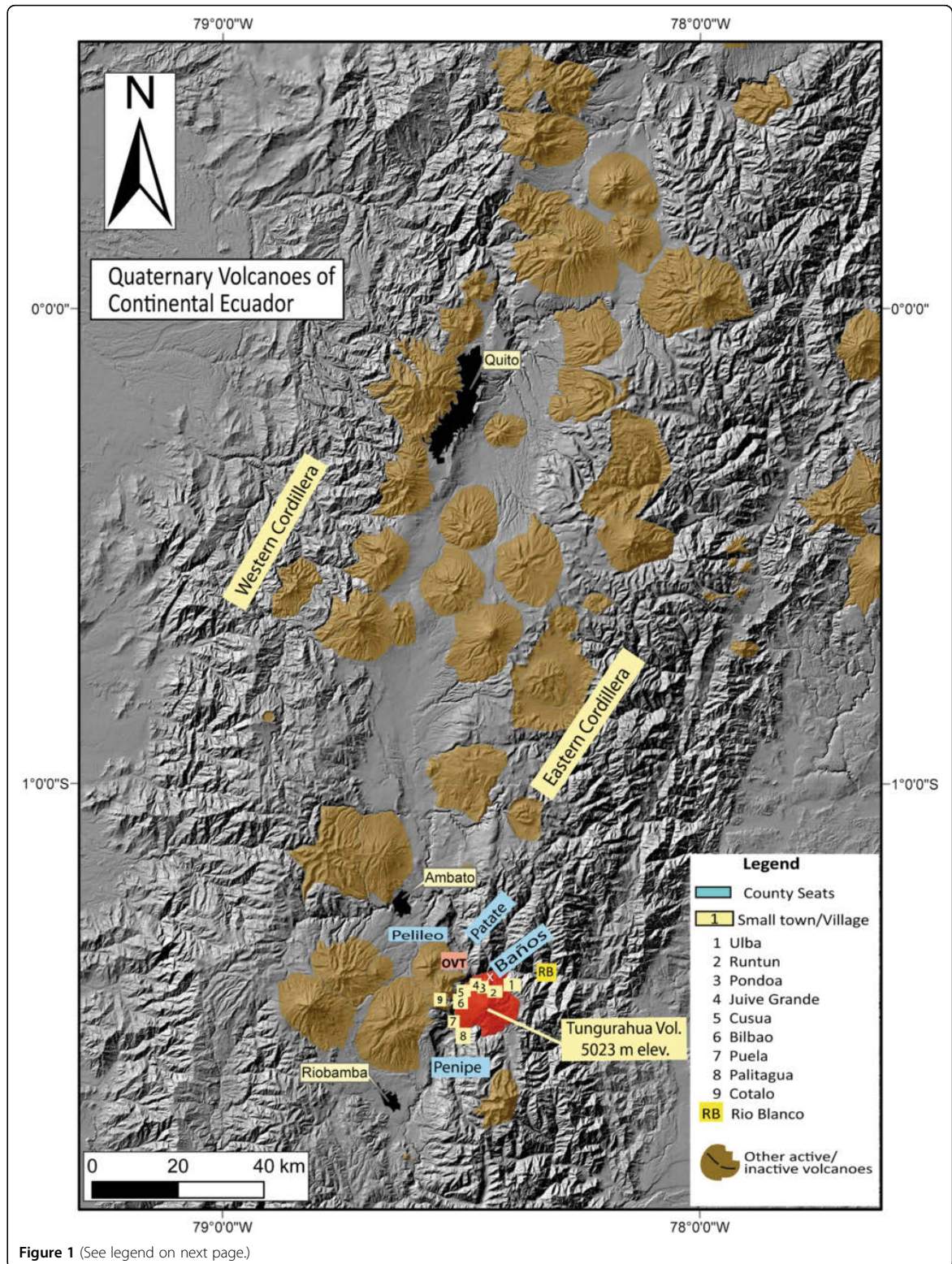
### Background

As described by Tobin and Whiteford (2002), after culmination of the 3 month-long forced evacuation of about 26,000 people in Baños and areas surrounding Tungurahua volcano in October, 1999, the affected population remained resentful and leery of scientists and their monitoring and hazard communication efforts. The local population openly blamed the volcano monitoring

scientists for this unfortunate situation. Such circumstances made it difficult over the next several years for IGEPN volcanologists to be fully accepted in the Baños area. Herein we describe the strategies the IGEPN embraced to change a negative situation, to one that is positive.

Tungurahua volcano (Latitude 01°28'S; Longitude 78° 27'W) is located in the southern portion of the Eastern Cordillera of the Ecuadorian Andes, 140 km south of Quito and 33 km southeast of Ambato, the capital of Tungurahua Province (Figure 1). The 5023-m-high active

\* Correspondence: pmothes@igepn.edu.ec  
Instituto Geofísico, Escuela Politécnica Nacional, Casilla 1701-2759, Quito, Ecuador



(See figure on previous page.)

**Figure 1 Map of most Quaternary volcanoes of continental Ecuador.** The two main cordilleras are highlighted– the Western and the Eastern, respectively. Tungurahua volcano is located near the southern end of the Eastern Cordillera. County seat cities mentioned in the text: Baños, Pelileo, Patate and Penipe are shown, as are smaller towns and villages and OVT. Modified from: Bernard, B and D. Andrade, 2012. "Volcanes Cuaternarios del Ecuador Continental". IGEPN internal publication, Quito- Ecuador.

stratovolcano is notable for its extreme relief of 3200 m, steep sides, and frequent eruptive cycles. Its 400-m-wide crater is situated slightly NW of Tungurahua’s summit with the lowest rim (at 4800 m) on its NW side, favoring spillage of pyroclastic and lava flows onto the upper NW and W flanks, and potentially lower down into the communities of Juive Grande, Cusúa and Bilbao, among others (Figures 1 and 2a and b).

The actual Tungurahua edifice is recent. After a catastrophic sector collapse of the previous cone some 3000 years ago, it has rebuilt itself at the same location with its current symmetrical shape (Hall et al. 1999). Important eruptive activity occurred between AD 1300 and 1700 (Le Pennec et al. 2008). Five major eruptive episodes are recognized in historical reports: 1641–46,

1773–81, 1886–88, 1916–18, and the present period. Andesitic lava flows, pyroclastic flows, ash falls, and secondary lahars characterize the volcano’s activity (Hall et al. 1999). Tungurahua is a dangerous volcano that threatens the tourist town of Baños (~20,000 residents; ≤ 50,000 on holidays) as well as small villages located around the base of the cone (Figures 1 and 2a, b).

Since 1999 the eruptive activity of Tungurahua volcano has varied between volcano explosivity index (VEI) levels of <1 to 3, generally allowing the continuance of tourism, agricultural, and other economic activities around the volcano’s edifice. On-off eruptive cycles occurring every 4–12 months have helped to maintain the attention of local and regional authorities and the population at large during this drawn-out eruptive process.

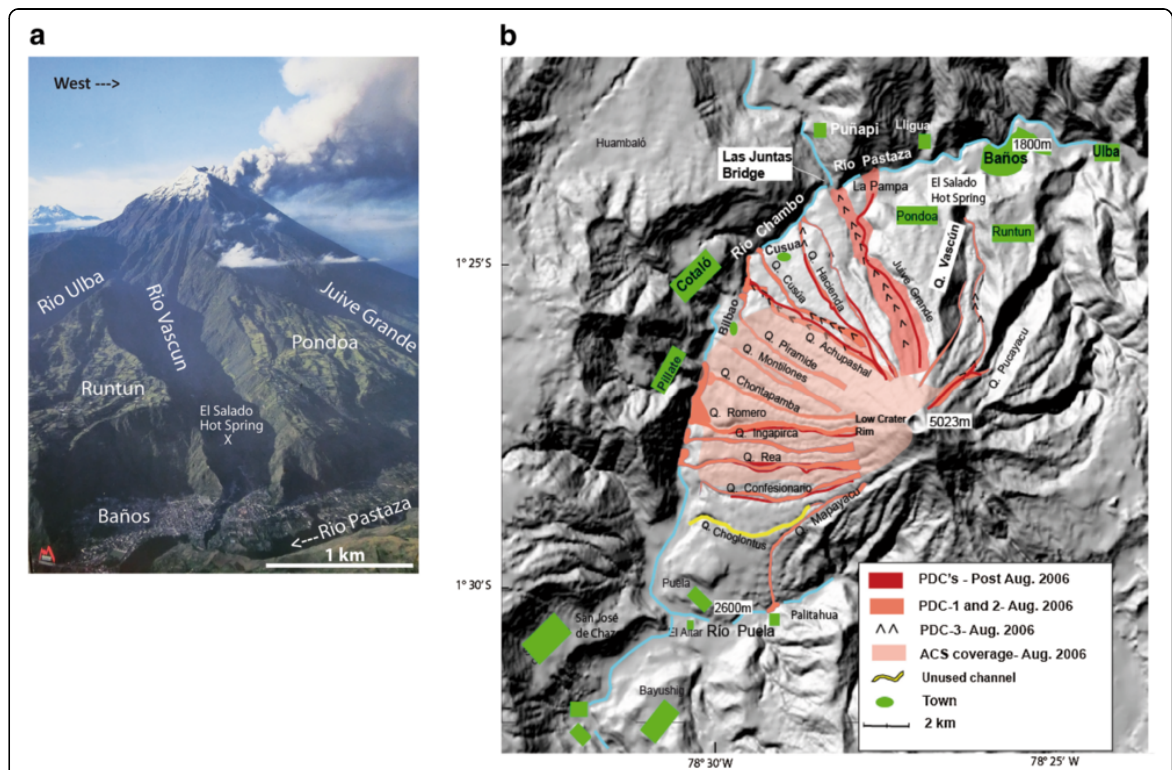


**Figure 2** Tungurahua volcano, location of Baños city and other communities and paths of the 2006 pyroclastic flows. **a:** Modified aerial photograph of Tungurahua volcano taken before the 2006 pyroclastic –flow forming eruptions. The tourist city of Baños is located at the northern foot of the cone, and partially on the fan of the Rio Vascun. The extreme relief between the summit and Baños is 3200 meters over a 7 km distance. Photo courtesy of Jorge Juan Anhalzer- Quito. **b:** Digital elevation map of the whole volcano showing all major quebradas on the north, west and SW flanks, pyroclastic flow paths of 2006 and post 2006, identified as pdcs in the legend, and ashcloud surge (ACS) of the same eruption, and main town and rivers.

From 1999 and to the present, eruptive activity has varied between intermittent periods of low to moderate Strombolian-style eruptive activity to notable Vulcanian and sub-Plinian events. In the first seven years the activity was mainly characterized by Strombolian episodes with frequent but small explosions, lava fountaining, and ejection of incandescent ballistics, sub-regional to regional ash falls, and rain-generated lahars (Leonard et al. 2005). However, no pyroclastic flows were produced in this 7 year period. Later, sub-Plinian eruptions on 17 August 2006 generated sizeable pyroclastic flows (40 Mm<sup>3</sup>, bulk volume) (Hall et al. 2013) (Figure 2b). During these eruptions and subsequently, Vulcanian-like explosive outbursts accompanied the most intense Strombolian eruptions and were characterized by powerful infrasound signals and audible booms during paroxysmal phases (Ruiz et al. 2006; Hall et al. 2013). From May 2010 to present, activity has been interspersed by Vulcanian-style eruptive outbursts of varying intensity, often producing explosions with high infrasound values as well as small-volume pyroclastic flows, some which reached the volcano's base (Figure 2b).

Since September, 1999 the IGEPN has maintained a permanently-staffed observatory (OVT) located 13 km NNW of the crater and at its principal office in the Escuela Politécnica Nacional, Quito, where it has operated 24 hours a day, 7 days a week. Continual monitoring of Tungurahua employs collocated seismic and infrasound instruments (short period and broadband), SO<sub>2</sub> gas emission detection (COSPEC and DOAS) and geodetic methods (EDM, tiltmeters, GPS and occasionally InSAR). In addition, thermal imagery (airborne and ground-based) during the past 10 years has proven to be invaluable for nighttime and foggy observations. Available satellite information is also used in the visible, infrared and radar ranges for the detection of ash plumes, hot spots, and thermal anomalies, and to measure SO<sub>2</sub> concentrations in the atmosphere and to obtain radar interferograms (InSAR). IGEPN uses twelve acoustic-flow-monitoring stations (AFM) (Hadley and LaHusen 1995) to detect and register secondary lahar activity (Figure 3). Lahars are frequently generated by the remobilization of loose volcanoclastics by rainfall on the cone's steep slopes; they are the most commonly occurring hazard and they affect the main roads that circumvent the volcano and also some infrastructure. During the 15 year eruptive episode more than 800 lahars have been registered by the AFM monitoring system, often resulting in lahar warnings issued to the public from OVT (Mothes and Vallance 2015).

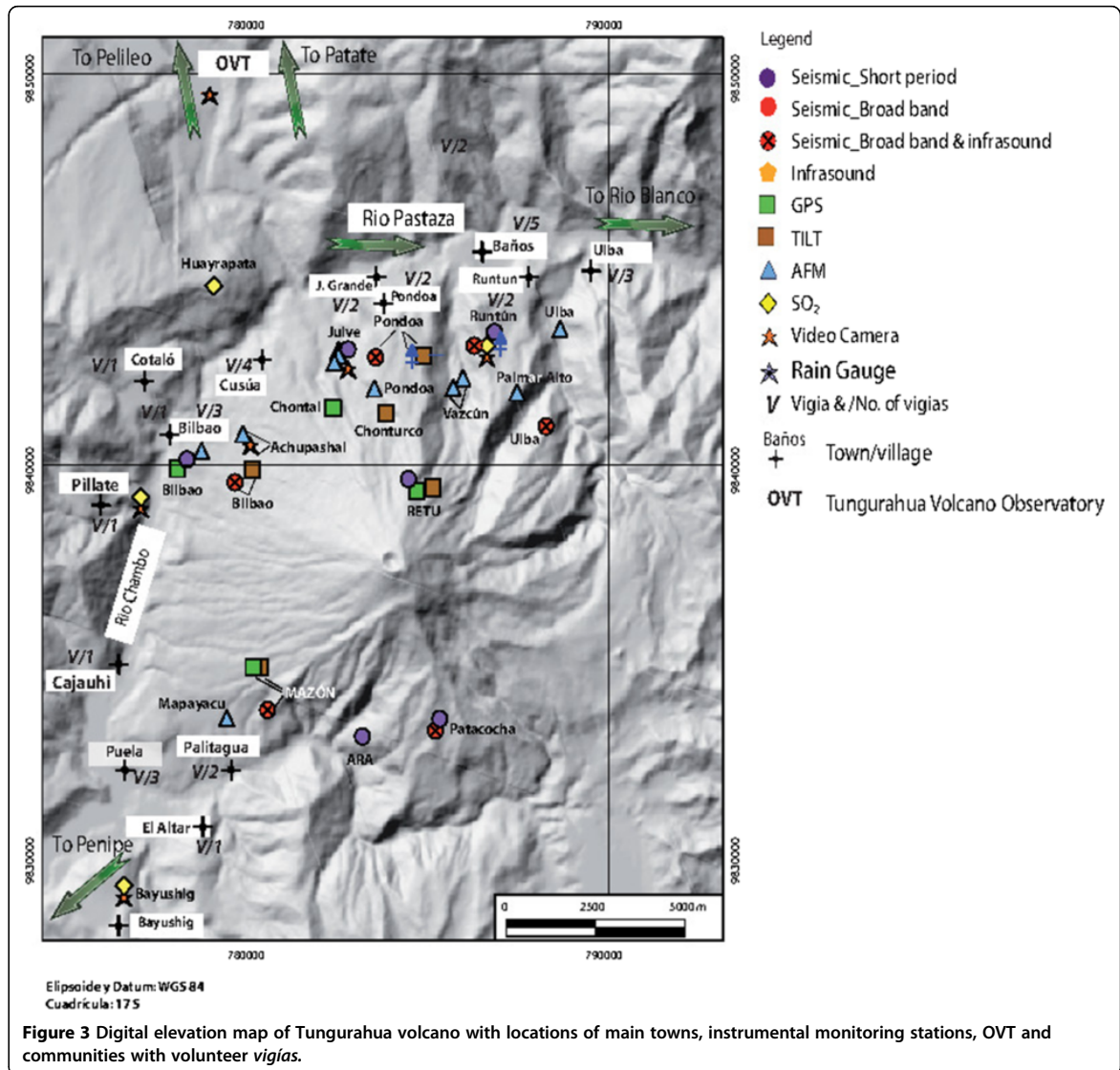
### **Methods: inputs for the IGEPN's monitoring and communication strategies**

#### **The importance of IGEPN's local observatory, OVT**

The strong onset of Tungurahua's unrest in September 1999 required that a local observatory be established.

The generous loan of a *hacienda* farmhouse 13 km NW of the volcano, provided an ideal line-of-sight view of the volcano (Figure 3). The *Observatorio del Volcán Tungurahua*, OVT, is staffed by a senior scientist and an assistant on rotating shifts of eight days, thus satisfying the need to have a sustained local scientific presence which greatly facilitates rapid recognition of changes on the volcano and in managing developing situations, if necessary. These two individuals record visual and audible activity, foster and evaluate incoming signals from the volcano's monitoring network, provide support to national and international scientists and students conducting fieldwork on the volcano, participate in meetings at the local and provincial level, communicate with the populace at large, give interviews for radio and TV stations and to the press, and provide frequent verbal updates about the volcanic activity over the regional UHF radio system. They also perform data collection from thermal springs, gas measurements with mini-DOAS, and make observations and sampling of fresh ash and lahar deposits. Observations made by the local volcano observers, *vigías*, reporting to OVT over the radio system, are recorded at all hours. During the months-long intervals of relative quiescence between strong eruptive periods, activities at OVT are in a lull and the demands are lower. Generally OVT scientists can catch up on field work, academic obligations, and perform upkeep of the monitoring network around the volcano.

During the eruptive period from 1999 to early 2006, the permanent presence of IGEPN scientists at the volcano assured people that the volcano was being monitored full time. Nonetheless this volcano monitoring service wasn't exempt from risk. In 2000 several of Baños' hotel owners blamed the OVT and IGEPN scientists for lack of tourist visitation to their facilities, proclaiming that excessive information about the volcano's behavior was being shown in the media and tourists were canceling their hotel reservations in Baños. Their hostile attitudes were perhaps a lingering response to the evacuation in 16 October 1999 to January 5, 2000, when all Baños' hotels closed, thus causing a local economic crisis (Lane et al. 2003). At the most critical moment some hotel owners threatened to chase out OVT scientists with *machetes* and even to set the observatory on fire! Eventually the difficulties were worked out and faded with time, mostly because the OVT personal began giving weekly live interviews on a Baños radio station in which the townspeople heard updates of the volcano's status and a daily interpretation of monitoring data. Many talks were also given to communities about the nature and benefits of volcano monitoring and trends in the eruptive process; some talks were done under the auspicious of a European Community-funded DIPECHO project, which at that time was involved in ameliorating social issues in



the affected areas to the west of the cone. Local people also became accustomed to the permanent presence of the IGEPN scientists in the area, eventually perceiving OVT operations and its mission as a benefit to their overall security. Meanwhile, the economic base improved around Baños and tourists again filled the hotels, even though the volcano remained active and the IGEPN continued normal reporting (Sword-Daniels et al. 2011).

Compared with the basic setup of fifteen years ago, the monitoring network in 2015 is considerably more robust. OVT relies on broad band (BB) and short period seismic networks and also infrasound sensors linked to the BB stations (Kumagai et al. 2010). Telemetered

electronic tiltmeters, continuous GPS stations, continuously recording video and thermal cameras, more lahar monitors and four telemetered SO<sub>2</sub> detection systems (DOAS) have greatly improved the IGEPN's capacity to provide better prognosis before eruptive activity's onset (Figure 3). Also, during eruptions a 25 station ash-collection network is used to evaluate rates of ash accumulation and volumes (Bernard et al. 2013).

**The social/political network around the volcano**

Since the onset of Tungurahua's eruptive activity the IGEPN has maintained broad working relationships with mayors, governors and other popularly-elected officials,

as well as central government-designated public servants and civil defense personnel. Elected public servants generally serve for 4 years. Between 1999 and 2006 risk management before and during natural hazard events was carried out by the Ecuadorian Civil Defense through personal in their local, provincial and national offices. Subsequently, after 2006 the newly formed National Secretary of Risk Management (SNGR) became the main coordinating entity charged with risk mitigation in the face of floods, landslides, volcanic and seismic activity. Since early 2014, each county throughout the country is required to designate a risk management coordinator whose job is to prepare local citizens before events of adverse nature and also to coordinate mitigating actions at the county level. The SNGR of the national government interacts with the governors of each province, overseeing the coordination of activities between county and provincial officials. Overall this setup has enabled the IGEPN to provide rapid and frequent briefings to authorities concerning increases in pre-eruption signals and to help them to make critical decisions before major eruptive events. Baños did not have evacuation plans prior to the reactivation of the volcano in 1999, nor when the city and high-risk areas around the volcano were forcefully evacuated for three months starting on 16 October, 1999, at which time the Ecuadorian military handled all procedures. The forced and prolonged evacuation of 26,000 residents generated deep resentment in the affected citizens and huge economic losses. They fully blamed the IGEPN for the actions taken, even though we had not made the decisions to evacuate them or keep them away from their homes and livelihoods for 3 months (Tobin and Whiteford 2002). It took years to overcome these accusations and part of the IGEPN's response was to develop positive interactions with the local community (Leonard et al. 2005).

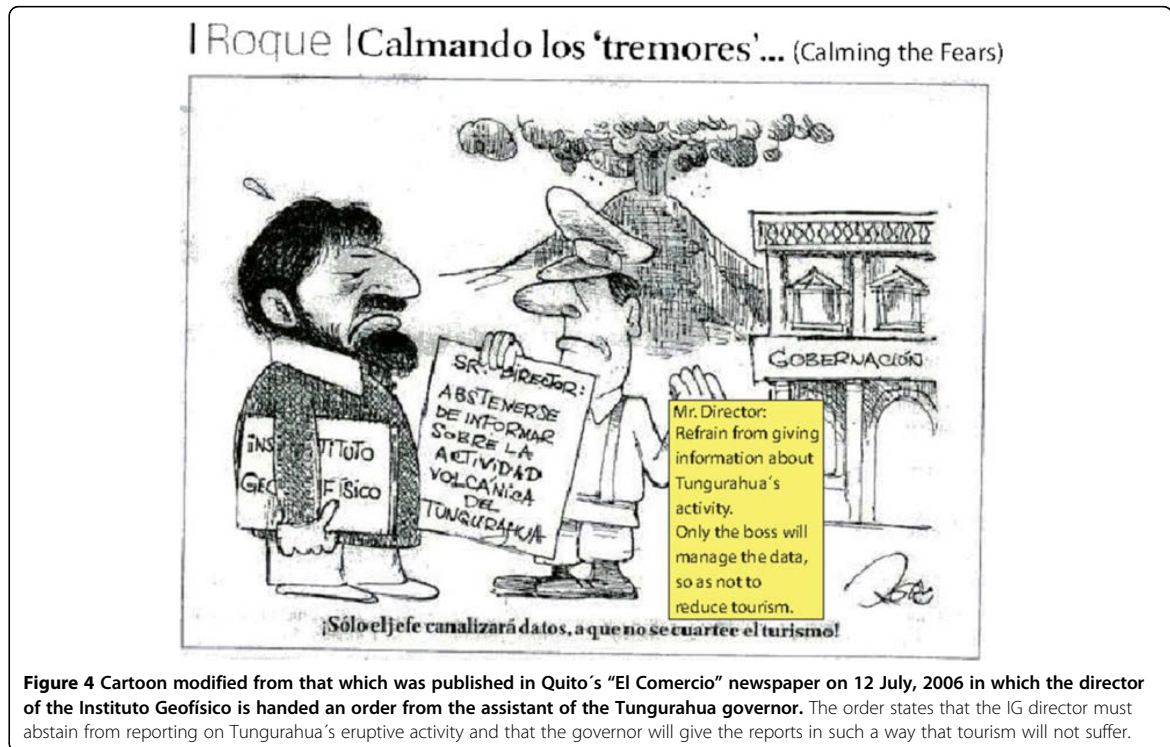
But evacuation plans existed and were used to evacuate Baños during the paroxysmal stage of the 17 August 2006 sub-Plinian eruption. In this instance, given the volcano's strong, overwhelming superficial manifestations, the townspeople willingly evacuated to safe zones. Subsequently, no other broad evacuations have occurred, however smaller village-specific evacuations have occurred before heightened eruptive activity in May 2010 and February, 2014. Also, in most cases when activity ramps up, members of the communities of Cusúa and Bilbao sleep in safe zones, and return in the morning to do chores.

Some officials are willing to act on pre-eruptive advisories from IGEPN scientists, while others are more reluctant to act due to the pressure from local hotel and tourist interests, again, particularly in Baños. Two cases illustrate these circumstances. Days before the 14 July 2006 eruption, the governor of Tungurahua province demanded in a written statement that the IGEPN desist

from reporting about the volcano's condition, claiming that it was chasing tourism away from Baños. He proclaimed that from then on he personally would be fielding all responses to inquiries from members of the press, local and national officials, and the population at large about the volcano's activity (Figure 4). At this time daily and special reports were being prepared at the IGEPN and sent out to 560 recipients via fax and internet, and up to 10 interviews with the media were granted daily from OVT and the Quito office. The IGEPN respectfully obeyed the written order and smartly redirected telephone calls and requests for scientific information and interviews to the governor's office and personal phones, so that he could explain to all concerned the rapidly evolving state of the volcano on a 24/7 basis. His readiness to take on this task quickly waned when he recognized his shortcomings to credibly answer questions about the volcano's heightened state of restlessness and in perceiving the constant and extraordinary social pressure to provide immediate and reliable scientific information. Within 24 hours, via a second written order, the governor reinstated the IGEPN's communication responsibilities, barely two days before the 14 July 2006 (VEI = 2) eruption.

A month later, on the morning of the 16<sup>th</sup> of August 2006, about 14 hours before onset of Tungurahua's largest eruption since 1918, amidst unceasing high-decibel explosions and continually felt vibrations throughout the region— due to low frequency volcanic tremor accompanying magma ascent, the principal authority of Baños was unreachable by telephone or radio at 10 am when the IGEPN director called to advise/warn him that a large eruption was believed to be imminent and that certain areas could be overrun by pyroclastic flows. Fortunately the local civil defense chief took responsibility and made the decisions to evacuate people from several threatened villages and Baños city before the paroxysmal finale at about 00H30 (local time) on August 17<sup>th</sup> (Hall et al. 2013). There were no serious casualties in Baños county, although about 60 homes were overrun and scorched by pyroclastic flows, particularly in the Juive Grande sector, where thankfully the residents had responded to the alert and were not injured. The hydroelectric facility of Agoyan (156 MW), 3 km downriver from Baños, also responded successfully to OVT's early warnings and their engineers carried out the company's emergency plans to close the intake tunnel to the turbines, thus avoiding damage to the turbines from severe abrasion or blockage by fresh volcanic products; they also opened the dam's floodgates to permit the flow-through of dense materials. A few days later after a general revision and filling of the reservoir, the facility was again operating normally.

The mayors of the neighboring counties of Penipe and Pelileo with their communities of Bilbao, Puela and



Cusúa, situated around the volcano's flanks, also had their roles to play during the ramping up to the 17<sup>th</sup> August eruption. On the evening of the 16<sup>th</sup> the mayor of Pelileo came to OVT to give a verbal order over the radio system that residents of Cusúa and other communities of his county must evacuate. Also, the mayor of Penipe personally drove around the villages of Puela and Palitagua beseeching the citizens to evacuate before the major eruption. Unfortunately, five people didn't heed the warnings and died in Palitagua due to descending pyroclastic flows. Another short-coming in Penipe county was the lack of coverage of the pan-volcano radio system, impeding a free-flow of critical information to this sector from both OVT and other actors during the crisis. Additionally, given the delays to get people motivated to leave their endangered properties, about 50 head of livestock, some grazing on the upper flanks of the volcano, perished from burns or asphyxiation. Decimeter-size ballistics fell out to 8 km, injuring people and livestock (Arellano et al. 2008). People living to the west and southwest of the cone—such as in the Cotaló area, and who stayed inside their homes, reported huddling beneath wooden tables to avoid impacts while the ballistics crashed through their roofs.

**The Vigía network and OVT— a collaborative effort**  
*Vigía*, a Spanish word for somebody who is watching and alert, describes the volunteer efforts of 25 mostly rural-based people who keep the IGEPN informed of happenings in the sector where they live and work around the volcano. As Stone et al. (2014) explained, the *vigía* network is a prime example of community-based monitoring that contributes to the strengthening of the whole operation. Since scientists at OVT can only observe the volcano's N and NW flanks, beginning in 2000 farmers living in other sectors of the volcano were asked by OVT staff and Civil Defense leaders to daily report the volcanic activity that they observed from their locations. This system was established with the help of the Tungurahua province Civil Defense director and his collaborators in order to further open lines of communication over all sectors of the volcano that were being affected by the eruption process. *Vigías* were chosen based upon their observational skills and the proximity of their homes to certain sectors of the volcano or to active lahar-frequented ravines—*quebradas*. They use hand-held radios that pertain to the local UHF network now operated by the SNGR. Verbal messages given by *vigías* are received around the clock at OVT and recorded in a logbook and corroborated with the IGEPN's

monitoring data. The area covered by the *vigía's* communication network includes the southern part of the volcano in Penipe county, the western flanks of the cone that comprise part of Pelileo county, the Baños area, and the communities of Pondoá and Runtun, above Baños and Ulba (Figure 3) (Stone et al. 2014). Reporting by *vigías* of the descent of secondary lahars after heavy rains or snow has been very successful and has contributed to the hastening of the closure of roads before vehicles get stuck or buried in lahars. One notable lahar in February 2005 was provoked by a local electrical storm and sent a wall of water and debris into the El Salado hot spring facility located in the Vascún *Quebrada*, one km upslope of Baños. The vibrations made by the descending lahar caused a notable jump in the data values of the AFM station in that quebrada. This combination strongly suggesting that a lahar of substantial volume ( $100 \text{ m}^3/\text{s}$ ) was in transit. Thanks to the alertness of OVT scientists and their immediate communication of this dangerous situation to Baños Civil Defense authorities and the mayor, plus timely reporting by several *vigías*, 13 bathers were rescued before the deadly lahar inundated the thermal pools where they were relaxing (Mothes and Vallance 2015; Williams et al. 2008).

Since most *vigías* have lived with the volcano for many years and are dedicated to agricultural activities and attending to livestock living on the high slopes, they know well their immediate surroundings and are quick to observe anomalous behavior. Their observations offer pertinent and dependable information regarding activity on the upper slopes of the cone; for example, the type of ash fall—lithic or scoria, ash color and grain size, intensity of rainfall and its persistence, the descent of lahars and their texture or the directions taken by ash fall columns and incandescent flows. Many times the information provided by *vigías* closely matches patterns of seismic and infrasound data. A visual confirmation sent over the radio to OVT, for example, about the descent of a pyroclastic flow or the increase in lahar activity in one of the many *quebradas* draining the volcano, is a welcome compliment to the instrumental monitoring data. Nightly at 8 pm a radio broadcast (*ronda*) is hosted in which each *vigía* reports observations concerning the volcano from his/her sector, and any other pertinent news. OVT personal record the observations of the *vigías* and then give an oral summation of the day's seismic and other instrumental recordings of events on the volcano and in the region.

OVT co-hosts an annual meeting/luncheon for *vigías*, key local officials, and OVT personal with the aim of sharing observational criteria, giving an annual scientific report on the overall trend of the volcano's activity, and maintaining collegial collaborative ties. Many *vigías* who live on opposite sides of the volcano might only see each

other at these special events, although they all participate in the nightly radio *rondas* and recognize each other's voices. The annual meeting thus serves to fortify this volunteer network and keep all involved interested in participating and being attentive when an eruption period is approaching.

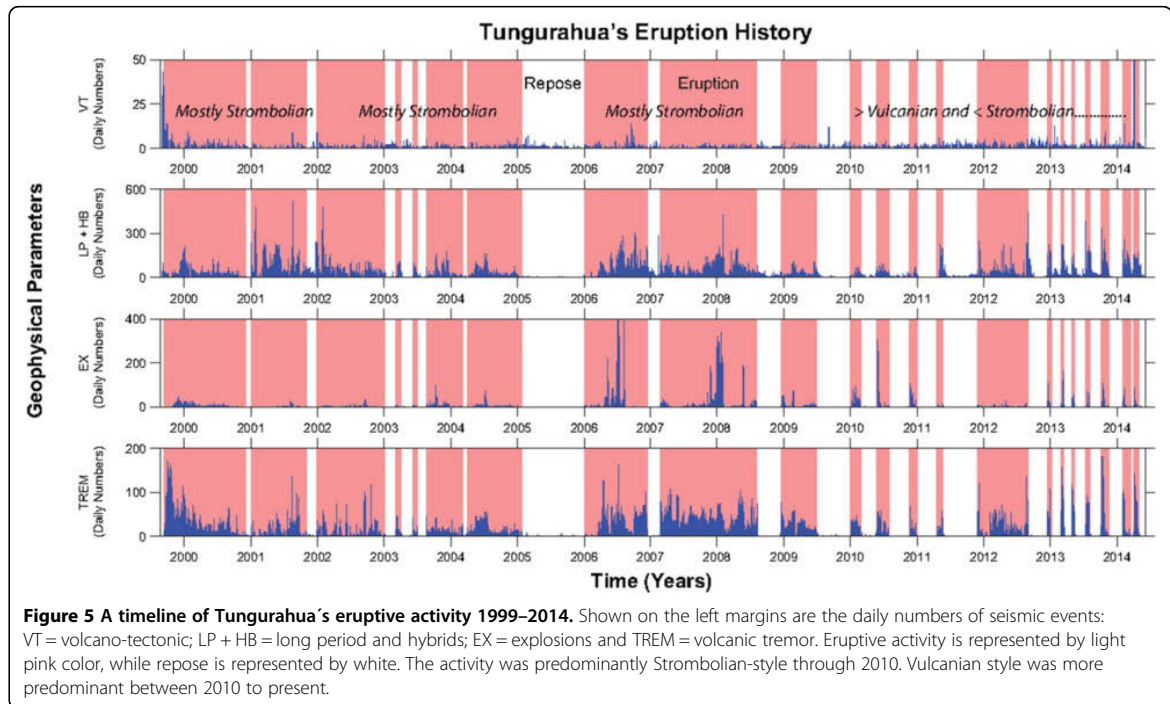
At the last two *vigía* meetings, all *vigías* verbally shared their observations of recent activity, but they also drew out on paper event time-lines that transpired in their sector during important eruptive periods and what actions they took to benefit their community. This activity fortified their collective memory. OVT personal keep *vigías* informed about scientific evaluations of the ongoing eruptive process. Special events planned for the future include discussions about strategies for fostering successful care of livestock during continual ashfall. Local university researchers will provide the know-how along with the experience of the *vigías* in handling their own livestock during multiple ashfall events.

*Vigías* also assist with the installation of IGEPN monitoring stations, cleaning ash and vegetation off solar panels, and the overall caretaking of monitoring infrastructure. At Tungurahua there have been few robberies of monitoring equipment, perhaps because people perceive that it is to their benefit that the instrumentation keeps working, but they also know that a *vigía* is attentive to the instrument's well-being. Through the years the *vigías* have become more fortified in their community leadership skills. This is because many of them have had to act responsibly during evacuations of their community when dangerous eruptive activity begins. Secondly, they are people with knowledge of how their community has dealt with the eruptive processes and they have perspective on what actions might have to be taken in the future in benefit of their community members.

## Results and discussion

### Challenges to providing early warnings before Vulcanian-style eruptions

From the onset of eruptive activity in 1999 to the August eruptions in 2006 the activity can be categorized as mainly Strombolian style (Figure 5) (Arellano et al. 2008; Hidalgo et al. 2014). This means that the vent is predominantly open and high gas pressures don't accumulate, rather the activity has a rhythmic continuum of pyroclast ejections and the eruptions tend to be long-standing (Vergnolle and Mangan 2000). Typically Tungurahua's eruptive periods commence with an increased number of low-frequency earthquakes that begin to produce mild explosions with moderate infrasound characteristics. With greater conduit opening, the lava fountains jet out of the crater and continuous roiling sounds are heard. Ash falls associated with low-level lava fountaining often continues for days and covers agricultural lands to the west with black scoriaceous



and lithic ash mantles. Notable ash fallout occurred in late 1999 and in August, 2001 (Eychenne et al. 2012). These events however did not produce pyroclastic or lava flows, and the limited ballistic trajectories kept bomb/block impacts high on the volcano's upper slopes.

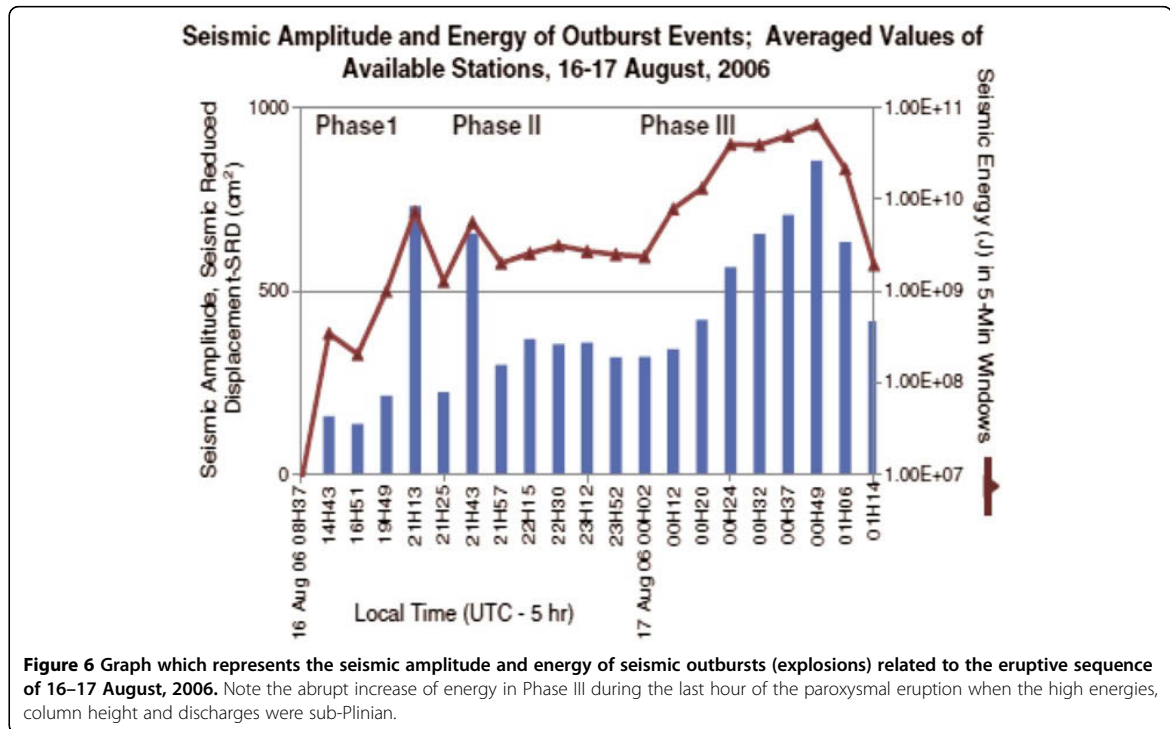
In contrast, the end of the 17 August 2006 eruption was associated with the rapid ascent of a large volume of gas-rich magma (Samaniego et al. 2011) that generated pyroclastic flows that descended most *quebradas* on the volcano's west side, as well as the Pucayacu and Vazcún *quebradas* above Baños (Kelfoun et al. 2009), and overran Palitagua village on the south flank, where five residents died who had not heeded warnings to evacuate (Ramón 2010; Hall et al. 2013). A total bulk volume of almost 0.1 km<sup>3</sup> of pyroclastic flow debris and airfall tephra was erupted (Hall et al. 2013). The last phase (Phase III) of the eruption had large Vulcanian-like outbursts and was notably more energetic than the earlier phases of eruptive activity (Figure 6) (Arellano and Hall 2007). The eruptive column rose 17 km above the volcano's summit (Steffke et al. 2010). Following the mid-2006 eruptions and continuing through April 2010, Strombolian-style eruptions occurred about every six months and lasted about six weeks; subsequently the volcano settled into repose.

Starting on 28 May 2010, however, another large Vulcanian-style eruption began. Its rapid onset, limited open-vent eruptive activity prior to the main explosion,

its loud audible characteristics, and the threat of pyroclastic flows and a broader ballistic distribution, made this event and subsequent Vulcanian events truly dangerous to local residents. Since the May 2010 event, six other Vulcanian-style eruptive episodes have occurred and have been interspersed with Strombolian-style activity (Table 1 and Figure 5). In general the Vulcanian-style eruptions are small to moderate-size, discrete explosive outbursts that last seconds to minutes. Nonetheless, the Vulcanian explosion recorded on 14 July 2013, had the highest seismic or acoustic energies ever recorded at Tungurahua (Table 1). A Vulcanian explosion occurs when an accumulation of magmatic gases beneath a sealed conduit plug or dome attains high overpressures that cause brittle failure of the impermeable plug and produces a discrete eruption in which the gases, clasts, and juvenile products are violently released (Morrissey and Mastin 2000; Clark 2013). After the initial conduit opening, Plinian and sub-Plinian eruptions with juvenile products may follow. Vulcanian eruptions typically emit volumes <0.1 km<sup>3</sup> of dense rock equivalent (DRE) (Morrissey and Mastin 2000).

Nonetheless, Strombolian-style activity briefly returned to Tungurahua in 2011 and the eruptions produced approximately 3.2 Mm<sup>3</sup> of magma (DRE), of which about 3.0 Mm<sup>3</sup> was new magma, as interpreted from deformation patterns at the highest tilt stations (Ruiz et al. 2012).

In most cases Vulcanian explosive events at Tungurahua were preceded by a marked brief increase in LP



seismic events—a swarm typically occurs a few days to several hours prior to the eruption. Other precursors include strong deformation signals registered by electronic tiltmeters several weeks prior to the eruption, especially at the station closest to the conduit (RETU) (Figure 3), and a decrease in the SO<sub>2</sub> values registered by the DOAS instrumentation.

**Early warning given before major Vulcanian eruption on 1 February 2014**

Early warnings before Vulcanian eruptions are often hard to provide because of the sudden onset of this style of eruption and the subtleness of precursors (Gottsmann et al. 2011). Nonetheless, there is a growing literature that reports on important ground deformation before such eruptions (Iguchi et al. 2008; Yamazaki et al. 2013).

Before Tungurahua’s Vulcanian eruption of 1 February 2014, the geophysical data patterns suggested that an eruption was imminent. Although seismic signals during the previous week had been relatively minor, a strong inflationary pattern registered by the electronic tiltmeter station at 4000 m elevation implied that internal pressures were building beneath a rocky plug in the volcano’s conduit (Figure 7). A marked shift in seismicity was observed 36 hours prior to the disruption of the conduit’s plug by the three principal explosions of the 1 February 2014 eruption. A swarm of long-period seismic events and continual high-amplitude tremor heralded the run-

away energy release that took place in this event (Figure 8). The 36 hr-long window of restlessness prior to the main eruption permitted the IGEPN to prepare special advisories that “a major eruption would likely occur in a short time frame (hours to days)” for the local, provincial and national authorities and the local populace. The internet, social media, phone calls, the *vigía* radio system, and reports on radio and television were all used to get the message out. Use of the UHF radio system at OVT was also fundamental to insure immediate updates of the ongoing activity. As the seismic swarms became more continuous and seismic and acoustic energy levels rose, another formal verbal report was issued by OVT scientists over the *vigía* radio system that an eruption was imminent two hours before the eruption. Accordingly, SNGR personal and the *vigías* advised people in their villages via loud speakers of the severity of the situation and most residents opted to self-evacuate. Military trucks and SNGR personal helped with the mobilization. Many of the farmers living on the threatened western slopes of the volcano have optional government-built housing at La Paz (a *barrio* of Pelileo) and Rio Blanco (east of Baños) and in Penipe town, where they and their families can spend the night. Each morning they return home and assess the damage to their property and crops, if any, and tend to livestock, which may be still grazing in the high hazard zone.

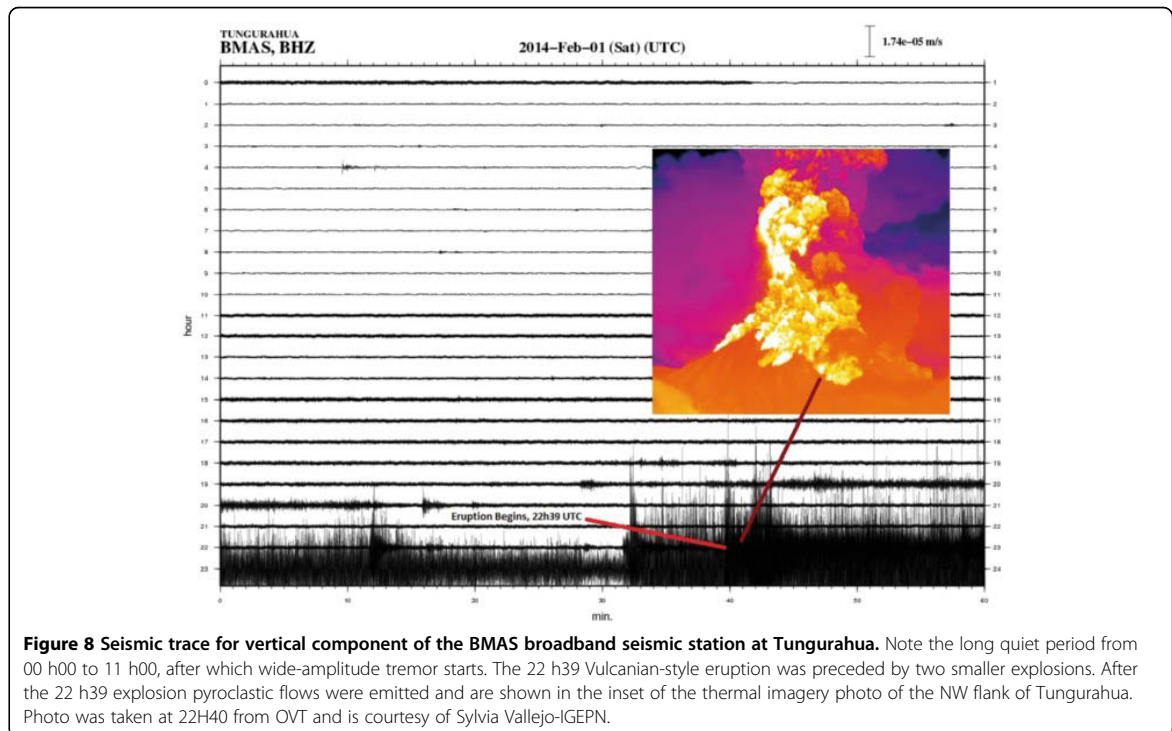
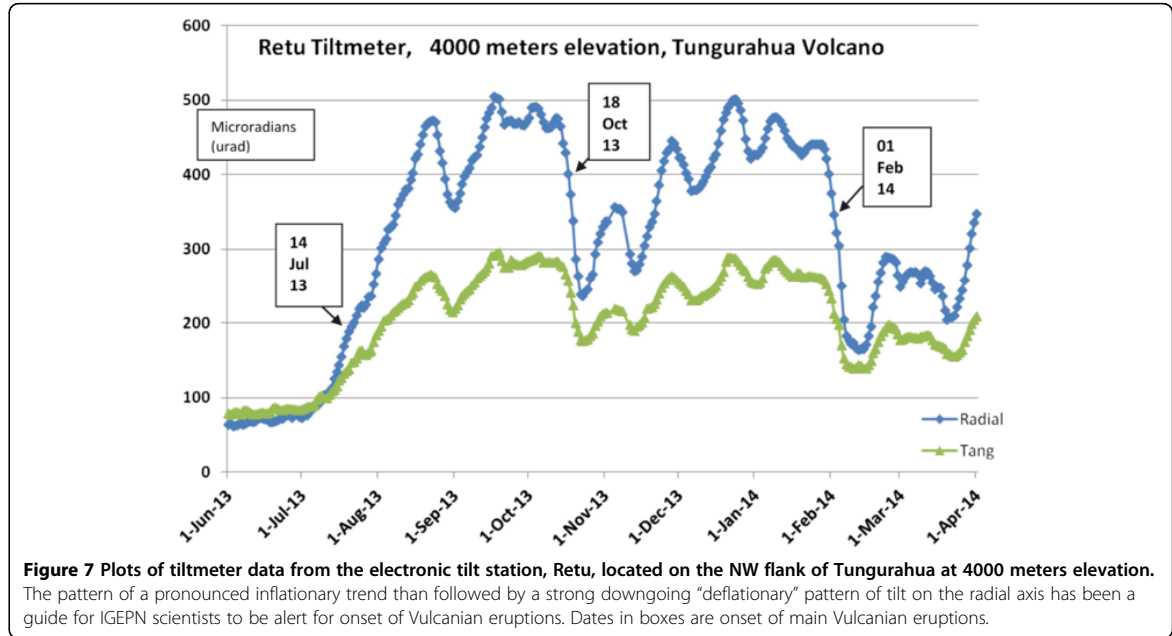
**Table 1 Registry of Vulcanian-style eruptions of Tungurahua volcano and their characteristics**

No	Date/Time (UTC)	Seismic and Audible Characteristics Of Vulcanian Explosions	Pf's and channels used	Hrs. of Advance Warning	Comments
1	28-05-2010; 11:13	Huge Explosion; N-shaped infrasound (IS) waveform. High seismic to acoustic ratio (low VASR).  <i>6.91E + 08 = Average Seismic Energy (Joules)*</i> <i>1.04E + 10 = Average Acoustic Energy (Joules)*</i>	Yes, Achupashal	None	Occurred after approximately 3 months of repose. It was the uncorking of the volcanic system after some period of pressure build up
2	21-08-2012; 15:52	Explosion; Sharp N-shaped IS signals are not consistent across the network  <i>2.85E + 08 = Average Seismic Energy (Joules)</i> <i>9.36E + 10 = Average Acoustic Energy (Joules)</i>	No	?	Occurred during a peak period in volcanic activity (one of the peak days of the eruptive phase), after a building of activity during the preceding days.
3	14-12-2012; 19:36	Huge Explosion; Sharp N-shaped IS signals. Compressional first seismic motions.  <i>1.33E + 08 = Average Seismic Energy (Joules)</i> <i>5.17E + 10 = Average Acoustic Energy (Joules)</i>	Yes, Mapayacu- SW flank.	6 hr. OVT staff recognized jump in activity.	Most of the energy of main event was released within the first 1 seconds and nearly all energy in the first 5 seconds.
4	16-12-2012; 10:53	Moderate Explosion; Emergent compressional seismic onset. Small, P-wave – not particularly clear.  <i>7.09E + 08 = Average Seismic Energy (Joules)</i> <i>4.79E + 10 = Average Acoustic Energy (Joules)</i>	No	None	Similar to activity on the 28th May 2010. The first explosion of this new phase of activity recorded on the 14 December 2012 had partially opened the conduit and vent.
5	14-07-2013; 11:46	Huge Explosion, very strong shock wave. Waveform structure is not of an expected and simple 'N-shape' despite shockwave presence, but instead comprises a more complex sequence.  <i>1.93E + 09 = Average Seismic Energy (Joules)</i> <i>3.20E + 11 = Average Acoustic Energy (Joules)</i>	Yes. Achupashal and others to the south; pf's arrived to Chambo river.	Yes, 1 Hr.	This was the largest discrete explosion recorded at Tungurahua since BB seismic and infrasound monitoring began in July 2006.
6	18-10-2013; 14:26	Moderate explosion.  <i>1.91E + 08 = Average Seismic Energy (Joules)</i> <i>2.60E + 10 = Average Acoustic Energy (Joules)</i>	Yes, Achupashal Alto.	Yes, volcano was already erupting.	Very clear, N-shaped IS signal. Impulsive compressional onset. Coda up to ~ 50 seconds. Most energy at <5 Hz.
7	01-02-2014; 22:39	Strong explosion.  <i>2.05E + 08 = Average Seismic Energy (Joules)</i> <i>3.40E + 10 = Average Acoustic Energy (Joules)</i>	Yes, Juive Grande and SW quebradas	36 hrs	Three distinct explosions at 22 h11; 22 h31 and 22 h39, the last opened the system and was followed by descent of pf's.

\*Mean seismic and acoustic values are calculated from 4 collocated broadband and acoustic sensors (Alex Steele\_IJEPN, pers. Comm. 2014).

Due to the presumed high gas pressures and accumulated magma beneath the conduit plugs, the last three Vulcanian events (Table 1) produced pyroclastic flows which sped relentlessly down *quebradas*, arriving to the

surrounding river channels 10 minutes after the main explosion (Figure 2b). Given the dynamics of the Vulcanian-style eruptions, early warnings based on geo-physical parameters and conveyed over a reliable radio



system are essential for the well-being of the local population who persist living on the volcano's flanks and also those who are transiting on main thoroughfares around the volcano. Since we have identified some of the precursor geophysical parameters that may be displayed before future major Vulcanian events at Tungurahua, the IGEPN hopefully can continue to provide timely early warnings before new eruption onsets.

After fifteen years of on and off eruptions, Tungurahua has produced both Strombolian-style and Vulcanian eruptive outbursts and a varied amount of ash and eruptive products. Estimates of the amount of volcanic material expelled up to March 2014 is based on the following data with the respective references: 1999 to July 2001 = 14 Mm<sup>3</sup> (Wright et al. 2012); August, 2001 = 4 Mm<sup>3</sup> (Le Pennec et al. 2011); Late 2001-December, 2005 = 5 Mm<sup>3</sup> (Wright et al. 2012); August, 2006 = 100 Mm<sup>3</sup> (Hall et al. 2013; Eychenne et al. 2012); 2007 unknown; February, 2008 = 1.5 Mm<sup>3</sup> (Biggs et al. 2010); December, 2008-November, 2012 = 20 Mm<sup>3</sup> (G. Ruiz and J. Bustillos, Pers. Comm); December, 2012 = 0.5 Mm<sup>3</sup> and March, 2013 = 0.2 Mm<sup>3</sup> (Bernard et al. 2013). Since July 2013 to present at least 8 Mm<sup>3</sup> were expelled in the form of pyroclastic flows (M. Hall and S. Vallejo, Comm. Pers.). A total reported bulk volume is approximately 153 Mm<sup>3</sup> of combined ashfall, lava and pyroclastic flows.

The sporadic nature of the eruptive activity and its relative predictability are important factors giving residents the confidence to keep living around the volcano. Most citizens have continued to maintain their homes and livelihoods, and that despite the explosive activity, crop yields are moderately good, some even bountiful, due to the frequent dressing of fine andesitic ash, which is quickly tilled into the soil to readily facilitate nutrient uptake by crops. Tourists travel to Baños to be close to the volcano, especially flocking to the city during the most spectacular and persistent Strombolian activity, viewing the volcano from safe hilltop perches. The city government promotes safe visitation to the volcano for local and international tourists.

Since the display of outright resentment by the population to the IGEPN monitoring scientists after the 1999-forced evacuations, the managerial aberrations that occurred in 2006 and especially after the large eruptions that same year spilled pyroclastic flows down three flanks and modified local topography, there was little doubt in people's minds that the volcano truly had the eruptive power to affect their lives and livelihoods. Until they experienced the 2006 eruptive events, residents whose grandparents had related to them the hardships they had faced following the yet bigger 1918 Tungurahua eruption, had been skeptical that the actual eruption would personally affect them or their families. Farmers still living persistently on Tungurahua's SW flanks relate

that their relatives in 1918 escaped the harshness of that eruptive episode by migrating to the piedmont zone at the foot of the Western Cordillera, about 80 km SW of Penipe, to start a new life.

Local people also developed greater respect for the IGEPN scientists, as OVT had given two successful early warnings before the July and August, 2006 eruptive episodes, and also for the recent Vulcanian-style eruptions of 2013 and that of 01 February, 2014. Good working relations with the provincial and local officials and the population-at-large around Baños, Pelileo and Penipe have typified the post-2006 eruptive period. While nobody knows what the final outcome will be at Tungurahua, if the eruption were to end now, the eruptive phase of 1999–2014 will have been more benevolent than the 1916–1918 eruptive events, whose incandescent products produced broader flow paths which were experienced and reported by deceased ancestors of families who still live around the volcano. Stratigraphy also shows us that previous historical eruptions produced larger volume ash falls and broader-reaching pyroclastic flows. For example, villages on the west flank were overrun by pyroclastic flows during earlier historical eruptions as was the western perimeter of Baños and Ulba (Le Pennec et al. 2008). The 1773 eruption brought a scoria bomb-rich pyroclastic flow into Baños center (Mothes et al. 2004).

## Conclusions

The founding of OVT on a local hacienda outside of Baños gave IGEPN scientists an opportunity to experience and monitor closely the evolution of eruptive activity and to issue early warnings to authorities and the populations living in high-risk zones. OVT has also benefitted from the implementation of a wide range of modern monitoring techniques that aide scientists in the interpretation of changing conditions in the volcano, and thus provides a means for giving early warnings. The persistent local presence at OVT has helped the IGEPN to have a close evaluation of evolving eruptive activity and be in close and immediate contact with local authorities and the public. Some IGEPN scientists have been serving regular monitoring shifts at OVT since inception of the observatory and are well recognized and trusted in the community. Trust is an earned attribute which is very important during volcanic crises, because people may feel that they are putting their lives in a scientist's hands (Haynes et al. 2008). This long association with monitoring at OVT has helped to create a collective "institutional memory" within the IGEPN and have fostered a well-founded knowledge of the volcano's behavior. This understanding has facilitated the induction of young scientists into OVT monitoring activities. Young scientists, who begin as students working on a thesis, are trained at OVT over a period of months, thus

learning the “*modus operandi*”. They learn the volcano’s geography, become acquainted with the local actors, but foremost they must learn the geophysical signs given by the volcano and the possible significance of these signals.

Personal interaction by OVT monitoring scientists with local people and *vigías* has helped cement relations and establish trust. The *vigías* are an important link between the monitoring scientists and the communities where individual *vigías* live. The continued real-time 24/7 monitoring done by the IGEPN has given people living around the volcano a greater level of security. The population has come to rely on receiving timely early warnings before eruption, and they believe that IGEPN monitoring scientists are keeping a constant eye on the volcano’s pulse and trends. The *vigía* network and radio system also promotes the interchange of critical observations which keeps community members informed as well as giving visual and audible observations to OVT scientists.

In this contribution we reported a clear shift over 15 years, from negative to eventually positive in the public’s perception of volcano monitoring and early warnings given by the IGEPN. Various circumstances played a role in this transformation, but the foremost contribution was maintaining a local observatory, staffed by scientists from a national university, the gradual insertion by various means into the local context and the scientific-community linkage that is effectively established through collaboration with *vigías*, being present to meet often with concerned people and officials, and to give orienting talks and debriefings on volcanic activity. Essentially the IGEPN, consciously or not, has carried out volcano monitoring and risk reduction with a “bottom-up” approach. This approach takes more time to implement compared to a top-down approach, where the people are forced to evacuate or stay out of a zone through enforcement by military or police, and perhaps where monitoring scientists have little contact with the public. Developing trust between local people, authorities and scientists is mutually beneficial, especially when the mission is long. Insertion into the local fabric is gradual and may take years if there is lingering resentment by the local population, and relies on key players at observatories who are credible, recognized and trusted. We believe that the public wants to know and hopefully trust the scientists who are providing critical information about possible impacts on their lives in decisive moments, ie, the decision to evacuate or not, being one of them.

As has been pointed out, overall moderate levels of eruptive activity of Tungurahua volcano, combined with the instrumental and human-based monitoring and warning system that is in place, has allowed local people to continue living in high risk areas. Their willingness to continue inhabiting some high risk zones is doubtless due to their connection to their land, their economic investments, the lack of another home, the custom volcano

monitoring provided by OVT and for some, the ability to stay in touch by communicating over the UHF radio system. Given the powerful eruptions that occurred in 2006 and later, local residents probably realize the possibility that a surprise large pyroclastic flow could travel far down the slopes and *quebradas* during rapid-onset Vulcanian-style eruptions, potentially affecting life and property. If, in the future large and multiple pyroclastic flows occur with a lead time of only minutes, not *all* the people who could be affected may receive an adequate warning that permits evacuation. This is because the people at highest risk, especially those living on the NW flanks, are served by evacuation routes that are cut by *quebradas* that may transport descending pyroclastic flows. Such a worst-case scenario, if it were to play out, could present severe complications for both the IGEPN and the SNGR and perhaps terminate inhabitation of families on the volcano’s immediate flanks.

Nonetheless, after 15 years, thus far the VEI = 3 or smaller eruptions have not surpassed the resilience of communities or of OVT scientists to adequately respond or recover from an eruption. OVT scientists continue living in this environment, communicating often with the local population via several media, including having frequent personal contact— essential actions which fortify the scientific-community interface in the area. Foremost, OVT scientists have the paramount responsibility of fingerprinting geophysical trends of Tungurahua’s activity and providing early warnings before heightened eruptive activity.

Finally we must honor Tungurahua, for unlike most volcanoes that erupt in hours or days of their awakening, then resume dormancy, Tungurahua has given us 15 years of study and practice in which to improve our response and reaction and has taught us many lessons.

#### Competing interests

The authors declare that they have no competing interests.

#### Authors’ contributions

PM developed the concept of the paper, wrote the draft and carried out the modifications. HY, PH and PR revised the manuscript and participated in discussions about the content. AS prepared data on Vulcanian explosions and read the text and made comments. MR discussed with all authors hazard mitigation strategies and improvements to monitoring during crises. All authors read and approved the final manuscript.

#### Acknowledgments

We are thankful for the Instrumentation upgrades that have been achieved in collaboration with JICA, USAID, USGS, SouthCom, UNAVCO, NOVAC, the SNGR, Proyecto BID (Early Warning System), the Ecuadorian NSF (SENESCYT) and SENPLADES. Cooperation with French IRD scientists has provided high-quality modeling of PDCs. We also extend gratitude to the Chavez Family who loans us their hacienda house for OVT operations. The DIPECHO Project helped in improving community relations and contributing to the concept of forming the Vigía group. Interactions with the STREVA project have provided stimulating conversations concerning resilience of local populations and volcano observatories. We extend thanks to the EPN for continuing support and the staff of the IGEPN. We recognize the commitment of the 25 *vigías* who provide invaluable observations during eruptive activity at Tungurahua. A USAID-OFDA project

also helped to strengthen the *vigía* network in 2013. We are grateful to the three reviewers whose suggestions improved the manuscript.

Received: 5 August 2014 Accepted: 26 January 2015

Published online: 25 February 2015

## References

- Arellano S, Hall M (2007) Velocidades de emisión de bombas expulsados por el volcán Tungurahua el 16–17 de agosto de 2006. 6ta Memorias Jorn. Cien. Tierra, Esc Poli Nac, Quito, pp. 185–188
- Arellano S, Hall M, Samaniego P, Le Pennec JL, Ruiz A, Molina I, Yepes H (2008) Degassing patterns of Tungurahua volcano (Ecuador) during the 1999–2006 eruptive period, inferred from remote spectroscopic measurements of SO<sub>2</sub> emissions. *J Volcano Geotherm Res* 176:151–162
- Bernard B, Bustillos J, Wade B, Hidalgo S (2013) Influence of the wind direction variability on the quantification of tephra fallout: December 2013 and March 2013 Tungurahua eruptions. *Avances* 5(1):A14–A21, Quito, Ecuador
- Biggs J, Mothes P, Ruiz M, Baker S, Amelung F, Dixon T, Hong S-H (2010) Stratovolcano growth by co-eruptive intrusion: the 2008 eruption of Tungurahua Ecuador. *Geophys Res Lett* 37:L05304, doi:10.1029/2009GL041644, 2010a
- Clark AB (2013) Unsteady explosive activity: Vulcanian eruptions. In: Fagents SA, Tracy KP G, Rosaly MC L (eds) *Modeling Volcanic Processes: The Physics and Mathematics of Volcanism*. Cambridge University Press, England, pp 129–152
- Eychenne J, Le Pennec J-L, Troncoso L, Gouhier M, Nedelec J-M (2012) Causes and consequences of bimodal grain-size distribution of tephra fall deposited during the August 2006 Tungurahua eruption (Ecuador). *Bull Volcanol* doi:10.1007/s00445-011-0517-5
- Gottsmann J, Angelis D, Fournier N, Van Camp M, Sacks S, Linde A, Ripepe M (2011) On the geophysical fingerprint of Vulcanian explosions. *Earth Planetary Sci Lett* 306:98–104, doi:10.1016/j.epsl.2011.03.035
- Hadley KC, LaHusen RG (1995) Technical manual for the experimental acoustic flow monitor. US Geologic Surv Open File Rep 25:95–114
- Hall M, Robin C, Beate B, Mothes P, Monzier M (1999) Tungurahua Volcano, Ecuador: structure, eruptive history and hazards. *J Volcanol Geotherm Res* 91(1):1–21
- Hall ML, Steele AL, Mothes P, Ruiz MC (2013) Pyroclastic density currents (PDC) of the 16–17 August 2006 eruptions of Tungurahua volcano, Ecuador: Geophysical registry and characteristics. *J Volcanol Geotherm Res* 265:78–93
- Haynes K, Barclay J, Pidgion N (2008) The issue of trust and its influence on risk communication during volcanic crisis. *Bull Volcanol* 70(5):605–621
- Hidalgo S, Battaglia J, Bernard B, Steele A, Arellano S, Galle B (2014) Identifying open and closed system behaviors at Tungurahua volcano (Ecuador) using SO<sub>2</sub> and seismo-acoustic measurements. EGU General Assembly, Vienna Austria, Abstract id 1615541H
- Iguchi M, Yakiwara H, Tamegair T, Hendrasto M, Hirabayashi J (2008) Mechanism of explosive eruption revealed by geophysical observations at the Sakurajima, Sawanosejima and Semeru volcanoes. *J Volcanol Geotherm Res* 178:1–9, doi:10.1016/j.jvolgeores.2007.10.010
- Kelfoun K, Samaniego P, Palacios P, Barba D (2009) Testing the suitability of frictional behaviour for pyroclastic flow simulation by comparison with a well-constrained eruption at Tungurahua volcano (Ecuador). *Bull Volcanol* 71(9):1057–1075
- Kumagai H, Nakano M, Maeda T, Yepes H, Palacios P, Ruiz M, Arrais S, Vaca M, Molina I, Yamashima T (2010) Broadband seismic monitoring of active volcanoes using deterministic and stochastic approaches. *J Geophys Res* 115:B08303, doi:10.1029/2009JB006889
- Lane LR, Tobin GA, Whiteford LM (2003) Volcanic hazard or economic destitution: hard choices for Baños, Ecuador. *Environ Haz* 5:23–34
- Le Pennec J-L, Jaya D, Samaniego P, Ramón P, Moreno S, Egred J, van der Plicht J (2008) The AD 1300–1700 eruptive periods at Tungurahua volcano, Ecuador, revealed by historical narratives, stratigraphy and radio-carbon dating. *J Volcanol Geotherm Res* 176:70–81
- Le Pennec J-L, Ruiz GA, Ramón P, Palacios E, Mothes P, and Yepes H (2011) Impact of tephra falls on Andean communities: the influences of eruption size and weather conditions during the 1999–2001 activity of Tungurahua Volcano, Ecuador. *J Volcanol Geotherm Res* (2011) doi:10.1016/j.jvolgeores.2011.06.011.
- Leonard GS, Johnston DM, Williams S, Cole JW, Finnis K, Barnard S, (2005) Impacts and management of recent volcanic eruptions in Ecuador: lessons for New Zealand. Institute of Geological & Nuclear Sciences, Geological and Nuclear Sciences Science Report 2005/20, 51 p. <http://civildefence.govt.nz/assets/Uploads/publications/GNS-SR2005-20-Ecuador-volcano-impacts.pdf>
- Morrissey MM, Mastin L (2000) Vulcanian Eruptions. In: *Surgurdsson H (ed) Encyclopedia of Volcanoes*. Academic Press, San Diego, USA, pp 463–476
- Mothes P, Vallance J (2015) Lahars at Cotopaxi and Tungurahua Volcanoes, Ecuador: Highlights from Stratigraphy and Observational Records and Related Downstream Hazards. In: Papale P et al (eds) *Volcanic Hazards, Risks and Disasters, Hazards and Disasters Book Series*. Elsevier, Amsterdam, Netherlands, pp 142–167
- Mothes P, Hall M, Hoblitt R, Newhall C (2004) Caracterización de los flujos piroclásticos producidos por el volcán Tungurahua (Ecuador): evidencia de dichos flujos en la ciudad de Baños. *Investigaciones en Geociencias*, vol 1. Instituto Geofísico & Corporación Editora Nacional, Quito, pp 19–27
- Ramón P (2010) Análisis Retrospectivo de la Evaluación de la Amenaza, el Monitoreo Volcánico y la Comunicación durante las Erupciones del año 2006 del Volcán Tungurahua. Master 2 SGT PREFALC "CIENCIAS Y GESTION DE LA TIERRA" GEOLOGIA, RIESGOS Y GESTION DEL TERRITORIO, Université Nice Sophia Antipolis, p 113, Instituto Geofísico, Quito
- Ruiz M, Lees JM, Johnson JB (2006) Source constraints of Tungurahua volcano explosion events. *Bull Volcanol* 68:480–490
- Ruiz AG, Mothes P, Bustillos J, Jarrin P, Yepes H (2012) Predicting Volumes of Magma Influx in 2011 using Ground Deformation Patterns at Tungurahua Volcano, Ecuador. *Cities on Volcanoes7*, Abstract, Colima, Mexico
- Samaniego P, Le Pennec J-L, Robin C, Hidalgo S (2011) Petrological analysis of the pre-eruptive magmatic process prior to the 2006 explosive eruptions at Tungurahua volcano, Ecuador. *J Volcanol Geotherm Res* 199:69–84
- Steffke AM, Fee D, Garcés M, Harris A (2010) Eruption chronologies, plume heights and eruption styles at Tungurahua volcano: integrating remote sensing techniques and infrasound. *J Volcanol Geotherm Res* 199:69–84
- Stone J, Barclay J, Simmons P, Cole PD, Loughlin SC, Ramón P, Mothes P (2014) Risk reduction through community-based monitoring: the *vigías* of Tungurahua, Ecuador. *J of Applied Volcanology* 3(11), doi:10.1186/s13617-014-0011-9.
- Sword-Daniels V, Wardman J, Stewart C, Wilson T, Johnston D, Rossetto T (2011) Infrastructure impacts, management and adaptations to eruptions at Volcán Tungurahua, Ecuador, 1999–2010. *GNS Science Report* 2011/24., p 73
- Tobin GA, Whiteford LM (2002) Community resilience and volcano hazard: the eruption of Tungurahua and evacuation of the *faldas* in Ecuador. *Disasters* 26(1):28–48
- Vergnolle S, Mangan M (2000) Hawaiian and Strombolian eruptions. In: *Sigurdsson H (ed) Encyclopedia of Volcanoes*. Academic Press, San Diego, USA, pp 447–461
- Williams R, Stinton AJ, Sheridan MF (2008) Evaluation of the Titan2D two-phase flow model using an actual event: case study of the 2005 Vazcún Valley Lahar. *J Volcanol Geotherm Res* 177:760–766
- Wright HMN, Cashman KV, Mothes PA, Hall ML, Ruiz AG, Le Pennec J-L (2012) Estimating rates of decompression from textures of erupted ash particles produced by 1999–2006 eruptions of Tungurahua volcano, Ecuador. *Geology* 40(7):619–622, doi:10.1130/G32948
- Yamazaki K, Teraishi M, Ishihara K, Momatsu S, Kato K (2013) Subtle changes in strain prior to sub-Plinian eruptions recorded by vault-housed extensometers during the 2011 activity at Shinmoe-dake, Kirishima volcano, Japan. *Earth Planets Space* 65:1491–1499

Submit your manuscript to a SpringerOpen journal and benefit from:

- Convenient online submission
- Rigorous peer review
- Immediate publication on acceptance
- Open access: articles freely available online
- High visibility within the field
- Retaining the copyright to your article

Submit your next manuscript at ► [springeropen.com](http://springeropen.com)

## **Résumé :**

Dans l'histoire de l'Équateur, les séismes ont causé beaucoup de victimes (~60 000) et de nombreux autres problèmes. Les événements récents de la fin du XXe siècle ont mis en évidence que les constructions existantes présentent une vulnérabilité physique importante et que l'impact économique des tremblements de terre pourrait être très élevé. Le risque sismique a trois composantes principales : l'aléa, la vulnérabilité et l'exposition. Par conséquent, pour réduire le risque en Équateur, il est primordial d'effectuer des évaluations probabilistes de l'aléa sismique (PSHA).

La première étape du développement du PSHA fut de construire un catalogue sismique dans lequel la sismicité historique et instrumentale est homogène et complète. Les données de sismicité instrumentale ont été rassemblées à partir des catalogues locaux et internationaux. Les événements ont été identifiés et, par l'utilisation d'un régime de hiérarchisation des endroits les plus fiables et des estimations de magnitude, les événements ont été regroupés dans un catalogue unique, unifié et homogénéisé. La sismicité historique réévaluée a ensuite été ajoutée. Le catalogue des séismes en Équateur entre 1587 et 2009 comprend ainsi 10 823 événements instrumentaux et 32 séismes historiques, avec une gamme de magnitude  $M_w$  de 3,0 à 8,8.

Un modèle de zonage des sources sismiques (SSZ) a ensuite été effectué. Dans le cadre de cette modélisation, une nouvelle vision de la géodynamique de l'Équateur a été conçue. Deux aspects des interactions des plaques à l'échelle continentale permettent d'expliquer plusieurs caractéristiques observées dans la génération des tremblements de terre observés, comme l'essai sismique d'El Puyo, ainsi que le couplage inter-sismique : les différences de rhéologie des plaques Nazca et Farallon et la convergence oblique provoquée par la forme convexe de la partie nord-ouest de la marge continentale sud-américaine. La paléomarge en extension Grijalva (GRM) marque la frontière entre les deux plaques. La sismicité et le couplage inter-sismique sont faibles et peu profonds au sud de la GRM et augmente vers le nord, avec un modèle de couplage hétérogène associé localement à la subduction de la ride de Carnegie. De grands séismes de décrochement ont rompu l'interface entre la ride de Carnegie et le nord. Au niveau continental, la frontière entre le bloc NA et le bloc stable Amérique du Sud est constituée par le système CCPP de failles. Il concentre la majorité de la libération du moment sismique dans la croûte Équateur. 19 SSZ ont été modélisées : une tranche-externe, trois interfaces, six intra-plaques et neuf croûtes.

Le catalogue sismique et une version préliminaire du modèle SSZ ont été appliqués pour déterminer le PSH à Quito et évaluer les incertitudes. La ville est construite sur le toit d'un système de failles inverses actif, qui se déplace de 4,3 à 5,3 mm/an. Les PSH ont montré que la contribution de la SSZ locale explique presque entièrement l'aléa correspondant à une période de retour (PR) de 475 ans. L'analyse a donc été concentrée sur cette zone. La source locale, la géométrie de la SSZ, la modélisation des distributions de fréquence-magnitude et/ou de taux de glissement avec des pourcentages de verrouillage variables, la sélection des GMPEs et l'intégration de l'effet du compartiment chevauchant ont apporté des accélérations avec cette PR avec une variabilité importante. Le PGA moyen obtenu sur un site au rocher est ~0,4g avec cette PR, avec une variabilité de 0,3 à 0,73g.

La mise à disposition du PSHA est cruciale pour la gestion des risques mais est compliquée, car les probabilités et les incertitudes ne sont pas facilement assimilées par la société. Suite aux pratiques des sciences sociales et les expériences acquises des alertes précoces d'éruption, une approche participative a été exposée pour construire collectivement des connaissances sur le risque de séisme à Quito, qui pourrait prendre la forme d'un observatoire citoyen.

## **Mots-clés :**

Catalogue sismique, zonage sismotectonique, géodynamique de l'Équateur, PSHA, communication de l'aléa, incertitudes

## **Abstract:**

Seismic hazard and risk are high in Ecuador. Earthquakes are notorious in the country's history for both the number of victims (~60.000) and the hardships they have brought. Moreover, late 20<sup>th</sup> century events have highlighted evidences that the physical vulnerability of present-day buildings is considerable and that the economic impact of earthquakes could be devastating for Ecuador's sustained growth. Therefore, it is an important contribution for reducing the seismic risk to construct methodologically sound models for probabilistic seismic hazard assessment, which is the main objective of this dissertation.

The first step was to construct a seismic catalog for the country where historical and instrumental seismicity is homogeneous and complete. The instrumental seismicity available in local and international catalogs since the beginning of the 20<sup>th</sup> century was collected. Events were singularized and, by means of a prioritizing scheme of most reliable locations and magnitude estimations, individual events were merged in a single, unified and homogenized catalog. Previously re-evaluated historical seismicity was appended. The 1587–2009 Ecuadorian earthquake catalog finally comprises 10,823 instrumental events plus 32 historical earthquakes with a  $M_w$  magnitude range from 3.0 to 8.8.

Next a seismic source zones (SSZ) model for probabilistic seismic hazard analysis was worked out. In the course of modeling the SSZ, a new view of Ecuador's complex geodynamics was conceived. This view emphasizes two aspects of the plates' interactions at continental scale: the differences in rheology of Farallon and Nazca plates and the convergence obliquity resulting from the convex shape of the South American northwestern continental margin. Both conditions satisfactorily explain several characteristics of the observed earthquake generation –such as the El Puyo seismic cluster– as well as the interseismic coupling. The Grijalva rifted margin (GRM) marks the boundary between the two plates. Seismicity and interseismic coupling are weak and shallow south of the GRM and increases northward, showing a heterogeneous coupling pattern locally associated to Carnegie ridge's subduction. Great thrust earthquakes have ruptured the interface from Carnegie to the north, not breaking through Carnegie. In the continental realm the CCPP localized fault system constitutes the boundary between the NA block and stable South America. It concentrates most of the seismic moment release in crustal Ecuador. 19 SSZs have been modeled accounting for this new scheme: 1 outer-trench, 3 interface, six intraplate and 9 crustal.

The catalog and a preliminary version of the SSZ model were applied in determining the PSH in Quito and assessing the uncertainties. The city is built on the hanging wall of an active reverse fault system that is moving at 4.3-5.3 mm/yr. PSH estimates showed that hazard levels at 475 years return period (RT) almost entirely proceed from the contribution of the local SSZ, therefore the analysis was concentrated on it. Significant variability in accelerations at that RT resulted from a variety of considerations: modeling the local source either as a zone or as fault source, the geometry of the SSZ, the way frequency-magnitude distributions and/or slip rates with variable locking percentages were modeled, the GMPEs selection and the inclusion of the hanging wall effect. The PGA mean value obtained for a rock site Quito is ~0.4 g in that RT with variability ranging from 0.3 to 0.73g.

PSHA communication is crucial for risk management, but is difficult since probabilities and uncertainties are not easily assimilated by society. Following the practices of the social sciences and of experiences acquired in issuing eruption early warnings to rural communities, a participatory approach has been outlined to collectively build up knowledge about the earthquake risk in Quito that could take the form of a citizens' observatory for seismic risk awareness and reduction.

## **Key words:**

Seismic catalog, seismic source zones, Ecuador's geodynamics, PSHA uncertainties, hazards communication.